JOHN E. HALKYARD & COMPANY
OCEAN ENGINEERING CONSULTANTS

FOR
U. S. GOVERNMENT
USE ONLY

# Inspectibility of Tension Leg Platform Tendons

FINAL REPORT - PHASE I

May 4, 1985

Prepared by:

R. H. Bossi (Sigma Research, Inc.)
J. E. Halkyard
C. A. Isaacson
B. F. Maki

This report was prepared under Contract No. 14-12-0001-30204 for the U.S. Department of Interior, Minerals Management Service, Technology Assessment and Research Branch.

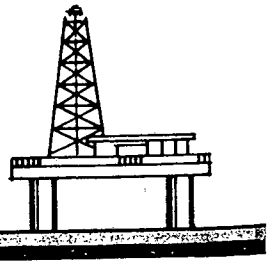

2949 EPAULETTE STREET • SAN DIEGO, CALIFORNIA 92123 • USA

PHONE (619) 569-6083 • TELEX 516-864

ATTACHMENT B

**U.S. DEPARTMENT OF THE INTERIOR**
**SMALL BUSINESS INNOVATION RESEARCH PROGRAM**
**PHASE I-FY 1984**
**DOI/SBIR 84-1**
**PROJECT SUMMARY**

| FOR DOI USE ONLY | | |
|---|---|---|
| Program Office | Proposal No. | Topic No. |
| | | |

**TO BE COMPLETED BY PROPOSER**

**Name and Address of Proposer**

John E. Halkyard & Company, 2949 Epaulette Street, San Diego, CA 92123

**Name and Title of Principal Investigator**

John E. Halkyard, President

**Title of Project**

Inspectibility of Tension Leg Platforms

**Topic**

Technology Assessment and Research Program (Topic # 7)

**SubTopic**

**Technical Abstract (Limit to two hundred words)**

Likely tension leg platform tendon designs have been identified. Fatigue loads have been estimated for four environments: the North Sea, Atlantic, Gulf of Mexico and the U. S. West Coast. Fatigue and crack growth analysis has been carried out to identify the residual life (deterministic analysis) and probability of structural failure (probabilistic analysis) for a given assumed initial flaw distribution. The level of inspection required to achieve a certain structural reliability over a given period was thus determined. A survey of possible inspection techniques was conducted and ultrasonic methods were identified as the most suitable for inspecting the threaded connections, flex elements and other tendon components. A theoretical model was developed to predict the level of flaw detection for a given geometry and ultrasonic parameters. From these results, it appears that a high reliability may be achieved in TLP tendons using relatively infrequent in place inspection techniques to detect cracks. The tendon designs selected for this study appear reliable enough to require only one inspection during their service lives, except possibly in the "worst case" North Sea environment. A plan for verifying the ultrasonic model has been proposed for Phase II.

**Keywords (8 max) Description of the Project, Useful in Identifying the Technology, Research Thrust and/or Potential Commercial Application**

Tension Leg Platforms, Compliant Structures, Ultrasonic Inspection, Fracture Mechanics, Corrosion Fatigue

**Anticipated Results/Potential Commercial Applications of the Research**

Assessment of state-of-the-art methods for inspecting Tension Leg Platform tendons and the potential impact of in place inspection on TLP reliability. Potential application in evaluating tendon designs and developing a commercial inspection method.

CONTENTS

CONTENTS (continued)

CONTENTS (continued)

LIST OF FIGURES

LIST OF FIGURES (Continued)

LIST OF FIGURES (Continued)

LIST OF TABLES

LIST OF TABLES (Continued)

## 1.0 Introduction

The oil industry has been developing alternate methods of producing oil from deeper waters for several years [Crooke]. Two novel deep water production platforms are currently being installed. The Exxon guyed tower [Lena Platform] is currently in place in the Gulf of Mexico, and the Conoco Hutton tension leg platform ("TLP", Figure 1.1) was installed in the North Sea in the summer of 1984*. Both the guyed tower and the tension leg platform are "compliant" structures in that they are designed to move with the waves without exerting undue stresses on their members. Compliant structures have a natural surge period that is greater than normal wave periods, while fixed structures have periods less than the wave periods.

A critical element of both the tension leg platform and the guyed tower are the mooring systems. These systems consist of the guy wires, in the case of the guyed tower, and tendons in the case of the TLP. The mooring system is designed to prevent the excursions of the platform from exceeding those which would be safe for the platform and well system, while at the same time keeping the loads on the moorings within acceptable stress and fatigue limits.

The reliability of these mooring systems is a key ingredient to the overall feasibility and safety of compliant structures. Ideally, once in place, the tethers would not need to be replaced over the lifetime of the structure. Whether this objective can be met depends on two factors:

a) can design criteria as conservative as those used for fixed structures be used in the design of these tethers and

b) can suitable methods of in place inspection of the tethers be utilized so that the risk of structural failure is adequately low.

Unfortunately, there is no prior operational experience to draw upon in order to verify the appropriateness of design criteria for this specific application. The reliability of tether components will not truly be known until a number of test programs are undertaken, and

*See Ocean Industry, Vol.19, No.8, Aug. 1984, p.35.

maybe not even until a structure has been in place for many years. This means that the ultimate reliability of the tether system depends on the ability to either perform accurate in-place inspections, or to periodically remove and replace tether components.

This latter approach has two drawbacks:

a) the costs of removing, inspecting and replacing tethers may be prohibitive in terms of both replacement costs and interruption of operations, and

b) risks associated with removing tethers during the course of operations operations (e.g. from damaging the latch or adjacent tendons) may exceed the potential benefits gained by having confidence in the structural integrity of the replaced part.

Thus, primary emphasis should be placed on developing "fail-safe" insitu inspection techniques and procedures. The primary focus of this research is to investigate the specific requirements for inspecting TLP tendons and the state of the art of applicable inspection methods.

In principle, several methods can be used to inspect for fatigue cracks or other defects: ultrasound, eddy current, x-ray, or acoustic emission. For reasons discussed in Section 6, ultrasonic NDT techniques are considered most suitable.

In addition to selecting the most appropriate inspection technique, there are questions about how to implement the procedure. In the case of the pipe sections with a small inner bore, internal inspection would have to be accomplished with an automated instrument, and even in pipes with an inner diameter of 20 inches or more manned inspection is unlikely. External inspection may be possible using divers or remotely operated vehicles, but it would be very expensive, especially in view of the huge amount of the steel to be inspected. External inspection would also be impeded by marine growth on the outside of the legs. Even a relatively thin layer of marine growth makes ultrasonic inspection difficult or impossible because the porosity of most of these organisms scatters and strongly attenuates signals.

In the case of gas-filled pipes, acoustic coupling may constitute a problem. It can be solved, however, by temporarily substituting a liquid for gas in all or part of the leg being inspected or by using a contacting acoustic device.

## Introduction

Emphasis in this study has been placed on the modeling of tendon failure mechanisms and on methods for inspecting tendons while in service. Since it is likely that the efficacy of any inspection scheme will depend on the particular form of the tendons, the first phase of this study focuses on the development of a methodology for quantitative assessment of the effectiveness of a given inspection method. The output of this methodology, or tendon inspection model, is a determination of risk, or failure probabilities, as a function of such things as inspection tool performance, structural form (shape) of tendon components, frequency of inspection, acceptance criteria (e.g. initial flaw size) and environmental loadings. This model may be utilized in the future to assess the relative effectiveness of various inspection methods together with various tendon structural forms. This assessment will combine an analysis of inspection methods with a fracture mechanics analysis of tendon components in order to determine the effectiveness of various inspection strategies.

This report defines the key parameters of possible TLP tendon designs, inspection systems and likely failure mechanisms which need to be considered in an inspection strategy. Section 3 defines fatigue load criteria derived from Spectral Ocean Wave Model (SOWM) hindcast data and various published tendon tension response functions. Sections 4 and 5 discuss the available data on appropriate material properties for candidate tendon materials, and typical tendon component designs and stress analysis, respectively. Section 6 contains a discussion of possible inspection schemes and an analysis of the likely performance of the preferred method of inspection, ultrasonic. Section 7 presents the results of a structural reliability model incorporating the results of the previous sections. The purpose of this model is to evaluate the effect on structural reliability of various levels of inspection - specifically the frequency of inspection, sensitivity and reliability of the inspection technique. Section 8 discusses recommendations for future research.

## 1.1 References

Crooke, R. C., Otteman, L. G., "Offshore Oil and Gas Technology Assessment", Panel Discussion presented to a symposium "A National Program for the Assessment and Development of Mineral Resources of the United States Exclusive Economic Zone", USGS, Reston, VA, Nov. 1983.

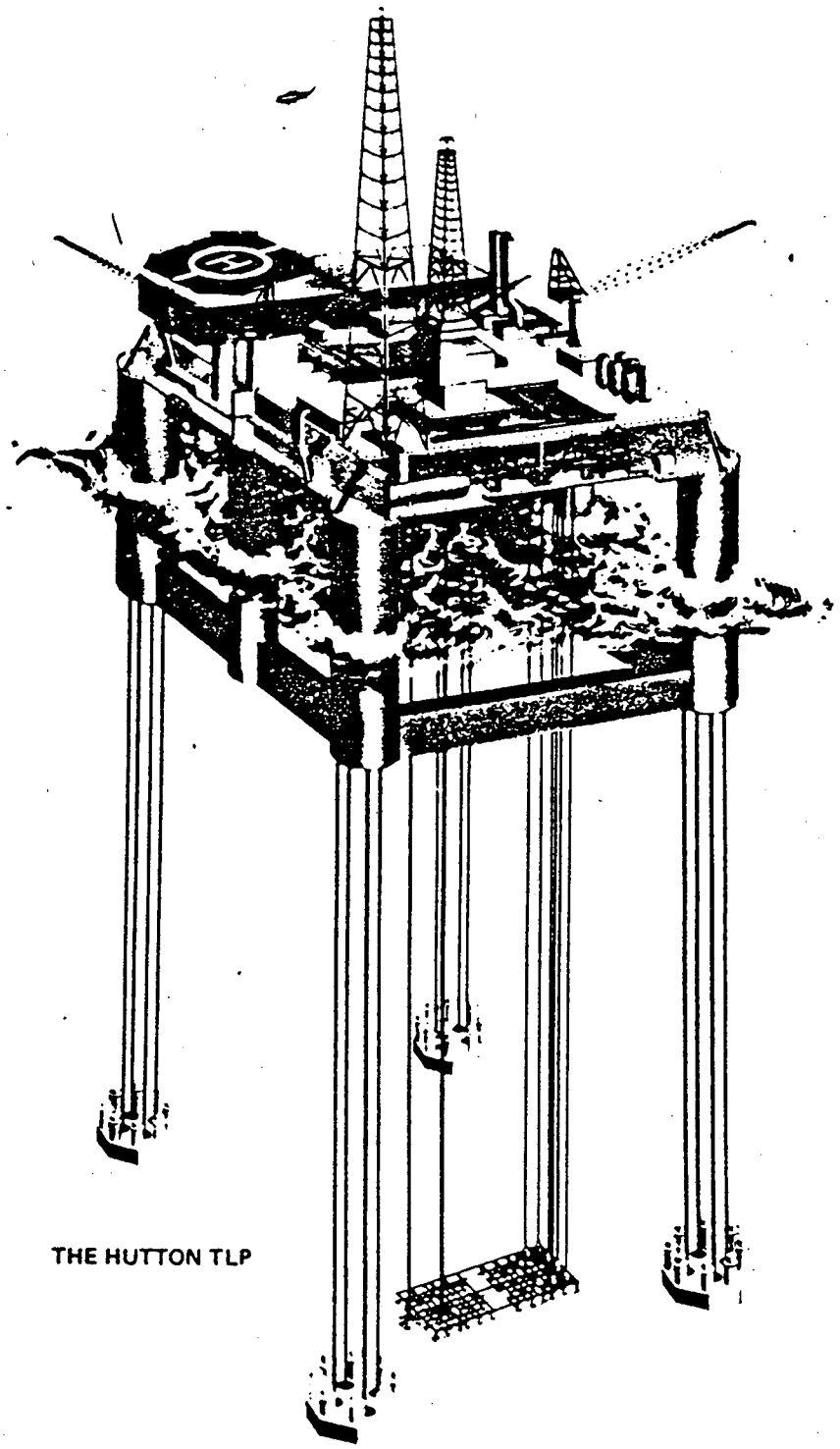


Figure 1.1 The Hutton TLP
(From Mercier, et al)

## 2.0 Summary and Conclusions

### 2.1 General

The objective of Phase I included an analysis of inspection requirements for likely TLP tendon designs, and appropriate inspection methodologies. The focus of the effort was on tendons consisting of tubular steel elements joined by threaded couplings and an internal inspection system similar in approach to that developed for the Hutton project [Salama and Ellis, Shilbeck, et al]. Surface cracks (e.g., welds or heat affected zones) may be detected using various techniques such as magnetic particle, eddy current, magnetic field disturbance or ultrasonic. Magnetic particle and eddy current methods are probably most applicable for direct inspection of external surface flaws, although only the eddy current (for external inspection) or an ultrasonic device would size the defect.

The Phase I study concentrated on modeling the performance of an internal ultrasonic device. The methodology is equally applicable, however, to an external device which might be required for buoyant tendons (i.e. with the tendon I.D. sealed). Mechanized systems for ultrasonic inspection of pipeline welds and offshore platforms have been developed which could be applicable to TLP's (see P.S. Tan, Leeuwen and Hooft).

Generic "thick walled" and "thin walled" connector designs have been considered, as shown in figure 2.1 and 2.2. The thick walled connector corresponds to the Hutton TLP tendon design, while the thin walled connector is more representative of those currently under consideration for U.S. waters.

### 2.2 Ultrasonic Inspection

A theoretical model of ultrasonic detection limits for inspection from the inner diameter has been developed. Figure 2.3 illustrates the acoustic beam angles proposed for the inspection of critical areas of the thin walled connector. Ultrasonic detection limits have been analyzed using assumed conditions for attenuation, reflectivity from boundaries, transmissivity and crack geometry. The model results in an estimate for ultrasonic echo response given as

Summary

$$\frac{P}{P_o} = C_1 R^2 e^{-\alpha 2d} \frac{S_s S_f}{d^2 \lambda^2} \qquad (2.1)$$

where

$C_1$ = transmittance coefficient
P = pulse echo sound pressure amplitude
$P_o$ = initial sound pressure
R = reflection coefficient at steel/water interface
$\alpha$ = attenuation coefficient
$S_s$ = acoustic source area
$S_f$ = area of crack reflecting the acoustic pulse
d = distance travelled by beam in material between source and reflector crack
$\lambda$ = acoustic wavelength

Values of attenuation coefficients, reflection coefficients and transmissivity are very dependent on material properties and surface finish. Values for smooth, fine grained low alloy steel were used in the Phase I analysis.

Plots of this relationship for various sections of the connector at various acoustic frequencies were generated. An example is shown in Figure 2.4. Detection limits will be a function of echo response, with values of .001 (0.1%) considered marginally detectible responses and .005 (.5%) being detectible with a high confidence. These limits result in the theoretical detection sensitivities shown in Table 2.1 for a 5 MHz source frequency.

Notice that the present model considers only far field ultrasonic effects and is not able to reliably predict detection thresholds less than 2mm. These would have to be determined experimentally or with a refined analytical model, although our failure analysis (see below) suggests that lower detection limits may not be necessary.

## 2.3 Analysis of Inspection Requirements

Inspection requirements were determined by carrying out loads analysis, fatigue and fracture mechanics analysis for four likely deep water environments:

- Gulf of Mexico (Green Canyon)
- Atlantic

- o Pacific (Central California)
- o North Sea

Fatigue (crack initiation) and crack growth times depend most critically on load amplitudes, environment and material properties.

Loads are very platform specific. In particular, tendon fatigue loads arise primarily from wave inertial forces on platform columns and pontoons. These loads vary directly with platform displacement and are dependent on a number of factors such as column spacing, ratio of column to pontoon volume, and total waterplane area. A number of published tendon tension Response Amplitude Operations (RAO) were used for the Phase I study recognizing that the RAO for specific applications could alter the results. In assessing inspection requirements, the worst case combination of RAO and environment were generally selected. Table 2.2 shows the effect of various environments and tendon response functions on the estimated crack initiation time for the last box thread.

Of more interest from an inspection standpoint is the time for cracks of various sizes to propagate to a critical size. For any given flaw detection threshold, this could be considered the minimum inspection interval.

Figure 2.5a-b shows the predicted life as a function of initial crack depth for the thick walled and thin walled connectors, respectively, under various environmental conditions. The loading for these cases was derived for worst case RAO of those published - corresponding to a large production platform with a large column to pontoon volume ratio. Table 2.3 summarizes the crack growth periods for an initial flaw size corresponding to the minimum size of a detectible flaw from Table 2.1. Clearly, if flaws of this size can be reliably detected in the connector threads, and our other assumptions are correct, then an initial inspection of the connector threads which shows no flaws larger than those indicated would insure against critical crack growth during typical platform service lives.*

*Note that this analysis does not consider other failure modes such as stress corrosion cracking, nor does it consider damage conditions which could lead to higher loads over part of the structure's life. Also, average crack rates, not upper bound, were used. See Phase I report for further discussion.

Flaw growth in the tendon pipe is expected to be more rapid than in the connector due to higher section stresses. Figure 2.6 shows expected time to failure as a function of critical flaw size for thin walled pipe in the worst case North Sea environment.

In this case a 2mm flaw would lead to critical flaw size in an estimated 35 years. These results could also apply to thin walled tendons with girth welds, where the potential for flaws is greater. Note, however, that crack growth data is sparse for the prevailing TLP conditions (i.e. high mean stress, cathodically protected) even for base metal, let alone for weld metal on the heat affected zone.

The above analysis does not consider the uncertainty in loadings, material properties or initial flaw distribution. A probabilistic crack growth analysis was carried out using Monte Carlo techniques and assumed distributions for these variables. The results for the last pin thread, freely corroding with a presumed inspection to 2 mm flaw size, are shown in Figure 2.7. The results are shown for a single component and a number of components in series representing the reliability of a tension leg taken as a whole.

The above 'worst case' assessment suggests that inspection sensitivities in the range of 2mm for the pipe and/or connector are more than sufficient for an inspection system. In fact, even under these assumptions, and inspection system with a 6-8mm detection limit would be adequate, although under the worst conditions an inspection to this level might be desireable every 10 years.

These conclusions need to be tempered by consideration of several factors:

a) The inspection model is contingent upon several assumptions. For example, external coatings on the tendons could effect the reflection coefficients used in equation 2.1 which in turn could reduce the echo response.

b) The fracture mechanics analysis assumed a single crack nucleation site. Multiple initiation sites could lead to circumferential crack growth which would lead to faster through wall propagation.

c) The material fatigue data is sparse for the conditions experienced by tendons. Our results are based in part by extrapolation of data taken at higher stress intensity and/or lower mean stresses.

d) Stress profiles used in the connector threads were derived from a simplified application of Neuber's rule. Actual thread stress profiles could be different and require finite element and/or experimental verification.

e) The large volume of critically stressed material in a TLP makes 100% inspection difficult. The probability of missing a flaw larger than the theoretically minimum size flaw needs to be considered.

Table 2.1

Theoretical Detection Limits for
TLP Tendon Inspection

| Connector | Location | Min. Detectible Crack Size (mm) | 100% Detection Probability (mm) |
|---|---|---|---|
| Thick Walled | Last Box Thread | 2.0 | 4.3 |
| Thick Walled | Last Pin Thread | <2.0 | <2.0 |
| Thick Walled | Pin Preload Shoulder | <2.0 | <2.0 |
| Thick Walled | Make Up Shoulder | <2.0 | <2.0 |
| Thick Walled | First Box Thread | 3.7 | 8.2 |
| Thin Walled | Last Box Thread | <2.0 | <2.0 |
| Thin Walled | Last Pin Thread | <2.0 | <2.0 |
| Thin Walled | Make Up Shoulder | <2.0 | <2.0 |
| Thin Walled | First Box Thread | <2.0 | 2.8 |

TABLE 2.2 Fatigue life in years for TLP tendon connector designs

| FATIGUE DATA | MAXIMUM TENSION | PRE-TENSION | THICK-WALLED CONNECTOR LIFE CURVE A | THICK-WALLED CONNECTOR LIFE CURVE B | THIN-WALLED CONNECTOR LIFE CURVE A | THIN-WALLED CONNECTOR LIFE CURVE B |
|---|---|---|---|---|---|---|
| 1 | 5300 | 1760 | 101 | 39 | 94 | 34 |
| 2 | 5300 | 1760 | 1083 | 1.2E+6 | 1013 | 1.1E+6 |
| 3 | 1720 | 1085 | 1977 | 1.5E+11 | 1885 | 1.4E+11 |
| 4 | 2075 | 1275 | 1590 | 5.9E+9 | 1513 | 4.75E+9 |
| 5 | 2075 | 1275 | 1557 | 2.0E+10 | 1481 | 1.9E+10 |
| 6 | 2475 | 1475 | 1370 | 2.0E+7 | 1299 | 1.83E+7 |
| 7 | 4275 | 2375 | 433 | 1123 | 403 | 949 |
| 8 | 3275 | 1875 | 382 | 9667 | 360 | 8534 |
| 9 | 2075 | 1275 | 1520 | 5.3E+8 | 1446 | 4.75E+8 |
| 10 | 3275 | 1875 | 277 | 1992 | 261 | 1760 |
| 11 | 2975 | 1725 | 807 | 11430 | 760 | 10250 |
| 12 | 3975 | 2225 | 101 | 376 | 90 | 325 |

Tensions in kips
Curve A is free corrosion S-N curve [Salama and Tetlow, Fig. 7]
Curve B is design S-N curve [Ibid]
MATERIAL: 3.5% NiCrMoV

Fatigue Data Key:

1. Webster Hutton
2. Webster tether
3. SOWM Pacific, Chou RAO
4. SOWM Gulf, Chou RAO
5. SOWM Gulf, Paulling RAO
6. SOWM Gulf, Tan RAO
7. SOWM Gulf, Dillingham RAO
8. SOWM Gulf, Mercier-Hutton RAO
9. SOWM Atlantic, Chou RAO
10. SOWM Atlantic, Mercier-Hutton RAO
11. SOWM North Sea, Chou RAO
12. SOWM North Sea, Mercier-Hutton RAO

Table 2.3

Results of Crack Growth Analysis (Summary)

| Connector | Location | Initial Crack Size (mm) | Residual Connector Life Assuming 100% Detectible Initially (years) North Sea | Atlantic | Gulf of Mexico | Pacific |
|---|---|---|---|---|---|---|
| Thick Walled | Last Pin Thread | 2.0 | 73+ | 633+ | 6319+ | 3720+ |
| Thick Walled | Last Box Thread | 4.2 | 62+ | 520+ | 4700+ | 2600+ |
| Thin Walled | Last Pin Thread | 2.0 | 140+ | 1250+ | 12500+ | 8400+ |
| Thin Walled | Last Box Thread | 2.0 | 160+ | 1300+ | 14000+ | 9000+ |

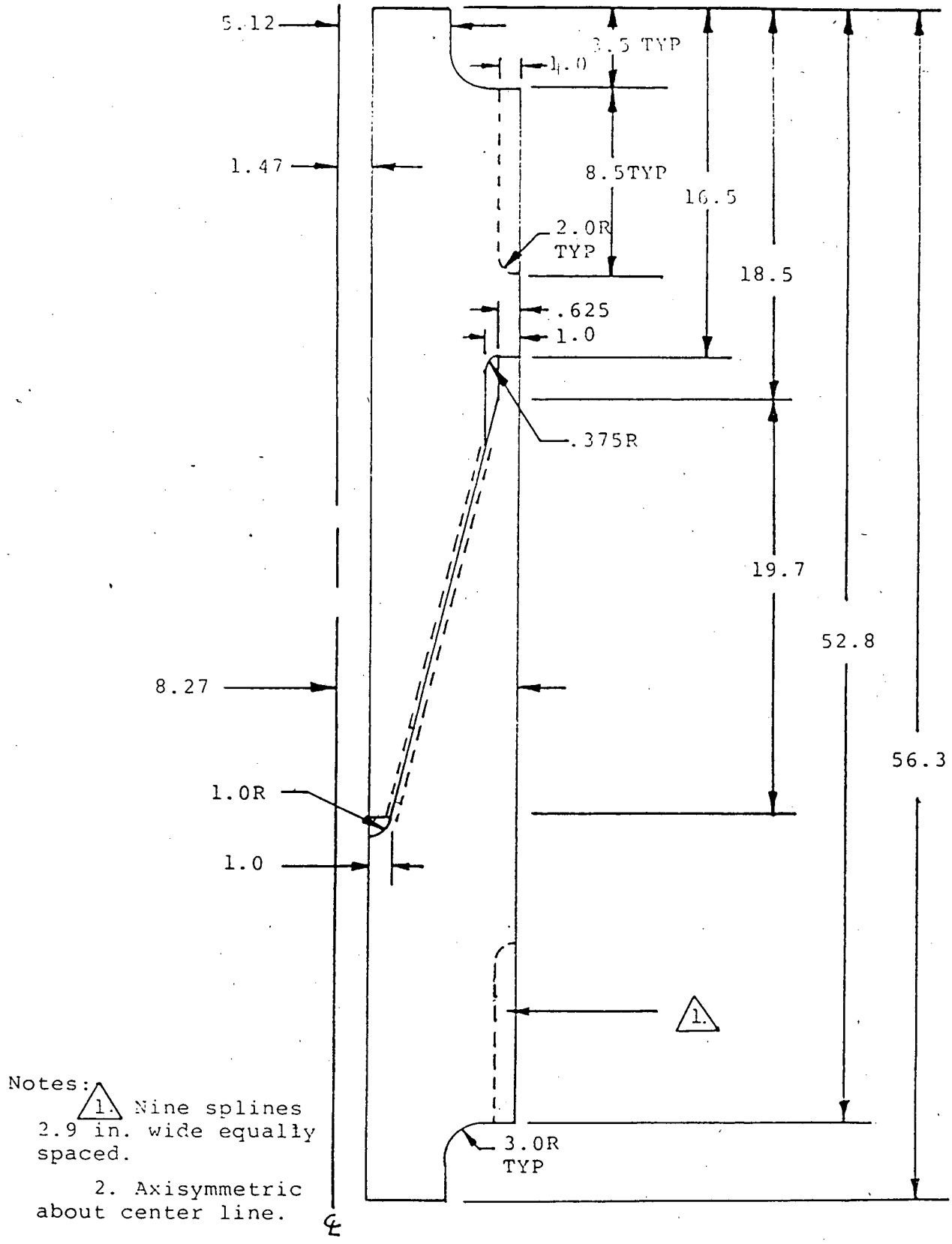


Figure 2.1 - Thick walled connector.

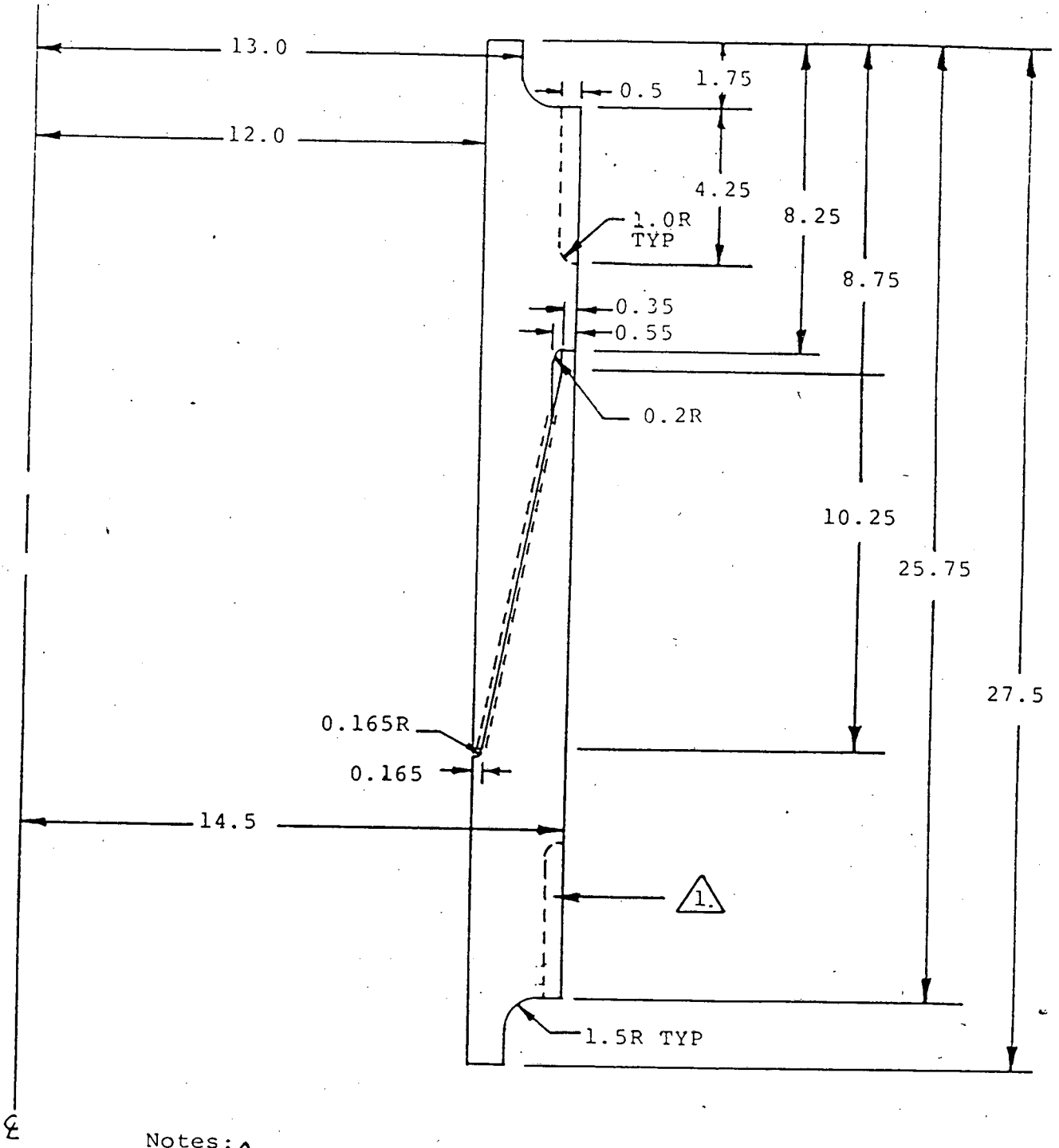


Notes:

1. Twelve splines 3.8 inches wide, equally spaced.
2. Axisymmetric about center line.

Figure 2.2 - Thin walled connector.

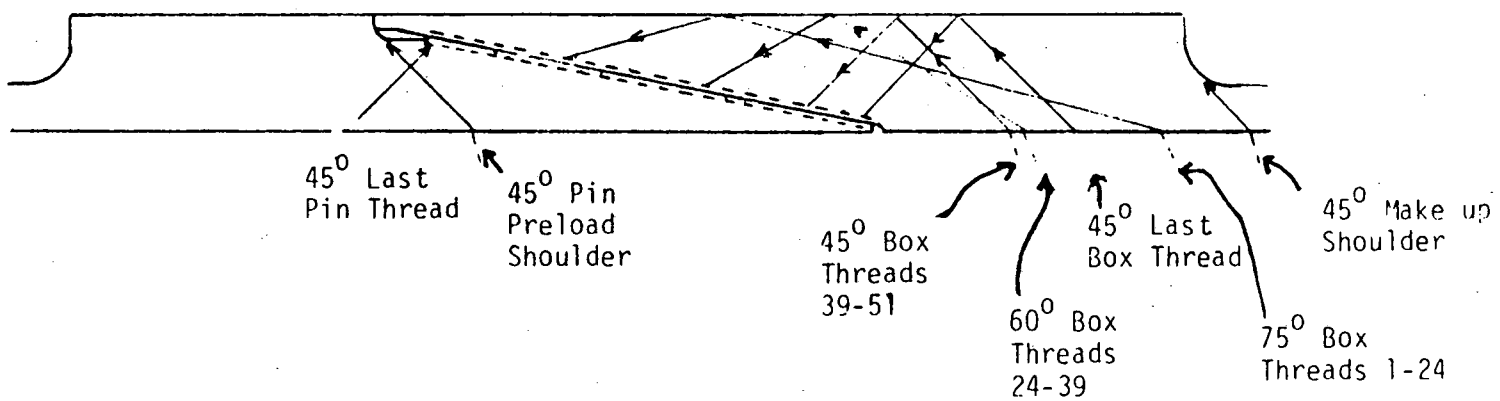


Figure 2.3- - Ultrasonic beam angles for the thin walled coupling

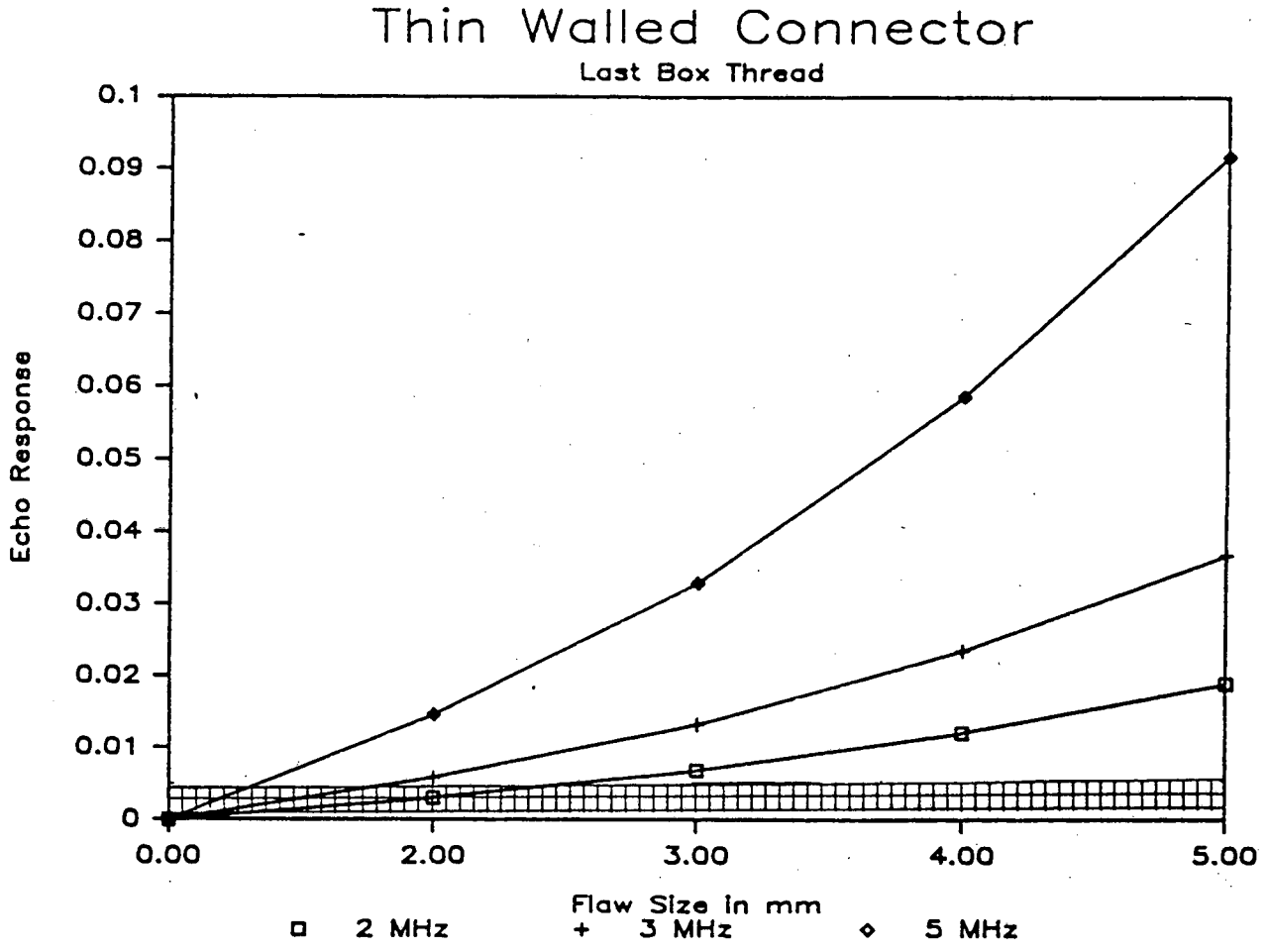


Figure 2.4 - Echo response vs. flaw size for the thin walled connector last box thread.

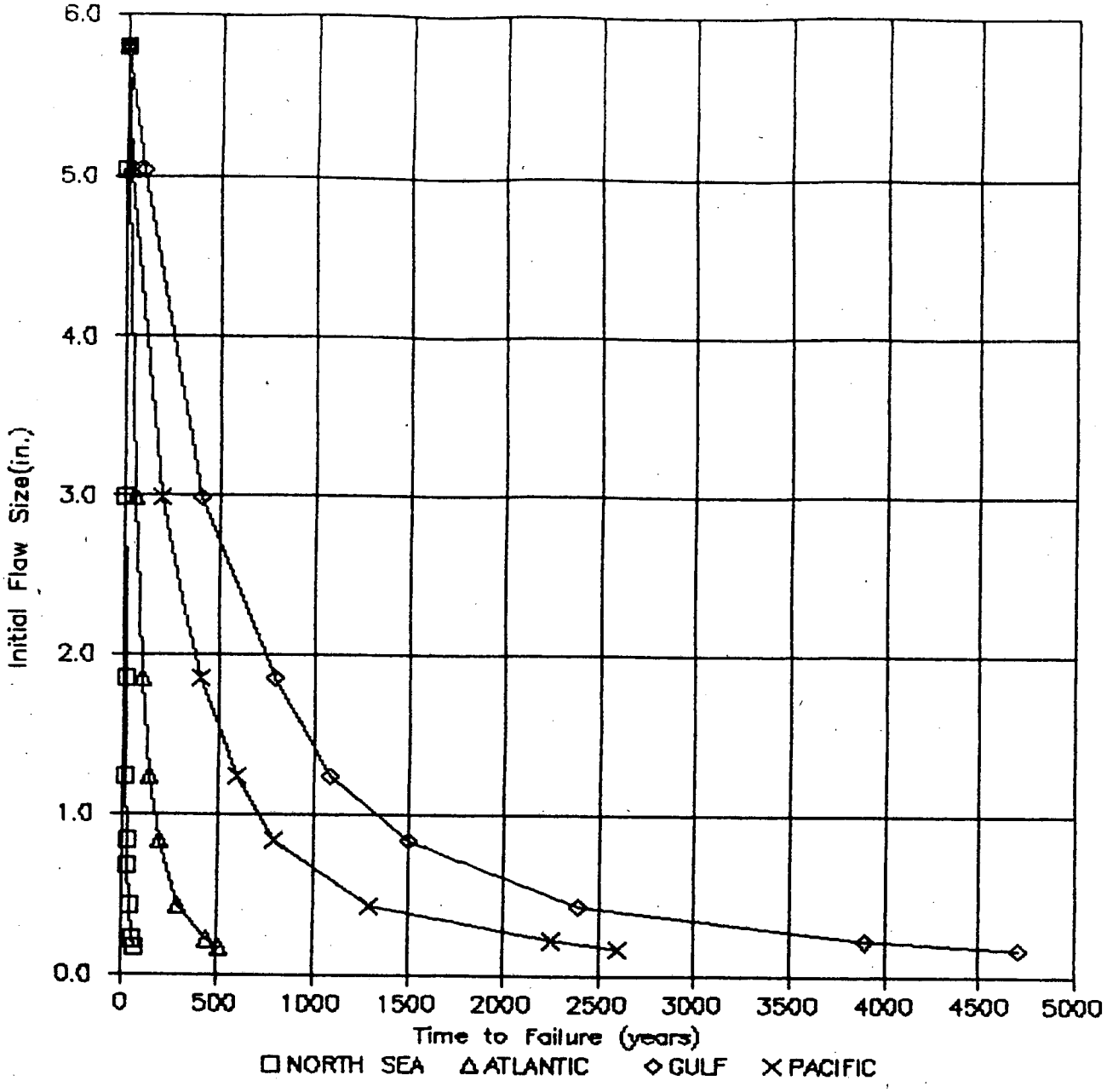


Figure 2.5a - Initial Flaw Size versus Time to Failure. A Comparison of Platform Environments (Thick Walled).
Material Environment: Free Corrosion
Platform Environment: Dillingham
Tendon Cross Section: Last Box Thread
Stress Intensity Model: Semi-Elliptical Crack

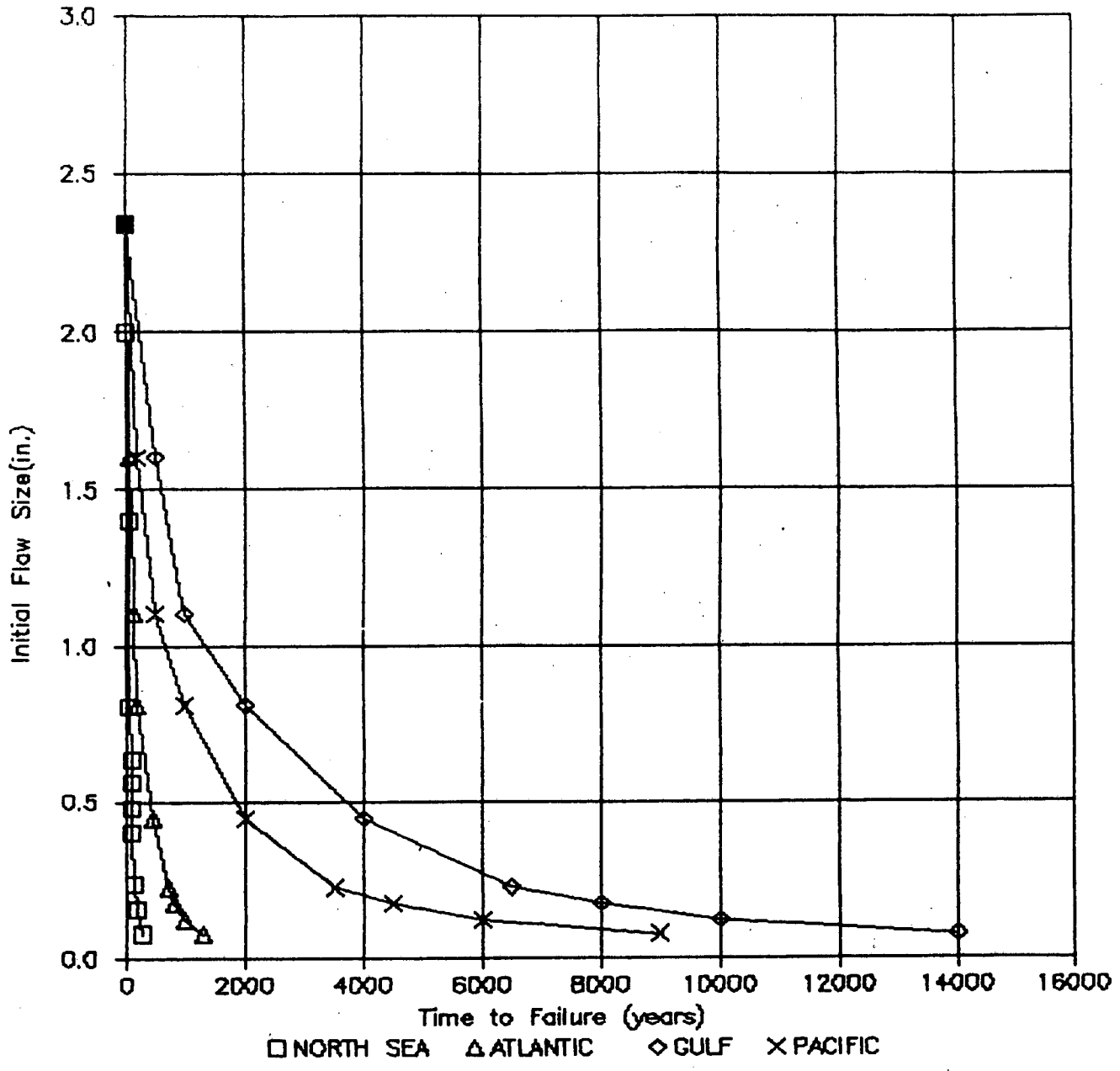


Figure 2.5b - Initial Flaw Size versus Time to Failure. A Comparison of Platform Environments (Thin Walled).
Material Environment: Free Corrosion
Platform Environment: Dillingham
Tendon Cross Section: Last Box Thread
Stress Intensity Model: Semi-Elliptial Crack

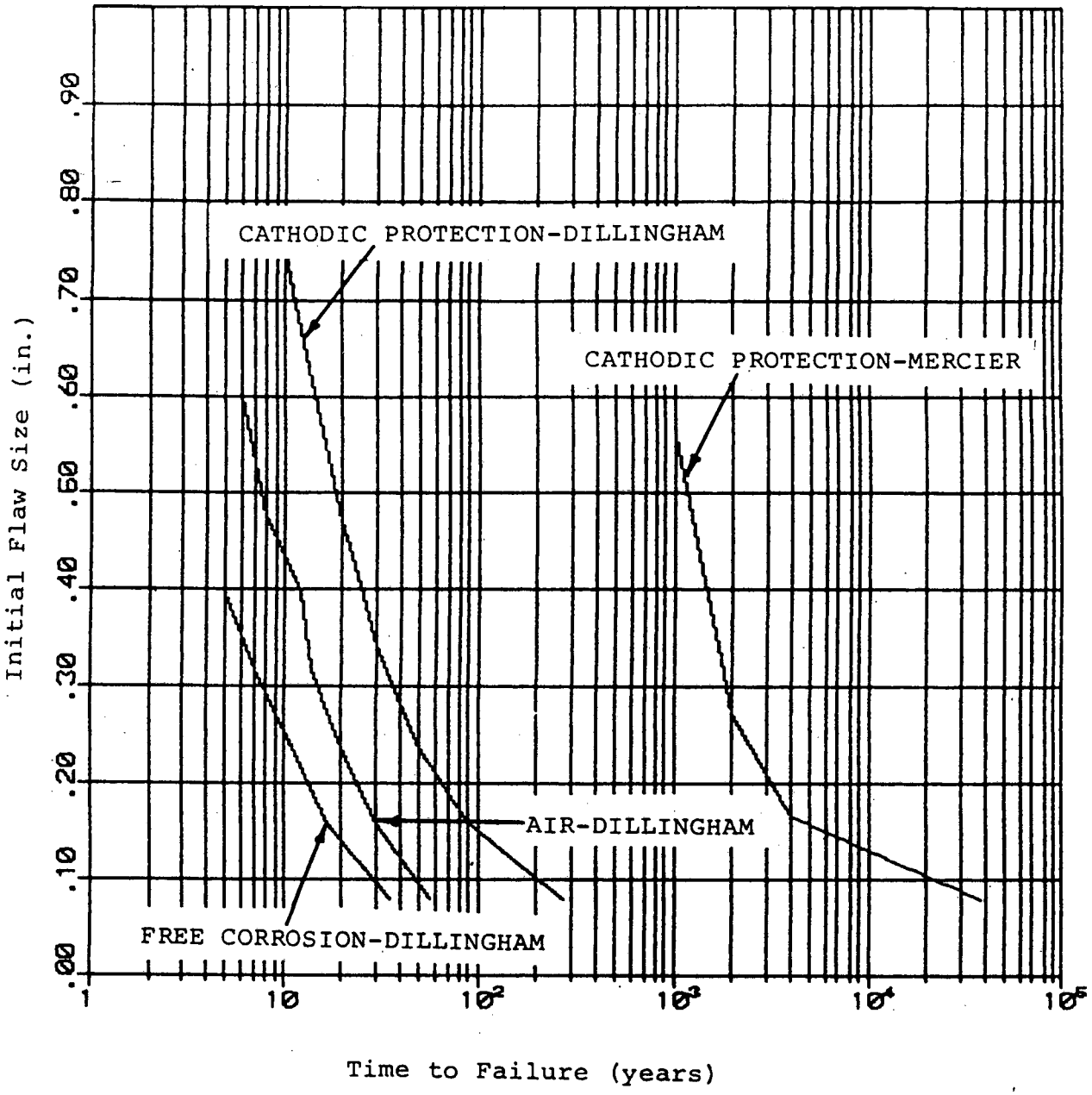


Figure 2.6 - Initial Flaw Size versus Time to Failure. A Comparison of Material Environments (Thin Walled).
Platform Environment: North Sea
Platform RAO: Dillingham/Mercier
Tendon Cross Section: Pipe
Stress Intensity Model: Semi-Elliptical Crack

Figure 2.7
(Last Pin Thread, Thin Walled Connector)

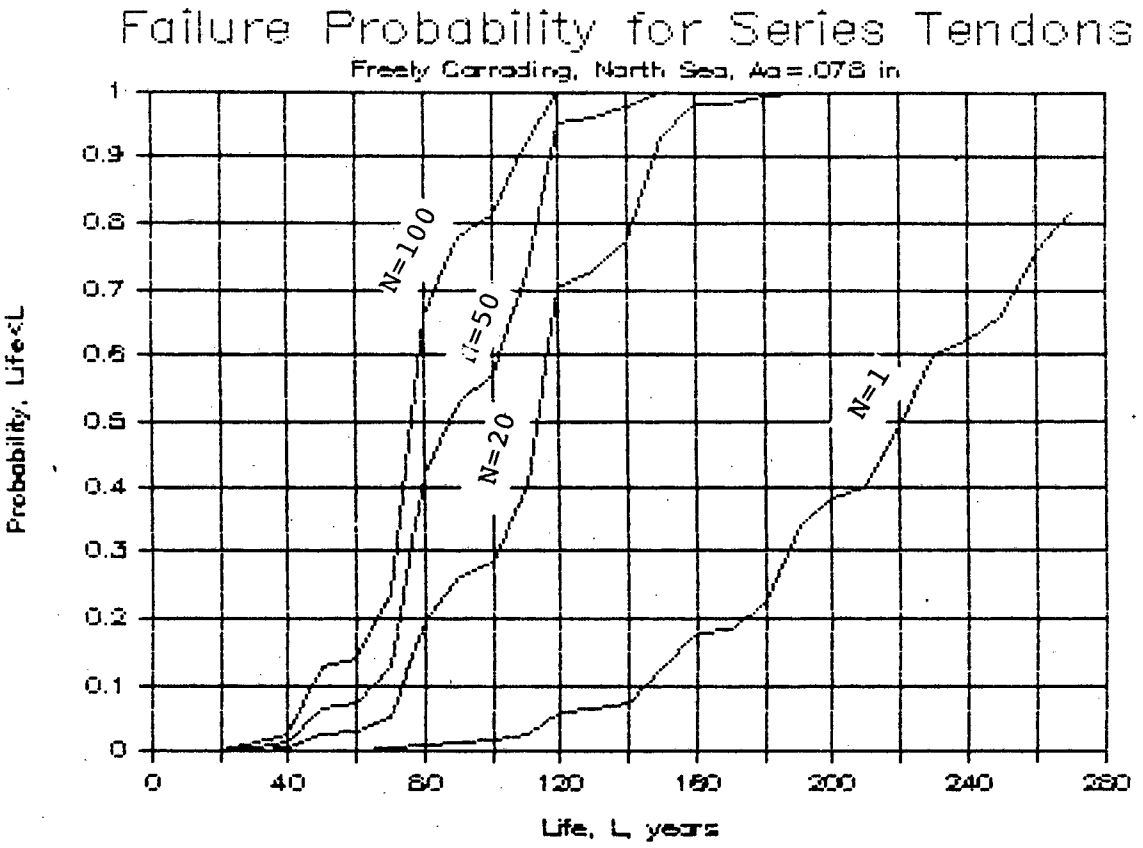

# 3.0 Tendon Fatigue Loads

## 3.1 Environmental Data

In order to determine fatigue loading of the TLP tendons, it is necessary to establish the environment to which the TLP is exposed. The significant environmental factors are wave height and period. Wind and current velocity only play a small part in fatigue although they should be considered in deriving maximum and minimum loads as well as other design criteria.

### 3.1.1 Regions of Study and Source of Data

Four regions used in this study are the offshore Central California area, Green Canyon in the Gulf of Mexico, Atlantic Ocean off the east coast, and the North Sea. These regions show promise to the oil industry and are potential TLP sites due to their large water depth (TLP's are economical and stable in deep water - 1500' and greater). Figure 3.1a-d shows maps of the four regions which indicate recent lease sites. Sources of environmental data for each of these locations is described below:

**North Sea**

1) Spectral Ocean Wave Model (SOWM) data produced by the National Climatic Center (NCC) has been processed by the NCC to give significant wave height versus frequency of occurance based on 20 years (29,000 records) of hindcast data. [NOCD]

2) [Webster] has published North Sea fatigue loads for two cases: The Hutton platform and a three column tethered buoyant platform.

**Atlantic Ocean**

1) SOWM data produced by NCC, required processing to achieve relevant environmental data (described below).

2) Hurricane data for Gulf is used [API RP2T].

**Gulf of Mexico**

1) SOWM data produced by NCC: required processing to achieve relevant environmental data (described below).

2) Data from [API RP2T] contains statistical data consisting of frequency of occurance of significant wave height versus wave period for both normal conditions and hurricane conditions.

Pacific Ocean

1) SOWM data produced by NCC: required processing to achieve relevant environmental data (described below).

See table 3.1a-f for the environomental data relevant to the computation of fatigue loads.

### 3.1.2 The SOWM Model

The SOWM uses barometric pressure readings to derive a wind velocity map and corresponding wave spectrum map. The model is updated every six hours using a new set of barametric pressure readings. SOWM data for a particular area consists of a 12 or 20 year record with a wave energy spectrum and wind velocity specified every six hours. The SOWM model does not account for hurricanes so storm data from other sources is used. A Fortran 77 program (SOWM.FOR) has been developed to process this data. The energy spectrum is a 12 by 15 element array representing variance in $ft^2$. There are 12 wave approach angles and 15 frequencies. SOWM.FOR output consists of two files. The first is a chronological record (six hour increments) of significant wave height ($H_s$), mean period ($T_m$), zero crossing period ($T_z$), and wind speed. The second is statistical data of $H_s$ versus frequency of peak energy, $H_s$ versus direction of maximum energy, $H_s$ versus wind speed, wind direction versus wind speed and mean energy versus $H_s$. Tables of the statistical data are presented in Appendix A.

The values of $H_s$, $T_m$, and $T_z$ were calculated with the formulas:

$$H_s = 4(M_o)^{1/2}$$
$$T_m = M_o/M_1$$
$$T_z = (M_o/M_2)^{1/2}$$

where $M_o$, $M_1$, and $M_2$ are the zeroth, first, and second spectral moments defined as:

$$M_n = \int_0^\infty f_i^n E_{ij} d\omega$$

$E_{ij}$ corresponds to the energy variance in [$ft^2$] given by the SOWM model.

## 3.2 Fatigue Loads

### 3.2.1 Method for Computation of Fatigue Loads

A fatigue load spectrum is derived from the statistical frequency of occurance data on significant wave height and period (see table 3.1 for this data). The number of waves/year at a particular wave height and period is determined from the frequency of occurance data. To compute the load spectrum $S_{Load}(f)$ the Bretshnieder wave spectrum $S_{Wave}(f)$ is multiplied by the square of the tendon tension response amplitude operator [RAO(f)]. This is integrated numerically over f ($0 < f < \infty$) to obtain the first moment of the load spectrum. The load probability distribution function is then known and the number of cycles per year within a load range can be determined. See Figure 3.2 for an outline of the above procedure.

### 3.2.2 Tendon Tension RAO

The RAO will vary as a function of platform geometry, water depth, and wave characteristics. In this report, nonlinear RAO variation with wave height is ignored in that RAO's as computed by various authors are used to compute tendon tension as a linear function of wave height. The non-linear effects have been shown to be small. In computer time domain similiations [Halkyard and Liu] the RAO at large wave heights has been shown to yield RAO's close to the linear RAO's. The RAO's at large wave heights can be less than at small wave heights due to the increased importance of drag and the phase relation between drag and inertia.

Some of the RAO's presented here were derived experimentally from random sea state spectra. Tan et al determined RAO's experimentally for 2 random sea state spectra and for regular waves of various heights. Data from the three experiments indicate that RAO has only a small dependence on wave spectrum and wave height. Thus the assumption that tendon tension will be linearly dependent on wave height is reasonable.

Five RAO's have been selected to study the effect of geometry on tendon fatigue loads produced by waves [Chou, et al], [Dillingham], [Mercier, et al], [Paulling, et al], [Tan, et al]. The RAO's are plotted in Figure 3.3.

In the range $3 < T < 5$ seconds authors seldom specify RAO's. In the $0 < T < 3$ second range wave energy is small and can be neglected

(RAO's are also small). At the heave and pitch natural period, significant tensions could occur due to resonance. We estimate an RAO of 290 kips/ft for a typical platform at an assumed natural period of 3 seconds (see calculation sheets, Appendix ). In a narrow bandwidth about the natural period an average RAO of 15 kips/ft is found. In the range outside of this bandwidth the RAO is assumed to vary from the author specified RAO at T=5 seconds to zero at the period equal to 3 plus the bandwidth/2.

Platform geometries specified by the five authors are summarized in Table 3.2. Information is not given by [Chou et al] and [Dillingham]. Qualitatively, some aspects of the RAO curves may be described from an examination of platform geometry. At large wave periods the tension RAO should approach the tidal tension RAO. For the platform Paulling analyzes the tidal tension is very small because this TLP has very thin columns which act primarily as support members. Thus the RAO at 24 seconds is nearly zero. The [Mercier] RAO for the Hutton Platform is large at large periods. This is due to the four large corner columns and two center columns which give rise to large buoyancy induced heave forces. The [Dillingham] RAO is extremely large at large periods indicating large columns or other members breaking the free surface. The various dips and peaks that the RAO's exhibit is produced by complicated wave induced water velocity and accelleration distributions over the columns and pontoons. At small periods the RAO has a spike at the TLP pitch natural period and is effectively zero at smaller periods. Large columns also introduce complicated wave diffraction effects which effect the RAO's for wave periods less than approximately 8 seconds.

### 3.2.3 Computed Fatigue Loads

Environments and platforms for which fatigue loads were derived are:

a) North Sea - SOWM Data: Mercier et al, (Hutton TLP), Chou et al.

b) Atlantic Ocean - SOWM Data: Mercier et al, (Hutton TLP), Chou et al.

c) Gulf of Mexico -

1) SOWM Data: Chou et al, Tan et al, Paulling et al, Dillingham, Mercier et al.

2) API RP2T: Chou et al.

3) API RP2T Hurricane Data: Chou et al, Tan et al, Paulling et al, Dillingham, Mercier et al.

d) Pacific West Coast - SOWM Data: Chou et al.

Tables of these ten cases as well as the two [Webster] data are given in Table 3.3a-1. Due to the lack of hurricane contributions in the SOWM data the fatigue load contributions due to hurricanes for the Gulf and Atlantic are given by the API RP2T Gulf Hurricane data. Plots of the table information are contained in figures 3.4a-c. Figure 3.4a shows a plot of the fatigue loads that the platform based on Chou's RAO would experience in the four environments. The increase in load from the mild Pacific environments to the most severe North Sea environment is evident. The API RP2T curve is the same as the SOWM curve, which implies that the two sets of environmental data are equivalent. The two data sets are probably based on different locations within the Gulf which could account for any discrepancy.

Figure 3.4b shows loads for the Gulf of Mexico based on the five RAO's. The number of cycles at each load amplitude differs significantly between each RAO. Thus fatigue and tendon size may be strongly dependent on platform geometry.

Figure 3.4c compares the Webster load data with load data derived from the SOWM data for the Atlantic and North Sea and the Mercier-Hutton RAO curve. The Webster-Hutton curve and the North Sea-Mercier curve are fairly close. The differences may be attributed to 1) a possible change in design of the Hutton platform between the time of the Webster study and the Mercier et al study, and 2) the variation in climate between the location the SOWM data represents and the location for which the Webster-Hutton loads were determined. The Atlantic-Mercier loads are more benign than the North Sea loads and the Webster-tether loads are the least of the four. The Webster-tether loads are based on a three column TLP which may explain their mildness since the tendon tension RAO's of most three column TLP are less than four column TLP's. The Webster-Hutton loads are based primarily on numerical calculations and some experimental data for a preliminary Hutton design

which has since been changed. The TBP loads were derived for a three leg platform from experiments simulating the Northern North Sea environment.

### 3.2.4 Pretension and Maximum Design Loads

Pretension was calculated from the formula

$$P_T = T_T + T_L + T_m + T_s + T_w + T_f + T_r$$

where

| | | |
|---|---|---|
| $T_T$ | = | maximum tidal load - 100 Kips |
| $T_L$ | = | weight of tendons - 513 thick connector<br>533 thin connector |
| $T_m$ | = | effect of wind/current moment - 100 Kips |
| $T_s$ | = | setdown - 0 |
| $T_w$ | = | maximum storm wave - variable of environment |
| $T_f$ | = | foundation mispositioning - 50 Kips |
| $T_r$ | = | springing effect - 50 Kips |

Generic values used are listed to the right.

The fatigue loads induced by the maximum storm wave was determined from the 100 year design wave in a manner analogous to that outlined in section 3.2.1. The primary design wave load was then taken as the maximum load whose probability of occurance was 100% during the 100 year storm.

Maximum design load was calculated from the equation:

$$T_{max} = P_T + T_t + T_m + T_s + T_w + T_f + T_r$$

Here $T_s$ = 50 Kips, other values remain the same.

Table 3.4 contains pretension and maximum design loads for the various environments and platforms.

### 3.2.5 Probabilistic Hurricane Fatigue Loads

Hindcast hurricane data has been produced in a paper by [Bea]. In particular, extreme value probabilities of expected maximum wave heights and probability of number of severe hurricanes in a year were used to derive fatigue loads in a manner similar to that outlined in Section 3.2.1. The peak wave period is assumed to equal 14 seconds and

the following relationship is used to relate maximum wave height $H_{max}$ to $H_S$:

$$H_S = 1.9\ H_{max}$$

An equation describing $H_S$ as a random variable was derived from figure 8 of Bea's paper and is

$$H_S = 21.57\ RND + 22.1 \qquad \text{(feet)}$$

where RND is a random number ranging from 0 to 1. The probability (P) of number of severe hurricanes (N) in a year was taken from figure 3 of Bea's paper and is approximated by the following table:

| P | N |
|---|---|
| 55% | 0 |
| 26% | 1 |
| 14% | 2 |
| 5% | 3 |

## 3.3 References

American Petroleum Institute, "Recommended Practice for Planning, Designing, and Constructing Tension Leg Platforms", API-RP2T (Draft).

Chou, Frank, S.F., Ghosh, Susobhan, Huang, Edward W., "Conceptual Design Process of a Tension Leg Platform", Society of Naval Architects and Marine Engineers, Annual Meeting, New York, N.Y., November 9-12, 1983.

Dillingham, Jeffrey T., "Recent Experience in Model-Scale Simulation of Tension Leg Platforms", Marine Technology, Vol.21, No.2, April 1984, pp.186-200.

Halkyard, J.E., Liu, Shin Lin, "Coupled vs. Uncoupled Analysis for the Determination of TLP Tendon Loads".

Mercier, John Allen, Leverette, Steven J., Bliault, Allen L., "Evaluation of Hutton TLP Response to Environmental Loads", OTC 4429, Vol.4, 1982.

Paulling, J.R., Horton, E.E., "Analysis of the Tension Leg Stable Platform", OTC 1263, 1970.

Tan, S. Gie, deBoom, W.C., "The Wave Induced Motions of a Tension Leg Platform in Deep Water", OTC 4074, 1981.

NOCD, "U.S. Navy Hindcast Spectral Ocean Wave Model Climatic Atlas: North Atlantic Ocean", Naval Oceanography Command Detachment, Asheville, N.C., Navair 50-1C-538, October 1983.

Oil and Gas Journal, pg. 96, May 2, 1983.

Ocean Industry, pg. 37, 39, and 47, November 1984.

Webster, S.E., Review of Information on The Fatigue Tethering Systems for Tethered Platforms, BSC Research Services.

TABLE 3.1A

DATA FOR GRID POINT 212(GULF OF MEXICO). BASED ON 26540 RECORDS-20 YEARS
LATITUDE=25.6; LONGITUDE=92.4.

PEAK FREQUENCY VERSUS H-SIGNIFICANT - FREQUENCY OF OCCURANCE

| FREQ | PERIOD | H-SIGNIFICANT [FEET] | | | | | | | | | | | |
|---|---|---|---|---|---|---|---|---|---|---|---|---|---|
| | | 0-1 | 1-3 | 3-5 | 5-7 | 7-9 | 9-11 | 11-13 | 13-18 | 18-25 | 25-35 | 35-45 | 45-60 |
| .308 | 3.25 | .644 | 2.961 | .000 | .000 | .000 | .000 | .000 | .000 | .000 | .000 | .000 | .000 |
| .208 | 4.81 | .000 | .844 | 1.876 | .000 | .000 | .000 | .000 | .000 | .000 | .000 | .000 | .000 |
| .158 | 6.33 | 3.591 | 17.128 | 12.746 | 4.404 | .053 | .000 | .000 | .000 | .000 | .000 | .000 | .000 |
| .133 | 7.52 | .904 | 5.150 | 5.147 | 6.446 | 2.490 | .053 | .000 | .000 | .000 | .000 | .000 | .000 |
| .117 | 8.55 | 1.533 | 7.328 | 4.740 | 3.278 | 3.086 | 1.413 | .173 | .004 | .000 | .000 | .000 | .000 |
| .103 | 9.71 | .452 | 2.400 | 1.567 | 1.074 | 1.006 | 1.243 | 1.100 | .373 | .000 | .000 | .000 | .000 |
| .092 | 10.87 | .147 | .550 | .426 | .294 | .117 | .124 | .173 | .588 | .026 | .000 | .000 | .000 |
| .081 | 12.35 | .038 | .241 | .147 | .064 | .109 | .034 | .030 | .154 | .166 | .004 | .000 | .000 |
| .072 | 13.89 | .113 | .203 | .064 | .030 | .004 | .019 | .008 | .000 | .026 | .000 | .000 | .000 |
| .067 | 14.93 | .015 | .185 | .068 | .011 | .000 | .000 | .004 | .004 | .004 | .008 | .000 | .000 |
| .061 | 16.39 | .132 | .347 | .075 | .011 | .008 | .015 | .004 | .000 | .000 | .000 | .000 | .000 |
| .056 | 17.86 | .000 | .000 | .000 | .000 | .000 | .000 | .000 | .000 | .000 | .000 | .000 | .000 |
| .050 | 20.00 | .000 | .000 | .000 | .000 | .000 | .000 | .000 | .000 | .000 | .000 | .000 | .000 |
| .044 | 22.73 | .000 | .000 | .000 | .000 | .000 | .000 | .000 | .000 | .000 | .000 | .000 | .000 |
| .039 | 25.64 | .000 | .000 | .000 | .000 | .000 | .000 | .000 | .000 | .000 | .000 | .000 | .000 |

TABLE 3.1B

DATA FOR GRID POINT 260(ATLANTIC-EAST COAST). BASED ON 27000 RECORDS-
20 YEARS. LATITUDE=34.5; LONGITUDE=74.9.

PEAK FREQUENCY VERSUS H-SIGNIFICANT - FREQUENCY OF OCCURANCE

| FREQ | PERIOD | H-SIGNIFICANT [FEET] | | | | | | | | | | | |
|---|---|---|---|---|---|---|---|---|---|---|---|---|---|
| | | 0-1 | 1-3 | 3-5 | 5-7 | 7-9 | 9-11 | 11-13 | 13-18 | 18-25 | 25-35 | 35-45 | 45-60 |
| .308 | 3.25 | .54 | 3.51 | .00 | .00 | .00 | .00 | .00 | .00 | .00 | .00 | .00 | .00 |
| .208 | 4.81 | .00 | 1.54 | 3.80 | .00 | .00 | .00 | .00 | .00 | .00 | .00 | .00 | .00 |
| .158 | 6.33 | 1.88 | 8.02 | 6.96 | 3.93 | .11 | .00 | .00 | .00 | .00 | .00 | .00 | .00 |
| .133 | 7.52 | 1.21 | 4.82 | 2.56 | 3.72 | 2.02 | .10 | .00 | .00 | .00 | .00 | .00 | .00 |
| .117 | 8.55 | 1.14 | 4.80 | 2.56 | 2.26 | 2.94 | 2.12 | .50 | .03 | .00 | .00 | .00 | .00 |
| .103 | 9.71 | 1.14 | 4.85 | 1.97 | 1.13 | .93 | 1.25 | .98 | .50 | .00 | .00 | .00 | .00 |
| .092 | 10.87 | .62 | 3.61 | 1.76 | .87 | .56 | .37 | .42 | .97 | .04 | .00 | .00 | .00 |
| .081 | 12.35 | .46 | 2.77 | 1.80 | .87 | .56 | .37 | .27 | .40 | .30 | .00 | .00 | .00 |
| .072 | 13.89 | .24 | 1.44 | .88 | .65 | .28 | .15 | .09 | .08 | .10 | .03 | .00 | .00 |
| .067 | 14.93 | .20 | 1.23 | .67 | .42 | .29 | .14 | .09 | .14 | .11 | .04 | .00 | .00 |
| .061 | 16.39 | .12 | .39 | .37 | .23 | .16 | .09 | .04 | .06 | .07 | .09 | .01 | .00 |
| .056 | 17.86 | .00 | .03 | .05 | .01 | .01 | .02 | .01 | .00 | .02 | .03 | .00 | .00 |
| .050 | 20.00 | .00 | .01 | .01 | .00 | .00 | .00 | .00 | .00 | .01 | .01 | .00 | .00 |
| .044 | 22.73 | .00 | .01 | .00 | .00 | .00 | .00 | .00 | .00 | .00 | .00 | .00 | .00 |
| .039 | 25.64 | .00 | .00 | .00 | .00 | .00 | .00 | .00 | .00 | .00 | .00 | .00 | .00 |

## TABLE 3.1C

DATA FOR GRID POINT 175(PACIFIC-WEST COAST). BASED ON 16070 RECORDS-20 YEARS
LATITUDE=32.8; LONGITUDE=119.5

PEAK FREQUENCY VERSUS H-SIGNIFICANT - FREQUENCY OF OCCURANCE

| FREQ | PERIOD | H-SIGNIFICANT [FEET] | | | | | | | | | | | |
|---|---|---|---|---|---|---|---|---|---|---|---|---|---|
| | | 0-1 | 1-3 | 3-5 | 5-7 | 7-9 | 9-11 | 11-13 | 13-18 | 18-25 | 25-35 | 35-45 | 45-60 |
| .308 | 3.25 | .959 | 3.953 | .000 | .000 | .000 | .000 | .000 | .000 | .000 | .000 | .000 | .000 |
| .208 | 4.81 | .000 | 3.000 | 5.845 | .000 | .000 | .000 | .000 | .000 | .000 | .000 | .000 | .000 |
| .158 | 6.33 | .622 | 4.177 | 8.273 | 4.893 | .081 | .000 | .000 | .000 | .000 | .000 | .000 | .000 |
| .133 | 7.52 | .430 | 2.714 | 3.019 | 4.413 | 2.359 | .044 | .000 | .000 | .000 | .000 | .000 | .000 |
| .117 | 8.55 | .342 | 2.235 | 1.849 | 1.500 | 2.608 | 1.401 | .162 | .000 | .000 | .000 | .000 | .000 |
| .103 | 9.71 | .510 | 2.944 | 2.017 | 1.338 | 1.120 | 1.127 | .822 | .162 | .000 | .000 | .000 | .000 |
| .092 | 10.87 | .293 | 2.011 | 1.226 | .859 | .548 | .311 | .149 | .243 | .000 | .000 | .000 | .000 |
| .081 | 12.35 | .454 | 2.135 | 1.345 | .691 | .479 | .249 | .106 | .143 | .006 | .000 | .000 | .000 |
| .072 | 13.89 | .380 | 2.179 | 1.357 | .909 | .305 | .143 | .056 | .068 | .000 | .000 | .000 | .000 |
| .067 | 14.93 | .560 | 2.378 | 1.550 | .784 | .342 | .137 | .081 | .062 | .000 | .000 | .000 | .000 |
| .061 | 16.39 | 1.226 | 5.235 | 2.340 | 1.208 | .367 | .230 | .100 | .056 | .000 | .000 | .000 | .000 |
| .056 | 17.86 | .012 | .243 | .174 | .093 | .075 | .056 | .025 | .019 | .006 | .000 | .000 | .000 |
| .050 | 20.00 | .012 | .075 | .112 | .068 | .025 | .044 | .019 | .031 | .006 | .000 | .000 | .000 |
| .044 | 22.73 | .000 | .019 | .025 | .006 | .019 | .019 | .006 | .000 | .006 | .000 | .000 | .000 |
| .039 | 25.64 | .006 | .037 | .006 | .006 | .012 | .000 | .000 | .000 | .000 | .000 | .000 | .000 |

## TABLE 3.1D

DATA FOR GRID POINT 124(NORTH SEA). BASED ON 29000 RECORDS -20 YEARS.
LATITUDE=57; LONGITUDE=5EAST. (FROM N.O.C.D.)

PEAK PERIOD VERSUS H-SIGNIFICANT - FREQUENCY OF OCCURANCE

| FREQ | PERIOD | H-SIGNIFICANT [FEET] | | | | | | | | | | | |
|---|---|---|---|---|---|---|---|---|---|---|---|---|---|
| | | 0-3 | 3-6 | 6-9 | 9-12 | 12-16 | 16-20 | 20-24 | 24-28 | 28-34 | 34-40 | 40-48 | 48-55 |
| .333 | 3 | 6 | 0 | 0 | 0 | 0 | 0 | 0 | 0 | 0 | 0 | 0 | 0 |
| .176 | 5.68 | 2 | 4.8 | 0 | 0 | 0 | 0 | 0 | 0 | 0 | 0 | 0 | 0 |
| .147 | 6.82 | 4 | 8 | 1.8 | 0 | 0 | 0 | 0 | 0 | 0 | 0 | 0 | 0 |
| .117 | 8.52 | 3 | 2.8 | 5.8 | .4 | 0 | 0 | 0 | 0 | 0 | 0 | 0 | 0 |
| .104 | 9.66 | 3.2 | 2.8 | 3.8 | 3 | 1 | 0 | 0 | 0 | 0 | 0 | 0 | 0 |
| .091 | 11.0 | 3.2 | 2 | 2.8 | 4 | 2 | .1 | 0 | 0 | 0 | 0 | 0 | 0 |
| .080 | 12.5 | 2.2 | 2 | 1 | 1.93 | 2 | 1 | .16 | 0 | 0 | 0 | 0 | 0 |
| .073 | 13.63 | 2.2 | 2 | 1 | .4 | 1.12 | 1.4 | 1.1 | .1 | .07 | 0 | 0 | 0 |
| .063 | 15.9 | 1 | 1 | 1 | .3 | .4 | .2 | .1 | .2 | .1 | 0 | 0 | 0 |
| .059 | 17.0 | 2 | 1 | 1 | .8 | .3 | .1 | .1 | .2 | .1 | .043 | 0 | 0 |
| .055 | 18.18 | .9 | .8 | .9 | .3 | .2 | .05 | .1 | .1 | .1 | .043 | .01 | 0 |
| .049 | 20.4 | 0 | .1 | .1 | .1 | .15 | .05 | 0 | 0 | .01 | 0 | 0 | 0 |
| .044 | 22.7 | .1 | .1 | 0 | .1 | .15 | .05 | 0 | 0 | 0 | 0 | .004 | .014 |

TABLE 3.1E

DATA FROM API RP2T (DRAFT) (GULF OF MEXICO).
LONG TERM STATISTICS.

SIGNIFICANT PERIOD VERSUS H-SIGNIFICANT - FREQUENCY OF OCCURANCE

| FREQ | PERIOD | H-SIGNIFICANT (FEET) | | | | | | | | | | | | | |
|---|---|---|---|---|---|---|---|---|---|---|---|---|---|---|---|
| | | 1 | 2 | 4 | 6 | 8 | 10 | 12 | 14 | 16 | 18 | 20 | 25 | 30 | 30+ |
| .167 | 6 | 12 | 22.4 | 21.6 | 7.4 | 1.75 | 0.7 | 0.20 | 0.1 | 0.05 | 0.01 | 0 | 0 | 0 | 0 |
| .125 | 8 | 1.4 | 2.5 | 7.2 | 7.6 | 3.05 | 1.3 | 0.40 | 0.18 | 0.10 | 0.01 | 0 | 0 | 0 | 0 |
| .1 | 10 | 0.2 | 0.6 | 1.0 | 1.7 | 1.35 | 0.8 | 0.30 | 0.20 | 0.10 | 0.02 | 0.01 | 0 | 0 | 0 |
| .083 | 12 | 0 | 0.6 | 0.33 | 0.3 | 0.4 | 0.3 | 0.20 | 0.10 | 0.10 | 0.06 | 0.03 | 0.01 | 0 | 0 |
| .071 | 14 | 0 | 0 | 0.2 | 0.1 | 0.1 | 0.1 | 0.05 | 0.05 | 0.05 | 0.05 | 0.03 | 0.02 | 0.01 | 0 |
| .071- | 14+ | 0 | 0 | 0 | 0.1 | 0.05 | 0.1 | 0.05 | 0.07 | 0.10 | 0.05 | 0.03 | 0.02 | 0.01 | 0 |

TABLE 3.1F

DATA FROM API RP2T (DRAFT) (GULF OF MEXICO).
HURRICANE STATISTICS

SIGNIFICANT PERIOD VERSUS H-SIGNIFICANT - FREQUENCY OF OCCURANCE

| FREQ | PERIOD | H-SIGNIFICANT (FEET) | | | | | | | | | | | | | |
|---|---|---|---|---|---|---|---|---|---|---|---|---|---|---|---|
| | | 1 | 2 | 4 | 6. | 8 | 10 | 12 | 14 | 16 | 18 | 20 | 25 | 30 | 30+ |
| .167 | 6 | 0 | 1 | 1 | 1 | 1 | 1 | 1 | 1 | 3 | 3 | 2 | 2 | 2 | 1 |
| .125 | 8 | 0 | 0 | 0 | 1 | 1 | 1 | 1 | 1 | 2 | 2 | 2 | 3 | 3 | 3 |
| .1 | 10 | 0 | 0 | 0 | 0 | 0 | 0 | 1 | 1 | 2 | 3 | 3 | 3 | 3 | 4 |
| .083 | 12 | 0 | 0 | 0 | 0 | 0 | 0 | 0 | 1 | 2 | 2 | 3 | 3 | 4 | 4 |
| .071 | 14 | 0 | 0 | 0 | 0 | 0 | 0 | 0 | 0 | 0 | 2 | 2 | 3 | 3 | 5 |
| .071- | 14+ | 0 | 0 | 0 | 0 | 0 | 0 | 0 | 0 | 0 | 0 | 0 | 0 | 3 | 3 |

Table 3.2

Platform Data for RAO's

| | [Chou] | [Dillingham] | [Mercier] | [Paulling] | [Tan] |
|---|---|---|---|---|---|
| Number of Columns | NA | NA | 6 | 3 | 4 |
| Column Diameter (ft.) | NA | NA | 58-corner<br>48-center | 3.1 | 55.4 |
| Column Spacing (ft.) | NA | NA | 256 | 196 | 283 |
| Column/Pontoon Volume Ratio | 2.5 | NA | 3.4 | 0.00124 | 1.44 |
| Total Displacement (tons) | NA | NA | 63,300 | 2574 | 54500 |
| Pitch Natural Period (sec.) | NA | NA | 2 | NA | 2.1 |
| Heave Natural Period (sec.) | NA | NA | 2 | NA | 2 |

NA - Not Applicable

**TABLE 3.3A**

NUMBER OF CYCLES AT LOAD AMPLITUDE PER YEAR BASED ON GULF OF MEXICO SOWM DATA AND CHOU'S RAO. HURRICANE DATA BASED ON API RP-2T AND CHOU'S RAO.

| LOAD AMPLITUDE (KIPS) | CYCLES SOWM | CYCLES HURRICANE |
|---|---|---|
| 0-25 | 6029665 | 457 |
| 25-50 | 254224 | 463 |
| 50-75 | 26086 | 287 |
| 75-125 | 3930 | 251 |
| 125-175 | 102 | 76 |
| 175-225 | 4.98 | 20 |
| 225-275 | 0.27 | 4.2 |
| 275-350 | 8E-3 | 0.74 |
| 350-450 | 1.1E-5 | 0.03 |
| 450-650 | 1.7E-10 | 2E-4 |

**TABLE 3.3B**

NUMBER OF CYCLES AT LOAD AMPLITUDE PER YEAR BASED ON GULF OF MEXICO SOWM DATA AND TAN et. al. RAO. HURRICANE DATA BASED ON API RP-2T AND TAN'S RAO.

| LOAD AMPLITUDE (KIPS) | CYCLES SOWM | CYCLES HURRICANE |
|---|---|---|
| 0-25 | 6078089 | 454 |
| 25-50 | 192716 | 400 |
| 50-75 | 31850 | 255 |
| 75-125 | 10136 | 270 |
| 125-175 | 978 | 111 |
| 175-225 | 116 | 45 |
| 225-275 | 13.3 | 17 |
| 275-350 | 1.9 | 7 |
| 350-450 | .06 | 1 |
| 450-650 | 2.2E-4 | 4E-2 |
| 650-850 | 3.8E-11 | 6E-6 |

**TABLE 3.3C**

NUMBER OF CYCLES AT LOAD AMPLITUDE PER YEAR BASED ON GULF OF MEXICO SOWM DATA AND PAULLING'S RAO. HURRICANE DATA BASED ON API RP-2T AND PAULLING'S RAO.

| LOAD AMPLITUDE (KIPS) | CYCLES SOWM | CYCLES HURRICANE |
|---|---|---|
| 0-25 | 6009961 | 456 |
| 25-50 | 268291 | 458 |
| 50-75 | 30232 | 290 |
| 75-125 | 5255 | 258 |
| 125-175 | 156 | 75 |
| 175-225 | 5.7 | 19 |
| 225-275 | .24 | 4 |
| 275-350 | 7E-3 | .6 |
| 350-450 | 1.1E-5 | 1.8E-2 |
| 450-650 | 2.1E-10 | 5E-5 |

**TABLE 3.3D**

NUMBER OF CYCLES AT LOAD AMPLITUDE PER YEAR BASED ON GULF OF MEXICO SOWM DATA AND DILLINGHAM'S RAO. HURRICANE DATA BASED ON API RP-2T AND DILINGHAM`S RAO.

| LOAD AMPLITUDE (KIPS) | CYCLES SOWM | CYCLES HURRICANE |
|---|---|---|
| 0-25 | 5562231 | 234 |
| 25-50 | 590595 | 288 |
| 50-75 | 112857 | 243 |
| 75-125 | 40623 | 317 |
| 125-175 | 5531 | 176 |
| 175-225 | 1326 | 102 |
| 225-275 | 440 | 63 |
| 275-350 | 199 | 56 |
| 350-450 | 68 | 39 |
| 450-650 | 28 | 31 |
| 650-850 | 2.5 | 9 |
| 850-1050 | 0.1 | 2.3 |
| 1050-1250 | 1.8E-3 | 0.5 |
| 1250-1450 | 1.3E-5 | 8.9E-2 |
| 1450-1650 | 4E-8 | 1E-2 |
| 1650-1850 | 6E-11 | 1.4E-3 |

**TABLE 3.3E**

NUMBER OF CYCLES AT LOAD AMPLITUDE PER YEAR BASED ON GULF OF MEXICO SOWM DATA AND MERCIER'S RAO. HURRICANE DATA BASED ON API RP-2T AND MERCIER'S RAO.

| LOAD AMPLITUDE (KIPS) | CYCLES SOWM | CYCLES HURRICANE |
|---|---|---|
| 0-25 | 4955956 | 145 |
| 25-50 | 981308 | 205 |
| 50-75 | 237352 | 207 |
| 75-125 | 110109 | 348 |
| 125-175 | 21599 | 238 |
| 175-225 | 5411 | 154 |
| 225-275 | 1495 | 99 |
| 275-350 | 547 | 85 |
| 350-450 | 112 | 51 |
| 450-650 | 14 | 25 |
| 650-850 | .2 | 2 |
| 850-1050 | 7E-4 | 9E-2 |
| 1050-1250 | 7.4E-7 | 2E-3 |
| 1250-1450 | 1.7E-10 | 1.6E-5 |
| 1450-1650 | 9.2E-15 | 6E-8 |

**TABLE 3.3F**

NUMBER OF CYCLES AT LOAD AMPLITUDE PER YEAR BASED ON ATLANTIC EAST COAST SOWM DATA AND CHOU'S RAO. HURRICANE DATA BASED ON API RP-2T AND CHOU'S RAO.

| LOAD AMPLITUDE (KIPS) | CYCLES SOWM | CYCLES HURRICANE |
|---|---|---|
| 0-25 | 5347247 | 457 |
| 25-50 | 325857 | 463 |
| 50-75 | 45468 | 287 |
| 75-125 | 10252 | 251 |
| 125-175 | 1063 | 76 |
| 175-225 | 197 | 20 |
| 225-275 | 34 | 4.2 |
| 275-350 | 6 | 0.74 |
| 350-450 | .28 | 0.03 |
| 450-650 | 2.1E-3 | 2E-4 |
| 650-850 | 3.6E-9 | 5E-10 |

**TABLE 3.3G**

NUMBER OF CYCLES AT LOAD AMPLITUDE PER YEAR BASED ON ATLANTIC EAST COAST SOWM DATA AND MERCIER'S RAO. HURRICANE DATA BASED ON API RP-2T AND MERCIER'S RAO.

| LOAD AMPLITUDE (KIPS) | CYCLES SOWM | CYCLES HURRICANE |
|---|---|---|
| 0-25 | 4262633 | 145 |
| 25-50 | 936261 | 205 |
| 50-75 | 296302 | 207 |
| 75-125 | 174142 | 348 |
| 125-175 | 41150 | 238 |
| 175-225 | 12314 | 154 |
| 225-275 | 4268 | 99 |
| 275-350 | 2139 | 85 |
| 350-450 | 727 | 51 |
| 450-650 | 183 | 25 |
| 650-850 | 6 | 2 |
| 850-1050 | .17 | 9E-2 |
| 1050-1250 | 3E-3 | 2E-3 |
| 1250-1450 | 2.9E-5 | 1.6E-5 |
| 1450-1650 | 1.1E-7 | 6E-8 |

**TABLE 3.3H**

NUMBER OF CYCLES AT LOAD AMPLITUDE PER YEAR BASED ON ATLANTIC EAST COAST SOWM DATA AND DILLINGHAM'S RAO. HURRICANE DATA BASED ON API RP-2T AND DILINGHAM`S RAO.

| LOAD AMPLITUDE (KIPS) | CYCLES SOWM | CYCLES HURRICANE |
|---|---|---|
| 0-25 | 4763187 | 234 |
| 25-50 | 657787 | 288 |
| 50-75 | 183399 | 243 |
| 75-125 | 90826 | 317 |
| 125-175 | 19100 | 176 |
| 175-225 | 6800 | 102 |
| 225-275 | 3285 | 63 |
| 275-350 | 2510 | 56 |
| 350-450 | 1610 | 39 |
| 450-650 | 1148 | 31 |
| 650-850 | 260 | 9 |
| 850-1050 | 50 | 2.3 |
| 1050-1250 | 8 | 0.5 |
| 1250-1450 | 1.1 | 8.9E-2 |
| 1450-1650 | .12 | 1E-2 |
| 1650-1850 | 1E-2 | 1.4E-3 |
| 1850-2050 | 6E-4 | 1E-6 |

**TABLE 3.3I**

NUMBER OF CYCLES AT LOAD AMPLITUDE PER YEAR BASED ON NORTH SEA SOWM DATA AND CHOU'S RAO.

| LOAD AMPLITUDE (KIPS) | CYCLES SOWM |
|---|---|
| 0-25 | 4504890 |
| 25-50 | 578716 |
| 50-75 | 119630 |
| 75-125 | 39169 |
| 125-175 | 5324 |
| 175-225 | 1211 |
| 225-275 | 333 |
| 275-350 | 135 |
| 350-450 | 49 |
| 450-650 | 20 |
| 650-850 | 1 |
| 850-1050 | 1.9E-2 |
| 1050-1250 | 1.2E-4 |

**TABLE 3.3J**

NUMBER OF CYCLES AT LOAD AMPLITUDE PER YEAR BASED ON NORTH SEA SOWM DATA AND MERCIER'S RAO.

| LOAD AMPLITUDE (KIPS) | CYCLES SOWM |
|---|---|
| 0-25 | 3247250 |
| 25-50 | 987284 |
| 50-75 | 447802 |
| 75-125 | 368884 |
| 125-175 | 122654 |
| 175-225 | 44751 |
| 225-275 | 17601 |
| 275-350 | 9240 |
| 350-450 | 3072 |
| 450-650 | 850 |
| 650-850 | 73 |
| 850-1050 | 12 |
| 1050-1250 | 2 |
| 1250-1450 | .3 |
| 1450-1650 | .03 |
| 1650-1850 | 2E-3 |
| 1850-2050 | 1E-4 |

## TABLE 3.3K

NUMBER OF CYCLES AT LOAD AMPLITUDE PER YEAR BASED ON NORTH SEA SOWM DATA AND DILLINGHAM'S RAO.

| LOAD AMPLITUDE (KIPS) | CYCLES SOWM |
|---|---|
| 0-25 | 3677139 |
| 25-50 | 813545 |
| 50-75 | 329631 |
| 75-125 | 245885 |
| 125-175 | 88596 |
| 175-225 | 41026 |
| 225-275 | 20873 |
| 275-350 | 15202 |
| 350-450 | 8918 |
| 450-650 | 6330 |
| 650-850 | 1645 |
| 850-1050 | 450 |
| 1050-1250 | 138 |
| 1250-1450 | 50 |
| 1450-1650 | 23 |
| 1650-1850 | 12 |
| 1850-2050 | 6 |
| 2050-3000 | 5 |

## TABLE 3.3L

NUMBER OF CYCLES AT LOAD AMPLITUDE PER YEAR BASED ON GULF OF MEXICO API RP-2T DATA AND CHOU'S RAO. HURRICANE DATA BASED ON API RP-2T AND CHOU'S RAO.

| LOAD AMPLITUDE (KIPS) | CYCLES API RP-2T | CYCLES HURRICANE |
|---|---|---|
| 0-25 | 6003915 | 457 |
| 25-50 | 229311 | 463 |
| 50-75 | 21762 | 287 |
| 75-125 | 4043 | 251 |
| 125-175 | 222 | 76 |
| 175-225 | 21 | 20 |
| 225-275 | 1.8 | 4.2 |
| 275-350 | 0.1 | 0.74 |
| 350-450 | 8E-4 | 0.03 |
| 450-650 | 2E-7 | 2E-4 |

## TABLE 3.3M

NUMBER OF CYCLES AT LOAD AMPLITUDE PER YEAR FOR HUTTON PLATFORM IN NORTH SEA [WEBSTER].

| LOAD AMPLITUDE (KIPS) | CYCLES SOWM |
|---|---|
| 21 | 2295000 |
| 60 | 1495000 |
| 90 | 128500 |
| 154 | 81500 |
| 203 | 3750 |
| 280 | 975 |
| 340 | 820 |
| 404 | 104 |
| 483 | 960 |
| 551 | 14500 |
| 637 | 335 |
| 712 | 142 |
| 796 | 270 |
| 856 | 142 |
| 922 | 2.7 |
| 1021 | .75 |
| 1085 | .75 |

## TABLE 3.3N

NUMBER OF CYCLES AT LOAD AMPLITUDE PER YEAR FOR THREE COLUMN TETHERED PLATFORM IN NORTH SEA [WEBSTER].

| LOAD AMPLITUDE (KIPS) | CYCLES SOWM |
|---|---|
| 5.5 | 2000000 |
| 19.3 | 1000000 |
| 35.8 | 1000000 |
| 102 | 100000 |
| 154 | 10000 |
| 215 | 1000 |
| 290 | 100 |
| 375 | 10 |
| 496 | 1 |
| 610 | .1 |
| 734 | .01 |

Table 3.4

Tendon Pretension and Maximum Design Load for
Various Platforms and Environments

| Environment/Platform | $P_t$ | $L_m$ |
|---|---|---|
| North Sea/Hutton [Webster] | 1760 | 5300 |
| North Sea/Tether [Webster] | 1760 | 5300 |
| Atlantic/[Chou et al] | 1275 | 2075 |
| Atlantic/[Mercier et al] | 1875 | 3275 |
| Gulf of Mexico/[Chou et al] | 1275 | 2075 |
| Gulf of Mexico/[Tan et al] | 1475 | 2475 |
| Gulf of Mexico/[Paulling et al] | 1275 | 2075 |
| Gulf of Mexico/[Dillingham et al] | 2375 | 4275 |
| Gulf of Mexico/[Mercier et al] | 1875 | 3275 |
| Pacific/[Chou et al] | 1085 | 1720 |

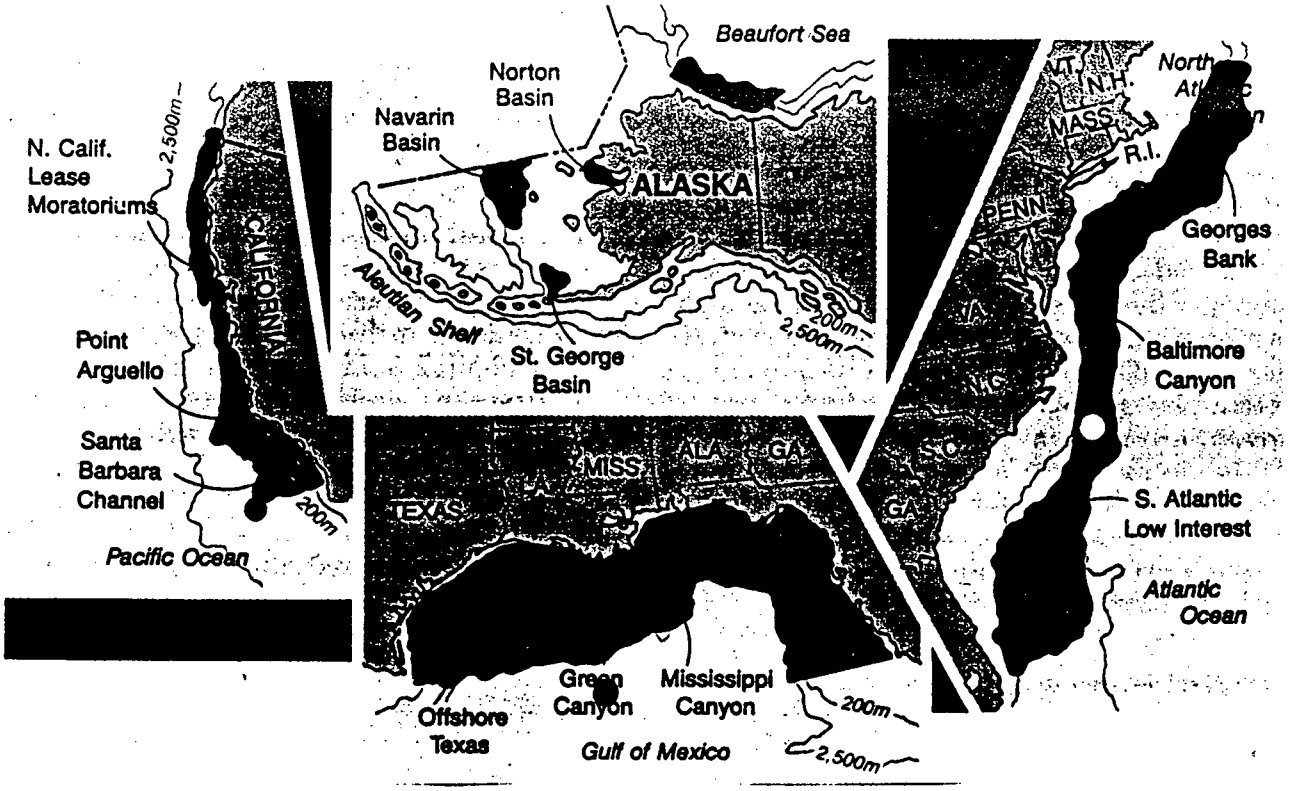


Figure 3.1a - Possible and existing U.S. offshore lease areas. Shading indicates extent of promising sedementary deposits. Circle indicates location SOWM data represents.(from Ocean Industry)

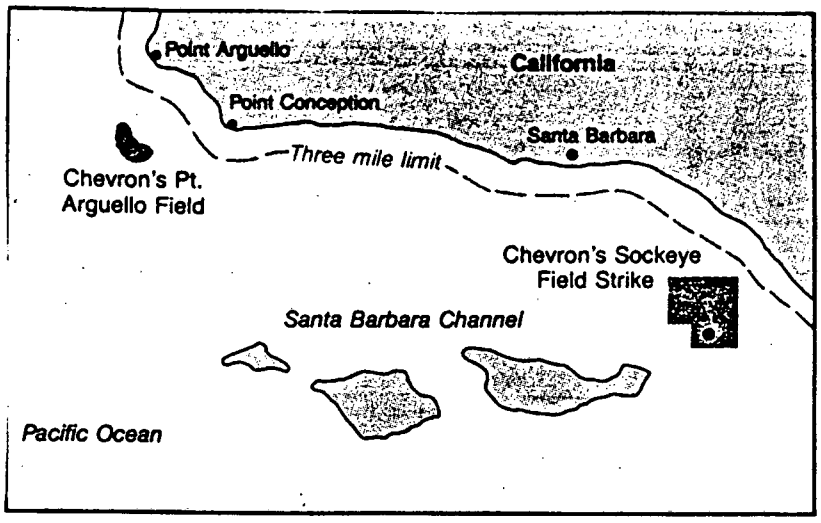


Figure 3.1b - Two major oil finds off the California Coast (from Ocean Industry)

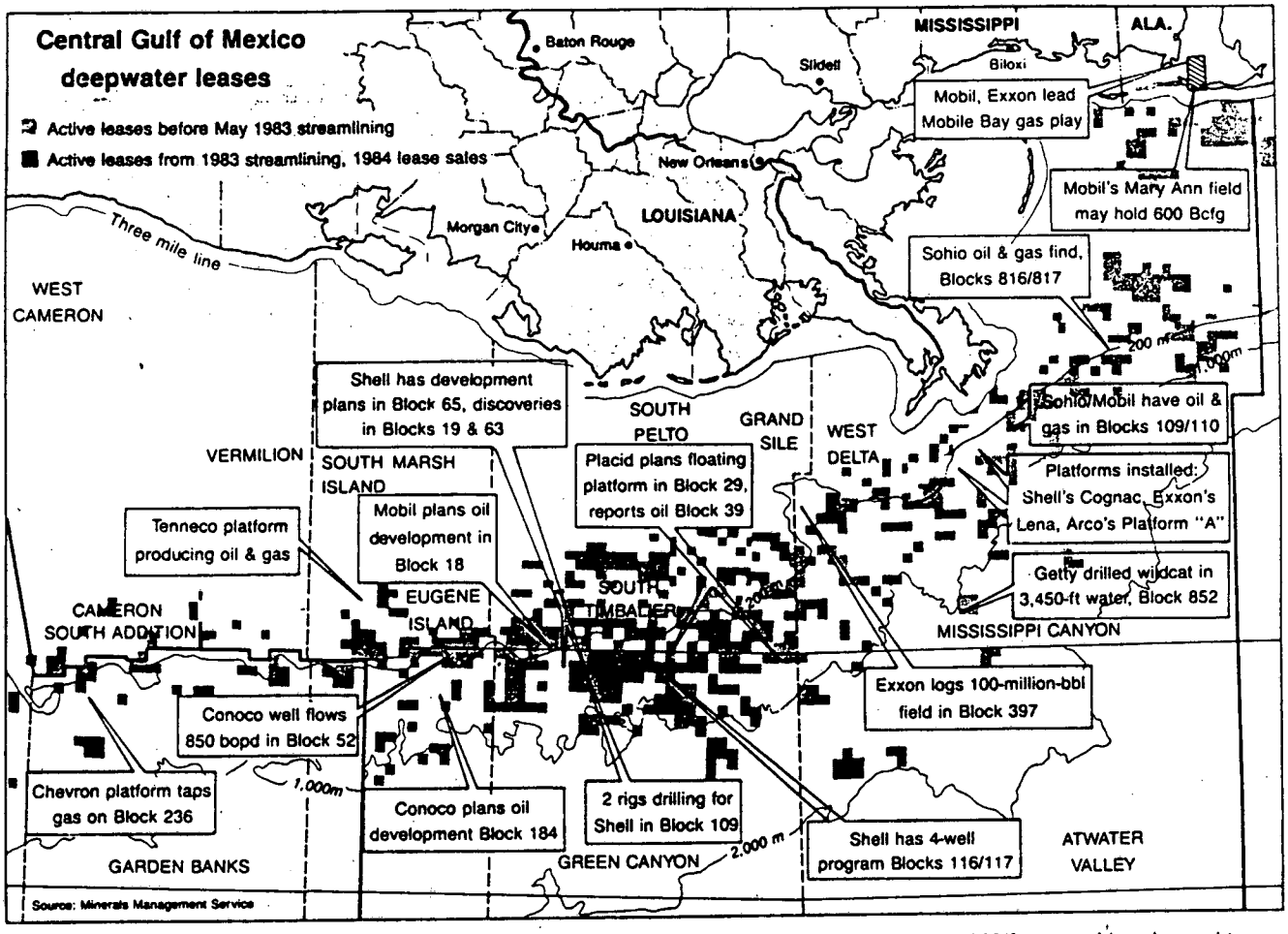


SURGE OF EXPLORATION DRILLING in Central Gulf of Mexico is keyed to deepwater tracts leased at 1983/84 area-wide sales and to gas prospects in and around Mobile Bay. Leases in most areas of conventional water depths have been deleted from map.

Figure 3.1c - Recent lease sites in the Gulf of Mexico.
(from Ocean Industry)

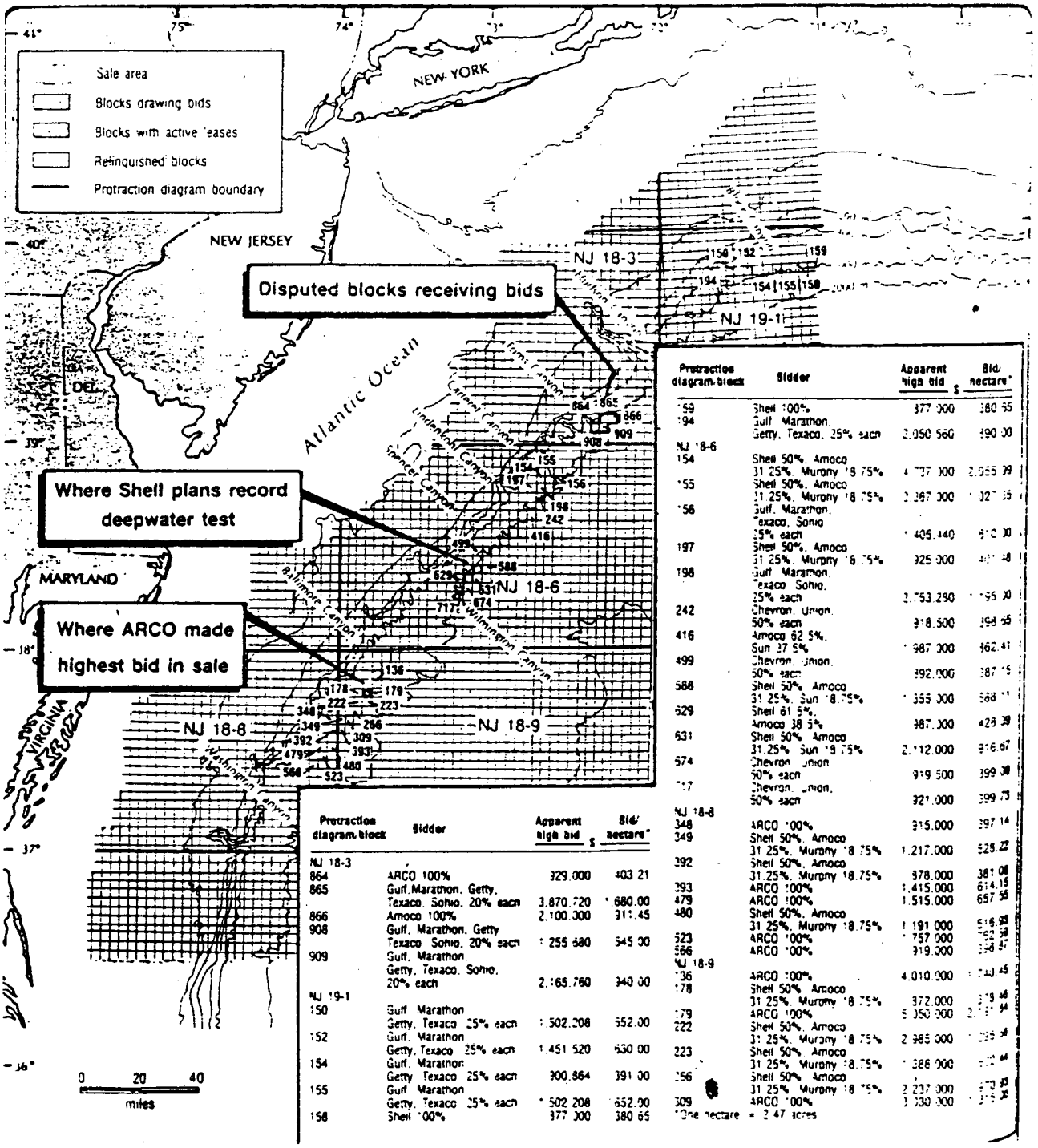


| Protraction diagram block | Bidder | Apparent high bid $ | Bid/ hectare* |
|---|---|---|---|
| NJ 18-3 | | | |
| 864 | ARCO 100% | 329.000 | 403.21 |
| 865 | Gulf, Marathon, Getty, Texaco, Sohio, 20% each | 3.870.720 | 1.680.00 |
| 866 | Amoco 100% | 2.100.300 | 911.45 |
| 908 | Gulf, Marathon, Getty Texaco, Sohio, 20% each | 1.255.680 | 545.00 |
| 909 | Gulf, Marathon, Getty, Texaco, Sohio, 20% each | 2.165.760 | 940.00 |
| NJ 19-1 | | | |
| 150 | Gulf, Marathon Getty, Texaco 25% each | 1.502.208 | 652.00 |
| 152 | Gulf, Marathon Getty, Texaco 25% each | 1.451.520 | 630.00 |
| 154 | Gulf, Marathon Getty Texaco 25% each | 900.864 | 391.00 |
| 155 | Gulf, Marathon Getty, Texaco 25% each | 1.502.208 | 652.00 |
| 158 | Shell 100% | 877.300 | 380.65 |
| 159 | Shell 100% | 877.300 | 380.65 |
| 194 | Gulf, Marathon, Getty, Texaco, 25% each | 2.050.560 | 890.00 |
| NJ 18-6 | | | |
| 154 | Shell 50%, Amoco 31.25%, Murphy 18.75% | 4.797.300 | 2.065.39 |
| 155 | Shell 50%, Amoco 31.25%, Murphy 18.75% | 2.367.300 | 1.027.35 |
| 156 | Gulf, Marathon, Texaco, Sohio 25% each | 1.405.440 | 610.00 |
| 197 | Shell 50%, Amoco 31.25%, Murphy 18.75% | 925.000 | 401.48 |
| 198 | Gulf, Marathon, Texaco, Sohio, 25% each | 2.753.280 | 1.195.00 |
| 242 | Chevron, Union, 50% each | 918.500 | 398.65 |
| 416 | Amoco 62.5%, Sun 37.5% | 1.987.300 | 862.41 |
| 499 | Chevron, Union, 50% each | 892.000 | 387.15 |
| 588 | Shell 50%, Amoco 31.25%, Sun 18.75% | 1.355.300 | 588.11 |
| 629 | Shell 61.5%, Amoco 38.5% | 987.300 | 428.39 |
| 631 | Shell 50%, Amoco 31.25%, Sun 18.75% | 2.112.000 | 916.67 |
| 674 | Chevron, Union 50% each | 919.500 | 399.30 |
| 717 | Chevron, Union, 50% each | 921.000 | 399.73 |
| NJ 18-8 | | | |
| 348 | ARCO 100% | 915.000 | 397.14 |
| 349 | Shell 50%, Amoco 31.25%, Murphy 18.75% | 1.217.000 | 528.22 |
| 392 | Shell 50%, Amoco 31.25%, Murphy 18.75% | 878.000 | 381.08 |
| 393 | ARCO 100% | 1.415.000 | 614.15 |
| 479 | ARCO 100% | 1.515.000 | 657.55 |
| 480 | Shell 50%, Amoco 31.25%, Murphy 18.75% | 1.191.000 | 516.93 |
| 523 | ARCO 100% | 1.757.000 | 762.59 |
| 566 | ARCO 100% | 919.000 | 398.87 |
| NJ 18-9 | | | |
| 136 | ARCO 100% | 4.010.000 | 1.740.45 |
| 178 | Shell 50%, Amoco 31.25%, Murphy 18.75% | 872.000 | 378.46 |
| 179 | ARCO 100% | 5.050.300 | 2.191.94 |
| 222 | Shell 50%, Amoco 31.25%, Murphy 18.75% | 2.985.000 | 1.295.36 |
| 223 | Shell 50%, Amoco 31.25%, Murphy 18.75% | 1.386.000 | 601.44 |
| 266 | Shell 50%, Amoco 31.25%, Murphy 18.75% | 2.237.300 | 970.93 |
| 309 | ARCO 100% | 3.330.300 | 1.445.36 |

*One hectare = 2.47 acres

Figure 3.1d - Recent lease sites in the Atlantic.
(from Oil and Gas Journal)

Figure 3.2

Outline of Fatigue Loads Determination .

1) Given a) joint frequency of occurance of $H_{sj}$, $T_{pi}$ $(f_{ij})$

$$\begin{array}{c} \\ T_{pj} \end{array} \begin{bmatrix} H_{si} & & \\ f_{11} & f_{12} & \\ f_{21} & & \\ & & f_{ji} \end{bmatrix}$$

b) Tendon tension RAO (f)

2) Compute total number of waves annually

$$N_{wij} = f_{ij} \times 31536000 \sum T_{pj} \quad \text{no sum on j}$$

3) Compute Bretschnieder spectrum

$$S_{ij}^{wave}(f) = \frac{5}{16} \frac{H_{si}^2}{f_{oj}} \frac{(f_{oj})^5}{(f)^5} \exp\left[-5(f/f_{oj})^{-4}/4\right]$$

$$f = 1/T, \; f_{oj} = 1/T_{pj} \quad \text{no sum on i, j}$$

4) Compute load spectrum

$$S_{ij}^{load}(f) = S_{ij}^{wave}(f) \times [RAO(f)]^2$$

5) Compute first moment of the load spectrum

$$M_{oij}^{load} = \int_0^\infty S_{ij}^{load}(f)\, df$$

6) Compute the probability distribution function

$$P_{ij}(L) = 1 - \exp\left[-L^2/2M_{oij}^{load}\right]$$

L = Load amplitude

The number of cycles per year in a particular load amplitude range ($L_1 < L < L_2$)

$$N\ (L_1 < L < L_2) = [P_{ij}(L_2) - P_{ij}(L_1)] \times N_{wij}$$

$$i = 1 \text{ to number of } H_s$$

$$j = 1 \text{ to number of } T_p$$

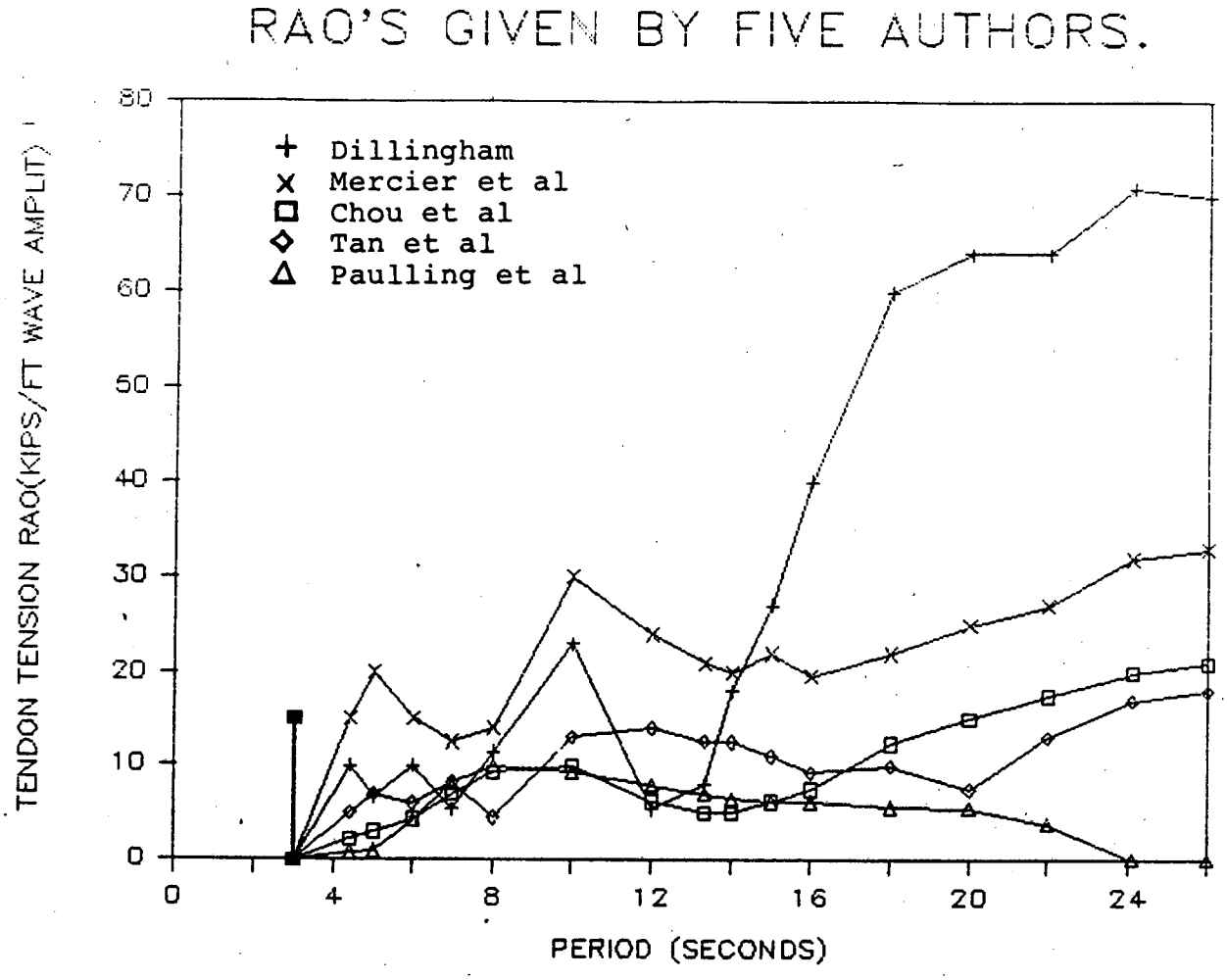


Figure 3.3 - Tendon tension RAO's as given by five author's.

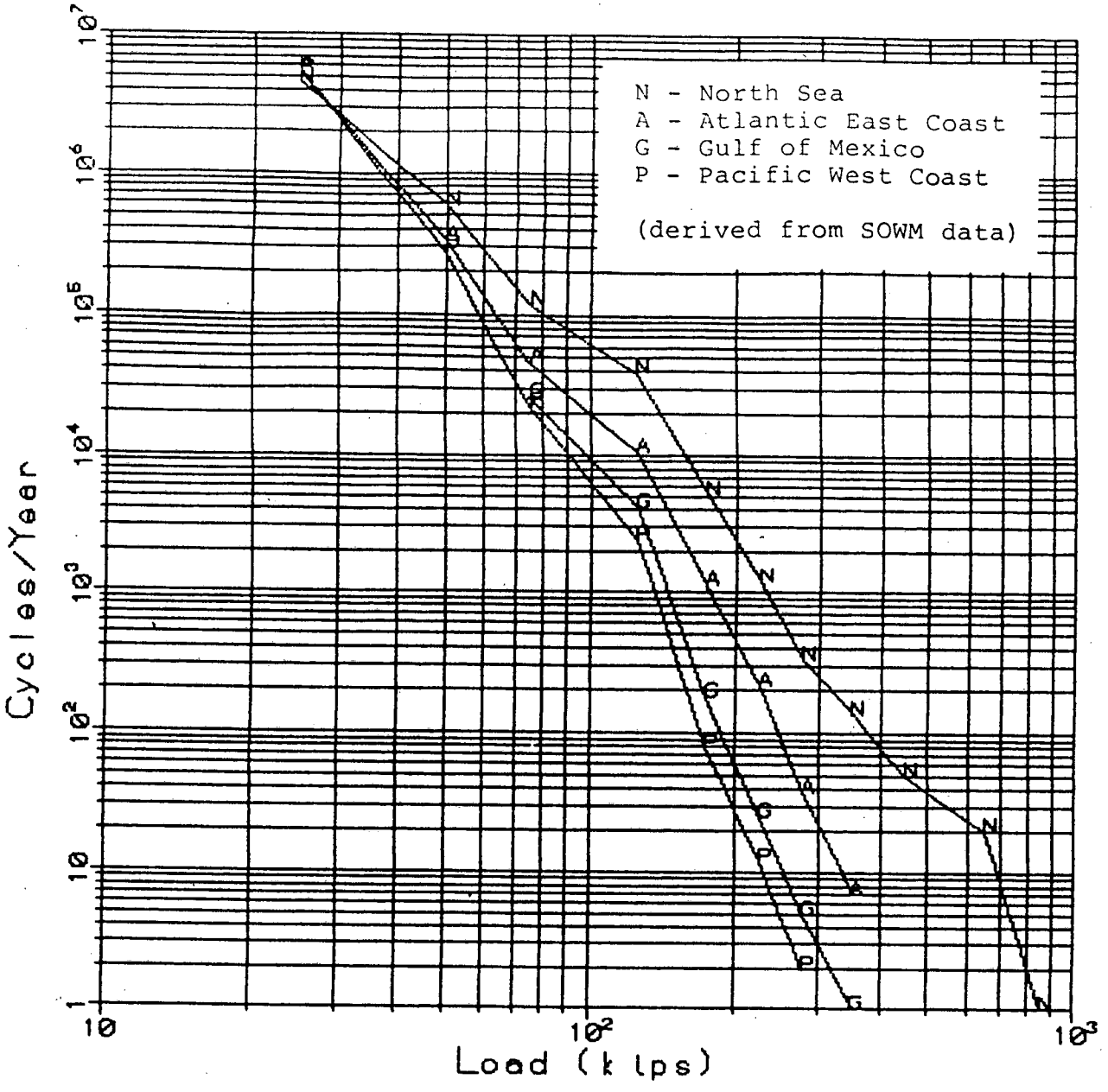


**Figure 3.4a - Values of Load Cycles per Year versus Load Amplitude for Four Environments. (Chou's RAO and SOWM data are used)**

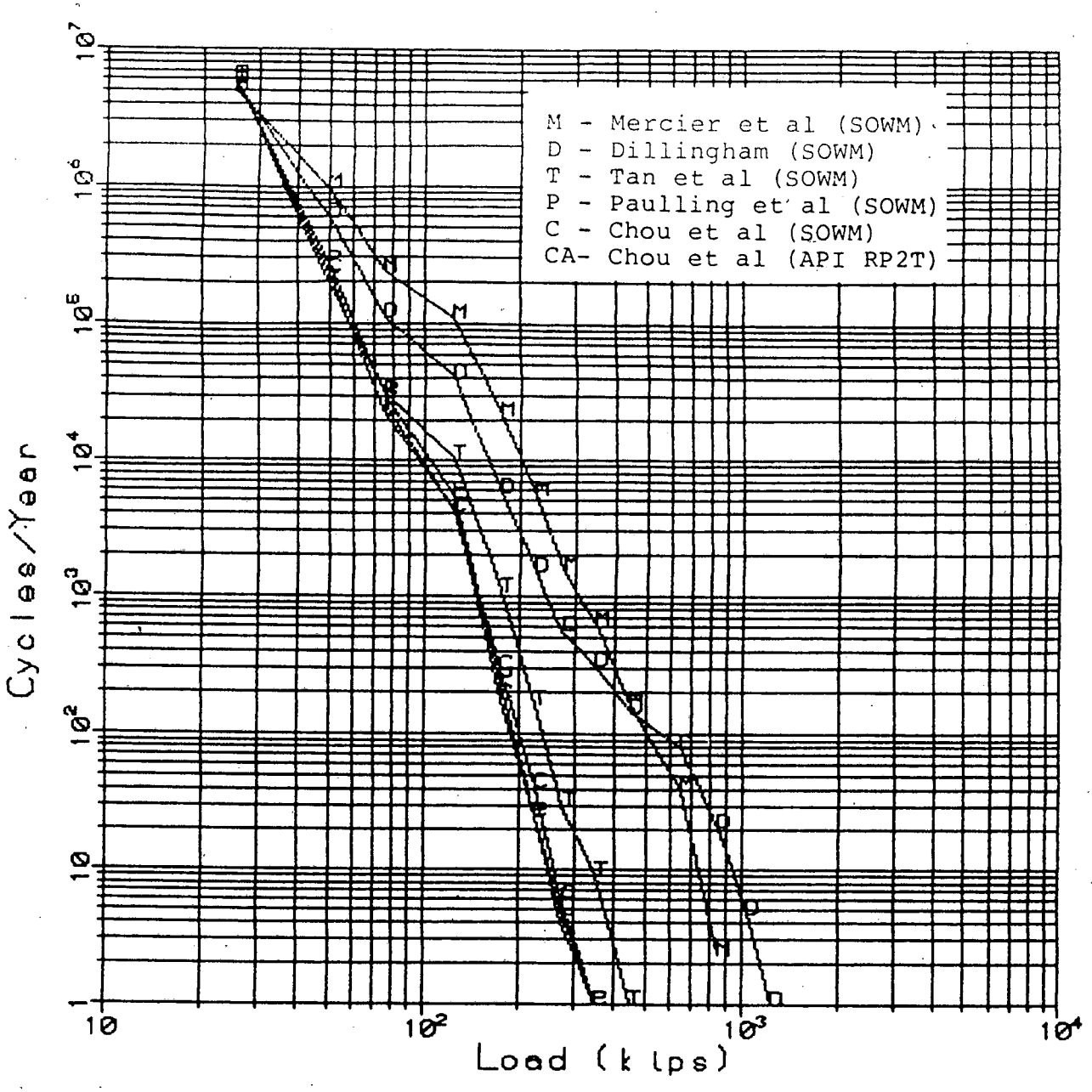


**Figure 3.4b - Values of Load Cycles per Year versus Load Amplitude for the Gulf of Mexico and Five Platforms.**

# 4.0 Tendon Materials and Material Properties

## 4.1 Types of Metals

High strength steels are required in tendons due to the large stresses induced by the combined preload and environmental loads. Steels of yield stress in the range $70 < \sigma_y < 120$ ksi may be applicable. An upper level of 120 ksi is assumed due to the undesirable brittle nature of steels with higher yield stresses.

## 4.2 Material Fatigue

### 4.2.1 SN Data

#### 4.2.1.1 Deterministic

Fatigue data (SN curves) used in this study are shown in figures 4.1a-b. Figure 4.1a,b represent data [Salama] for 3 1/2 NCMV 115 ksi yield stress steel used in the Hutton platform. The design curve and the free corrosion curve of figure 4.1a and the air curve of figure 4.1b were used in evaluation of the tendon fatigue life (see section 5).

#### 4.2.1.2 Probabilistic

A scatterband representing data from [Salama et al] was produced. This was achieved using the outermost data points as the upper and lower bounds. The free corrosion scatterband is shown on figure 4.1a and the air and cathodically protected scatterbands are shown on figure 4.1b.

The saltwater environment is extremely severe in comparison to the air and the cathodically protected case primarily because no endurance limit is assumed for the free corrosion case while an endurance limit of about 50 ksi and 65 ksi occur for the air and cathodically protected environments, respectively.

### 4.2.2 Environmental and Other Effects

Effects which will alter the fatigue characteristics of the tendon

are:

1) Preload
2) Cathodic Protection
3) Seawater (free corrosion)
4) Air Environment
5) Sealed Environment

The modified Goodman criterion is used to account for the effects of mean stress (see section 5.2).

Cathodic protection increases fatigue life many orders of magnitude over the free corrosion fatigue life (figure 4.1a). The scatterband of figure 4.1a for different applied voltages shows little change in fatigue life for the voltages used. The effect of voltage on crack growth may be more pronounced.

The fatigue curve for air gives slightly longer fatigue life than does the cathodically protected curve.

For the sealed environment to which the threaded couplings are expected to experience there is no fatigue data. To approximate this air environment is assumed.

It is possible that the tendon will experience any of the environments listed above requiring that the fatigue life be examined under all cases.

### 4.2.3 Final Fatigue Crack Size

It is assumed that when the damage ratio as computed by Miner's rule attains a value of 1.0 that a crack size has been reached which results in threshold stress intensities. Thus, from the formula

$$a_{th} = Q\ (\Delta K_{th}/\Delta\sigma_{eq})^2/\pi$$

where

$\Delta\sigma_{eq}$ = equivalent historical stress range
$Q$ = flaw shape parameter
$a_{th}$ = threshold crack size
$\Delta K_{th}$ = threshold stress intensity range

the crack size at which fatigue ends and crack growth begins is found. As an approximation the following values are used:

$Q = \pi^2/4$

$\Delta\sigma_{eq} = 4[\Gamma(1+k/2)]^{1/k}\ \Delta\sigma/\ \pi$

$\Delta K_{th}$ = value of $\Delta K$ between region I and region II crack growth (Section 4.3.2)

$\Delta\sigma_{avg}$ = average historial stress range

K = exponent in SN equation

## 4.3 Fracture Mechanics

### 4.3.1 da/dN versus ΔK Data

#### 4.3.1.1 Deterministic

Fracture mechanics data used for the deterministic fracture mechanics model are shown in figure 4.2a through figure 4.2c. Figure 4.2a and figure 4.2b [Burnside et al] are for BS4 360:50D steel in air and 521 DIN17100 and BS4 360:50D steels in sea water, respectively. The curves represent data for R ($K_{min}/K_{max}$) greater than 0.5. Figure 4.2c is for 3 1/2 NCMV 115 ksi yield stress steel [Salama et al] at R=0.5 in air and under cathodic protection. While the data from [Burnside et al] is not for metals of the appropriate yield stress range it is assumed that these curves are representative of the higher yield stress steels.

#### 4.3.1.2 Probabilistic

A scatterband was produced representing the data given by [Burnside et al]. The upper and lower bounds are shown in figure 4.2b,d for free corrosion and cathodic protection respectively. The upper and lower bounds were assumed to be the $3\sigma$ deviation from the mean [see Burnside et al page 8.9]. The mean was taken as the mean curve between the upper and lower bounds. The distribution across the scatterband is assumed to be log-normally distributed. The da/dN bandwidth in region I (low ΔK) of crack growth was taken to be the same as that in region II. The slopes are assumed to equal to that given by [Burnside et al] for the appropriate cases.

For the cathodically protected case (figure 4.2d) the $A_1$, scatterband upperbound passes through the two low ΔK values of figure 4.2d. These two points are assumed to represent the lower bound on ΔK threshold.

### 4.3.2 da/dN versus ΔK Equation

A three parameter equation as presented by [Burnside et al] is used. Its form is:

$$\frac{1}{da/dN} = \frac{1}{A_1(\Delta K)^{n1}} + \frac{1}{A_2(\Delta K)^{n2}} - \frac{1}{A_2[(1-R)K_c]^{n2}} \qquad (1)$$

where

$R$ = $K_{min}/K_{max}$

$K_c$ = fracture toughness

$\Delta K$ = $K_{max} - K_{min}$

$A_1$ = da/dN intercept at ΔK=1 (for region I described below)

$n_1$ = slope of da/dN vs. ΔK curve in region I.

$A_2$ = da/dN intercept at ΔK=1 for region II.

$n_2$ = slope of da/dN vs. ΔK curve in region II.

The three parts on the right of equation 1 each represent a region of crack growth. The first represents micro-crack growth (macro crack formation) for which SN curves may also be used, the second macro-crack growth and the third rapid crack growth and failure. These regions as well as the constants used in equation 1 are outlined in figure 4.3. Table 4.1 presents the values of these constants for the three environments.

### 4.3.3 Environmental and Other Effects

Crack growth as a function of stress intensity range will vary among the five cases listed in section 4.2.2.

Preload is exhibited by the R ratio. da/dN vs. ΔK curves are affected by R. Crack growth increases with R at constant ΔK. For TLP loads and pretension the value of R is almost always above 0.5. Thus the curves given in figures 4.2a-c can be used directly with equation 1 in computing crack growth characteristics of the tendons.

Cathodic protection may decrease crack growth rates for appropriate applied voltages while for large voltages (greater than -1.05 mV) crack growth rate is enhanced. The effect of cathodic protection may differ also depending on whether the crack is very small or large.

The effect of free corrosion is to increase crack growth rates

over those in air. As for the fatigue data, crack growth life is computed for all possible environments.

## 4.4 Effect of Load History

Due to the effect of loads on the plastic zone size at the crack tip, a retardation of crack growth can occur when variable amplitude loads occur. A large load will produce a large plastic zone with resulting compression at the crack tip during future lower loads. The compression will reduce crack growth rate by a factor which is proportional to the ratio of plastic zone size over the previous largest plastic zone size [Broek]. The exact form of the relation is itself a function of material and loading sequence. No experimental data has been found which addresses this concept for the high strength steels and loading sequences which are typical of TLP's.

## 4.5 References

Broek, D., Elementary Engineering Fracture Mechanics, Sijthoff and Noordhoff International Publishers, 1978, pg. 256-259.

Burnside, O.H., Hudak, S.J., Oelkers, E., Chan, K., and Dexter, R.J., "Long Term Corrosion Fatigue of Welded Marine Steels, Southwest Research Institute, March 1984.

Salama, M.M. and Tetlow, J.H., "Selection and Evaluation of High Strength Steel for Hutton TLP Tension Leg Elements", Offshore Technology Conference, Paper OTC 4449, 1983.

Table 4.1

Values of the Crack Growth Material Constants *

Deterministic:

| Environment | A1 | A2 | n1 | n2 | Kc |
|---|---|---|---|---|---|
| air | 3.94E-13 | 4.33E-10 | 13.3 | 3.15 | 228 |
| free corrosion | 3.937E-13 | 2.315E-10 | 13.3 | 3.65 | 228 |
| cathodic protection | 9E-23 | 2.5e-8 | 1.8 | 14.91 | 266 |

Probabalistic:

| Environment | A1 | A2 | n1 | n2 | Kc |
|---|---|---|---|---|---|
| free corrosion | | | | | |
| upper bound | 4.62E-12 | 1.37E-9 | 13.3 | 3.65 | 228 |
| lower bound | 3.29E-14 | 9.75E-12 | 13.3 | 3.65 | 228 |
| median | 3.9E-13 | 1.156E-10 | 13.3 | 3.65 | 228 |
| Cathodic Protection | | | | | |
| upper bound | 3.99E-21 | 5.85e-10 | 32 | 4.78 | 228 |
| lower bound | 1.596E-23 | 2.34E-12 | 32 | 4.78 | 228 |
| median | 2.523E-22 | 3.7E-11 | 32 | 4.78 | 228 |

* units of A1, A2 in inches/cycle
units of Kc in KSI*in^.5

a)

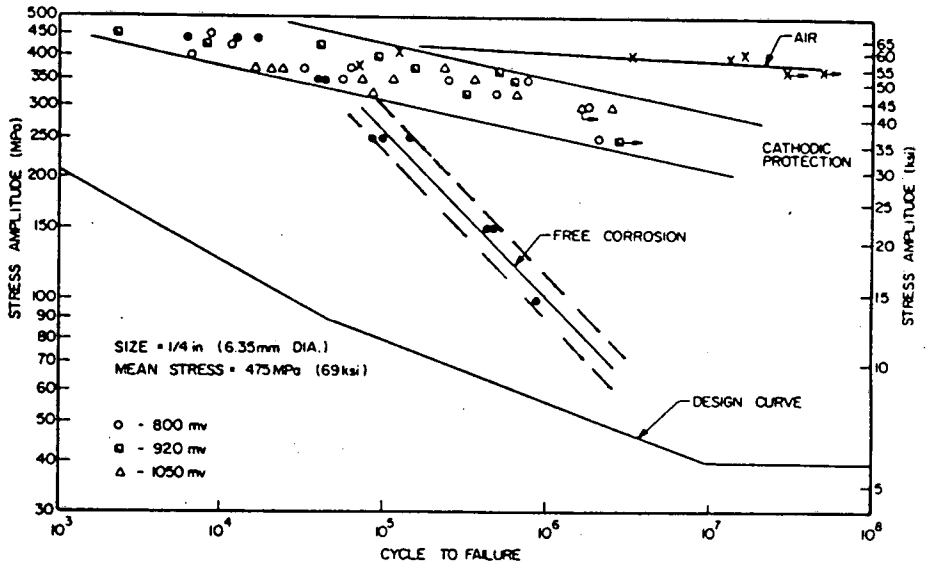


b)

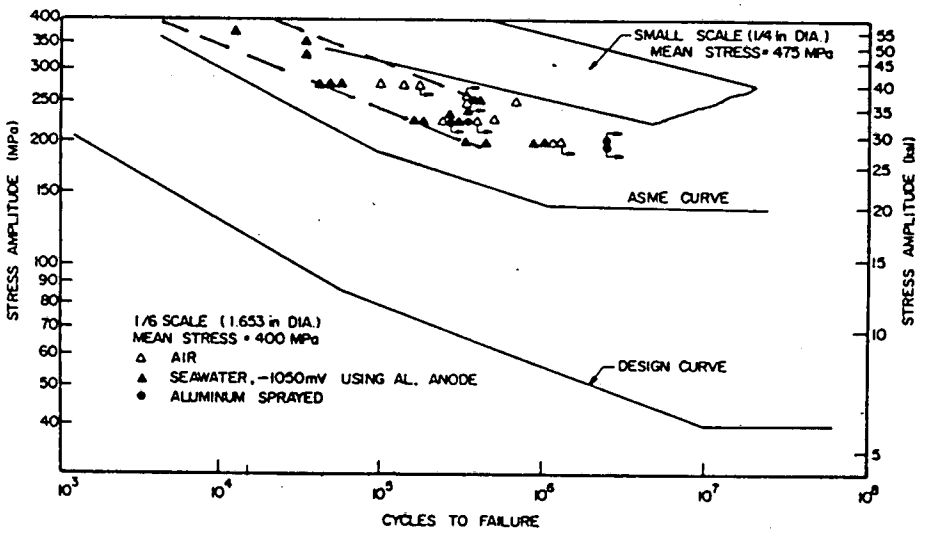


Figure 4.1 a) SN Curves in free corrosion, cathodic protection, and air for 3 1/2 NCMV steel.

b) SN Curve in air for 3 1/2 NCMV steel. (Salma, et al)

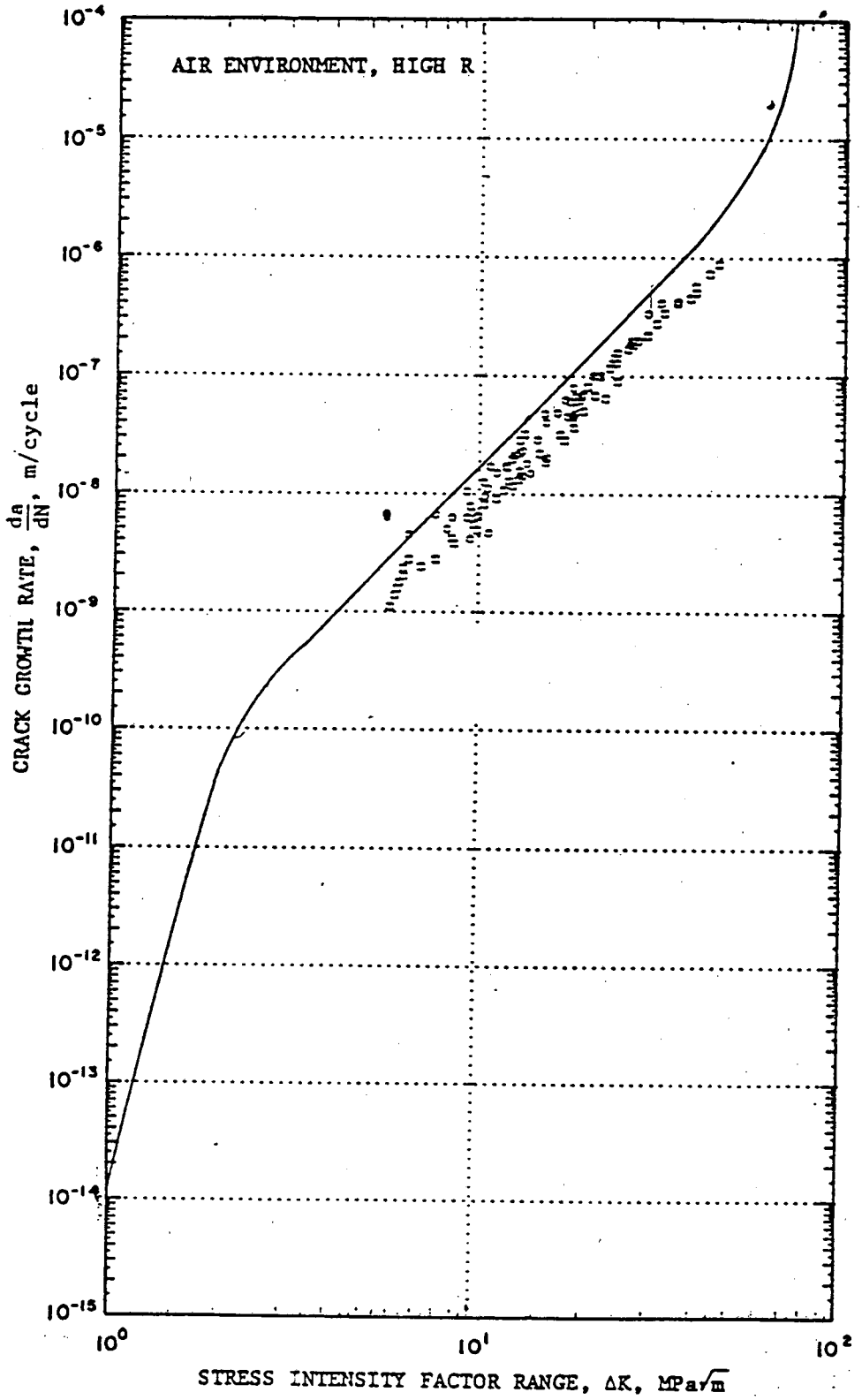


Figure 4.2a- CRACK GROWTH DATA, AIR ENVIRONMENT, HIGH R
[Burnside et al]

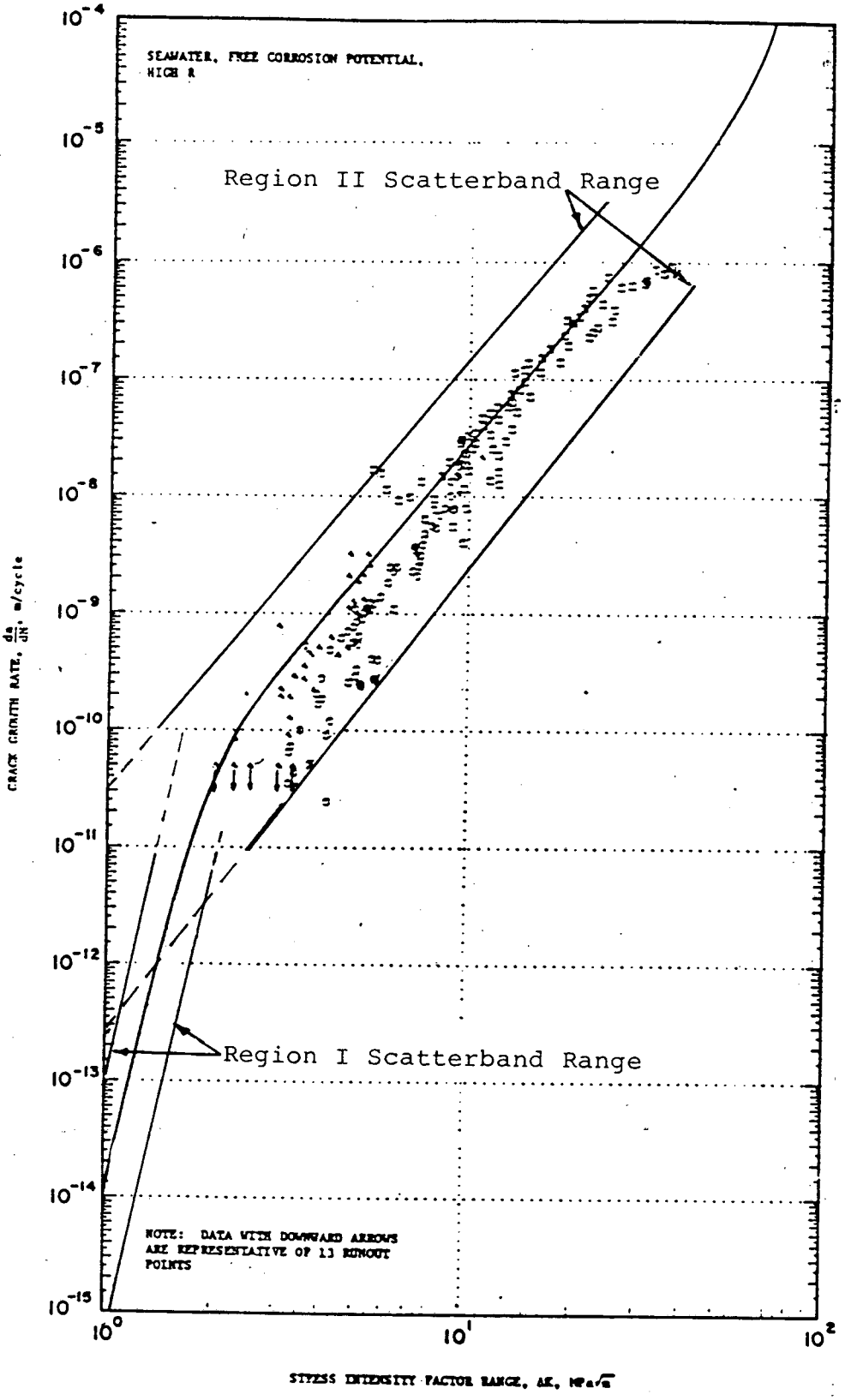


Figure 4.2b - CRACK GROWTH DATA, SEAWATER, FREE CORROSION POTENTIAL, HIGH R

[Burnside et al]

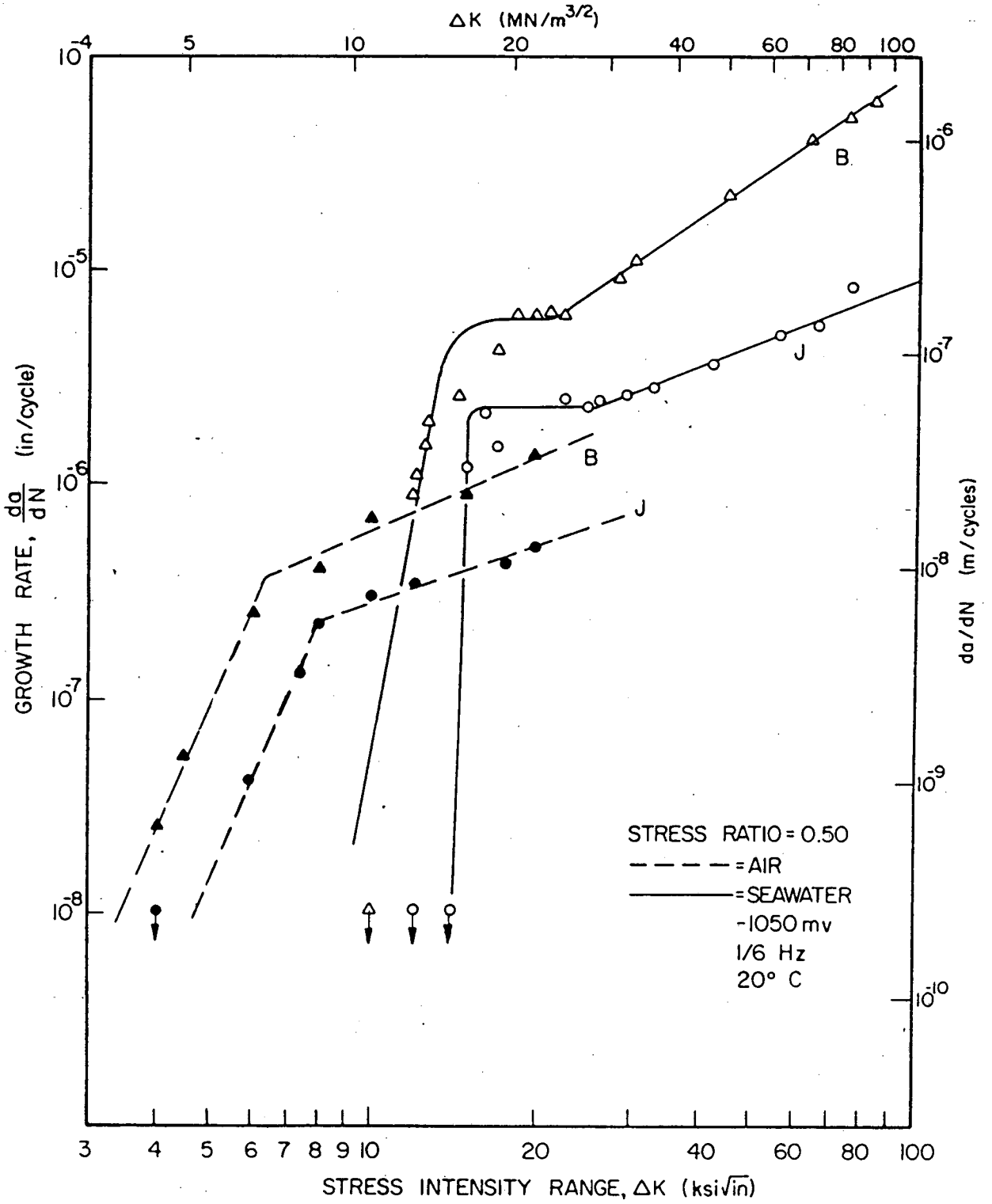


Figure 4.2c - Crack growth data, air, cathodic protection. 3 1/2 NCMV steel. For 2 producers (J,B) of test samples. [Salama et al]

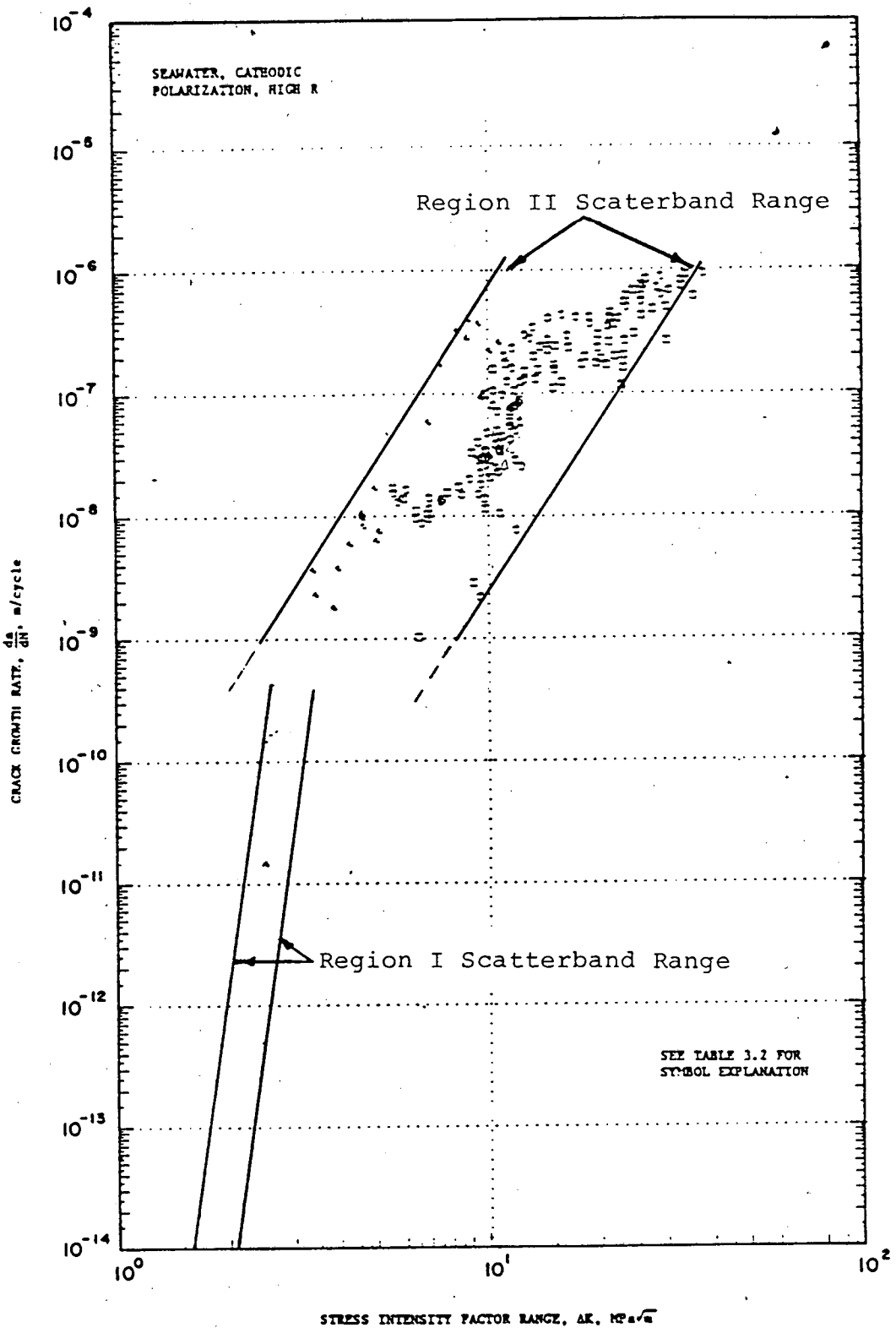


Figure 4.2d - CRACK GROWTH DATA, SEAWATER, CATHODIC POLARIZATION, HIGH R

[Burnside et al]

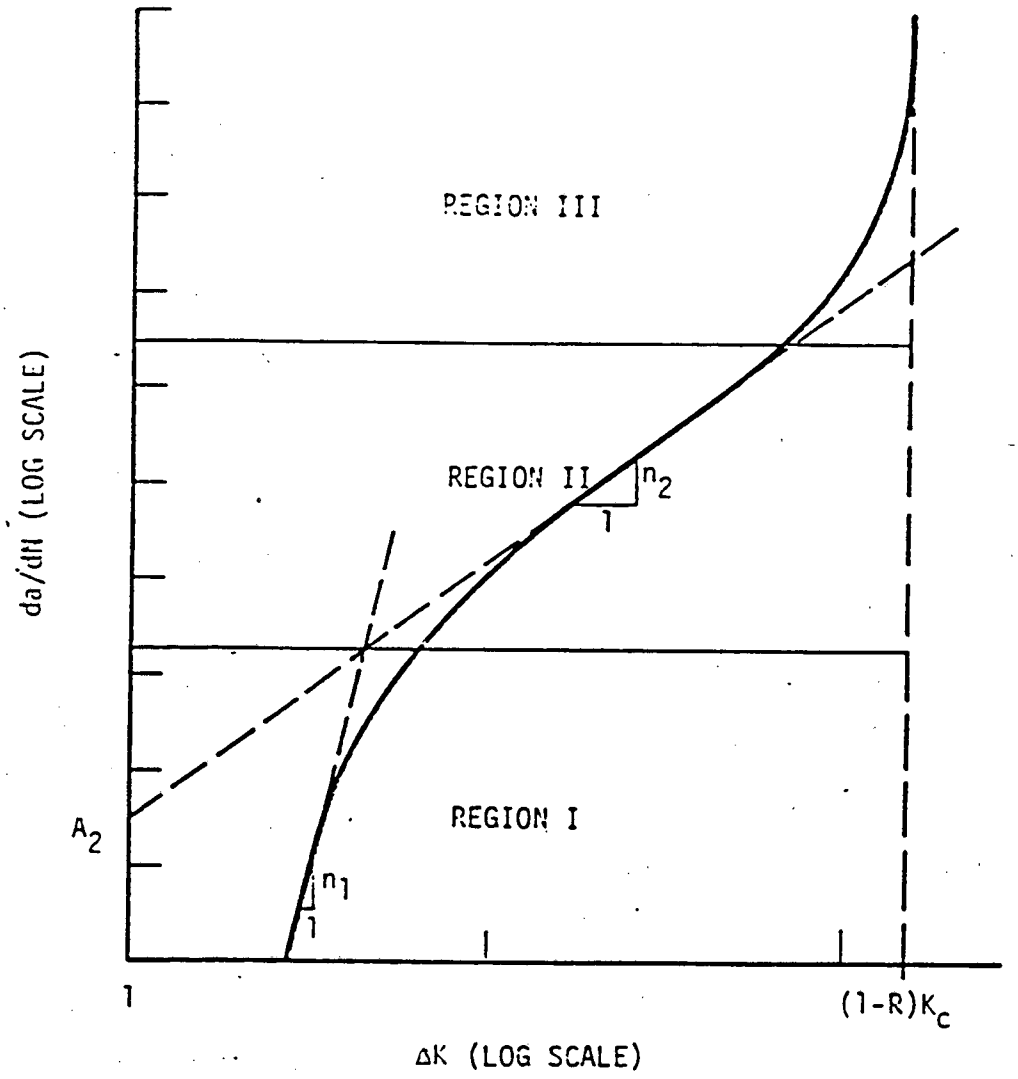


Figure 4.3 - Schematic of Three Component Crack Growth Model.

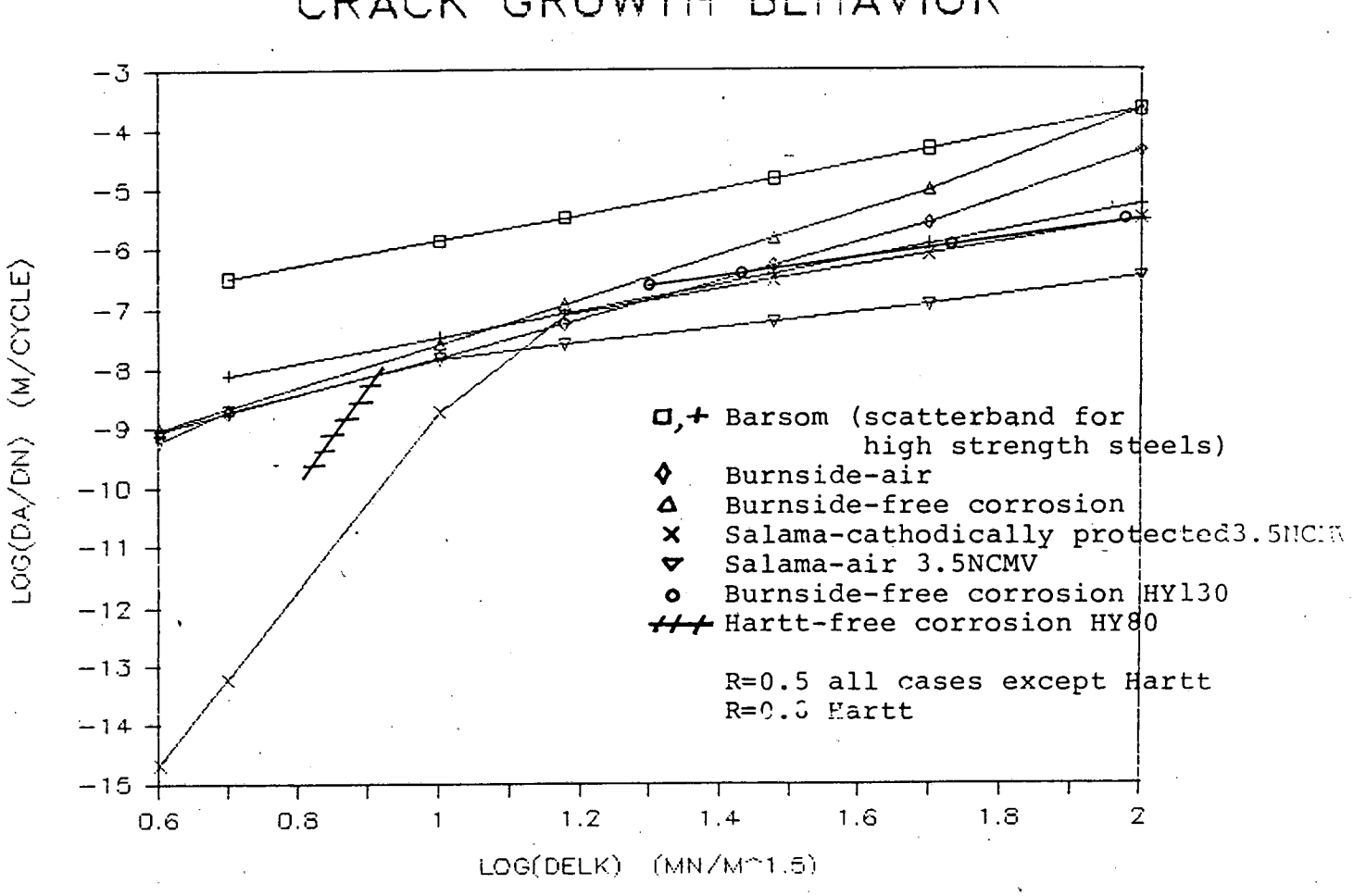


Figure 4.4 - da/dN ΔK for various materials.

# 5.0 Tendon Component Design

## 5.1 Discussion of Tendon Designs

Tendon systems make up the structural link between the TLP and its foundation. The principal components are (figure 5.1):

- Top Tendon Connector
- Cross Load Bearing
- Upper Flex Element
- Tendon Segment (2)
- Bottom Flex Element

The top tendon connector transfers the load from the tendon to the platform. It should have jacking capabilities to adjust for slight load variations between tendons.

The cross load bearing and upper flex element prevent tendon bending at the platform heel. Current TLP designs use an elastomeric bearing for both lateral and angular motion (figure 5.2).

The lower flex element performs a similar funtion with respect to the interface between the tendon and the bottom tendon template (figure 5.3).

The tendon segment consists of a tubular element and coupling. Continuous tendons consisting of cables or welded pipe are being considered, however, to date none have been seriously proposed for a TLP (see, e.g. Webster). The focus of this study is on tubular segments with threaded couplings, as this is the only concept which has been carried to the prototype stage.

These segments may be constructed in one of several methods:

a) integral forged construction
b) seamless pipe welded to forged coupling
c) formed pipe welded to forged coupling

The Hutton TLP tendons were constructed from forgings [Webster]. To minimize cost, a relatively small diameter and small bore configuration was selected [Tetlow]. Alternately, a relatively large bore, thin walled tendon may also be considered if the pipe is welded to the coupling [Webster].

The inner bore may be filled with a liquid (e.g. water or

air] or it may be evacuated for more buoyancy.

Two 'Generic' tendon configurations have been selected for this study, a 'thick walled connector' and a 'thin walled connector'. Dimensions for the thick walled connector are based on the Hutton design [Tetlow]. The pipe inner and outer diameters are 2.94 inches and 10.24 inches, respectively (figure 5.4). The maximum load for the Hutton tendons was 5300 Kips (see section 3, table 3.4) resulting in a 70 KSI working stress and a 117 KSI yield stress using a 1.67 safety factor.

For the thin walled case, the section areas of the thick walled pipe and connector were scaled to a 24 inch O.D. pipe (figure 5.5). This size was selected because it corresponded to 1 inch pipe wall thickness, which is a standard size and readily formed.

The working stress levels in the pipe will be identical to those in the thick walled case, hence similar material strength levels would be required, assuming the same wave environment.

Actually, the Hutton tendon design criteria exceed those of most potential U.S. sites. Table 5.1 shows maximum wave loads for the 100 year storm environments using a Bretschneider spectrum and the various response amplitude operations (RAO's) discussed in Section 3 (see table 3.4). Considering lower storm tides, wind loads and currents for U.S. sites, plus more favorable platform 'tuning', maximum loads could be reduced by 1500-2000 Kips over those reported for Hutton (we are ignoring the other obvious means of lowering loads by means of using more tendons).

Table 5.1

Maximum Tension Amplitude Due to Waves

| | Gulf, Atlantic | North Sea [Webster] |
|---|---|---|
| Maximum Tension Amplitude | 600-1500 Kips | 1760 Kips |

Thus, for our 'Generic Designs', the working membrane stress could be as low as 55 KSI. Using the AISC criteria, the minimum yield strength would be 73 KSI.

While it is obviously possible to design a lighter weight tendon with higher strength material, we believe the generic designs using 70-129 KSI yield strength material are representative of tendons which are likely to be built. This is primarily due to the problems encountered with stress corrosion cracking in steels greater than around 120 KSI yield strength, and the lower ductility of these steels generally.

From a fatigue and crack growth point of view, the critical areas of concern are the girth welds (for the thin walled connector) and the fillets and thread roots of both connectors. The couplings themselves represent integral pin and box type tapered joints similar to rotary shouldered connections for drill pipe or extreme line casing joints. A critical design criteria for these joints is to minimize stress risers which could result in fatigue crack formation.

Figure 5.4 and 5.5 show the coupling dimensions for the two cases. Again, these dimensions are representative of the Hutton connections [Tetlow] and are not necessarily optimum for any specific application.

We have considered several different thread forms derived from various specifications. No attempt has been made to optimize thread forms, however those selected should be representative in terms of thread pitch and gross dimensions.

The couplings are presumed sealed from sea water by means of an O-ring and/or a metal to metal seal in the external preload shoulder. The internal fluid is assumed to be non-corrosive.

From a fatigue/reliability point of view, the possibility of some sea water leakage into the thread area needs to be considered, although the preload shoulder is designed to maintain its seal through the entire range of loadings.

In order to evaluate connector fatigue life and material requirements, a computer program was developed to perform

approximate stress analysis. The following section discusses this analysis.

## 5.2 Coupling Analysis

The base case 'Thick-Walled' and 'Thin-Walled' TLP connector configurations were defined with the aid of a computer program which analyzed stresses and fatigue damage at critical sections. These configurations are shown in figures 5.4 and 5.5.

A sketch of the model connector which the program analyzed is shown in figure 5.6. The critical sections are:

a) Last Thread of Pin
b) Last Thread of Box
c) Pin Neck
d) Inside Fillet in Box
e) Weld/Fillet Sections of Pin and Box

These sections are pointed out in figure 5.7 for clarity. Compression stresses in the tang, shear in the shoulder, and shear in the splines were also computed to ensure structural adequacy.

In addition, approximate volume and weight of the connector as well as preload force and torque required for preload were determined within the program.

Inputs to the program consisted of:

1. Geometry (refer to figure 5.6)
   a) Diameters
   b) Lengths
   c) Fillet Radii
   d) Thread Root Radii
   e) Thread Pitch
   f) Thread Angle
   g) Thread Height
   h) Spline Depth
   i) Spline Length
   j) Number of Splines
2. Material Properties
   a) Alloy Designation
   b) Yield Strength
   c) Ultimate Strength
   d) Curve-Fit Parameters for a Corrosion Fatigue S-N Curve and a Design S-N Curve
   e) Friction Coefficient (assumed lubricated)

3. Fatigue Environment
   a) Fatigue Loads
   b) Number of Cycles Corresponding to each Load

4. Other Loads
   a) Maximum Load
   b) Pretension Load

The program considers only axial tension loads in the tendon.

To begin the analysis, stress in the tendon tube is computed for maximum load. If the tube stress was greater than the allowable stress, the entire run was aborted and new geometry is determined or higher strength materials are specified.

Once the tube stress was demonstrated to be acceptable, the analysis proceeded as follows (see Appendix - for list of symbols).

Allowable stress is computed from $\sigma_y$, the yield stress based on allowables defined in [13]:

For tensile stresses, $\sigma_{all}=0.8\sigma_y$ (ksi)

For bending and membrane stresses, $\sigma_{all}=1.2\sigma_y$ (ksi) [Ref.11]

Areas for all critical sections are computed as:

$$(\pi/4)\ (D^2_{outer} - D^2_{inner})$$

Stress concentration factors at all critical sections are computed as if the section were a square shoulder with a fillet in a circular shaft under axial tension (see figure 5.8) [Ref. 8].

Volume and weight of the connector is approximated from:

$$\text{Volume} = 2\ A_1\ L_1 + A_2\ (L_6 - L_1)\ (in^3)$$

$$\text{Weight} = (\gamma_s)(\text{Volume})\ (lbs)$$

where $\gamma_s$ = Density of Steel = .283 $lb/in^3$

Preload force is chosen such that separation force was 1.1 times the maximum anticipated load. By defining separation force ($P_s$) as

$$P_s = P_o\ (A_3 + A_4)/A_3 \quad \text{(see figure 5.9)}$$

then preload ($P_o$) is computed as

$$P_o = 1.1\ P_{max}\ A_3/(A_3 + A_4)\ \text{(kips)}$$

Torque (T) required to obtain preload is then computed from [Ref. 7]:

$$T = (P_o/12)\ [(R_t K_f/\cos\theta) + (R_s K_f) + (P_t/2\pi)]\ \text{(ft/kips)}$$

where $R_t$ = Mean Thread Radius = $(D_6 + D_7)/4$

$R_s$ = Mean Radius to Shoulder = 1/2 $D_7$ + 1/2 Tang Thickness

Stresses for preload were then computed.

In the Box:

Shear in Tang during make-up = $\dfrac{K_f T r}{J} = \dfrac{12 K_f T (D_5/2)}{(\pi/32)(D_5^4 - D_7^4)}$

Axial Stress in Tang = $-P_o/A_3$

Hoop stress at thread nearest tang [Ref.6] =

$$\frac{EI(D_6^2 - D_4^2)(D_6^2 + D_5^2)}{2\,D_6^3(D_5^2 - D_4^2)}$$

where I is the pin/box interference = $T_d\ n_t\ P_t$

where $T_d$ = Taper on diameter = $\dfrac{D_6 - D_8}{2(L_4 - L_3)}$

$n_t\ P_t = -\sigma_{tang}\ (L_3 - L_2)/E$ = number of turns x pitch

E = modulus of elasticity

Giving $EI = -\sigma_{tang}(L_3 - L_2)(D_6 - D_8)/2(L_4 - L_3)$

The Von Mises equivalent stress at the tang was computed from $\sigma_{eq} = [\sigma^2_h + \sigma^2_{tang} + \sigma_h\ \sigma_{tang} + 3\ \tau^2]^{1/2}$ (ksi)

In the Pin:

Shear in neck during make-up

$$\tau = \frac{K_f T r}{J} = \frac{12 K_f T (D6/2)}{(\pi/32)(D^4_6 - D^4_4)}\ \text{(ksi)}$$

Peak Axial Stress in Neck

$\sigma_p = P_o K_{t3}/A_4$ (ksi)

Peak Axial Stress at First Thread in Pin

$\sigma_p = P_o K_{tt1}/A_4$ (ksi)

Hoop Stress in Pin at First Thread [Ref.6]

$$\sigma_h = \frac{-EI\ (D_5^2 - D_6^2)}{D_6(D_5^2 - D_4^2)} \quad (ksi)$$

where EI is as previously described.

Von Mises equivalent stress in neck

$$\sigma_{eq} = (\sigma_h^2 + \sigma_{pneck}^2 + \sigma_h\sigma_{pneck} + 3\,\tau^2)^{1/2} \quad (ksi)$$

Von Mises equivalent stress in first thread:

$$\sigma_{eq} = (\sigma_h^2 + \sigma_{pft}^2 + \sigma_h\sigma_{pft}^2 + 3\,\tau) \quad (ksi)$$

Shear in the splines during make-up:

$\tau$ = Force/Area

where Force = $12T/[(D_5 - d_s)/2]$ (kips)

Area = $(\pi/4)\ [(D_5 - d_s)^2\ (ls)]/ns$

Shear in Shoulder

Force/Area

where Force = $P_o$

Area = $\pi D_7\ (L_2 - L_1)$

When external load is applied to the connector, the change in stress in the neck or tang per incremental change in load is dependent upon the ratio of the tang or neck area to the sum of these areas (see figure 5.9 for a graphic explanation). For example, stress in the neck under external load is:

$$\sigma = P_o/A_4 + P\,\frac{\partial\sigma}{\partial P}$$

where $$\frac{\partial\sigma}{\partial P} = \frac{1}{A_4}\,[1 - (A_3/(A_3+A_4))]$$

and stress in the tang under external load is

$$\sigma = P_o/A_3 + P\,\frac{\partial\sigma}{\partial P}$$

where $$\frac{\partial\sigma}{\partial P} = \frac{1}{A_3}\,[1 - (A_4/(A_3+A_4))]$$

Stresses under maximum load are computed as follows:

In the Box:

Axial Stress in the Tang

$$\sigma = P_o/A_3 + P_{max} \frac{\partial \sigma}{\partial P}$$

where $$\frac{\partial \sigma}{\partial P} = \frac{1}{A_3} [1 - (A_4/(A_3+A_4))]$$

Peak Axial Stress at Inner Fillet

$$\sigma_p = P_{max} K_{t2}/A_6$$

Peak Axial Stress at Last Thread in Box

$$\sigma_p = P_{max} K_{tt2}/A_6$$

Peak Von Mises equivalent stresses are computed for the tang using the previous equation and assuming the hoop stresses are the same at maximum load as they are at preload.

Equivalent bending and membrane stresses are computed for the inner fillet and the last thread in the box. Membrane stresses are found from dividing the peak stress by the stress concentration factor. Bending stresses are computed from

$$\sigma_b = 6 \frac{|\sum \sigma_i \Delta x(x_i - x_c)|}{(\sum \Delta x)^2}$$

where $x_i$ = Centroid of incremental section
$x_c$ = Centroid of entire section
$\Delta x$ = Width of increment
$\sigma_i$ = Stress at $x_i$
(see figure 7)

The σi's are found from the equation of the stress profile

$$\sigma_i = K_t \sigma [\rho/(\rho + kx_i)$$ [Ref.10]

where $\rho$ is the fillet radius
$K_t$ is the stress concentration factor
$\sigma$ is the mean stress
k is a stress profile parameter

See figure 5.10 for an explanation of determination of k.

The criterion for allowable equivalent bending and membrane stress is defined as $\sigma_b + 1.5\ \sigma_m < 1.2\ \sigma_y$ [Ref.11].

In The Pin:

Peak axial stress in the weld/fillet section $\sigma_p = P_{max} K_{t1}/A_1$

Peak axial stress in the neck

$$\sigma_p = P_o K_{t3}/A_4 + P_{max} K_{t3} \frac{\partial \sigma}{\partial P}$$

where $\frac{\partial \sigma}{\partial P} = \frac{1}{A_4} [1 - (A_3/(A_3+A_4))]$

Peak axial stress at last thread of pin

$$\sigma_p = P_o K_{tt1}/A_4 + P_{max} K_{tt1} \frac{\partial \sigma}{\partial P}$$

Von Mises equivalent stresses and equivalent bending and membrane stresses were computed for the critical sections of the pin under the previous assumptions.

Fatigue Analysis:

Fatigue is analyzed at the section where the highest stress amplitude occured between preload and maximum load conditions. Fatigue load amplitudes $\Delta P$ and their corresponding number of cycles per year $N_i$ are inputted. Stress amplitude $\Delta\sigma$ is computed for each $\Delta P$ from $\Delta\sigma = \Delta P \partial\sigma/^2 P$. An equivalent stress amplitude $\Delta\sigma_{eq}$ according to a modified Goodman criterion was computed from $\Delta\sigma_{eq} = \Delta\sigma [\sigma_u/(\sigma_u - \sigma)]$ where $\sigma_u$ is the ultimate strength of the material and $\sigma$ is the mean stress due to pretension in the tendon. The modified Goodman criterion gives a conservative estimate of the effect of mean stress on the fatigue resistance.

The number of allowable cycles $N_{fi}$ at each $\Delta\sigma_{eq}$ was then computed from $N_{fi} = C\Delta\sigma^M$ where C and M are fit to the S/N curve of the chosen material. Cumulative fatigue damage per year d was computed from $d = N_i/N_{fi}$ and life in years was obtained from LIFE = 1/d.

Acceptance criteria for fatigue life was based on a cumulative damage ratio (Miner's No.) of 1.0 for a 100 year design life.

If the S/N curve already had assumed a mean stress, it was corrected by $S=S_m/(1 - \sigma_m/\sigma_u)$, where $\sigma_m$ is the assumed mean stress. It should be pointed out that the choice of $\partial\sigma$ is dependent upon which section is being analyzed. If the most critical section is at the last thread in the pin or the neck (i.e. a preload section), then $\partial\sigma/\partial P = 1 [1 -$

$(A_3/(A_3+A_4))]/A_4$. At any other section which is not preloaded, $\partial\sigma/\partial P = \sigma_{max}/P_{max}$.

## 5.3 Discussion of Results

The thick-walled connector design (figure 5.4) was modeled after the Hutton TLP connector design [Ref.1].

From the given .95 in. thread pitch [Ref. 12], a standardized buttress type power thread (figure 5.11) was chosen such that the thread height of 0.63 in. and the thread radius of .068 in. were defined as a function of pitch [Ref.9]. The fillet radii at the neck, in the box near the last thread, and at the ends of the connector were chosen such that the circular radius of the fillet was the difference in the axial radii of the sections joined by the fillet. The spline dimensions were estimated from a drawing in the cited reference. A spline depth of 1.0 in. and length of 8.5 in. were used. Spline width was determined from the diameter and the number of splines (9 splines).*

The thin-walled connector configuration (figure 5.5) was determined by equating the tube area of the thick-walled design to API line pipe of 1 in. wall thickness [Ref.5]. Connector diameters were then determined by equating section areas with the thick-walled configuration. Lengths were scaled down proportionately with wall thickness. Fillet radii were determined in the same manner as the thick-walled case. The thread chosen for the thin-walled connector is an API buttress casing thread [Ref.4] modified to fit the thread taper and scaled to 3 threads per inch (see figure 5.12). Spline length and depth were scaled proportionately with length and wall thickness. The number of splines was arbitrarily chosen at 12.

Fatigue calculations were carried out for a harsh North Sea environment using fatigue data taken from published sources [2]. Maximum load and pretension were taken from [1].

*In subsequent drawings of the connector, a 2:1 elliptical fillet was used. This reduces stress concentration by approximately 20%.

The designated material was a 3 1/2% Ni Cr Mo V steel with a minimum yield strength of 115 ksi and a minimum ultimate strength of 130 ksi [2]. Fatigue data for 3 1/2 Ni Cr Mo V steel is shown in section 4, figure 4.1a. Fatigue calculations were based on the free corrosion S/N curve and the design S/N curve. The curves in figure 4.1a assume a mean stress of 69 ksi. Since this is not the mean stress used in the connector, it was removed by $S=S_{69}/[1-\sigma_m/\sigma_u)]$ where $\sigma_m$=69 ksi. Subsequent calculations used a Goodman criterion to account for mean stress assuming a mean tension of 1760 Kips [1]. The equations for these curves, after correcting for mean stress, are as follows:

$$N_f = C\,\Delta\sigma^{-m}$$

where $\Delta\sigma$ is load amplitude (ksi)

$N_f$ is allowable number of cycles at $\Delta\sigma$

free corrosion curve:

$C = 3.5289 \times 10^{9}$ ksi$^{-1}$

$m = -2.357$

design curve:

$C = 5.9255 \times 10^{11}$ ksi$^{-1}$

$m = -4.837$

$C = 1.5362 \times 10^{14}$ $\Delta\sigma > 28.4$ ksi

$m = -6.524$ $\Delta\sigma < 28.4$ ksi

No damage at $\Delta\sigma < 12.8$ ksi

Stresses in ksi at critical sections for thick-walled and thin-walled connectors under preload and maximum load conditions are listed in tables 5.2, 5.3, 5.5 and 5.6. Torque required to achieve preload is also shown in tables 5.2 and 5.4. This torque is based on a 0.1 coefficient of friction and could change appreciably with a different value. It can be seen that all stresses lie well within the specified limits.

Fatigue data and results for Webster Hutton loading are shown in table 5.4 and 5.7. As previously mentioned, fatigue analysis was carried out for the section of the connector where the highest peak stress amplitude occured between preload and maximum load coanditions. In both thick-walled and thin-walled connectors, the section of highest stress amplitude was the last

thread of the pin. Parameters listed in the tables are described as follows:

Pamp = $\Delta P$ = Fatigue Load Amplitude

N = $N_i$ = Number of Cycles of $\Delta P$ per year

Sigamp = $\Delta\sigma_{eq}$ = Goodman Equivalent Stress Amplitude induced by $\Delta P$

NF = $N_f$ = Number of Allowable Cycles at $\Delta\sigma_{eq}$

Damage = d = $N_i/N_f$ = Damage per year from $\Delta\sigma_{eq}$

Total Damage = d = Total Damage per year

Life = 1/Total Damage

S/N curve A is the free corrosion curve and S/N curve B is the design curve.

The same fatigue analysis was done for various load spectra. Fatigue life of both connectors for curves A and B at each spectrum are shown in table 5.8. An acceptance criterion for fatigue life was set at 100 years for the design curve and a factor of safety of 30 for a 20 year life (i.e. 600 years) for the free corrosion curve. In all cases, the fatigue life corresponding to the design curve met the criterion. Extremely long life is attributable to many of the stress amplitudes falling below the 12.8 ksi endurance limit of the design curve. Fatigue life corresponding to the free corrosion curve met the criterion for all load environments except:

Webster Hutton

SOWM Atlantic, Mercier-Hutton RAO

SOWM North Sea, Mercier-Hutton RAO

## 5.4 References


1. OTC 4428, J.H. Tetlow, Hutton TLP Mooring System, Proceedings OTC 1982.

2. OTC 4449, M.M. Salama and J.H. Tetlow, Selection and Evaluation of High Strength Steel for Hutton TLP Tension Leg Elements, Proceedings OTC 1983.

3. ASME Boiler Code, Section VIII (Pressure Vessels) Div. 2.

4. API Std. 5B

5. API Spec. 5L

6. W.P. Schneider, Casing and Tubing Connection Stresses, J. Petroleum Technology, Vol. 34, No.8, August 1982.

7. A.P. Farr, Torque Requirements for Rotary Shouldered Connections and Selection of Connections for Drill Collars, ASME Paper No. 57-PET-19.

8. R.J. Roark and W.C. Young, Formulas for Stress and Strain, McGraw-Hill, 1982.

9. H.A. Rothbart, Mechanical Design and Systems Handbook, McGraw-Hill, 1964.

10. M.M. Hammouda, R.A. Smith, K.J. Miller, Elastic-Plastic Fracture Mechanics for Initiation and Propagation of Notch Fatigue Cracks, Fatigue of Engineering Materials and Structures, Vol. 2, pp.139-154, 1979.

11. ANSYS Post-Processor Manual.

12. Correspondence with Geoff Dearden, Hunting Oilfield Products.

13. API RP2T, "Recommended Practice for Planning, Designing and Constructing Tension Leg Platforms", (Draft), Sept. 1, 1984.

Table 5.2 Preload stresses for thick-walled connector (Webster Hutton loading)

Preload force is 957 kips
Torque required is 144 ft-kips

| | Shear due to make-up | Axial | Peak axial | Hoop | Von Mises equivalent |
|---|---|---|---|---|---|
| Tang | 0.72 | -30.61 | | | -30.2 |
| Box, first thread | | | | 0.90 | |
| Box, last thread | | | | 1.09 | |
| Neck | 0.286 | 6.02 | 12.85 | | 11.71 |
| Pin, last thread | | 6.02 | 20.41 | -0.241 | 19.16 |
| Pin first thread | | | | -2.83 | |

Table 5.3 Maximum load stresses for thick-walled connector (Webster Hutton loading)

MAXIMUM LOAD=5300 KIPS

| | Axial (Membrane) | Peak Axial | Von Mises Equiv. | Bending | Eq. bending +Membrane |
|---|---|---|---|---|---|
| Tang | -2.78 | | -2.46 | | |
| Box, inner fillet | 27.09 | 43.09 | 43.65 | 10.09 | 50.73 |
| Box, last thread | 27.09 | 92.89 | 93.44 | 12.78 | 53.42 |
| Weld/Fillet | 70.19 | 81.77 | | 19.66 | 124.93 |
| Neck | 33.84 | 72.38 | 72.26 | 14.94 | 51.44 |
| Pin, last thread | 33.84 | 114.97 | 114.85 | 16.50 | 67.25 |

Allowable axial (membrane) stress = 92 ksi.

Allowable eq. bending + membrane stress = 138 ksi.

TABLE 5.4 FATIGUE DATA:

THICK-WALLED CONNECTOR, WEBSTER HUTTON FATIGUE DATA

MAXIMUM STRESS AMPLITUDE OCCURS AT LAST THREAD IN PIN

| | | | S/N CURVE A | | S/N CURVE B | |
|---|---|---|---|---|---|---|
| PAMP(KIPS) | N | SIGAMP(KSI) | NF | DAMAGE | NF | DAMAGE |
| 2.070E+01 | 2.296E+06 | 4.779E-01 | 2.011E+10 | 1.142E-04 | 1.930E+13 | 0.000E+00 |
| 5.940E+01 | 1.495E+06 | 1.371E+00 | 1.676E+09 | 8.918E-04 | 1.178E+11 | 0.000E+00 |
| 9.020E+01 | 1.285E+06 | 2.082E+00 | 6.262E+08 | 2.052E-03 | 1.561E+10 | 0.000E+00 |
| 1.540E+02 | 8.150E+04 | 3.555E+00 | 1.775E+08 | 4.592E-04 | 1.174E+09 | 0.000E+00 |
| 2.024E+02 | 3.750E+03 | 4.673E+00 | 9.320E+07 | 4.024E-05 | 3.131E+08 | 0.000E+00 |
| 2.794E+02 | 9.750E+02 | 6.451E+00 | 4.359E+07 | 2.237E-05 | 6.583E+07 | 0.000E+00 |
| 3.388E+02 | 8.200E+02 | 7.822E+00 | 2.767E+07 | 2.963E-05 | 2.591E+07 | 0.000E+00 |
| 4.026E+02 | 1.040E+02 | 9.295E+00 | 1.843E+07 | 5.644E-06 | 1.125E+07 | 0.000E+00 |
| 4.818E+02 | 9.600E+02 | 1.112E+01 | 1.207E+07 | 7.955E-05 | 4.718E+06 | 0.000E+00 |
| 5.500E+02 | 1.450E+04 | 1.270E+01 | 8.833E+06 | 1.641E-03 | 2.487E+06 | 0.000E+00 |
| 6.358E+02 | 3.350E+02 | 1.468E+01 | 6.277E+06 | 5.337E-05 | 1.233E+06 | 2.716E-04 |
| 7.106E+02 | 1.420E+02 | 1.641E+01 | 4.829E+06 | 2.940E-05 | 7.202E+05 | 1.972E-04 |
| 7.942E+02 | 2.700E+02 | 1.834E+01 | 3.716E+06 | 7.267E-05 | 4.206E+05 | 6.420E-04 |
| 8.536E+02 | 1.420E+02 | 1.971E+01 | 3.135E+06 | 4.530E-05 | 2.967E+05 | 4.786E-04 |
| 9.196E+02 | 2.700E+00 | 2.123E+01 | 2.630E+06 | 1.027E-06 | 2.070E+05 | 1.305E-05 |
| 1.019E+03 | 7.500E-01 | 2.352E+01 | 2.067E+06 | 3.629E-07 | 1.262E+05 | 5.943E-06 |
| 1.082E+03 | 7.500E-01 | 2.499E+01 | 1.791E+06 | 4.187E-07 | 9.407E+04 | 7.973E-06 |

TOTAL DAMAGE USING CURVE A: 5.53858E-03
LIFE (YEARS) USING CURVE A: 180.5517

TOTAL DAMAGE USING CURVE B: 1.616297E-03
LIFE (YEARS) USING CURVE B: 618.6983

TABLE 5.7 FATIGUE DATA:

THIN-WALLED CONNECTOR, WEBSTER HUTTON FATIGUE DATA

MAXIMUM STRESS AMPLITUDE OCCURS AT LAST THREAD IN PIN

| | | | S/N CURVE A | | S/N CURVE B | |
|---|---|---|---|---|---|---|
| PAMP(KIPS) | N | SIGAMP(KSI) | NF | DAMAGE | NF | DAMAGE |
| 2.070E+01 | 2.296E+06 | 4.879E-01 | 1.916E+10 | 1.199E-04 | 1.746E+13 | 0.000E+00 |
| 5.940E+01 | 1.495E+06 | 1.400E+00 | 1.597E+09 | 9.363E-04 | 1.066E+11 | 0.000E+00 |
| 9.020E+01 | 1.285E+06 | 2.126E+00 | 5.965E+08 | 2.154E-03 | 1.413E+10 | 0.000E+00 |
| 1.540E+02 | 8.150E+04 | 3.630E+00 | 1.691E+08 | 4.821E-04 | 1.063E+09 | 0.000E+00 |
| 2.024E+02 | 3.750E+03 | 4.770E+00 | 8.877E+07 | 4.224E-05 | 2.933E+08 | 0.000E+00 |
| 2.794E+02 | 9.750E+02 | 6.585E+00 | 4.152E+07 | 2.348E-05 | 5.957E+07 | 0.000E+00 |
| 3.389E+02 | 8.200E+02 | 7.985E+00 | 2.636E+07 | 3.111E-05 | 2.345E+07 | 0.000E+00 |
| 4.026E+02 | 1.040E+02 | 9.489E+00 | 1.755E+07 | 5.925E-06 | 1.018E+07 | 0.000E+00 |
| 4.819E+02 | 9.600E+02 | 1.136E+01 | 1.150E+07 | 8.351E-05 | 4.270E+06 | 0.000E+00 |
| 5.500E+02 | 1.450E+04 | 1.296E+01 | 8.414E+06 | 1.723E-03 | 2.251E+06 | 6.443E-03 |
| 6.358E+02 | 3.350E+02 | 1.499E+01 | 5.979E+06 | 5.603E-05 | 1.116E+06 | 3.001E-04 |
| 7.106E+02 | 1.420E+02 | 1.675E+01 | 4.600E+06 | 3.087E-05 | 6.518E+05 | 2.179E-04 |
| 7.942E+02 | 2.700E+02 | 1.872E+01 | 3.539E+06 | 7.629E-05 | 3.806E+05 | 7.094E-04 |
| 8.536E+02 | 1.420E+02 | 2.012E+01 | 2.986E+06 | 4.756E-05 | 2.685E+05 | 5.289E-04 |
| 9.196E+02 | 2.700E+00 | 2.167E+01 | 2.505E+06 | 1.078E-06 | 1.873E+05 | 1.442E-05 |
| 1.019E+03 | 7.500E-01 | 2.401E+01 | 1.969E+06 | 3.810E-07 | 1.142E+05 | 6.567E-06 |
| 1.082E+03 | 7.500E-01 | 2.551E+01 | 1.706E+06 | 4.396E-07 | 8.513E+04 | 8.810E-06 |

TOTAL DAMAGE USING CURVE A: 5.81482E-03
LIFE (YEARS) USING CURVE A: 171.9744

TOTAL DAMAGE USING CURVE B: 8.22906E-03
LIFE (YEARS) USING CURVE B: 121.5206

TABLE 5.8. Fatigue life in years for TLP tendon connector designs

| FATIGUE DATA | MAXIMUM TENSION | PRE-TENSION | THICK-WALLED CONNECTOR LIFE CURVE A | THICK-WALLED CONNECTOR LIFE CURVE B | THIN-WALLED CONNECTOR LIFE CURVE A | THIN-WALLED CONNECTOR LIFE CURVE B |
|---|---|---|---|---|---|---|
| 1 | 5300 | 1760 | 181 | 619 | 172 | 122 |
| 2 | 5300 | 1760 | 1944 | NO DAMAGE | 1851 | NO DAMAGE |
| 3 | 1720 | 1085 | 2641 | 2.8E+11 | 2537 | 2.6E+11 |
| 4 | 2075 | 1275 | 2261 | 1.1E+10 | 2171 | 9.9E+9 |
| 5 | 2075 | 1275 | 2213 | 4.3E+10 | 2126 | 4.0E+10 |
| 6 | 2475 | 1475 | 2030 | 4.8E+7 | 2005 | 4.5E+7 |
| 7 | 4275 | 2375 | 986 | 7857 | 941 | 7112 |
| 8 | 3275 | 1875 | 683 | 31895 | 654 | 29169 |
| 9 | 2075 | 1275 | 2161 | 1.1E+9 | 2075 | 9.9E+8 |
| 10 | 3275 | 1875 | 495 | 6569 | 474 | 6007 |
| 11 | 2975 | 1725 | 1508 | 205823 | 1445 | 188526 |
| 12 | 3975 | 2225 | 242 | 2609 | 231 | 2375 |

Tensions in kips
Curve A is free corrosion S-N curve (Fig. 7 OTC 4449, mean stress removed)
Curve B is design S-N curve (Fig. 7 OTC 4449, mean stress removed)
MATERIAL: 3.5% NiCrMoV

Fatigue Data Key:

1. Webster Hutton
2. Webster tether
3. SOWM Pacific, Chou RAO
4. SOWM Gulf, Chou RAO
5. SOWM Gulf, Paulling RAO
6. SOWM Gulf, Tan RAO
7. SOWM Gulf, Dillingham RAO
8. SOWM Gulf, Mercier-Hutton RAO
9. SOWM Atlantic, Chou RAO
10. SOWM Atlantic, Mercier-Hutton RAO
11. SOWM North Sea, Chou RAO
12. SOWM North Sea, Mercier-Hutton RAO

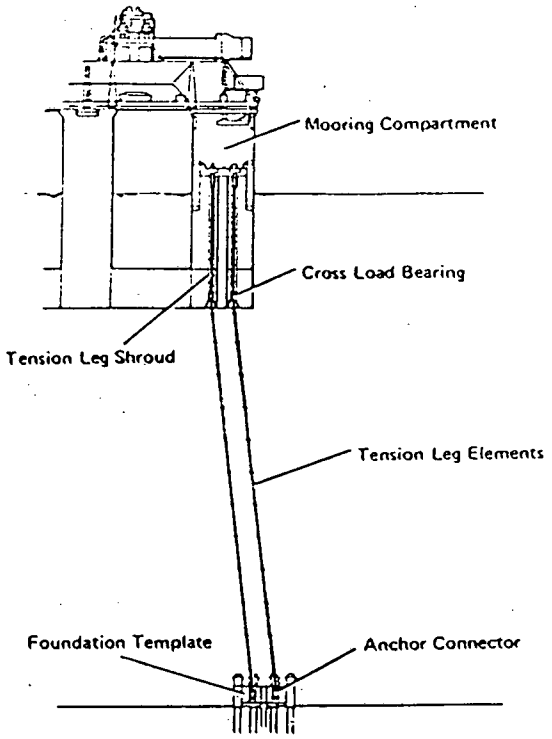


Figure 5.1 (from Tetlow)

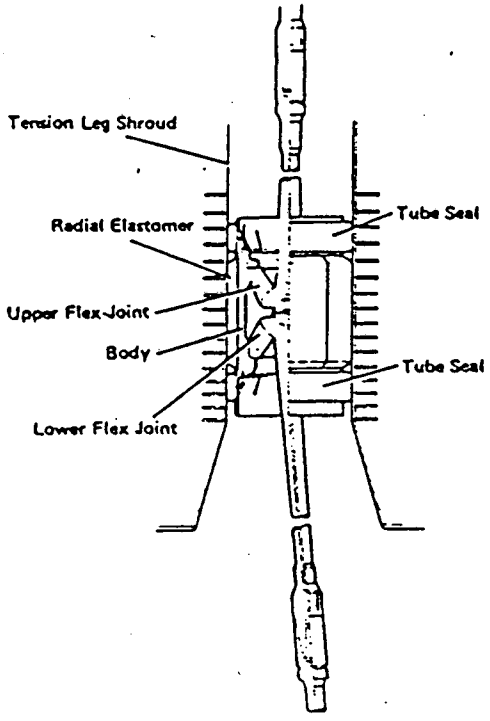


Cross Load Bearing
(From Tetlow)

Figure 5.2

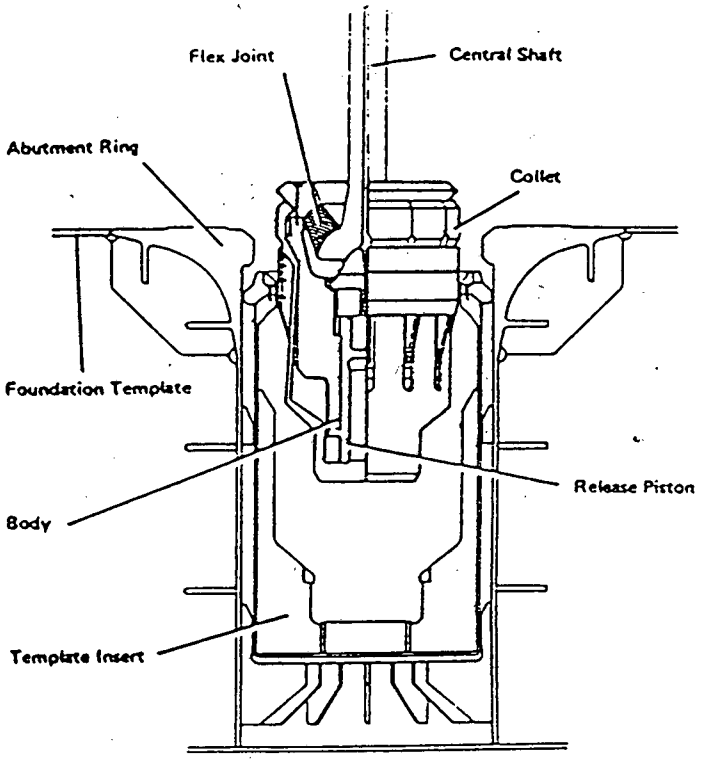


Anchor Connector
(Deployment/Retrieval Position)
(From Tetlow)

Figure 5.3

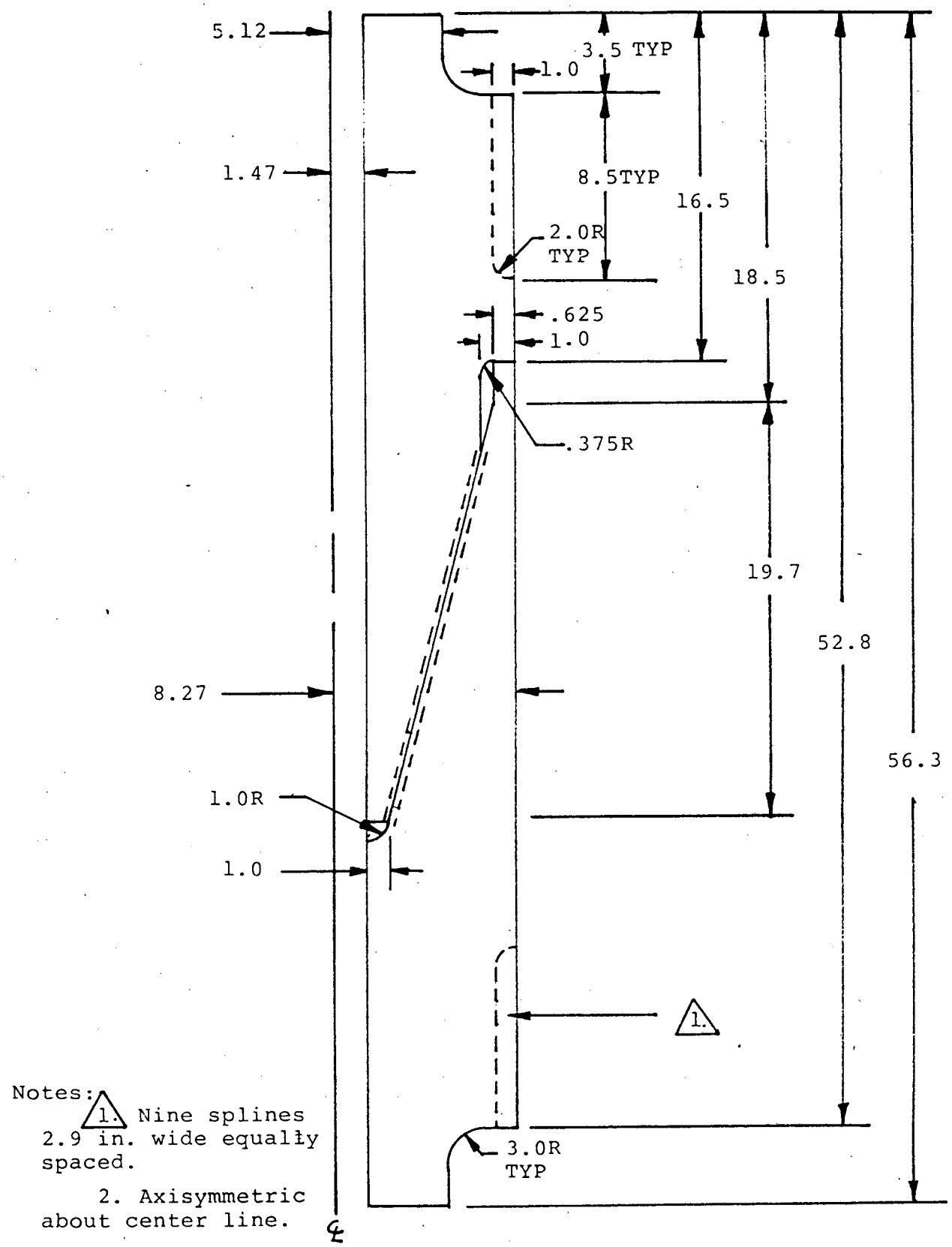


Notes:

1. Nine splines 2.9 in. wide equally spaced.

2. Axisymmetric about center line.

Figure 5.4 - Thick walled connector.

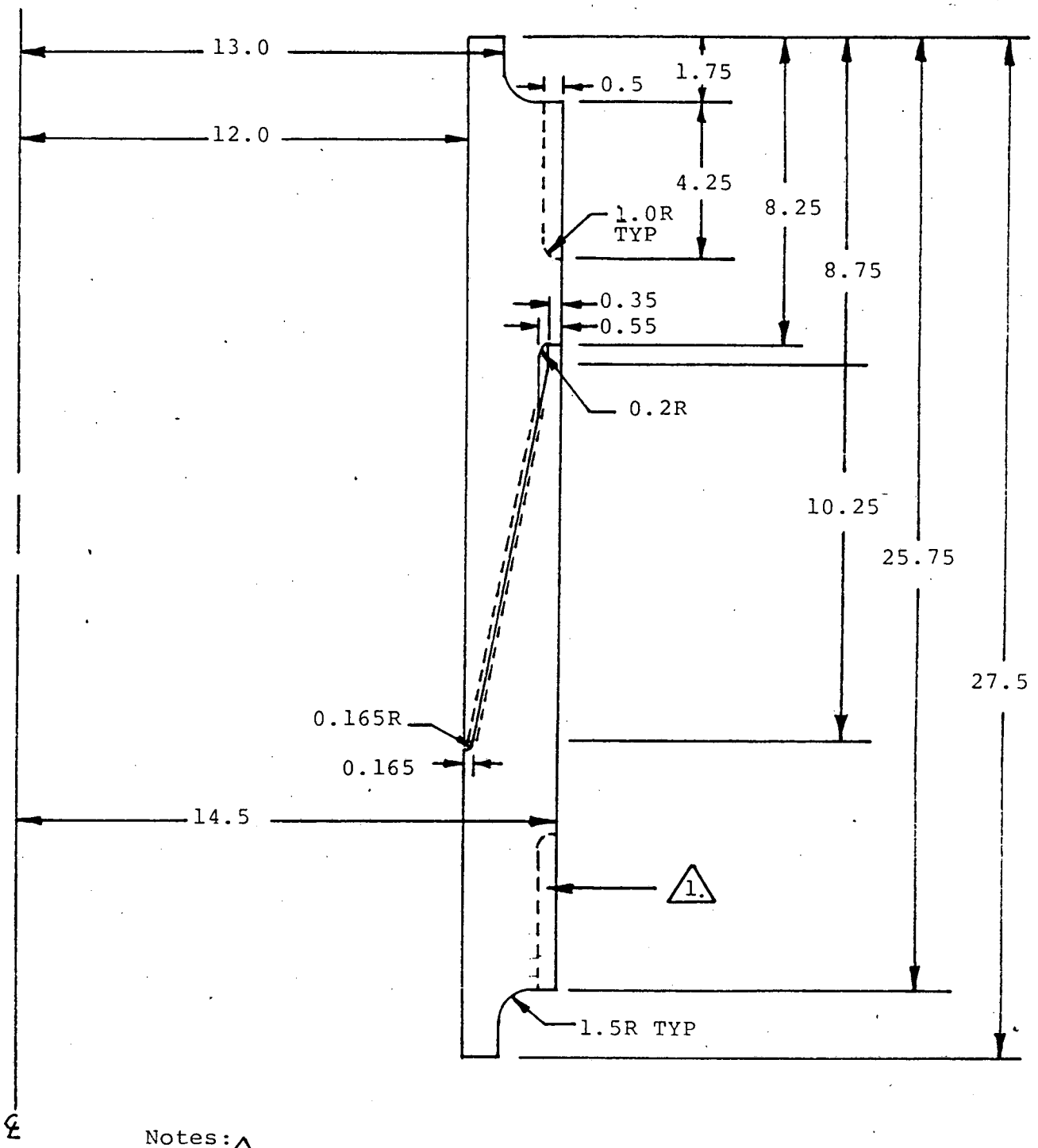


Notes:
1. Twelve splines 3.8 inches wide, equally spaced.
2. Axisymmetric about center line.

Figure 5.5 - Thin walled connector.

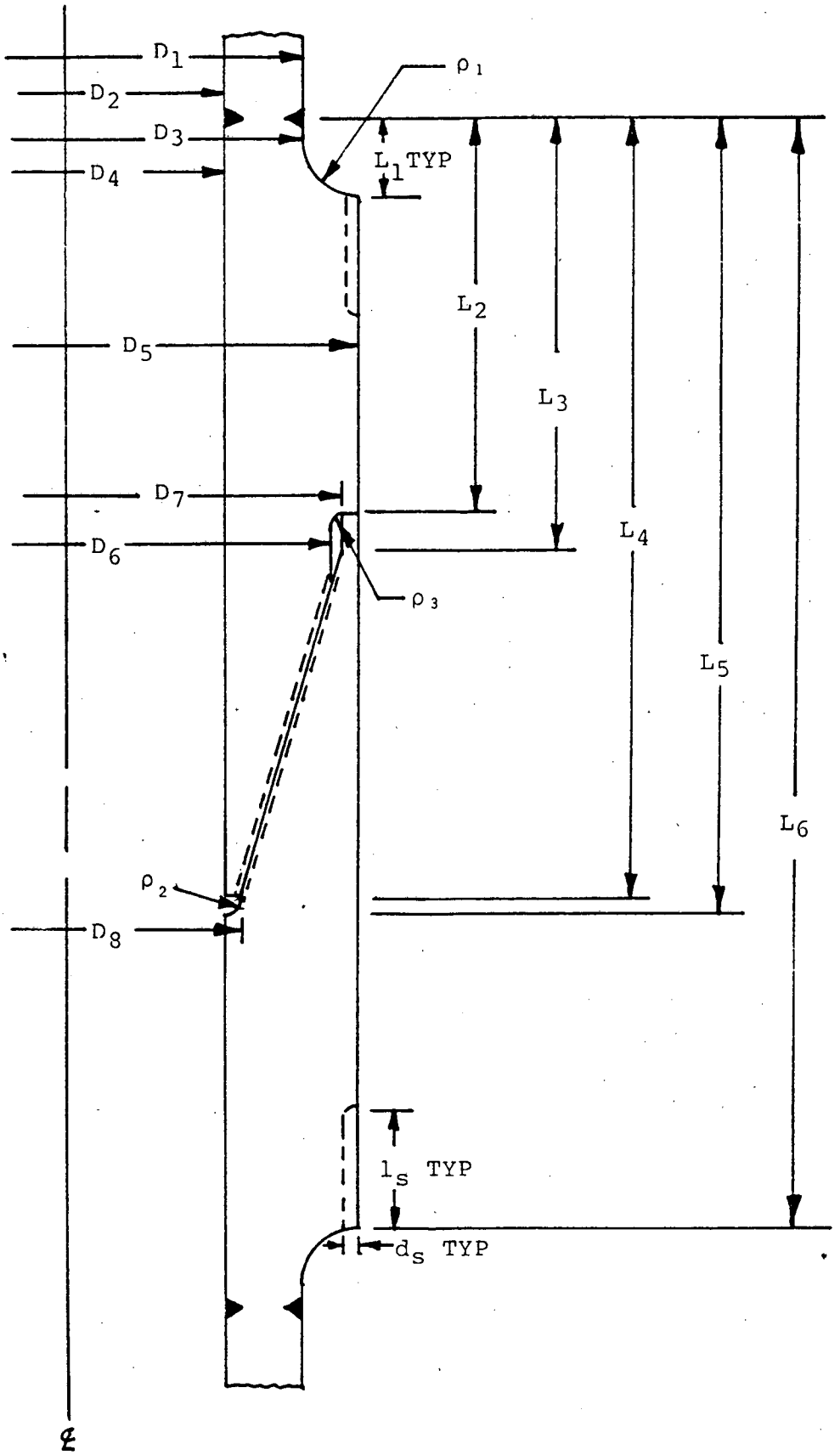


Figure 5.6 - Computer analysis connector model.

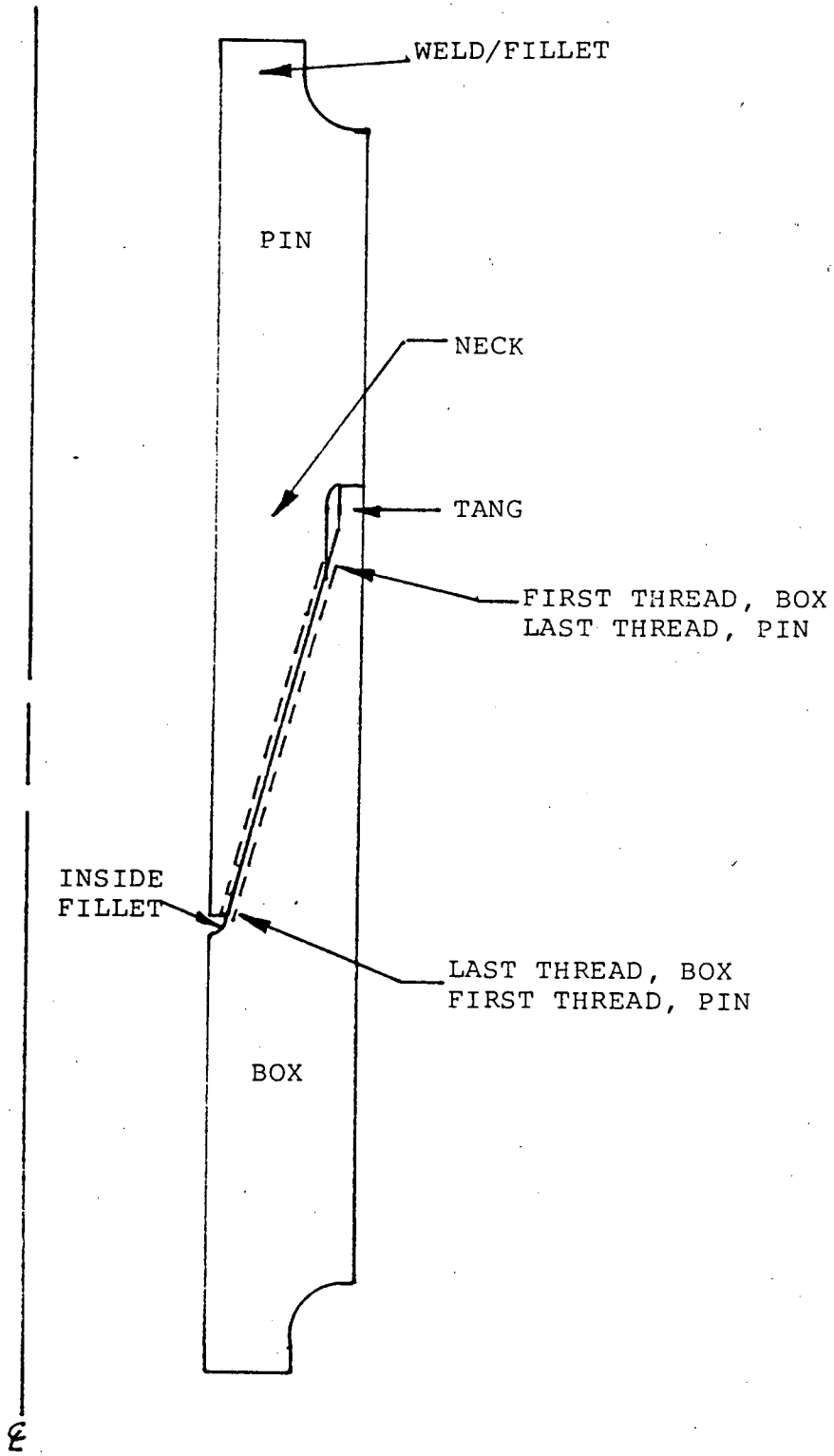


Figure 5.7 - Identification of connector sections.

Stress Concentration Factor for Square
Shoulder Fillet in Circular Shaft
(Elastic Stress, Axial Tension)

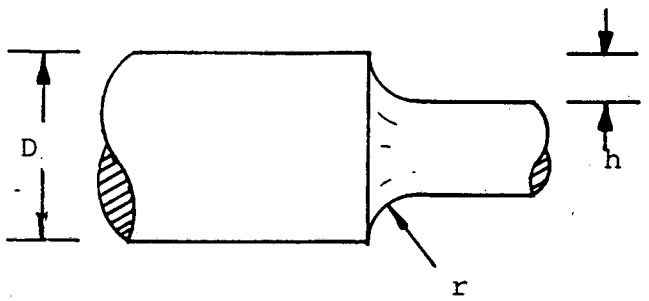


$$k_t = K_1 + K_2\ (2h/D) + K_3\ (2h/D)^2 + K_4\ (2h/D)^3$$

where

| | $0.25 < h/r < 2.0$ | $2.0 < h/r < 20.0$ |
|---|---|---|
| $K_1$ = | 0.927+1.149 h/r -0.086 h/r | 1.225+0.831 h/r -0.010 h/r |
| $K_2$ = | 0.011-3.029 h/r +0.948 h/r | -1.831-0.318 h/r -0.049 h/r |
| $K_3$ = | -0.304+3.979 h/r -1.737 h/r | 2.236-0.522 h/r -0.176 h/r |
| $K_4$ = | 0.366-2.098 h/r +0.875 h/r | -0.630 +.009 h/r -0.117 h/r |

ref. Roark and Young, Formulas for Stress and Strain, McGraw-Hill

Figure 5.8 - Model of Stress Riser used in Connector Analysis.

$P_s$ = Separation Force

$P_o$ = Preload Force

$A_3$ = Area of Tang

$A_4$ = Area of Neck

$\sigma_o$ = Preload Stress=$P_o/A_4$

$\sigma_s$ = Stress at Separation=$P_s/A_4$

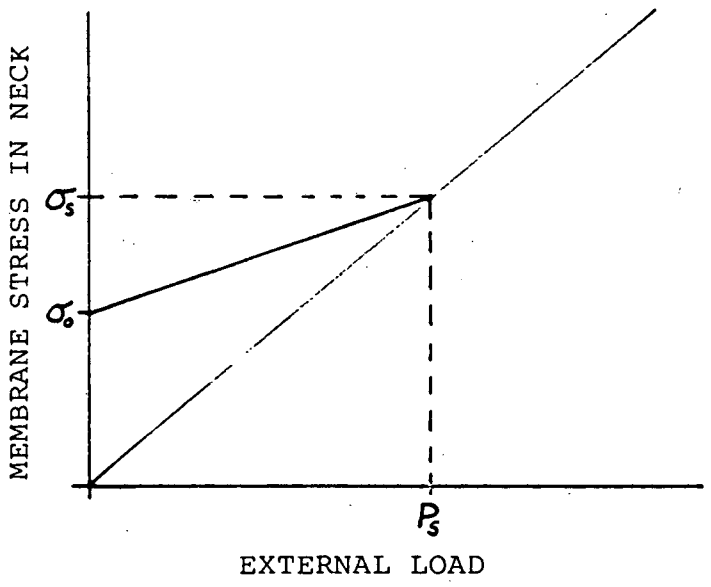


For preload connector, $\sigma = \left(\frac{\partial\sigma}{\partial P}\right) P + \sigma_o$ at neck

$$\frac{\partial\sigma}{\partial P} = \frac{\sigma_s-\sigma_o}{P_s-0} = \frac{P_s/A_4-P_o/A_4}{P_s} = \frac{1}{A_4}\left(\frac{P_s-P_t}{P_s}\right)$$

Using the defination of separation force: $P_s=P_o\left(\frac{A_3+A_4}{A_3}\right)$

$$\frac{\partial\sigma}{\partial P} = \frac{1}{A_4}\left(\frac{P_o[(A_3+A_4)/A_3]-P_o}{P_o[(A_3+A_4)/A_3]}\right) = \frac{1}{A_4}\left(\frac{[(A_3+A_4)/A_3]-1}{[(A_3+A_4)/A_3]}\right) = \frac{1}{A_4}\left(1-\left(\frac{A_3}{A_3+A_4}\right)\right)$$

Derivation is similar for $\frac{\partial\sigma}{\partial P}$ at tang

Figure 5.9 - Derivation of $\frac{\partial\sigma}{\partial P}$ at Neck of Preloaded Connector.

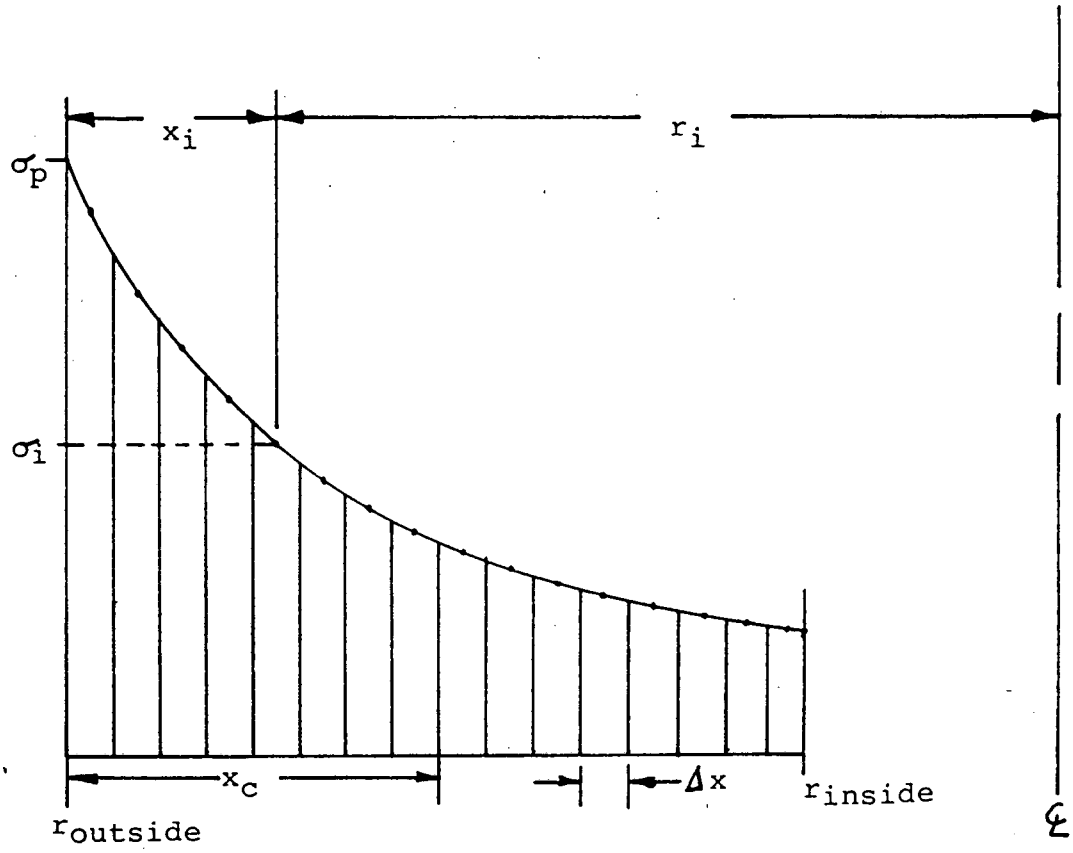


$X_i = r_{outside} - r_i$, $\sigma_i = \sigma_p [\rho/(\rho+KX_i)]^{1/2}$ $\sigma_p = \sigma_m K_T$, $\sigma_m = P/A$

$X_c = (r_{inside} + r_{outside})/2$, $K_T$=stress concentration factor, $\sigma_b = 6\left|\sum \sigma_i \Delta_x (x_i - x_c)\right| / (\sum \Delta X)^2$

To find K in modified Neuber equation, define incremental force: $\Delta F = \sigma_i \Delta_r (2\pi r_i)$, and total force: $F_T = 2\pi \Delta r \sum \sigma_i r_i$

Find K for which $\frac{F_t}{A} = \frac{2\pi\Delta r}{\pi(r_{outer}^2 - r_{inner}^2)}$ $\sum \sigma_i r_i = P = \sigma_m \overline{A}$

Note: This modified Neuber equation is for the entire thickness of the section. Close to the stress riser, K=4 as referenced.

Figure 5.10 - Representation of Stress Profile Showing Parameters.

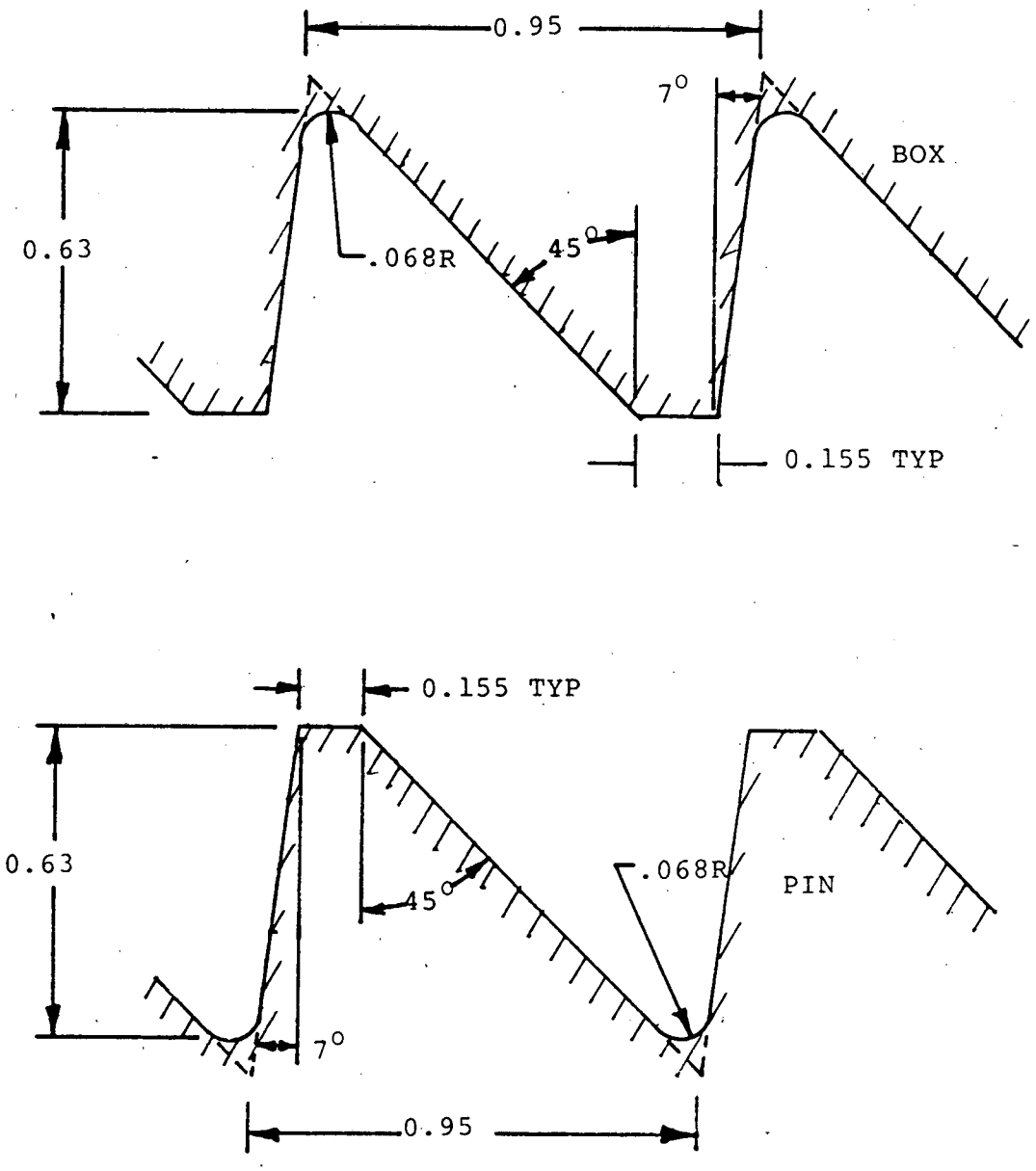


Note:

1. Crests are parallel to cone.

Figure 5.11 - Buttress thread for thick walled connector.

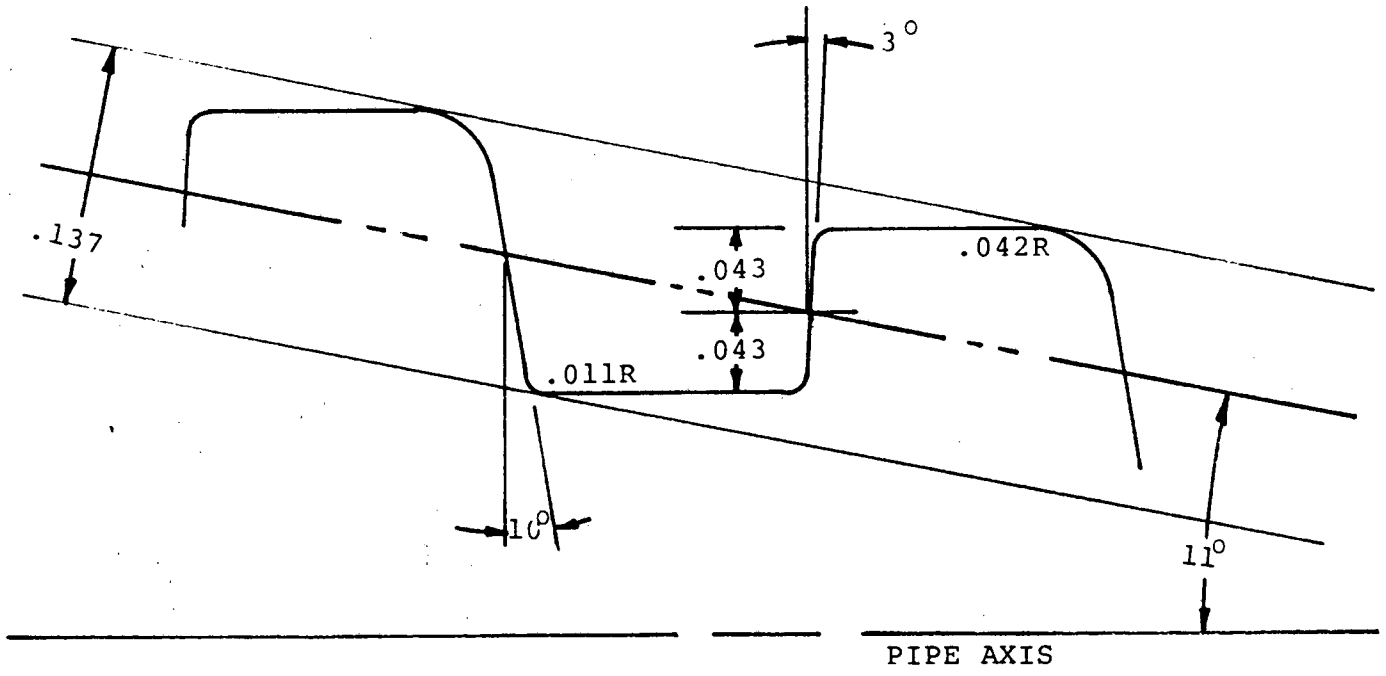


Notes:

1. Scale = 10x  3 threads/inch
2. Crests are parallel to pipe axis.

Figure 5.12 - Thin wall connector, buttress casing thread.

# 6.0 TLP Inspection Systems

## 6.1 Survey of methods for TLP inspection

### 6.1.1 Introduction

Tension leg platforms operate with legs that are subject to long term exposure to seawater, high mean-tensile stress, and a high number of cycles at relatively low stress ranges over their lifetime. Fatigue life is an important criteria in leg design. The Draft API (American Petroleum Institute) recommended practice on TLP design calls for materials with toughness to avoid unstable crack growth for readily detectable flaw sizes [14]. Thus, the inspection methodology and sensitivity is critical to the design. The inspection methodology should detect deterioration and allow corrective action in a timely manner. Inservice inspection is preferred even if it is less thorough because all tendons in the platform may be covered rather than a selected few.

The in service inspection method must inspect for defects smaller than the critical flaw size. The technique must be repeatable and capable of observing crack growth. Because of the tension legs' stress direction, crack growth in the legs will be radial/circumferential. Locations of crack initiation and growth will be at areas of geometric discontinuity where stress concentrations exist, such as thread roots, shoulders, grooves, and upset transitions. In welded structures cracks may initiate at weld defects and in the heat affected zone. The method of examination must be sensitive to cracks at these locations.

In service inspection requires the equipment be adaptable to the environment and geometric configuration under evaluation. This implies operation around marine environments, deployment on an offshore platform, operation at pressures with depth of inspection and inspection over long lengths on cylindrical geometry. Presently, nondestructive evaluation techniques employed offshore are applied underwater by divers and manned or unmanned submersible vehicles. These techniques include visual, magnetic particle, ultrasonic and radiographic inspections (Ref.1). In practice, these techniques have not been used in fully automated modes for offshore work but have required manual operation to some degree. Tension leg designs with central bores offer an environment for development of fully automated inspection systems.

The nondestructive evaluation techniques that have been employed in offshore applications or that could be considered for tension leg in service examination include visual, magnetic particle, magnetic field disturbance, eddy current, radiography, tomography, ultrasonics, and acoustic emission.

### 6.1.2 Visual Inspection

Visual inspection, often using optical aids, is the most common means of inspecting offshore structures. The probing medium is visual light that is reflected from the surface to detectors such as the human eye or television cameras. This technique is sensitive to cracks that are open to the surface and of sufficient size to be resolved by the detector. In many cases the cracks cause deformation of surface layers, such as aluminum flame spray, which aids in the detectability of the presence of cracks. Marine life coverings must be removed for inspection and limitations such as small field of view, reflections in water, and visibility allow only the detection of large open cracks (Ref.2).

For tension leg inspection, critical size defects will be subsurface such that visual inspection is of little value. Although visual inspection of the external leg for corrosion effects and structural damage is recommended, it cannot be the primary technique for tension leg in service evaluation.

### 6.1.3 Magnetic Particle

Magnetic particle inspection is the most commonly used method for offshore underwater structural inspection except visual (Ref. 1, Ref. 3). The probe media is a magnetizing current. Defects which distort the magnetic field also distort the magnetic particle pattern applied to the part surface indicating the defect presence. The technique is applicable to ferromagnetic materials. Sensitivity to surface cracks is superior to visual inspection. Subsurface defects may also be detected, but the detectability will be restricted by the field strength, object thickness, and flaw size. The surface of the part must be clean and relatively smooth.

Application in the marine environment on the outside of the leg is

difficult. Magnetic particles sprayed on the test area may not be fully attracted by the magnetic flux, water currents may take away material resulting in a reflecting cloud when black light is applied to observe the fluorescent particles, and loose particles may assemble on the diver's mask. Magnetic particles suspended in a foil package can be used for better control and permanent image (Ref.2), or magnetic tape (magnetographic method) may be used to detect and record the stray magnetic flux due to defects (Ref.4).

For tension leg inspection, magnetic particles would not be sensitive to the thread root flaws of critical size in threaded connector designs. It would be applicable to defects where cracks initiate at an accessible surface for inspection. However, magnetic particle inspections do not accurately indicate flaw depth (Ref. 1, Ref. 5).

### 6.1.4 Magnetic Field Disturbance

Magnetic fields can be used similarly to the magnetic particle inspection but with the use of a detector rather than the particles. This technique will be less sensitive to flaws and insufficient for the tension leg inspection requirements. An automated system could be developed for internal or external application.

### 6.1.5 Radiography

Radiographic inspection is sensitive to flaws throughout a body under inspection. The probe medium is electromagnetic radiation in the x-ray/gamma ray range. Changes in material are detected by changes in the beam attenuation. Cracks must be oriented along the axis of the radiation beam for detection.

Inspection of structural welds using radiography is routine in industry, but may not be practical as an in service tool in the offshore tension leg application. Cracks at the root of threads in the threaded connector may also be detected with radiography but would require technical sophistication. Sensitivity to two parts in one hundred is typical such that a crack of 2 mm depth should be detectable in a 4 inch thick region provided the orientation is optimized. However, access to both sides of the object is required. In the tension

leg application, the x-ray source and detector would be located with one inside the leg and one outside. The outside dimensional changes for shoulder and grooves could be difficult to accommodate adequately.

High voltages and/or radioactive materials would be required to be handled over the entire length of the leg. Inspection times could be long depending on the x-ray beam strength, detection method, and sensitivity requirement. For the thin walled threaded connector design presented in this report, a relatively high energy source would be desired (Ir-192 or a 1MeV x-ray machine). The Ir-192 would require several minutes per exposure and many exposures (perhaps every thread) would be required to assure optimized orientation. Detection by film techniques requires post inspection development and examination. Handling in the offshore environment would be difficult. Digital image detection techniques could be developed to provide real-time or near real-time imaging. In threaded regions, the complex geometry would be confusing for the image analysis. In welded regions the interpretation would be less difficult but equipment handling would remain difficult. The development of radiographic techniques would be desired only if no other methods were acceptable.

### 6.1.6 Tomography

An innovation in radiation detection techniques, that has potential application to leg inspection, is computed tomography (CT). The CT device takes data by passing a beam of radiation through the object at a variety of angles and reconstructing a cross sectional view image (Ref.6). The equipment is large and requires accurate positioning. Data acquisition and reconstruction times may be on the order of tens of minutes. These systems have been used with success on nuclear power plant system pipe (Ref. 7). Although sensitivity should be acceptable, deployment and expense are prohibitive.

### 6.1.7 Eddy Current

Eddy current methods are used for crack detection in a variety of industrial products and in service inspection in the utility and aerospace industries. The probing medium is an induced current. The technique, although sensitive to small cracks, has relatively low penetra-

tion and would not be applicable to the threaded region of the tension leg coupling (Ref.5). Welded regions, shoulders and grooves could be inspected with eddy currents. The depth of penetration for the inspection is inversely proportional to the square root of the electrical conductivity, frequency and magnetic permeability. In ferromagnetic materials, local variations in magnetic permeability can make cracks difficult to size accurately. Coatings of variable thickness or properties can also inhibit accurate measurement of crack size. Eddy current equipment is rugged and and can be used at relatively high speeds of inspection.

### 6.1.8 Acoustic Emission

Acoustic emission has been used for offshore structure evaluations (Ref. 1) and has been considered for monitoring tension legs (Ref.3). This technique uses passive ultrasonic listening devices to detect acoustic energy generated during the growth of a crack. Unfortunately, acoustic emission cannot accurately size defects and would have difficulty in accurately locating defects in the complicated thread geometry.

### 6.1.9 Ultrasonic

Ultrasonic inspection is a common method of crack detection in in service examination. An acoustic beam probes the material reflecting the beam at surfaces and cracks. Ultrasonics is one of the most suitable methods for crack detection because it responds to the presence of a crack surface, not associated aspects such as the volume in the case of radiography.

The sensitivity of ultrasonics is a function of the frequency, material, and geometry. It can be a very sensitive method for detecting cracks in the millimeter range in structural applications. Ultrasonics can be transmitted over relatively long distances in most structural metals.

Both offshore welded structure and threaded connectors can be inspected (Ref. 15, 3). Near surface resolution can be difficult with ultrasonics. Bounce path techniques overcome this provided the surface

is regular (i.e. weld crowns removed). The equipment used to perform ultrasonic inspection can also be deployed in a variety of configurations. This includes fully automated schemes. Inspection time is dependent on the volume of material to be inspected and the beam size. Relative to other NDE methods, ultrasonic inspections can be rapid.

The preferred method for adaptation to the tension leg in service inspection problem, ultrasonics has several inherent advantages (Ref. 5):

- o penetrates substantial depths in many materials,
- o tests from one surface,
- o sensitive to minute flaws,
- o comparatively accurate in determining flaw depth and size,
- o electronic operation for rapid inspection, adaptable to automatic inspection and harsh environments.

Ultrasonic systems are used for flaw detection in offshore application with success (Ref. 1, 9). The only existing tension leg platform (Hutton, Conoco, U.K.) uses a fully automated ultrasonic examination system (Ref. 8).

## 6.2. Ultrasonic Inspection

### 6.2.1 Introduction

Ultrasonic inspection is the most suitable NDE method for tension leg in service examination. The method is excellent for crack detection, is sensitive to flaws in the millimeter range, can provide sizing information, is useful in structural steels over large distances, can be used from one side of a part, can be adapted to complex geometries, and can be fully automated. In threaded connector designs no other method can provide all of the above mentioned capability. In tension leg designs where surface defect detection is sufficient other methods may be preferred.

For this study, thread connector tension leg designs have been considered. Welded structure inspections schemes may be found in handbook literature (Ref. 16). Inspection schemes for large threaded connectors have not been addressed until recently (Ref. 3). The pulse echo ultrasonic method is employed for the tension leg inspection.

An ultrasonic transducer is pulsed at a specific frequency. The ultrasonic beam is reflected and refracted by surfaces which intercept the wavefront. Defects, such as cracks, will reflect the ultrasonic beam back on itself. The reflected beam will interact with the ultrasonic transducer generating a signal indentifying the defect.

### 6.2.2 Assumptions

The ultrasonic inspection of tension leg elements assumes that ultrasound can be coupled into the element under inspection. The designs considered in this report contain a central bore of the tension leg. The bore may be filled with a liquid couplant such as water. In actual practice, a corrosion inhibiting water solution or oil would be used. For calculational purposes, the assumption of water is sufficiently accurate. It is assumed that there is access to the central bore for a mechanical tool which holds the ultrasonic transducer or transducer array. The ultrasonic beam angles are then determined by geometric considerations.

The steel structural material is assumed to be fine grained and homogenous for the most part. Fine grained means grain sizes on the

order of 1/100th of the wavelength of ultrasound. Table 6.1 lists the wavelengths of ultrasound in steel as a function of frequency. When the grain size approaches 1/10th the wavelength grain scattering of the ultrasonic beam becomes appreciable and testing may become impossible.

The detectability of a defect will be affected by the wavelength. At defect sizes smaller than a wavelength, Rayleigh scattering reduces the amount of coherently reflected energy and therefore reduces detectability. From Table 6.1, the use of transverse (or shear) waves has an advantage because the wavelength at a given frequency is smaller than for longitudinal (or compressional) wave.

### 6.2.3 Geometry Considerations

The ultrasonic inspection technique sends ultrasonic beams into the tension leg at various angles. The beam angle is determined by geometric considerations for access and to the degree that can be accommodated by orientations to optimize back reflection or shadowing effects from flaws. The ultrasonic beam may be generated in the inner bore of the leg or on the outside of the leg. For this study, two tension leg designs are considered: thick walled tubular and thin walled tubular steel with threaded couplings. In both cases, access to the inner bore is possible. This is, therefore, the preferred location because it is protected and controlled, not in the open sea/marine environment. Ultrasound entering the leg from the inner bore will be directed such that refractions at water-steel interface will create the proper beam angle in the tension leg. The acoustic beam cannot be passed through the threaded region. Therefore, to inspect the box thread region, the ultrasound must be reflected off the outer wall to the thread roots. The signal will be reflected back along its original path for detection.

The complete tension leg is composed of elements consisting of a shaft region with a box and pin at each end. These elements are joined at the box and pin with a threaded coupling. The leg is connected to the anchor plate with an anchor connector and at the platform has a crossload bearing element which allows flexing of the leg relative to the platform. The central portion of the anchor connector and crossload bearing can be inspected in the same manner as the main shaft of the

leg elements. The other portions of the anchor connector and crossload bearing cannot be readily inspected with the same system proposed in this study. Material changes, access, and geometry all complicate the anchor connector and crossload bearing. These components are in compression, however, and are not considered as critical as the tension member.

Ultrasound can be used in the form of longitudinal or transverse waves. The selection of the mode to be used is a function of the required beam angles and the optimization of transmittance across boundaries as a function of those angles. For the tension leg examination, the angles to be used for regions of interest around the box/pin joint are indicated in Table 6.2. Transverse (shear waves) are used in order to create beams at these angles. And, as stated earlier, transverse waves will be more sensitive to small flaws. Figure 6.1 shows the beams considered for the regions of interest. The shaft portion of the elements and the central shaft in the flex joint and box and pin will be inspected by beams equivalent to the make-up shoulder and pin preload shoulder examination. Sensitivity to defects in the shaft region will be in the same range as the equivalent regions at the coupling.

The overall time to perform an inspection is a function of the volume of material to be tested, speed of data acquisition and analysis equipment, and the capability of the mechanical scanning equipment. The thick walled tubular design is inspectable in a time frame of about 2.5 to 5 hours per element (Ref. 9) for a state-of-the-art data acquisition and analysis system. The thin walled tubular design should be inspectable in approximately the same time frame.

### 6.2.4 Equations of Interest

Several equations are of interest for calculations regarding the inspectability of the tension leg. The law of refraction determines the angle of the ultrasonic beam in the bore fluid to generate the proper transverse wave angles in the steel.

$$\frac{\sin \phi_w}{\sin \phi_s} = \frac{V_w}{V_{st}} \qquad (6.1)$$

where $\phi_w$ = angle from the normal in water,

$\phi_s$ = angle from the normal in steel leg component,

$V_w$ = velocity of ultrasound in water, and

$V_{st}$ = velocity of transverse waves in steel

Using values of V from Table 6.1 and angles $\phi_s$ from Table 6.2, the angles $\phi_w$ are calculated for Table 6.2.

The echo transmittance is a value that accounts for the losses experienced by a beam passing into and out of the leg boundary. The beam, when it meets an interface, will be refracted and/or reflected. The amount of energy that passes across the boundary to enter a material, and later returns for the pulse echo detection will be a function of the materials, water/steel, and the angle. Figure 6.2 is a plot of the values of the coefficient for the transmittance labelled $C_1$ as a function of angle.

Attenuation of ultrasound is given by

$$p = p_o \, e^{-\alpha 2d} \qquad (6.2)$$

where p = sound pressure

$p_o$ = initial sound pressure

d = distance in material travelled to reflector and 2d is total path for a pulse echo beam

$\alpha$ = the attenuation coefficient in Nepers/unit distance.

The value of the attenuation coefficient is a strong function of manufacturing parameters. Worked steel has low attenuation below 1 Np/m, slightly alloyed cast steel is typically 1 to 10 Np/m, and highly alloyed cast steel is greater than 10 Np/m for typically employed ultrasonic frequencies of inspection (Ref. 10).

The attenuation coefficient is composed of an absorption and a scattering term.

$$\alpha = \alpha_s + \alpha_a \qquad (6.3)$$

For steel used in tension leg applications a value of $\alpha$ = 0.1 dB/cm = 1.2 Np/m at 5 MHz is typical (Ref. 11). The scattering term of equation 6.3 is a strong function of the frequency. In the case where the wavelength is greater than the grain size, the scattering attenua-

tion coefficient is given by

$$\alpha_s = Tf^4 K \qquad (6.4)$$

where T = the grain volume

f = frequency in MHz

K = scattering coefficient.

using a value of K = 3260 dB/cm $(MHz)^4$ $cm^3$ (Ref. 12) and assuming an average grain size of about 10 microns, equation 6.4 can be modified to

$$\alpha_s = (3.26 \times 10^{-7})\ f^4\ dB/mm/MHz^4$$
$$= 3.8 \times 10^{-8}\ f^4\ Np/mm/MHz^4 \qquad (6.5)$$

The $\alpha_a$ term may be approximated by

$$\alpha_a = Af \qquad (6.6)$$

Assigning A = .00024 Np/mm/MHz (Ref. 10)

$$\alpha = (2.4 \times 10^{-4})f + (3.8 \times 10^{-8})f^4 \qquad (6.7)$$

An acoustic beam is generated by the oscillation of an ultrasonic transducer. Close to the transducer, diffraction phenomena influences the sound field causing regions of maximum and minimum. The range of the sound field characterized by extreme interferences is referred to as the near field. Beyond the near field, in the far field, the sound pressure field becomes less complex. The near field distance is closely approximated by

$$N = \frac{S}{\pi\lambda} \qquad (6.8)$$

where S is the area of the transducer and $\lambda$ is the wavelength.

Table 6.4 lists values of for near field lengths in steel as a function of wavelength for typical transducer diameters.

For acoustic beams in the far field, the sound pressure on axis of a reflected wave is given by

$$p = p_o \frac{S_s S_f}{d^2 \lambda^2} \qquad (6.9)$$

where $S_s$ is the area of the source and $S_f$ the area of the reflector (Ref. 10).

Combining equations, the sound pressure for pulse echo examination will be given by

$$p = p_o C_1 e^{-\alpha 2d} \frac{S_s S_f}{d^2 \lambda^2} \qquad (6.10)$$

If the beam path requires a reflection such as the outer wall of the leg for the box inspection, then a reflection coefficient R must be included. The coefficient R for an incident transverse wave angle $\phi_1$ at a steel/water interface is given by:

$$R = \frac{Z_2 \cos \phi_1 - Z_1 \cos \phi_2}{Z_2 \cos \phi_1 + Z_1 \cos \phi_2} \qquad (6.11)$$

where $Z_1$ and $Z_2$ are the acoustic impedances for the steel and water respectively, and $\phi_1$ and $\phi_2$ are the incident beam and reflected beam angles. Table 6.5 lists values of the reflection coefficient for angles considered in this study.

The equation for the ratio of the measured sound pressure to the initial pressure, which will be called echo response, becomes

$$\frac{p}{p_o} = C_1 R^2 e^{-\alpha 2d} \frac{S_s S_f}{d^2 \lambda^2} \qquad (6.10)$$

### 6.2.5 Calculation of the Echo Response

The echo response for regions of interest in the coupling designs can now be calculated as a function of flaw size and ultrasonic frequency. The following regions are considered:

Last box thread
Last pin thread
Groove on pin preload shoulder
Make up shoulder
Box thread roots

Table 6.6 lists the region for each type of connector and the ultrasonic beam path to the points of interest. The box thread roots

are divided into three sections over which a selected beam angle is used for inspection. An average distance to the threads in each region is used for the calculations.

The frequency range of 2 to 5 MHz will be considered. At lower frequencies, 1 MHz and below, the wavelength is 3.2 mm or longer for transverse waves in steel and will decrease in effective response for the detection of flaws with dimensions smaller than 3.2 mm. Frequencies greater than 5 MHz are not considered because attenuation will be too great for the long path length cases. In the regions where short path lengths are used, acceptable resolution is anticipated in the 2 to 5 MHz frequency range.

A transducer of 19 mm diameter size is assumed for the calculations. Flaw size is based on area where $S_f = \pi/2$ (flaw size)$^2$. This assumes a semicircular flaw with depth equal to the given flaw size. The flaw is assumed to be oriented perpendicular to the incoming beam. Figures 6.3 to 6.15 show plots of echo response vs flaw size for the regions of interest in the connector design. The plots are extended through the origin although detection of flaws smaller than a wavelength (1.6 mm at 2 MHz, 1.1 mm at 3 MHz, and .64 mm at 5 MHz) is not valid by the model employed. The minimum echo response that can be expected to be detectable is a function of the transducer type and electronics. Experience from testing in thick walled couplings (Ref. 8) indicates that an echo response value of 0.001 to 0.005 in the model would be expected to be the minimum required for equivalent flaw detection found in practice. This region is shaded in Figures 6.3 through 6.15. The experience results include factors such as beam focusing coatings, flaw angulation, and noise not specifically included in this model. Nevertheless, this serves as a baseline for comparison using the model.

### 6.2.6 Results

The results of the calculations plotted in Figures 6.3 to 6.15 are summarized in Table 6.7. The calculations indicate improved response with higher frequencies. Values above 5 MHz were not calculated because attenuation due to scattering for long path lengths becomes significant and in practice frequencies above 5 MHz would normally be only used on

thinner sections. Pin thread inspection will have as good or better sensitivity than that for the last pin thread.

The thin walled connector is shown to have improved inspectability over the thick walled connector. The most critical zone is the last box thread. In the thick walled connector, a defect on the order of 2 to 4 mm in depth should be detected. In the thin walled connector, defects on the order of 1 mm should be detectable.

Increased sensitivity may be obtained by two methods. Focusing the transducer beam will reduce the beam spreading. This would change the

$$\frac{S_s\, S_f}{d^2\, \lambda^2}$$ term in equation 6.12 to K $$\frac{S^2_t}{S_s d}$$

where K is a focusing factor term at the flaw. Shadowing, rather than flaw reflection, will also increase sensitivity. The flaw shadows cut the strong reflections from threads located behind it along the acoustic beam path. This technique is more sensitive to flaws because orientation of the flaw to maximize reflection is not necessary. This technique should be employed wherever possible in the detection scheme for a tension leg inspection device.

Decreased sensitivity must be expected by changes in material properties which affect the attenuation coefficient. The addition of a protective layer to the tension legs will affect the reflection coefficient R. Flame spraying, which is common in offshore application, can introduce a position and frequency dependent attenuation factor (Ref. 12).

### 6.2.7 Effect of Threads

The above analysis has not considered how the thread pattern may affect the detectability of defects. The threads will serve as reflectors and have a complicated image pattern depending on their shape and spacing. Large threads will reflect a strong signal. Defects at the root of the large thread will be detected as a small signal in addition to the large thread signal. Small threads will produce signals over which defects at the root should be more readily detected. The small thread designs also have more threads per unit length. This can be useful for shadowing effect. As a crack increases in depth, it will shadow more threads. Figure 6.16a shows the detection of notch defects in an ultrasonic C-scan image for relatively small (approximately 2 mm deep) threads. Figure 6.16b shows an ultrasonic B-scan presentation showing thread shadowing effects as a function of notch size.

The thread shape will also affect the reflected acoustic signal. This is a complicated effect depending on the thread surface orientation to the ultrasonic beam angle and the multiple acoustic reflections that may occur. Square threads should provide adequate reflections from the corner of the thread. Rotary shoulder threads will have a stronger reflection due to the larger, angulated surface depending on beam angle. Flaw detection and sizing by shadowing may be easier in the square thread design.

### 6.2.8 Conclusions

Ultrasonic inspection is the most suitable technique for tension leg examination. In the thin walled coupling design, detection of small defects 2 mm and smaller is anticipated using conventional ultrasonic pulse echo methods. The thick walled coupling design involves greater ultrasonic path lengths in material and thus ultrasonic sensitivity will not be as good as in the thin walled design.

The threaded coupling is the most difficult region for inspection, particularly box threads. Other regions such as the shaft, crossload bearing, and anchor connector will have flaw detectabilities similar to those found for the pin preload shoulder. The thread pattern in the connector will affect the ultrasonic data from which the flaw is extracted. Small, square threads may offer a pattern suitable for

relatively easy flaw detection and sizing based on shadowing. Inspection time is a function of the volume of material and the speed of the data acquisition and analysis equipment. Roughly 2.5 to 5 hours per element is required based on current technology.

The model proposed in this study is very useful for comparison of coupling designs. Absolute values from the model should be verified by experimentation, particularly to evaluate the effects of attenuation in the material, the minimum detectable echo response range using conventional ultrasonic systems, compensation for the orientation of the flaw to the beam, and the thread pattern.

## 6.3 Phase II Plan

### 6.3.1 Summary

Based on the results of the Phase I study, tension leg platform legs should be inspected using inservice ultrasonic examination to ensure their integrity. The Phase I study proposed a model for the ultrasonic inspection of the tension leg which allowed for the estimation of the detectable flaw size as a function of the position. The model proposed an echo response factor for defects and an anticipated sensitivity level. The results on two designs of tension leg coupling showed that the smallest detectable flaw size was a strong function of beam path length. The study showed that the threaded coupling was the most difficult region to inspect and the most critical. The material attenuation, a function of alloy and grain size was a factor. The thread pattern in the coupling was noted to influence the inspectability but a model was not proposed within the Phase I scope. Some general comments and an example were provided.

A Phase II effort on the inspectability of tension legs is warranted to verify experimentally the model and to refine the sensitivity level for the echo response by standard instrumentation.

### 6.3.2 Phase II Study Plan

The Phase II study plan calls for the testing of a standard coupling to observe fatigue crack growth. The study will refine the ultrasonic model through experiment and inspect the fatigue test specimen.

The ultrasonics model evaluation will be performed as follows:

### 6.3.3 Tasks

1. Define flaw types to be used. Type of flaw, quantity, and position. (1mm, 2mm, 4mm, and 8mm deep)
2. Fabricate test samples - Attenuation sample 4x4x4 in. and 4x4x8 in.

Plate representations for box and pin consisting of electric discharged machined notches of appropriate size at the last box

thread, last pin thread, center box thread, and 1/6 distance from farthest box thread (approximately two, 8 in. wide blocks of material for each connector type.) For:

Thick Walled Connector

Thin Walled Connector

Standard coupling to be used in the fatigue tests.

3. Testing on fabricated samples. Flaw size detected vs. frequency and location.
4. Evaluate thread patterns. Design test thread program for test blocks. Three thread types for last six box threads.
5. Fabricate thread test pattern blocks with flaws.
6. Test thread patterns.
7. Correlate results with model and refine model analysis for thick, thin, and fatigue test couplings.
8. Design inspection system for fatigue test specimen.
9. Inspect specimen during fatigue cycle.
10. Correlate UT test results with fatigue test results.
11. Prepare final report on UT.
12. Design flame spray experiment.
13. Fabricate flame spray test piece.
14. Test flame spray effect.

Equipment Needed:

UT flaw detector mainframe

Transducers

Fixturing

Testing, supplies

## 6.4 References


1. Underwater Inspection/Testing/Monitoring of Offshore Structures, February 1978, U.S. Department of Commerce.

2. Wulther K.G., "The Magfoil Method", Materials Evaluation 41, April 1983.

3. Hein, N.W. Jr., et al, " Requirements for a Nondestructive Inspection System for the Hutton Tension Leg Platform (TLP) Mooring System", Offshore Mechanics and Artic Engineering Conference, ASME, February 1984, New Orleans, LA.

4. NASA, Nondestructive Testing, A Survey, NASA SP-5113, 1973.

5. Stumm W., "Magnetographic Weld Inspection Systems for Underwater Installations", Materials Evaluation 41, April 1983.

6. Reimers P., and Goebbels J., "New Possibilities of Nondestructive Evaluation by X-Ray Computer Tomography", Materials Evaluation, May 1983.

7. Polichar R., "X-Ray Computed Tomography of Thick Steel Castings and Forgings", EPRI NP-2728-RR, February 1983, Section 7.

8. Bossi R.H., et al, "Computer Aided Ultrasonic Inspection of an Offshore Tension Leg Platform", ASME Pressure Vessel and Piping Conference, San Antonio, TX, June 1984.

9. Larson K., Durand Y., "Inspection of Pipelines, Risers, Steel, or Concrete Structures. A Comprehensive Range of Equipment to be Operated from Manned or Unmanned Submersibles", Underwater Technology, L. Alteraas Ed. Pergamon Press, Norway, April 1980.

10. Krautkramer, Ultransonic Testing of Materials, 2nd edition, Springe-Verlay, NY, 1977.

11. DeVries A., Sigma Research, Inc.

12. Papadakis Emmanuel, "Ultransonic Attenuation Caused by Scattering in Polycrystalline Media", Chapter 15, Physical Acoustics, Vol. IV, Academic Press, 1968.

13. Cox R., Almond D., Reiter H., "Ultrasonic Attenuation in Plasma Sprayed Coating Materials", Ultrasonics, January 1981.

14. American Petroleum Institute, "Recommended Practice for Planning, Designing, and Constructing Tension Leg Platforms", API-RP2T (Draft).

Table 6.1

Wavelengths of Ultrasound

| Frequency MHz | Steel Longitudinal Wavelength (velocity=5.9mm/ µsec.) | Transverse Wavelength (3.2 mm/µsec.) | Water Longitudinal Wavelength (1.5 mm/µsec.) |
|---|---|---|---|
| 1 MHz | 5.9 | 3.2 mm | 1.5 mm |
| 2 MHz | 3.0 | 1.6 | .75 |
| 3 MHz | 2.0 | 1.1 | .50 |
| 4 MHz | 1.5 | .80 | .38 |
| 5 MHz | 1.2 | .64 | .3 |
| 6 MHz | 1.0 | .53 | .25 |

Table 6.2

Ultrasonic Beam Angles for Regions of Interest

in the Tension Leg Inspection

| Region | Beam Angle In Steel (angle from normal) | Transducer Angle in Bore Fluid (water assumed) |
|---|---|---|
| **Thick Walled Connector** | | |
| Last box thread | 45 degrees | 19 degrees |
| Last pin thread | 45 | 19 |
| Preload Shoulder on Pin | 45 | 19 |
| Make up Shoulder | 45 | 19 |
| Box Threads | | |
| 14-20 | 45 | 19 |
| 8-14 | 60 | 24 |
| 1-7 | 70 | 26 |
| **Thin Walled Connector** | | |
| Last box thread | 45 | 19 |
| Last pin thread and preload shoulder | 45 | 19 |
| Make up shoulder | 45 | 19 |
| Box threads | | |
| 39-51 | 45 | 19 |
| 24-39 | 60 | 24 |
| 1-25 | 75 | 28 |

Table 6.3

Coefficient for Echo Transmission (Ref. 10)

| Angle (degrees) | Coefficient $C_1$ |
|---|---|
| 45 | .17 |
| 50 | .16 |
| 60 | .15 |
| 70 | .14 |
| 75 | .13 |

Table 6.4

Nearfield Lengths in Steel

| Frequency | Transducer Size 13mm dia. | 19mm dia. | 25mm dia. |
|---|---|---|---|
| 1 MHz | 13mm | 28mm | 50mm |
| 2 | 25 | 57 | 101 |
| 3 | 39 | 85 | 151 |
| 4 | 50 | 114 | 202 |
| 5 | 63 | 142 | 252 |
| 6 | 78 | 170 | 302 |

Table 6.5

Reflection Coefficient for Steel/Water Interface

| Incident Angle | Refracted Angle | R |
|---|---|---|
| 45 degrees | 19.4 degrees | .950 |
| 50 | 21 | .955 |
| 60 | 24 | .964 |
| 70 | 26 | .975 |
| 75 | 27 | .981 |

Table 6.6

Distance to Inspection Points

| Regions | Angle of Beam | Distance d (mm) |
|---|---|---|
| <u>Thick Walled Connector</u> | | |
| Last pin thread | 45 | 453 |
| Last pin thread | 45 | 198 |
| Preload shoulder | 45 | 208 |
| Make up shoulder | 45 | 131 |
| Box thread roots | | |
| 14-20 | 45 | 424 |
| 8-14 | 60 | 518 |
| 1-7 | 70 | 640 |
| <u>Thin Walled Connector</u> | | |
| Last box thread | 45 | 173 |
| Last pin thread | 45 | 70 |
| Preload shoulder | 45 | 70 |
| Make up shoulder | 45 | 50 |
| Box thread roots | | |
| 39-51 | 45 | 160 |
| 24-39 | 60 | 196 |
| 1-24 | 75 | 320 |

Table 6.7

Results of Calculations

| Region | Minimum Flaw Size | Comments |
|---|---|---|
| Thick Walled Connector | | |
| Last box thread | 2 to 4.3 mm | |
| Last pin thread | <2mm | |
| Pin preload shoulder | <2mm | |
| Make up shoulder | <2mm | |
| Box threads | | |
| 14-20 | 2mm to 4mm | |
| 8-14 | 2.5mm to 5.5mm | |
| 1-7 | 3.7mm to 8.2mm | |
| Thin Walled Connector | | |
| Last box thread | <2mm | |
| Last pin thread and preload shoulder | <2mm | Path length is less than near-field length. |
| Make up shoulder | <2mm | Path length is less than near-field length. |
| Box Threads | | |
| 39-51 | <2mm | |
| 24-39 | <2mm | |
| 1-24 | <2mm to 2.8mm | |

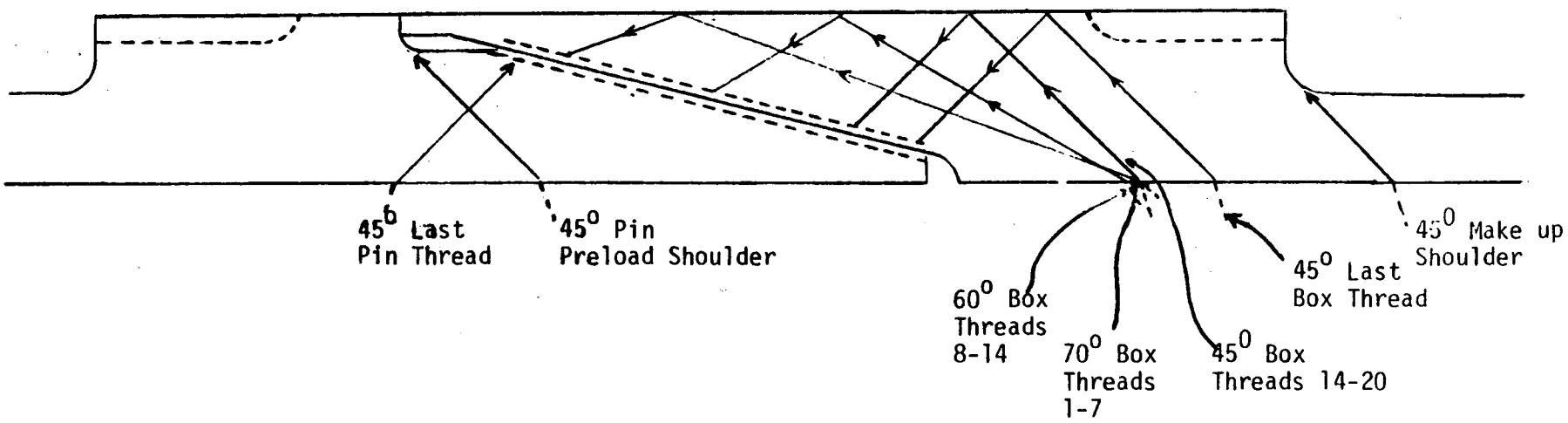


Figure 6.1a - Ultrasonic beam angles for the thick walled coupling.

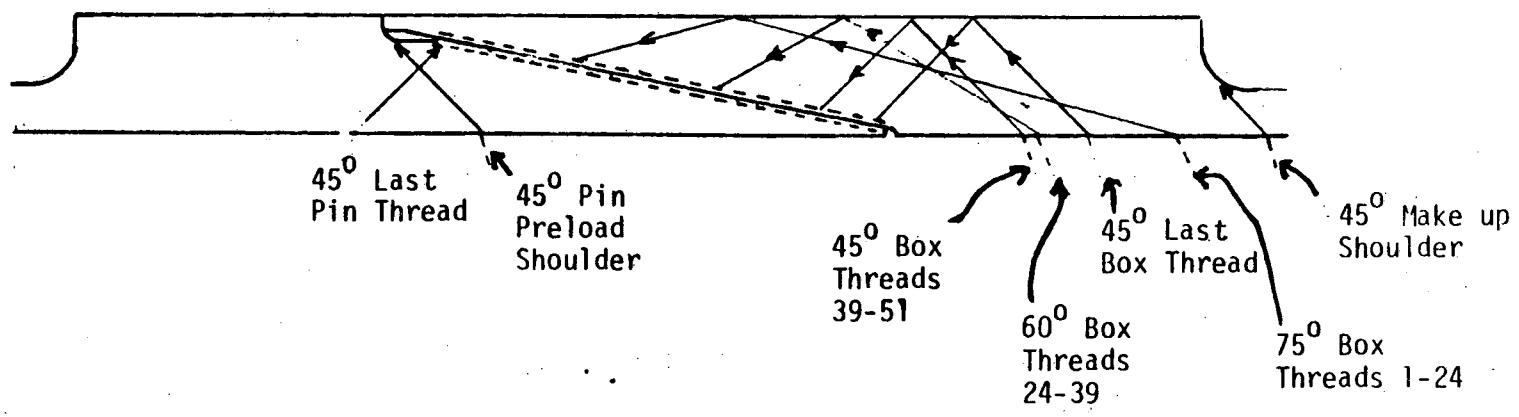


Figure 6.1b - Ultrasonic beam angles for the thin walled coupling

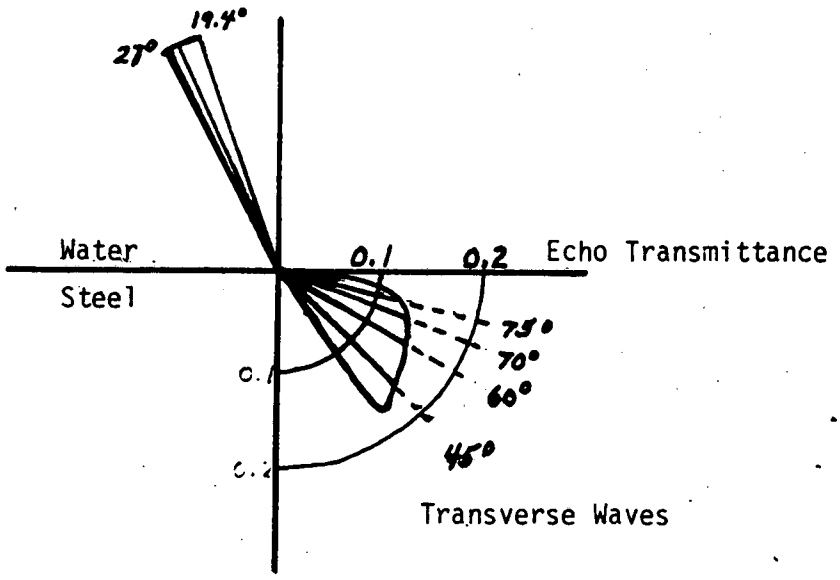


Figure 6.2 - Echo transmittance for water/steel interface (Ref. 3).

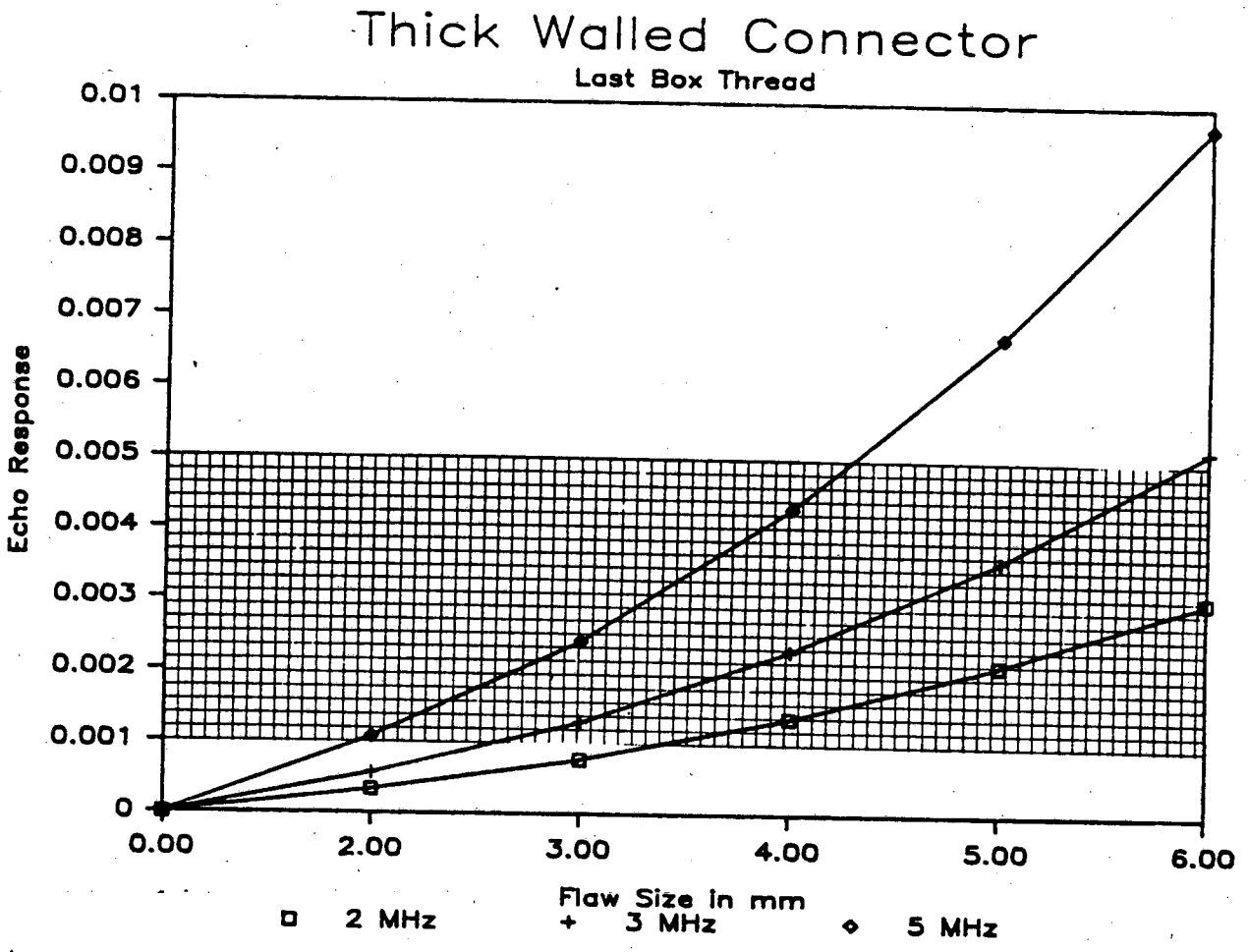


Figure 6.3 - Echo response vs. flaw size for the thick walled connector last box thread.

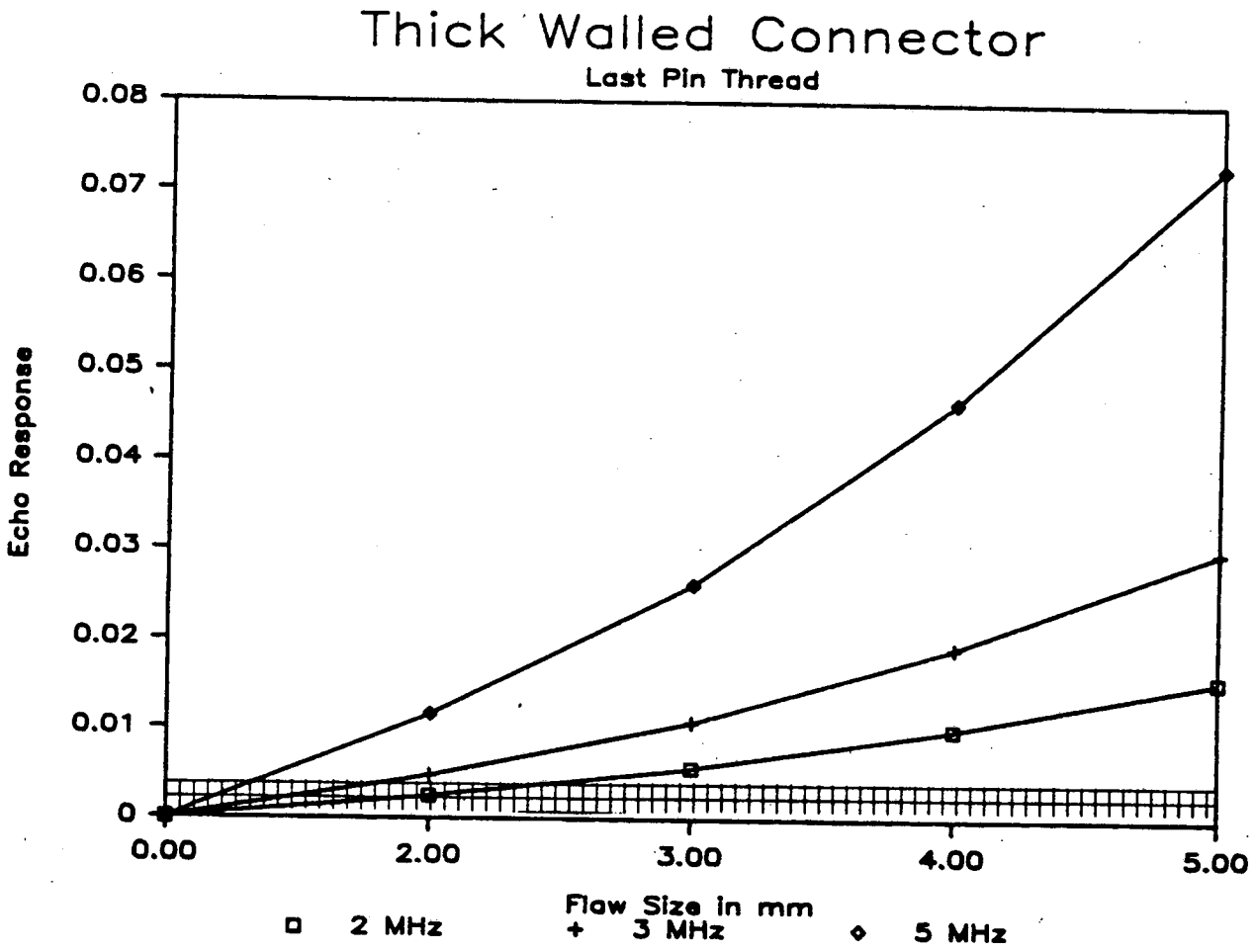


Figure 6.4 - Echo response vs. flaw size for the thick walled connector last pin thread.

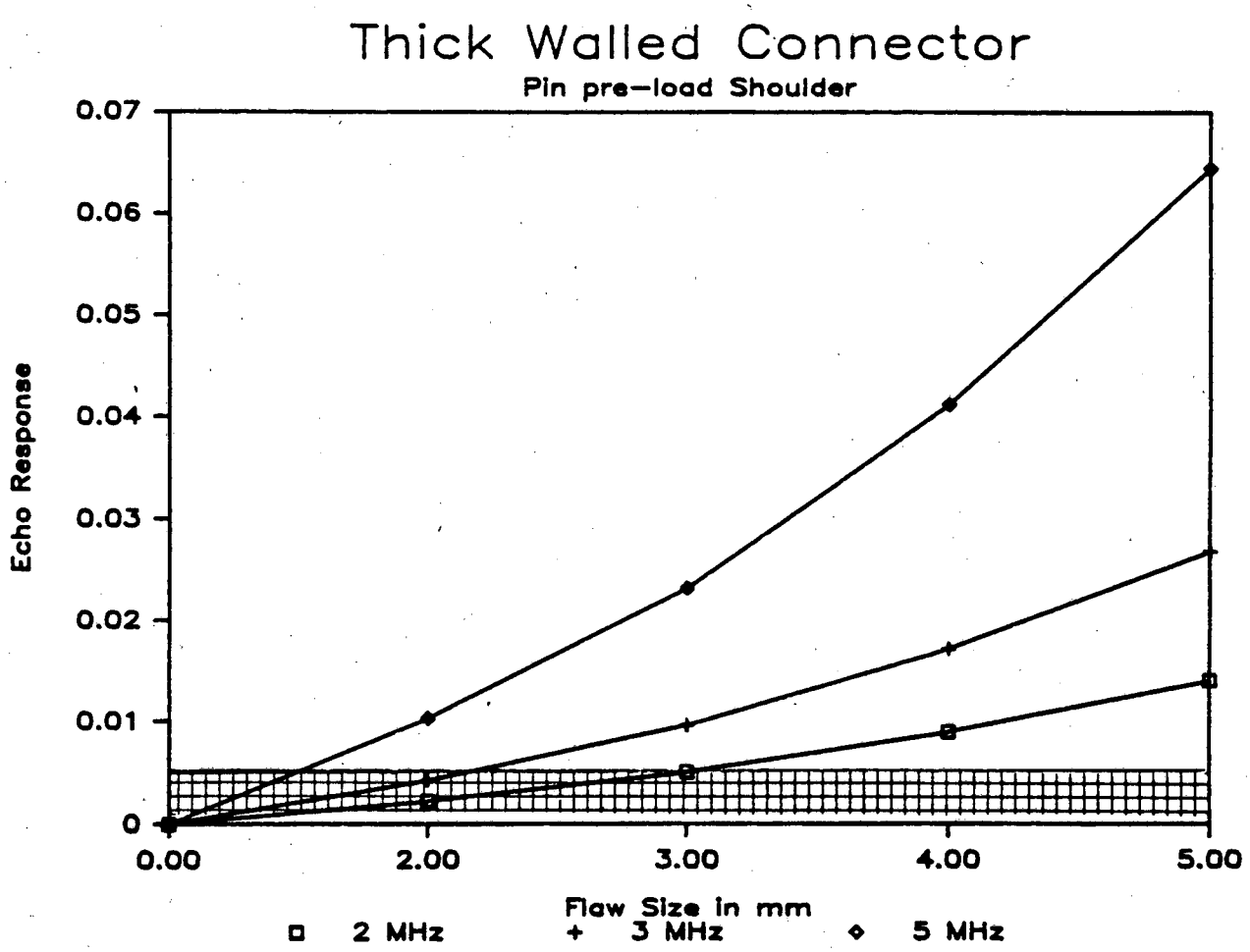


Figure 6.5 - Echo response vs. flaw size for thick walled connector pin preload shoulder.

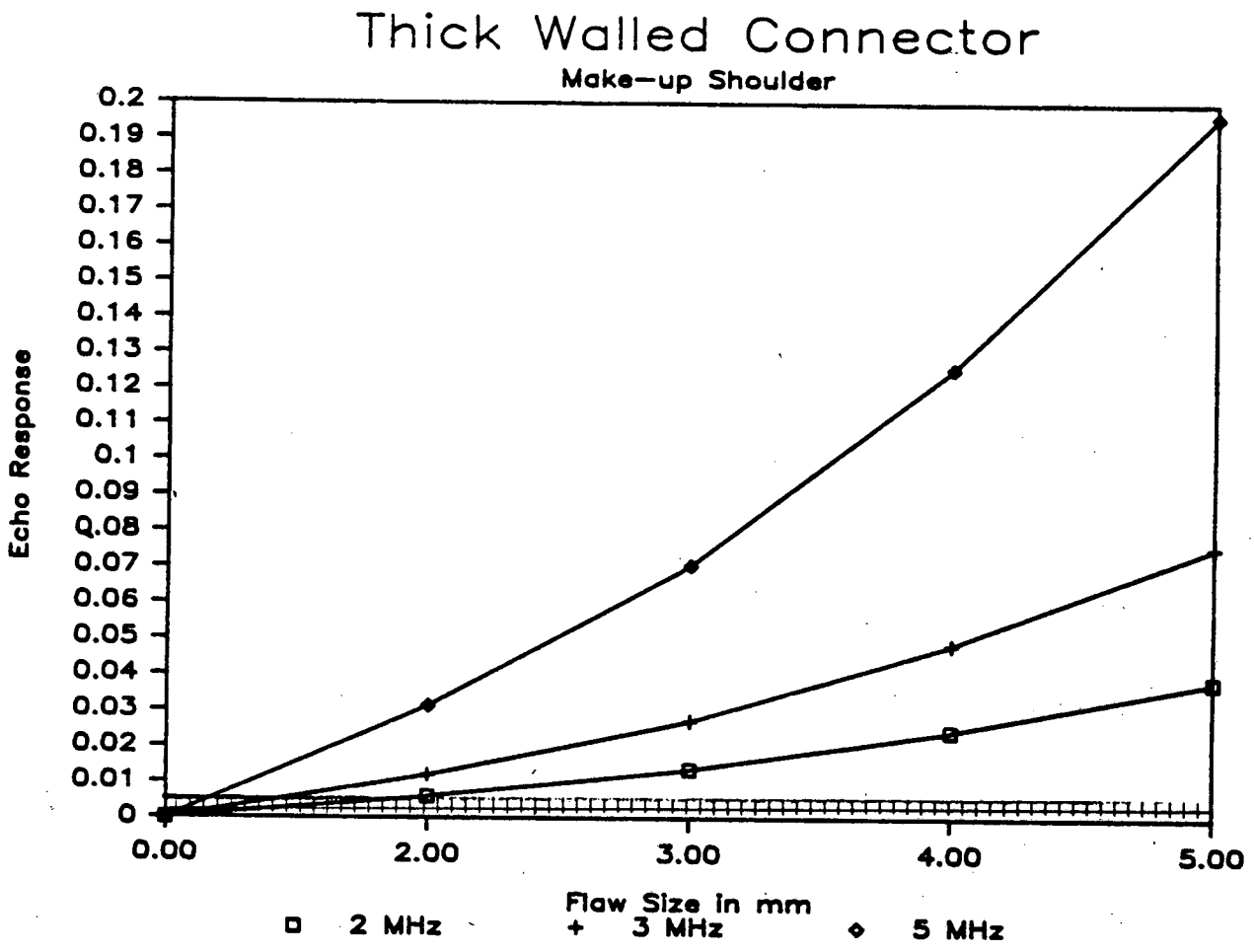


Figure 6.6 - Echo response vs. flaw size for the thick walled connector makeup shoulder

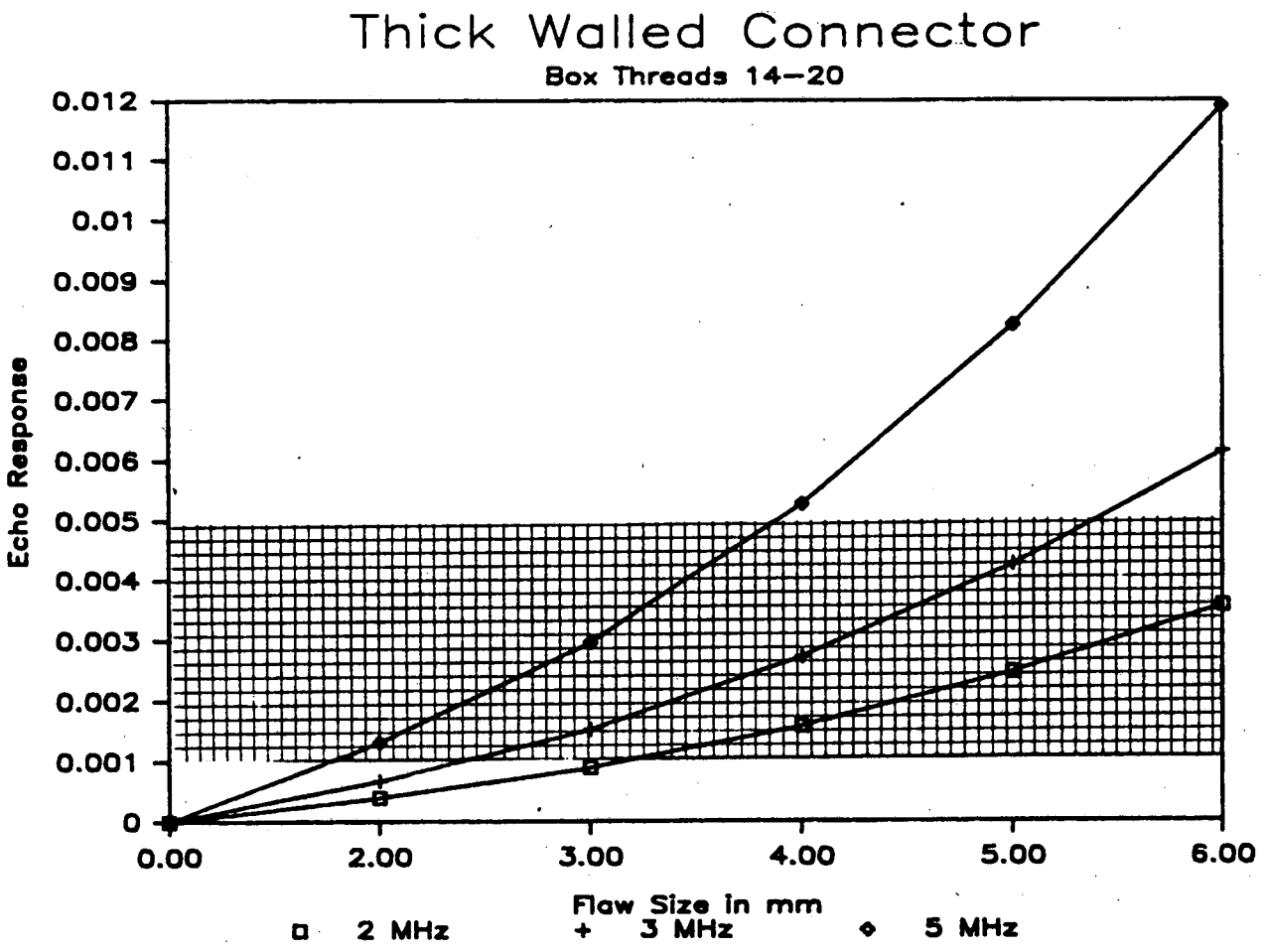


Figure 6.7 - Echo response vs. flaw size for the thick walled connector box threads 14-20.

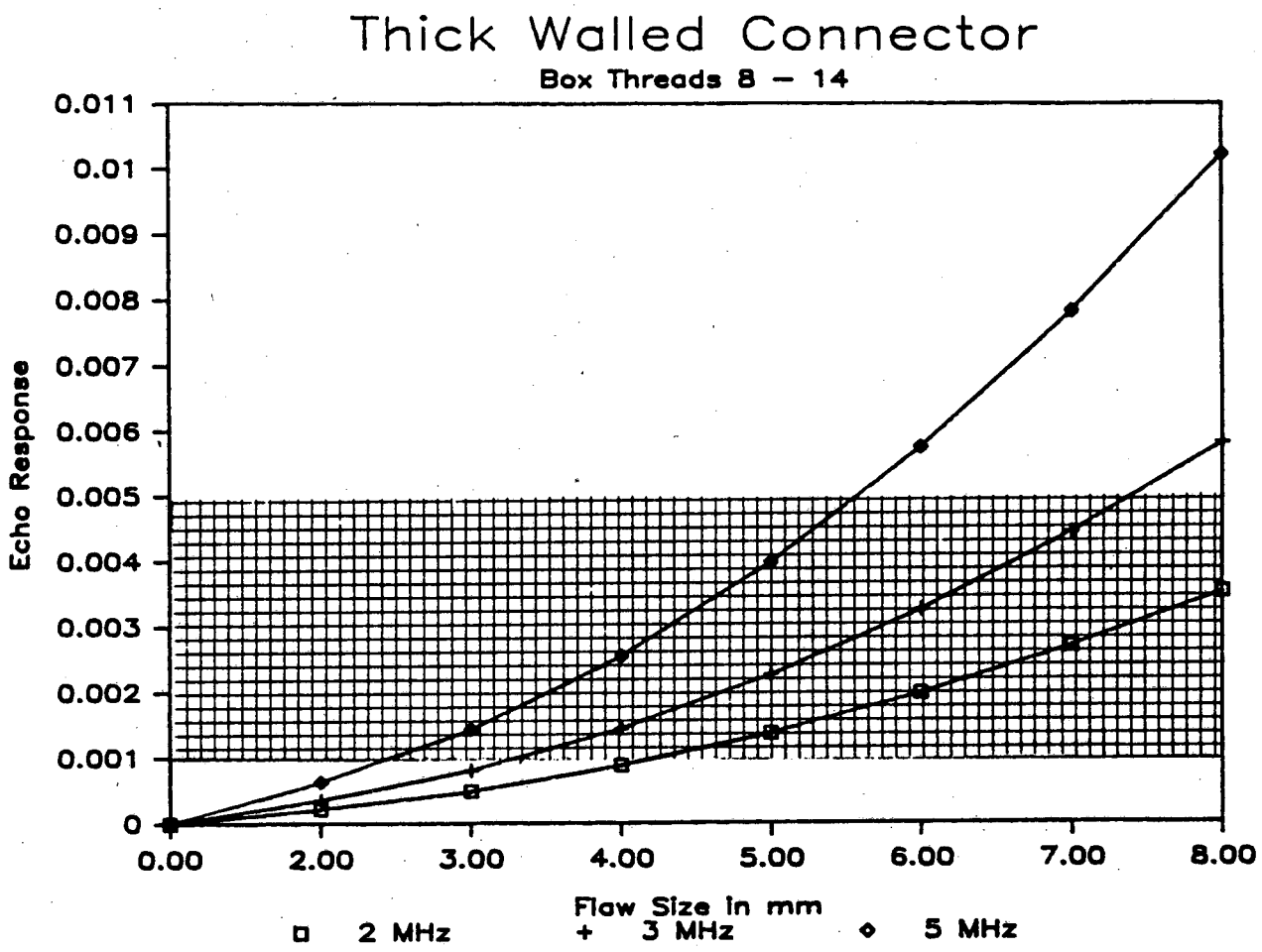


Figure 6.8 - Echo response vs. flaw size for the thick walled connector box threads 8-14.

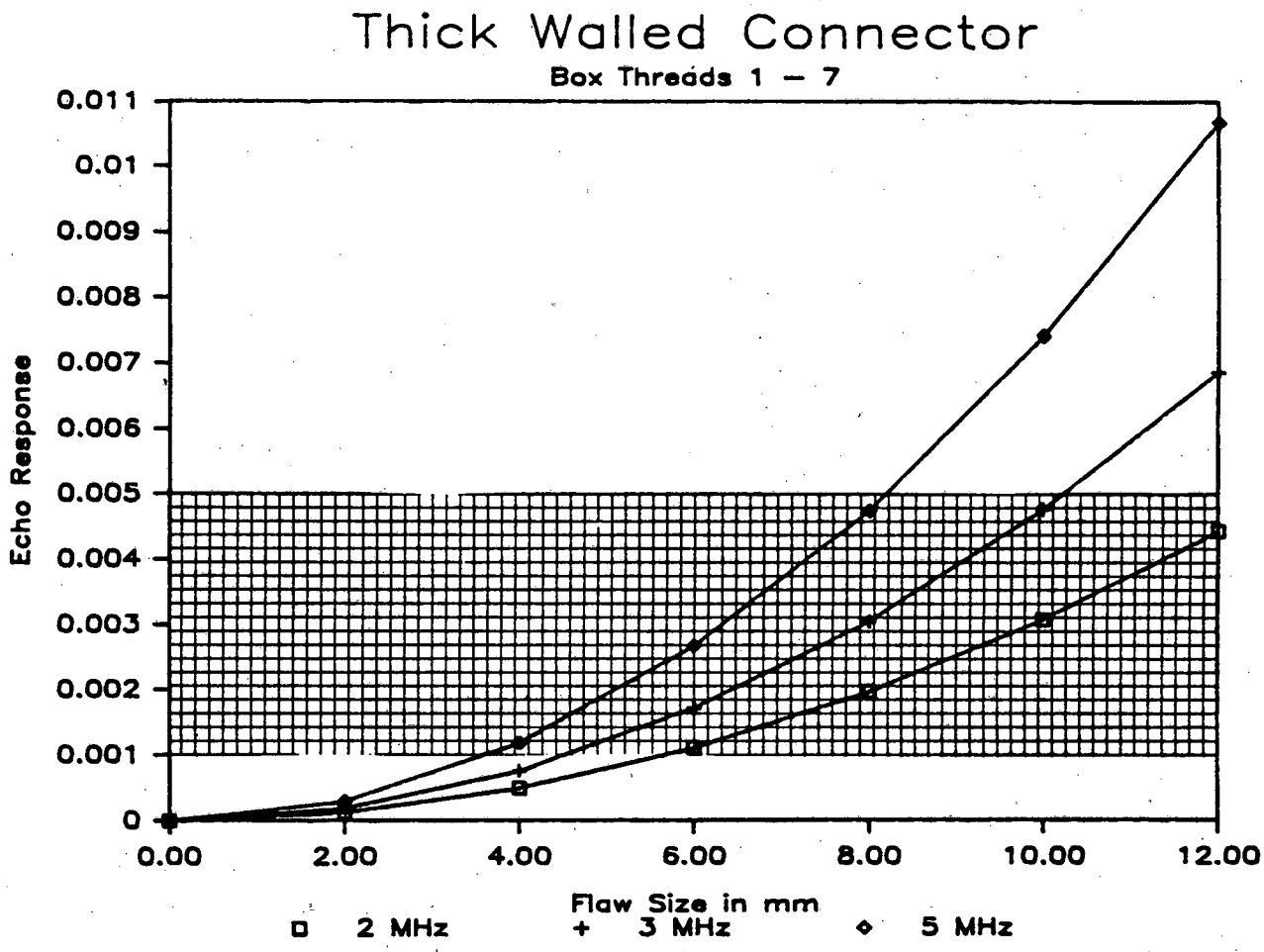


Figure 6.9 - Echo response vs. flaw size for the thick walled connector box threads 1-7.

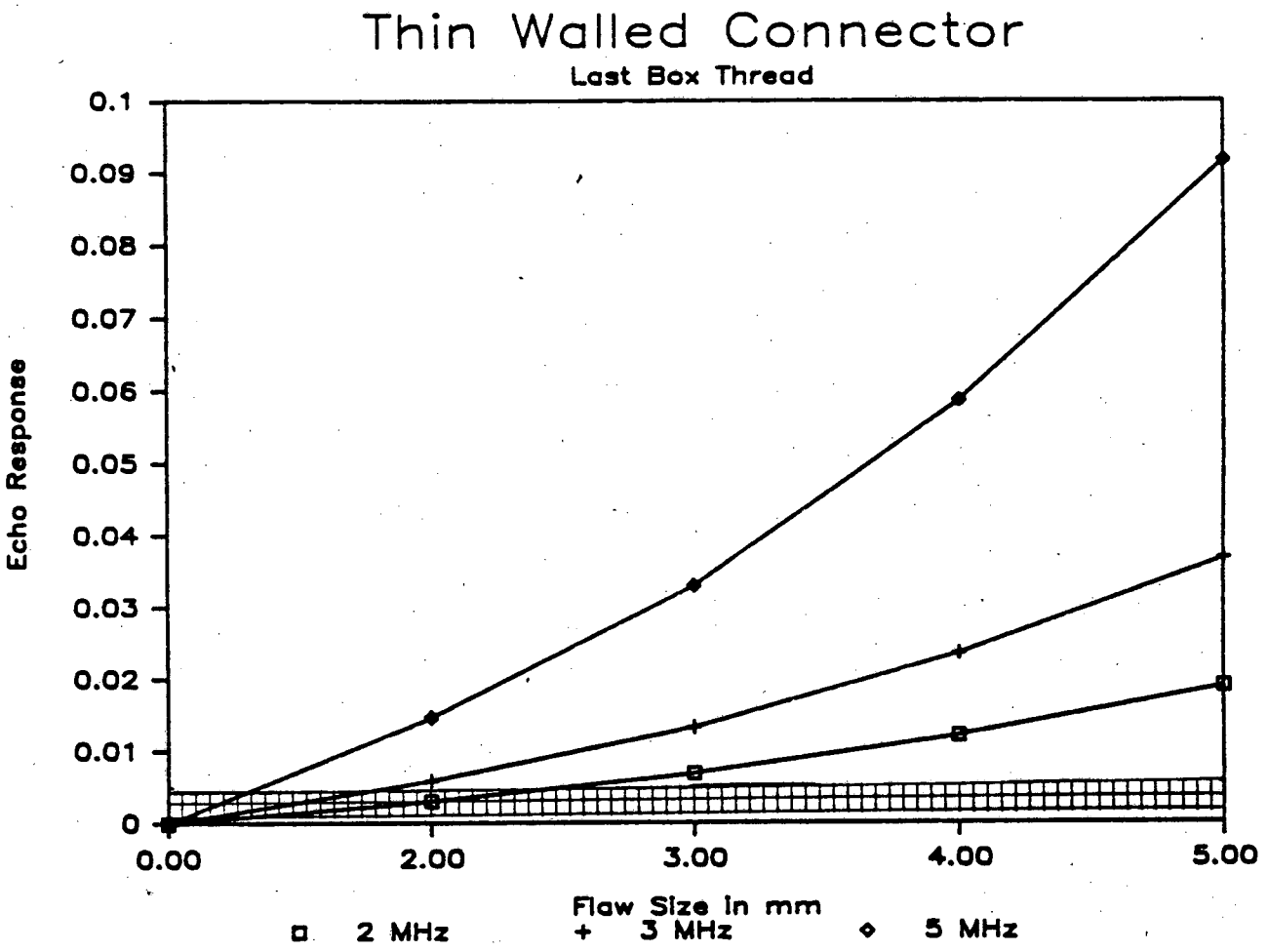


Figure 6.10 - Echo response vs. flaw size for the thin walled connector last box thread.

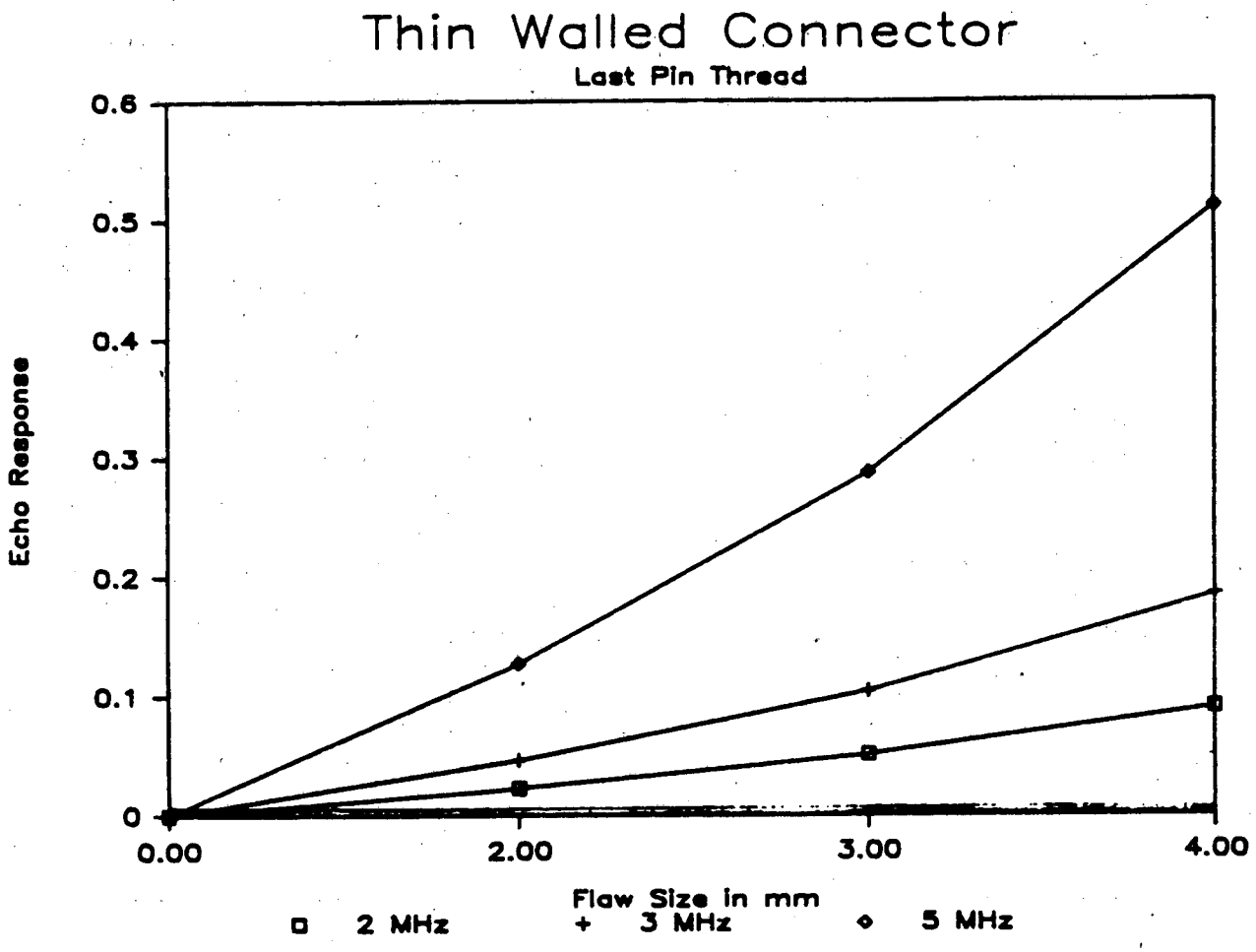


Figure 6.11 - Echo response vs. flaw size for the thin walled connector last pin thread and preload shoulder.

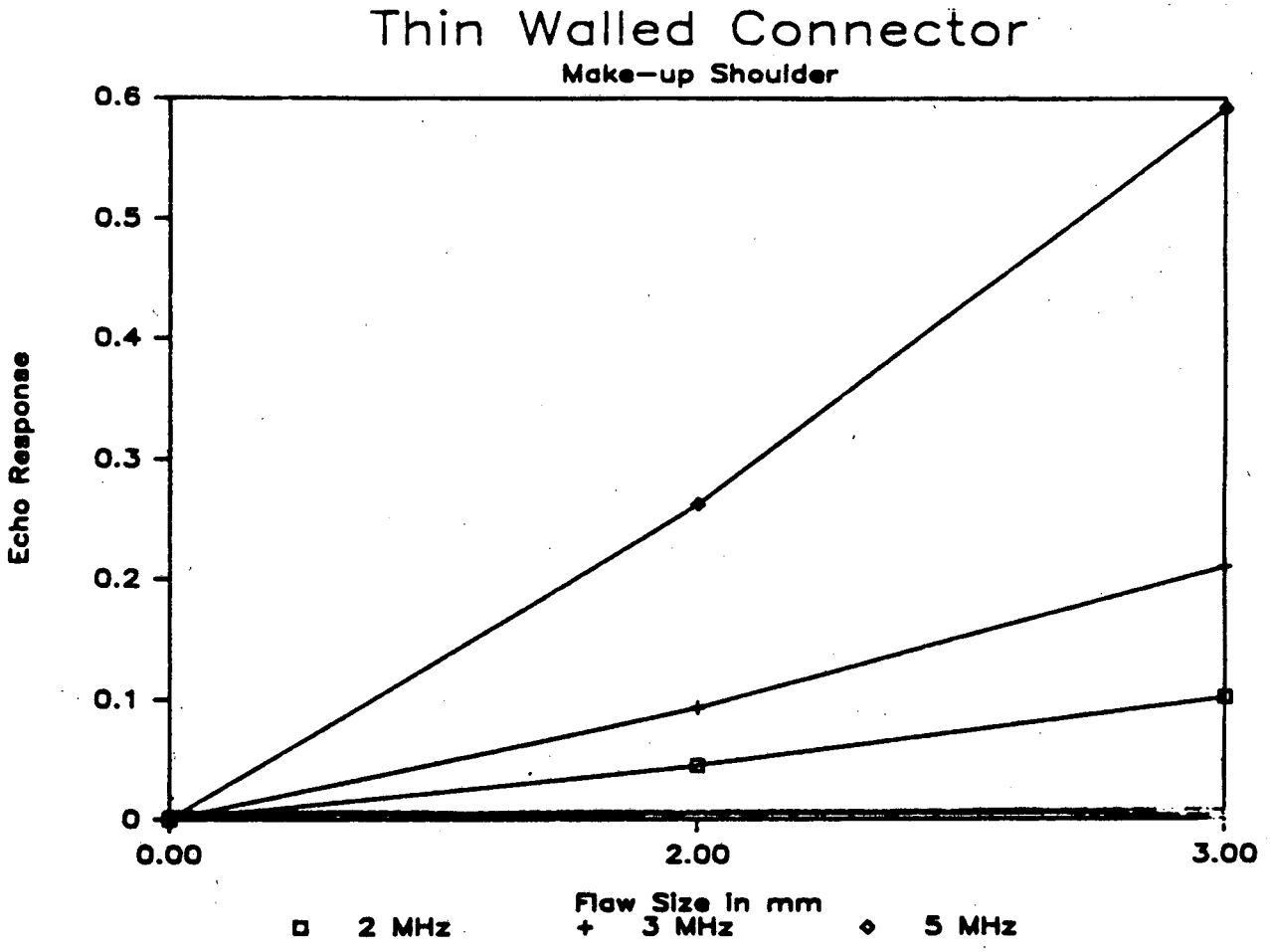


Figure 6.12 - Echo response vs. flaw size for the thin walled connector makeup shoulder.

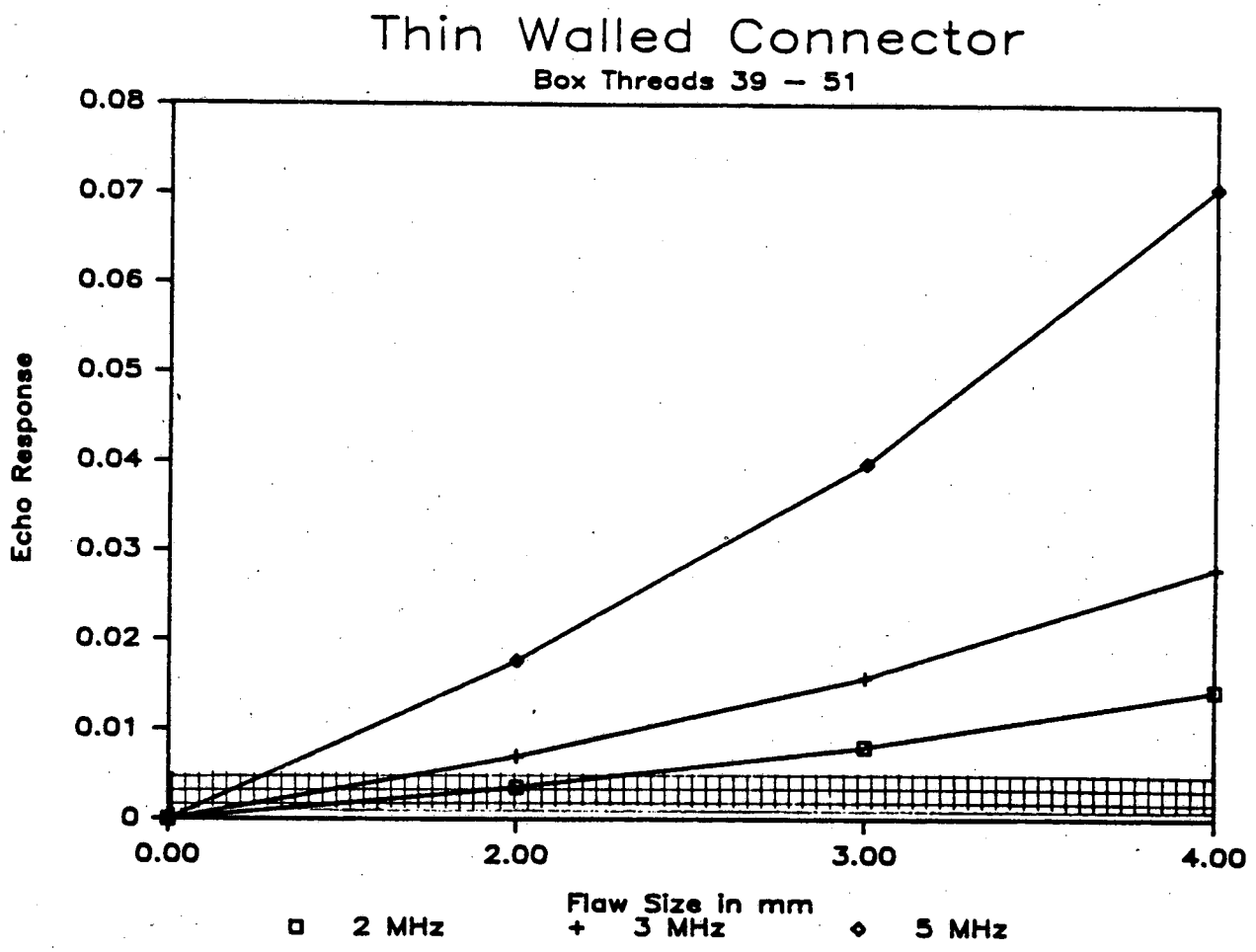


Figure 6.13 - Echo response vs. flaw size for the thin walled connector box threads 39-51.

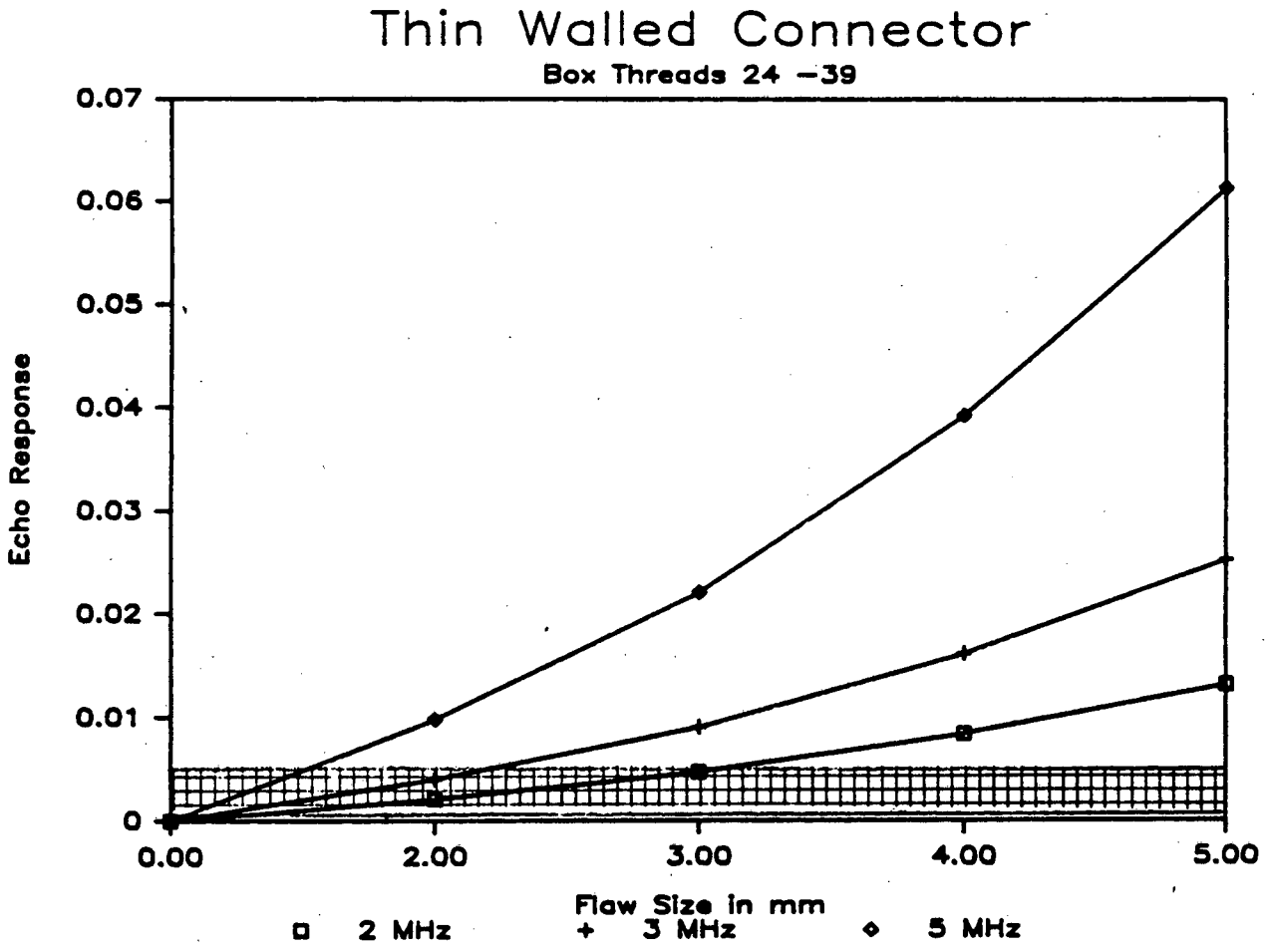


Figure 6.14 - Echo response vs. flaw size for the thin walled connector box threads 24-39.

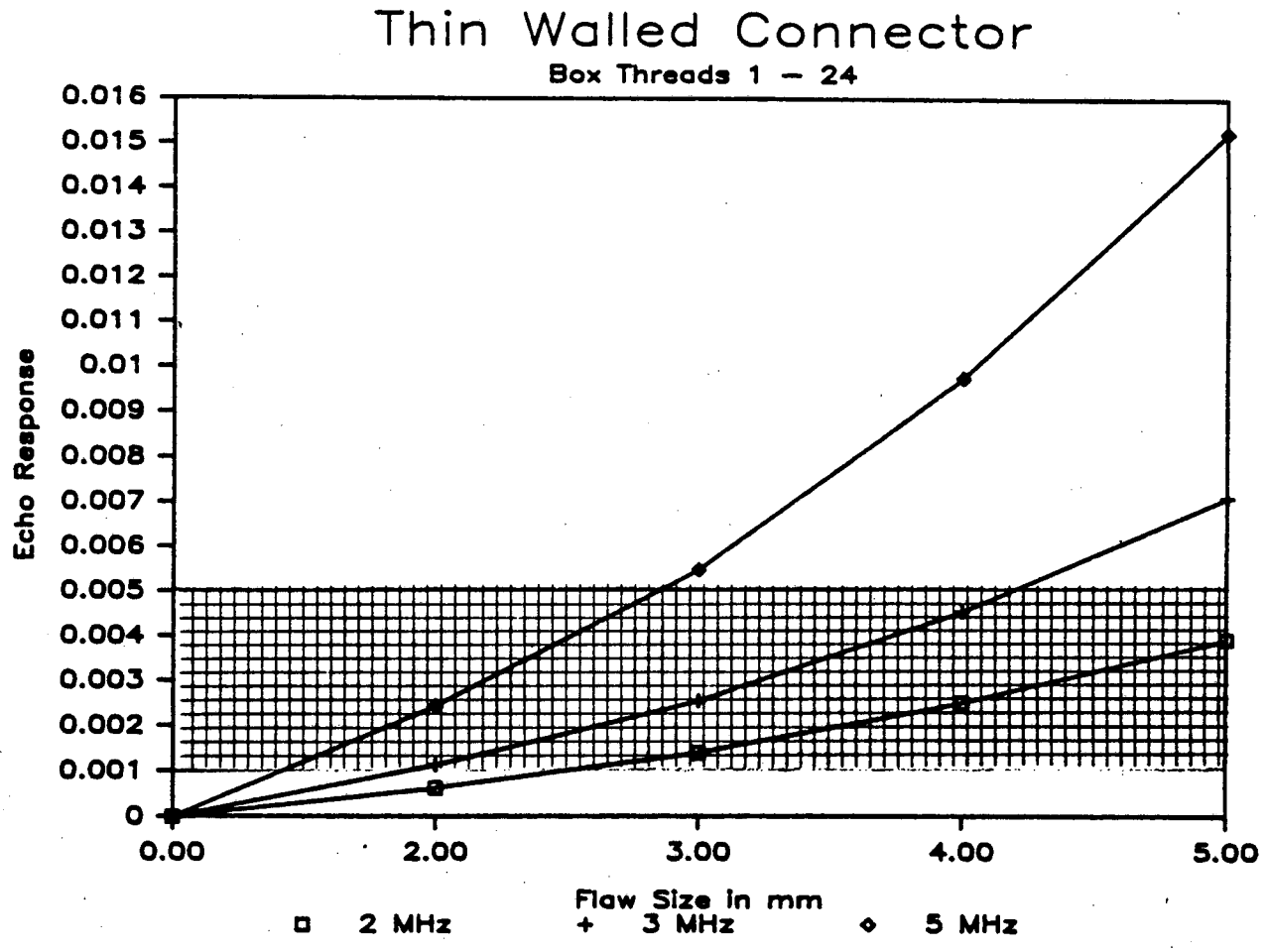


Figure 6.15 - Echo response vs. flaw size for the thin walled connector threads 1-24.

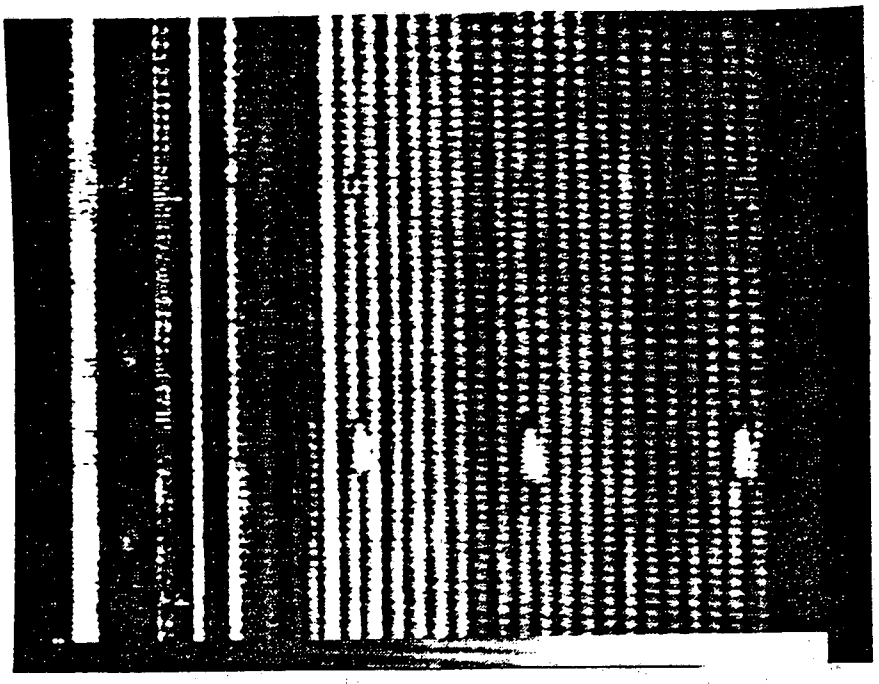

2 mm deep

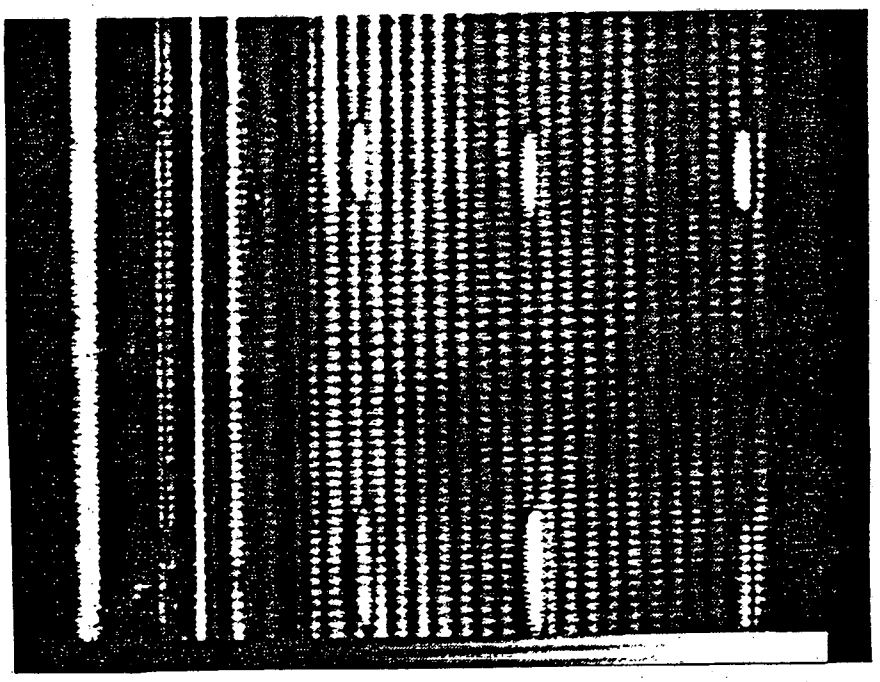

3 mm deep

4 mm deep

Figure 6.16a - Amplitude C-scans of EDM notches in small threads (2- x 6-mm 3- x 9-mm, and 4- x 12-mm).

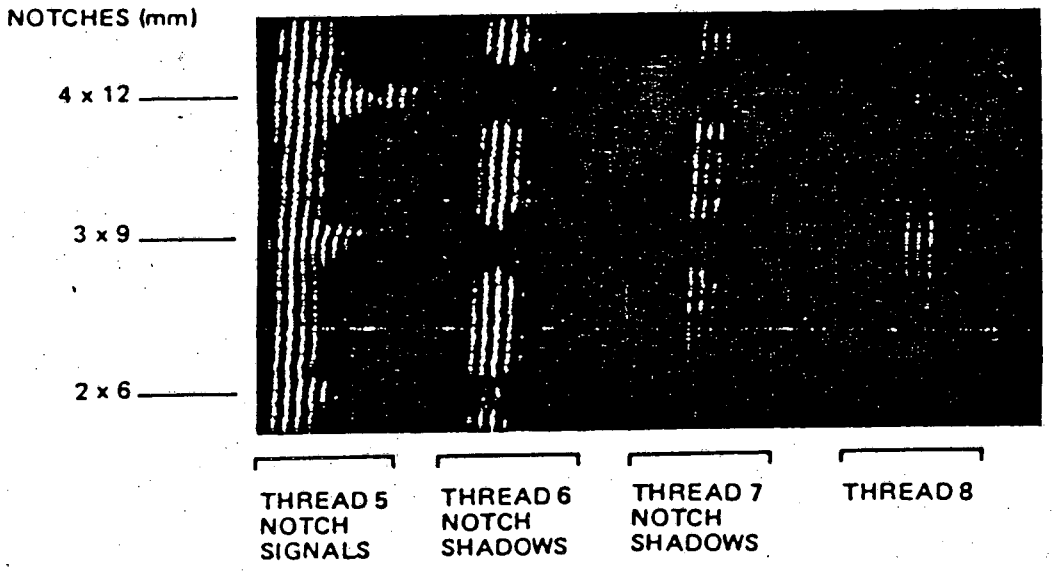


Figure 6.16b - B-scan images showing thread shadowing effect for 4 mm, 3 mm, and 2 mm deep notches.

# 7.0 Structural Reliability Model

## 7.1 Crack Growth Model

### 7.1.1 da/dN vs. ΔK

The three parameter da/dN vs. ΔK equation is used as described in section 4.3.2.

### 7.1.2 Stress Intensities

The macro-crack growth that the connector will experience can be one of four possibilities:

1) A semi-elliptical crack at the thread root (see figures 7.1a, b).
2) A circumferential crack at the thread root.
3) A semi elliptical crack in the pipe body.
4) A circumferential crack in the pipe body.

To model the stress intensities of the semi-elliptic crack at the thread root, an equation proposed by [Shah] for a semi-elliptic crack in a hole through a thick plate is used. The different stress profile at the thread root as compared to the profile at a hole in a plate is accounted for by use of an equivalent thread root radius. The equivalent thread root radius is derived from Neuber's formula for the actual stress profile of the thread root [see Hammouda et al]. A through wall semi-elliptical crack is modeled as a crack in a flat plate whose stress intensities are given by

$$K = \sigma[\pi a \sec(\pi a/w)]^{1/2}$$

where

$\sigma$ = membrane stress

a = 1/2 the crack width

w = circumference of section

The stress intensities which accompany the circumferentially cracked connector are derived from a model proposed by [Buchalet et al] and is given by

$$K_I = (\pi a)^{1/2} [A_o F_1 + 2a A_1 F_2/\pi + a^2 A_2 F_3/2 + 4a^3 A_3 F_4/3\pi]$$

where

$F_1$, $F_2$, $F_3$, $F_4$ are functions of crack depth

and

$A_0$, $A_1$, $A_2$, $A_3$ are the constants describing the cubic stress profile of the uncracked region of interest,

$$\sigma(x) = A_0 + A_1 x + A_2 x^2 \times A_3 X^3$$

Cracks initiating in the weld region or the pipe are analyzed using stress intensity factors derived for flat plates and pipes (see, e.g. Erdogan and Wei).

## 7.2 Variables

There are three variables (other than loading) which influence the life of a connector. They are:

1) Initial Flaw Size
2) Material Properties
3) Environment (seawater, air, cathodic protection)

These may be treated deterministically or probabilistically.

## 7.3 Deterministic Tendon System Failure Analysis

### 7.3.1 Introduction

Two types of crack growth were studied: semi-elliptical crack growth and radial growth of a circumferential crack. Three regions of the connector that were assumed to be the most critical are the last pin thread, the last box thread, and the pipe region (specifically, the pipe/upset transition). The last thread regions are critical because of the high peak stresses and the last box thread is critical in particular do to the difficulty of crack detection in that section with an internal inspection device. The pipe section is critical because of its small cross sectional area (compared to the connector) which results in a high membrane stress and potential for more rapid crack growth.

### 7.3.2 Analytical Procedure

#### 7.3.2.1 Input

Input to the deterministic failure analysis consists of

1) Initial or minimum detectible flaw size
2) Material environment/properties
3) Cyclic stress history

The minimum detectible flaw size size is defined as that flaw size

which has a 95% chance of detection (see Section 6, table 6.7). This flaw size is used as the initial flaw size. The material properties for each possible environment are described in Section 4.3.1.1. Figures 4.2 a, b and c are used to describe material properties in air, seawater and under cathodic protection, respectively. Fatigue loads will vary as a function of the location and design as described in Section 3. Component stress as a function of tendon tension is determined as in Section 5.

#### 7.3.2.2 Calculations

Stress intensities are computed as previously described, and the three parameter da/dN vs. $\Delta K$ equation is used to determine crack growth rate. This means there is no absolute threshold stress intensity. The time interval used for cycle counting is chosen to be small enough so that significant crack growth does not occur before the update of crack size.

### 7.3.3 Results

#### 7.3.3.1 Outline of Results

In this study there is a wide range of variables which are described in Table 7.1. Not all of the possible 720 cases have had fatigue calculation performed for them, but rather a sampling of various key variables with a concentration in the most severe cases. To summarize the results, the effect of the six variables on fatigue life are addressed.

#### 7.3.3.2 Effect of Tendon Type

The difference in crack growth life between the two designs (thick walled, thin walled) is significant. There are three reasons for this difference:

1) Flaw inspection sensitivity (i.e. larger possible initial flaws in the thick walled connector)
2) Crack growth behavior
3) Stress profiles

Figure 7.3 shows the residual life of connectors and pipe as a

function of initial crack size for the 'worst case' North Sea environment. For initial cracks up to .25 inches, the thin walled connector exhibits the longer life due largely to the lower stress concentration factors in the finer threads. From this standpoint, the higher resolution of inspection devices for the thin walled case (.08 inch vs. .17 inch for the thick walled connector) is the reverse of the desired situation, however for the assumptions used here the lifetimes are sufficiently long to eliminate concern for very small cracks.

The pipe sections exhibit nearly equal lives for small cracks due to the fact that the membrane stresses are equal in both cases.

#### 7.3.3.3 Effect of Tendon Section

Crack growth life differences between the three sections studied varies with the assumed crack growth behavior. Figure 7.4a shows life for the thin walled connector at the three sections based on semi-elliptical crack growth. The pipe proves to be the most critical section with a life of 35 years (for a .078 inch flaw) compared to 165 years and 190 years for the last pin thread and last box thread, respectively. This is due to the higher membrane stresses in the pipe.

Figure 7.4b shows life based on a circumferential crack growing radially. For this assumed crack growth behavior the life is least for the thread regions due to high peak stresses which occur at the thread roots. As the crack grows radially this peak stress shifts to the crack front which is not the case for the semi-elliptical crack.

#### 7.3.3.4 Effect of Material Environment

The life of the tendon varies with material properties to a large degree. Figure 7.5 shows the life for the last box thread for the free corrosion, cathodically protected, and air environments. Results for two RAO's are plotted. Compared to predicted lives for freely corroding conditions, the air environment results in an increase in life by a factor of two (approximately) while cathodic protection increases life by a factor of ten. This suggests that most fatigue damage occurs in region I of the da/dN curves where cathodic protection is most effective in reducing crack growth. This conclusion is supported by the relatively greater increase in life due to cathodic protection marked

by the Mercier curve in Figure 7.5, which represents a milder response (i.e. more cycles in region I).

7.3.3.5 Effect of Assumed Crack Growth Behavior

Crack growth behavior could vary significantly depending on the aspect ratio of the crack. While fatigue cracks typically eminate from a single nucleation site and assume a semi-elliptical shape, in cases of extremely sharp notches (e.g. at the toe of a weld bead), a surface crack can grow circumferentially by fatigue or the merger of cracks from multiple nucleation sites. This can also be the case for tubulars with any significant stress risers subject to rotary bending superimposed on a large axial force. The tendon designs being considered generally do not have sharp notches. Girth welds will probably be ground smooth, and the threaded connectors have relatively low stress concentration factors. Nevertheless, for purposes of this study, we have considered both semi-elliptical and circumferential surface cracks. The aspect ratio for an initial semi-elliptical crack was assumed to be 2:1. In the thread regions, the ratio generally stabilized at about 5:2 and 3:1 for the thin walled and thick walled cases, respectively, indicating faster circumferential growth initially. The semi-elliptical flaw growth may be taken to give an upper bound to life and the circumferential flaw growing radially may be the lower bound to life. Comparing figures 7.4a-b the life varies by over an order of magnitude between the two assumed crack growth possibilities. Fatigue tests on prototype connectors should be conducted to determine the mode of crack initiation and growth appropriate to this application.

7.3.3.6 Effect of Environment

The effects of environment are examined in figure 7.6. In all cases the North Sea is the most severe followed by the Atlantic and then the Pacific and Gulf of Mexico. The relative severity of the Pacific and Gulf of Mexico is a function of the platform response. For example the Gulf is most severe for Mercier's RAO and the Pacific is most severe for Dillingham's RAO. There are approximately two orders of magnitude difference crack growth life between the severe environment and the mild environment.

### 7.3.3.7 Effect of RAO

The effect of RAO on life is more dramatic than is environment. There are up to three orders of magnitude difference in life between the most severe and mild RAO's. Figure 7.7 shows life for the Gulf of Mexico with Mercier's and Dillingham's RAOs. The other three RAO's used in this study (Figure 3.3) yield the following lives for a Gulf of Mexico environment and an initial flaw size of .078 inches:

| | | |
|---|---|---|
| Tan | - | 95,000 Years |
| Paulling | - | 520,000 Years |
| Chou | - | 880,000 Years |

Note that all of these RAO's were developed for production platforms with displacements of approximately 10,000 to 55,000 tons. Small wellhead type platforms such as that currently being considered by Conoco for Green Canyon may have more benign responses than those used here. Thus, it appears that the proposed tendons may be overdesigned for likely U. S. OCS applications. From this analysis, it can be seen that optimizing tendon response is an important design problem and is a function of environment.

## 7.4 Probabilistic Model for Tendon System Failure

### 7.4.1 Introduction

The key statistical variables include the initial flaw size ($a_o$), crack growth rate coefficient (A), and severity of environmental fatigue loads. The attached flow sheet (figure 7.8) summarizes a Monte Carlo model for tendon system reliability. The basic approach is to employ Monte Carlo techniques to select key variables and thus arrive at a calculated value for the time to failure of a tendon system. The effect of inspection to various levels of sensitivity can be determined statistically by examining the effect on life of inspection vs. no inspection.

### 7.4.2 Model Description

The tendon performance model consists of the following major elements:

1. Material Conditions (material, environment, cathodic protection level, S-N and da/dN relationships)

2. Flaw Characteristics (flaw geometry, location, cummulative fatigue damage ratio, plastic zone size)

3. Load Conditions (cyclic loads, number and magnitude, stress profiles)

4. Flaw Growth and Fatigue Damage Calculations

5. Inspection Characteristics (frequency of inspection, sensitivity of inspection method, decision criteria for replacing tendons)

The model is executed as a time series in increments ranging from 6 hours (the interval of hindcast wave data records) upwards. Fatigue and crack growth estimates are performed by cycle counting over the specified time increment.

Key input variables are selected via a Monte Carlo technique and the model is executed a number of times to get a probability distribution (histogram) for time to failure. This distribution applies to each component.

### 7.4.3 Material Inputs

It is assumed that tendon materials will be high strength (60-120 KSI) quenched and tempered steels. Available S-N and da/dN data for these steels in shown in figure 4.1a-b and figure 4.2a-c*. The applicable curves depend on the exposure to sea water and the level of cathodic protection, if any.

S-N curves are interpreted to represent the crack initiation phase, i.e. the number of cycles required for at least one macrocrack to form. The transition from crack initiation to crack growth is not easily defined and is, in fact, a function of stress level (i.e. the crack size corresponding to critical stress intensity). The model assumes that once the cummulative damage ratio reaches a number of 1.0, that a crack width, a, has been attained as described in Section 4.2.3.

---

* The data included in these figures actually includes lower strength steels as well as high strength steels. The scatterband used here is therefore much wider than that which would be appropriate to use for a single material or class of materials.

### 7.4.4 Fatigue Loads

Fatigue loads are derived from hindcast analysis (SOWM) and from historical data on the occurance of tropical storms and hurricanes. Since tropical cyclones are not modeled in the hindcast data, they are modeled separately.

Fatigue load cycles have been derived from spectral wave data by using a bivariate distribution for height and period. This, coupled with the tendon tension RAO, results in the expected number of cycles within fixed load ranges over each time interval.

### 7.4.5 Results

The model described above was used to provide a conditional probabilty function for tendon life given an initial flaw size and crack growth rate coefficient. The joint distribution on tendon life was then determined from

$$P(T) = \int_0^T \int_0^\infty \int_0^\infty p(t|A,a)p(A)p(a)dadAdt$$

$p(t|A,a)$ were derived from the Monte Carlo simulation. A log-normal distribution was assumed for A, and an exponential distribution for a. The minimum detectible flaw size, $a_o$, was assumed to represent the 95% percentile of the exponential distribution.

Results presented here are limited to the 'worst' case North Sea environments assuming freely corroding conditions. As shown in the previous section, life estimates using cathodic protection are approximately an order of magnitude longer than under free corrosion conditions, and the more benign environments extend the lifetimes even further.

Figure 7.9 shows the probabilties associated with a flaw in the pipe wall. As stated, $a_o$ is interpreted here to be the 95th percentile detectible flaw size assuming an exponential distribution. For a 20 year life and an inspection with this tolerance to .078 inches (2 mm), the probability of failure is .005. For an assumed .031 (6 mm) inspection criteria, the comparable probability is .096.

Figures 7.10 and 7.11 show the results for the last pin thread for a semi-elliptical crack growth and circumferential crack growth, res-

pectively. These results correspond to a single tendon element or component. The analysis was extended to estimate the failure probabilities for 20, 50 and 100 tendon elements in series. Results for the pipe are plotted in Figure 7.12, and the corresponding last pin thread results are shown in Figures 7.13 and 7.14. Considering the series effect with 50 elements, the probability of failure in 30 years is .21,

the probabilities are .01, .04 and .20. Thus, based on these worst case assumptions, a freely corroding tendon should be inspected to something on the order of .08 inch detectible flaw size every 10 years.

## 7.5 Conclusions

The above analysis is believed to present a conservative view of inspection requirements based on fracture mechanics and corrosion fatigue considerations. While these results are indicative, the number of assumptions and lack of data on material properties and loads should be considered in drawing any firm conclusions. For any specific application, the following data is needed as a minimum:

1) Site specific wave and wind data derived from observed or hindcast information over a sufficiently long period of time to determine a true fatigue environment.
2) Platform specific tendon tension (and bending if applicable) RAO's in the period of waves of interest. Significant second order loads (e. g. resonant springing) should also be included.
3) Accurate stress analysis of the critical components.
4) Material data derived for loadings similar to those expected in service. Also, the material should be the same as the component under consideration and under the same expected cathodic protection level.

## 7.6 References

1. Buchalet, C.C. and Bamford, W.H., 'Stress Intensity Factor Solutions for Continuous Surface Flaws in Reactor Pressure Vessels', Mechanics of Crack Growth, ASTM STP 590, 1976, pp.385-402.

2. Shah, R.C., 'Stress Intensity Factors for Through and Part-Through Crack Originating at Fastener Holes', Mechanics of Crack Growth, ASTM STP 590, ASTM, 1976, pp.429-459.

3. Hammouda, M.M., Smith, R.A., and Miller, K.J., Elastic-Plastic Fracture Mechanics for Initiation and Propagation of Notch Fatigue Cracks, Fatigue of Engineering Materials and Structures, Vol. 2, pg. 139-154, 1979.

4. Erdogan, F. and Wei, R.P., 'Fracture Mechanics and Corrosion Fatigue in Pipelines', Annual Report for Contract DTRS 58 82-C-00014, Lehigh University, Sept. 1983.

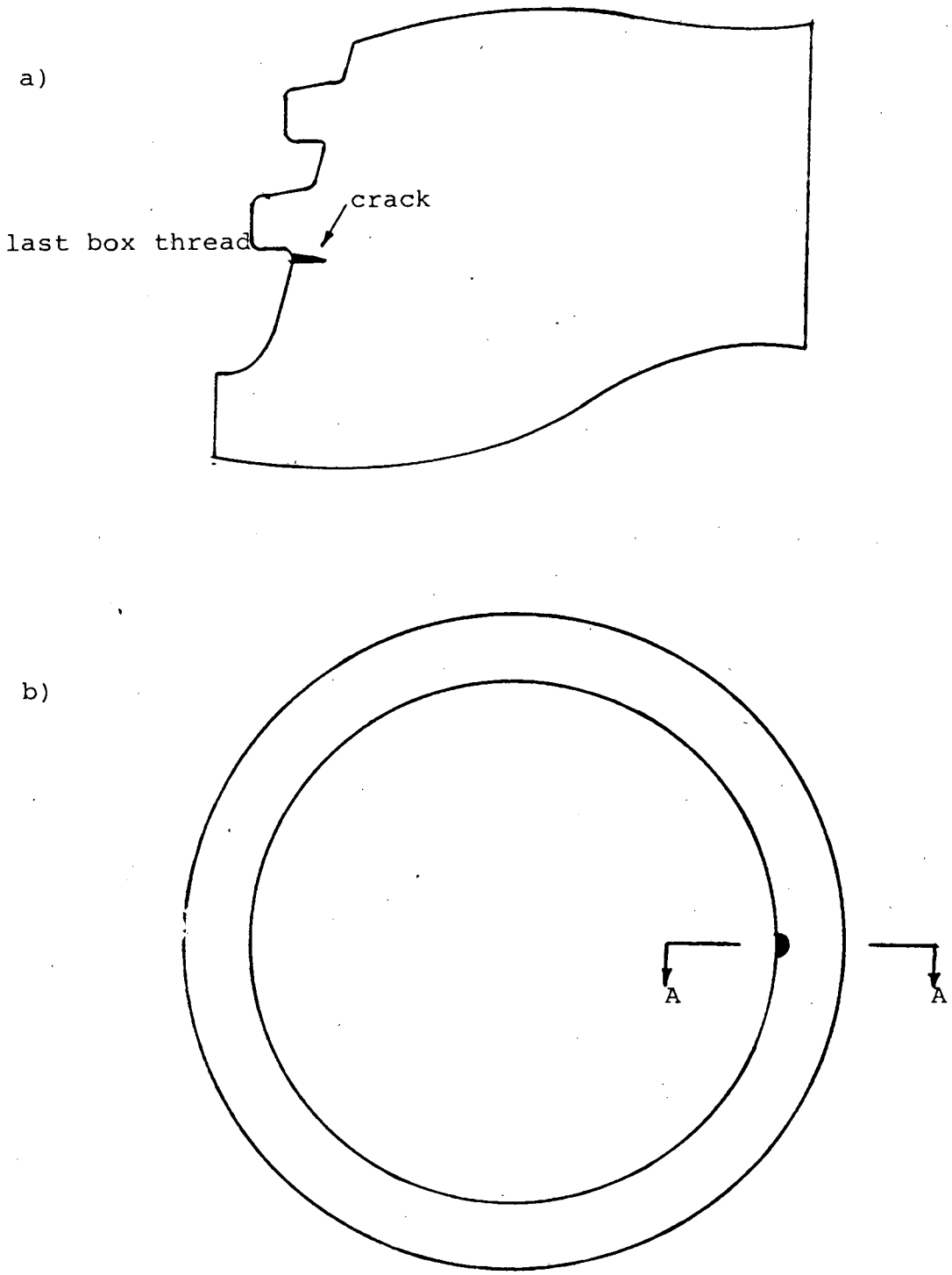


Figure 7.1 - a) side view of last box thread (view A-A)
b) cross section of first box thread with semi-elliptical crack(plan view)

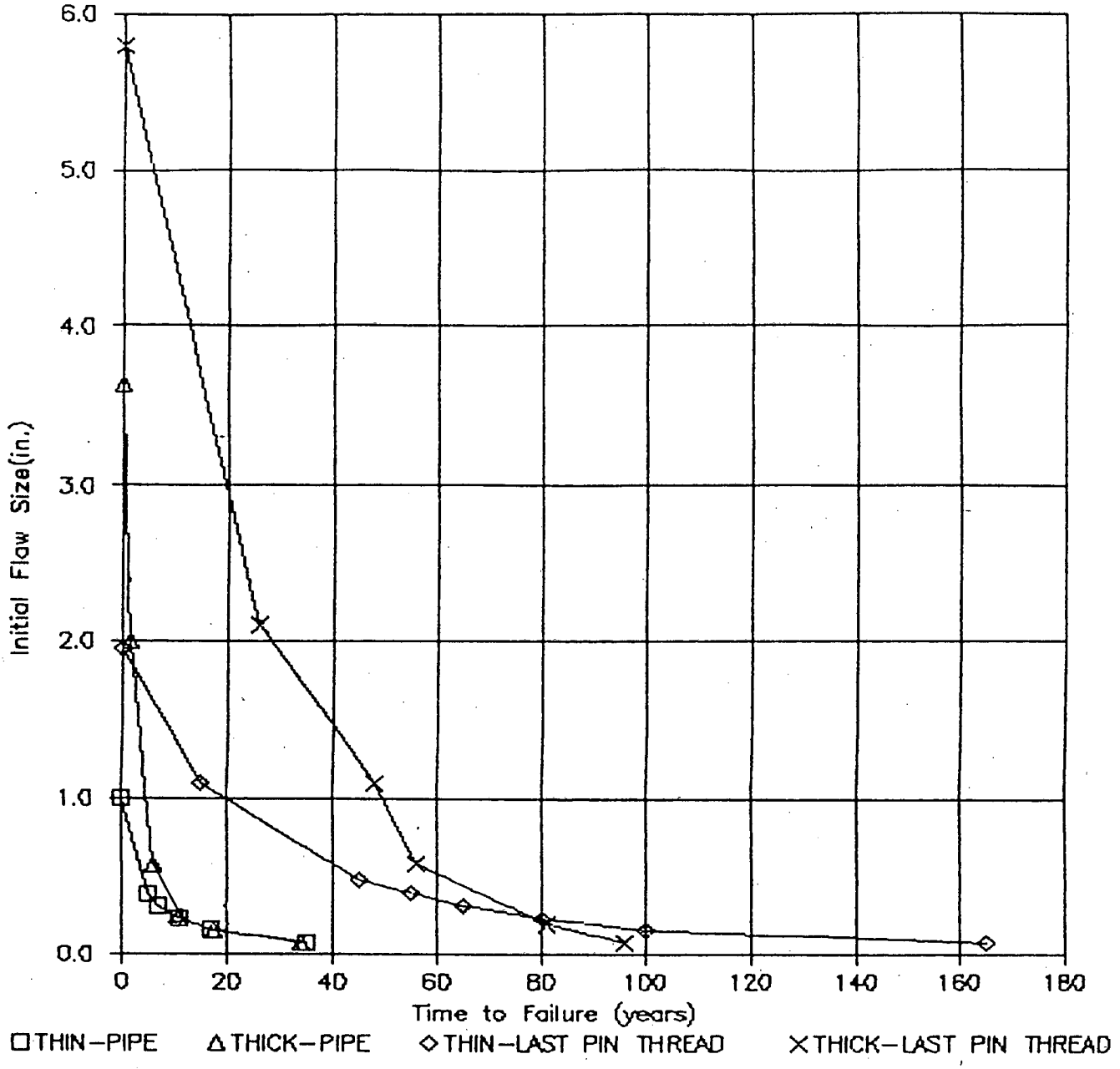


Figure 7.3 - Initial Flaw Size versus Time to Failure. A Comparison of Thick/Thin Walled Connectors.
Material Environment: Free Corrosion
Platform Environment: North Sea
Platform RAO: Dillingham
Stress Intensity Model: Semi-Elliptical Crack

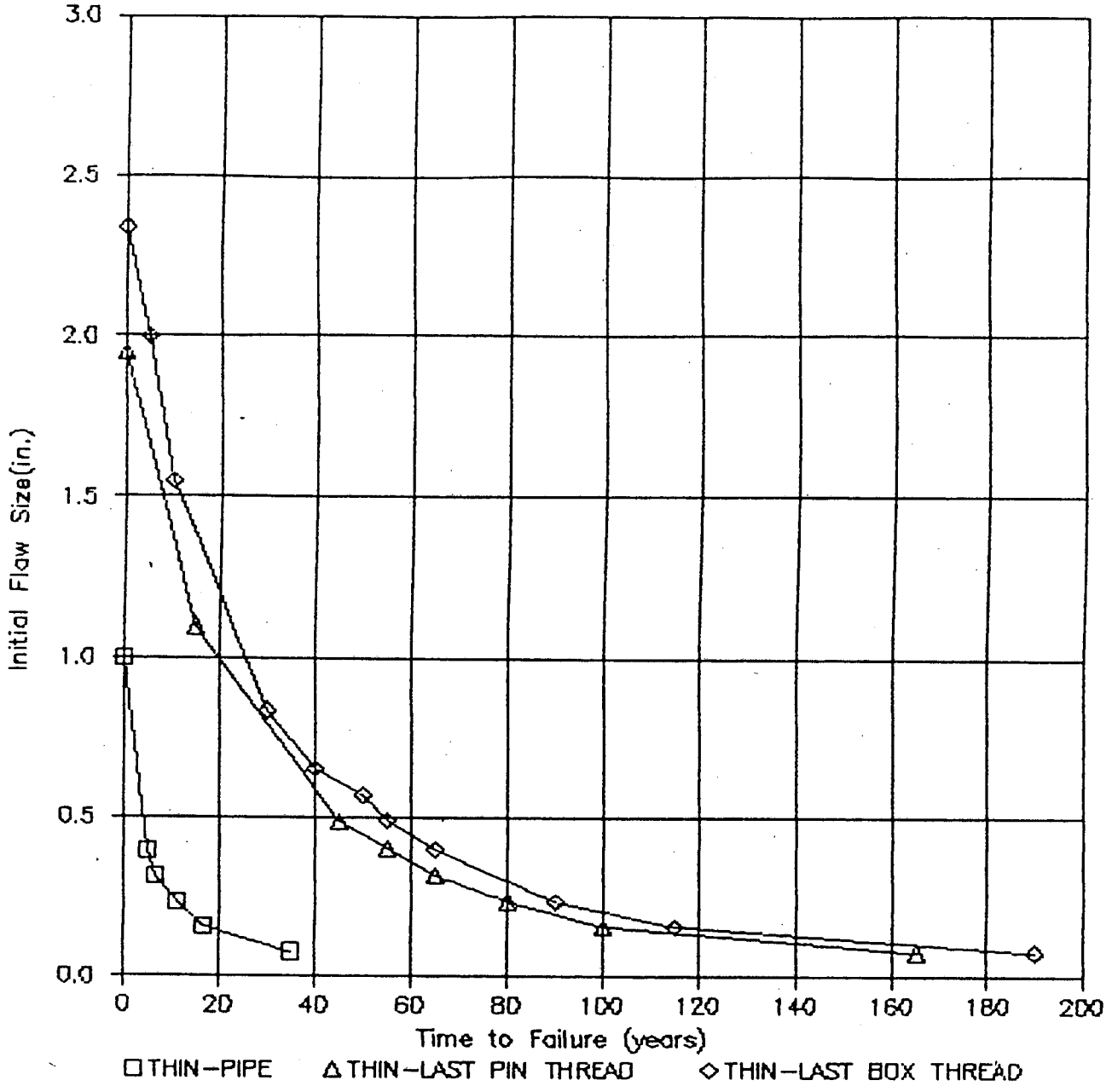


Figure 7.4a - Initial Flaw Size versus Time to Failure. A comparison of Tendon Cross Sections (Thin Walled).
Material Environment: Free Corrosion
Platform Environment: North Sea
Platform RAO: Dillingham
Stress Intensity Model: Semi-Elliptical Crack

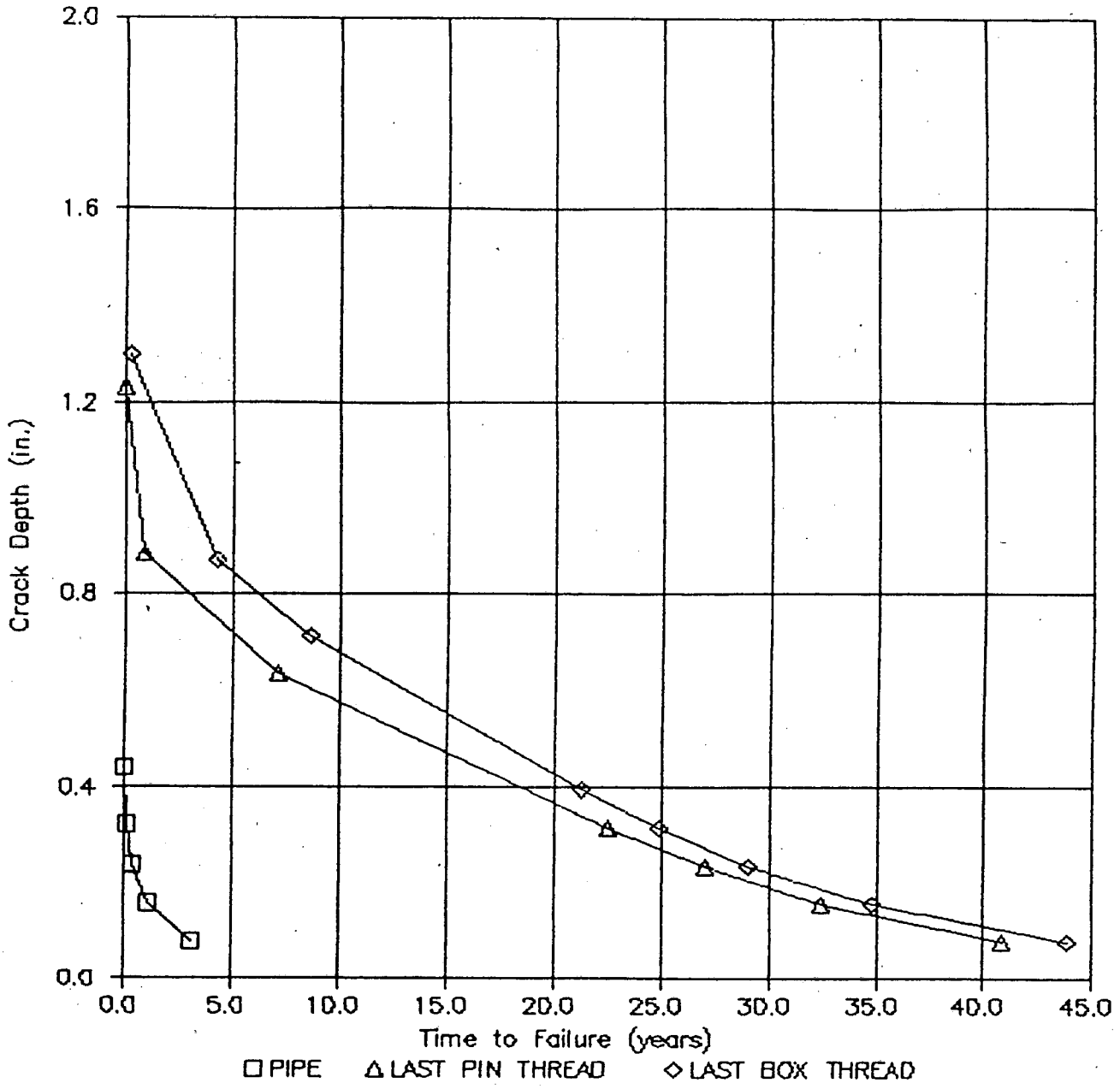


Figure 7.4b - Initial Flaw Size versus Time to Failure. A Comparison of Tendon Cross Sections (Thin Walled).
Material Environment: Free Corrosion
Platform Environment: North Sea
Platform RAO: Dillingham
Stress Intensity Model: Circumferentially Cracked Cylinder

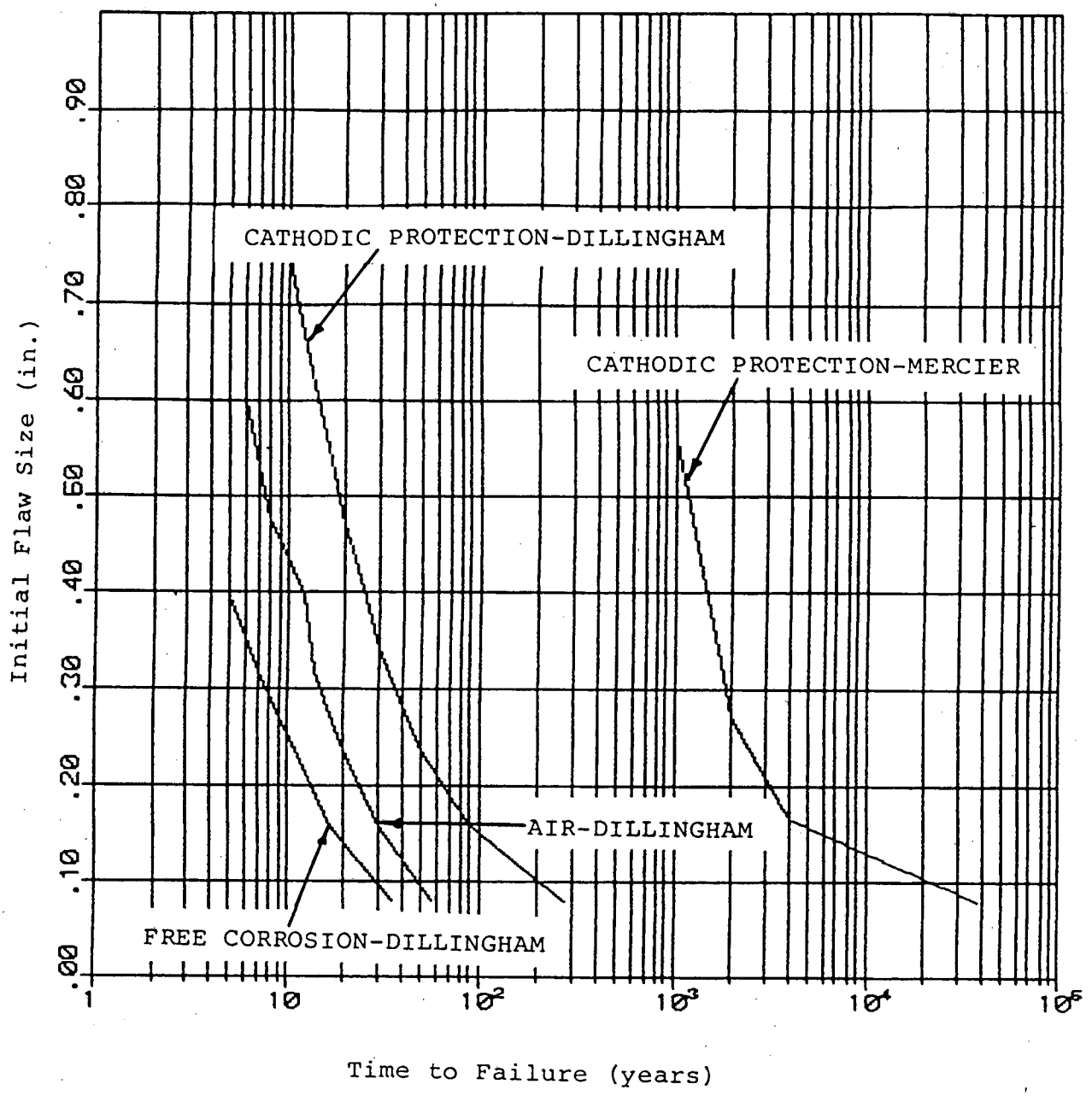


Figure 7.5 - Initial Flaw Size versus Time to Failure. A Comparison of Material Environments (Thin Walled).
Platform Environment: North Sea
Platform RAO: Dillingham/Mercier
Tendon Cross Section: Pipe
Stress Intensity Model: Semi-Elliptical Crack

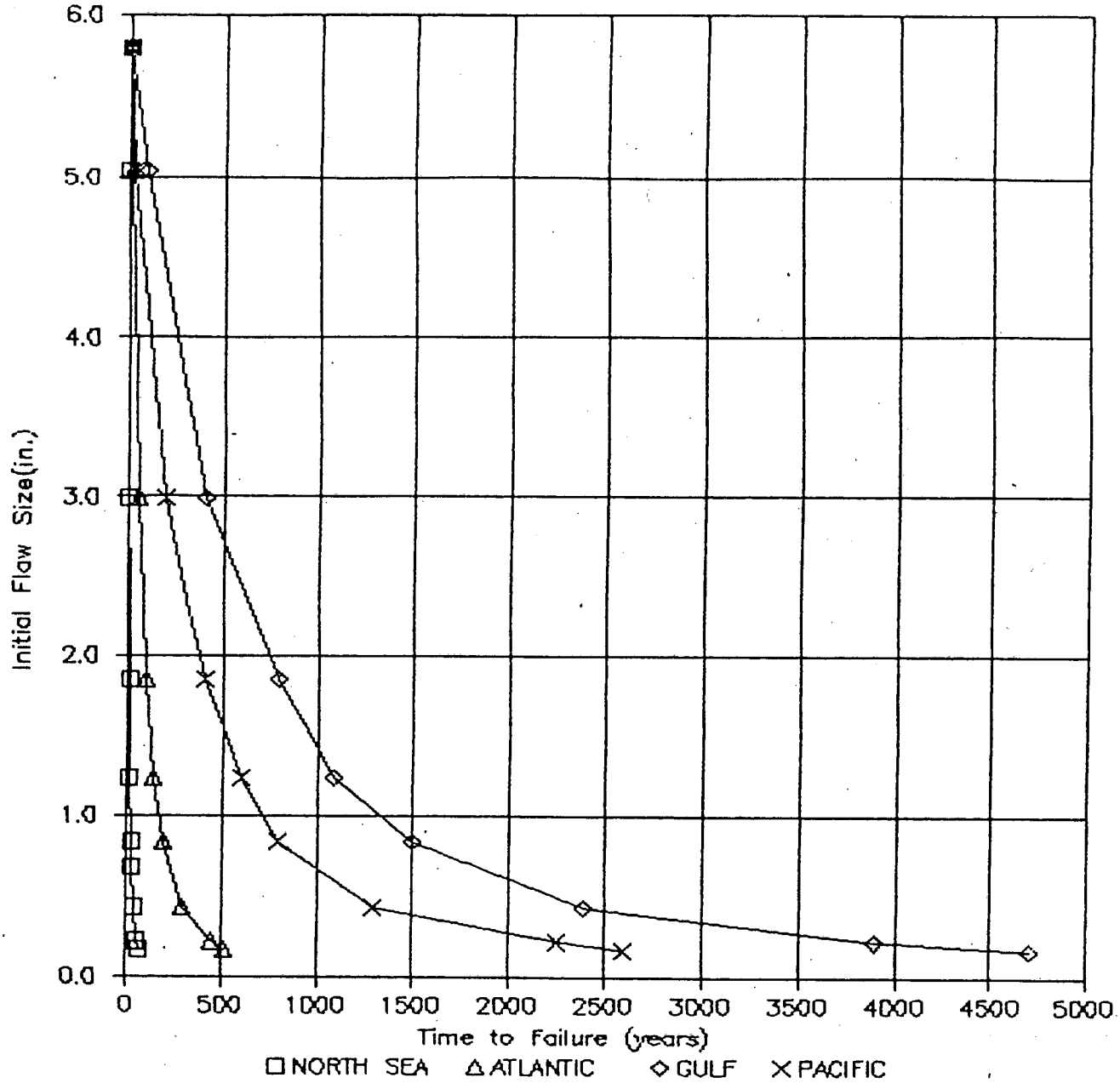


Figure 7.6a - Initial Flaw Size versus Time to Failure. A Comparison of Platform Environments (Thick Walled).
Material Environment: Free Corrosion
Platform RAO: Dillingham
Tendon Cross Section: Last Box Thread
Stress Intensity Model: Semi-Elliptical Crack

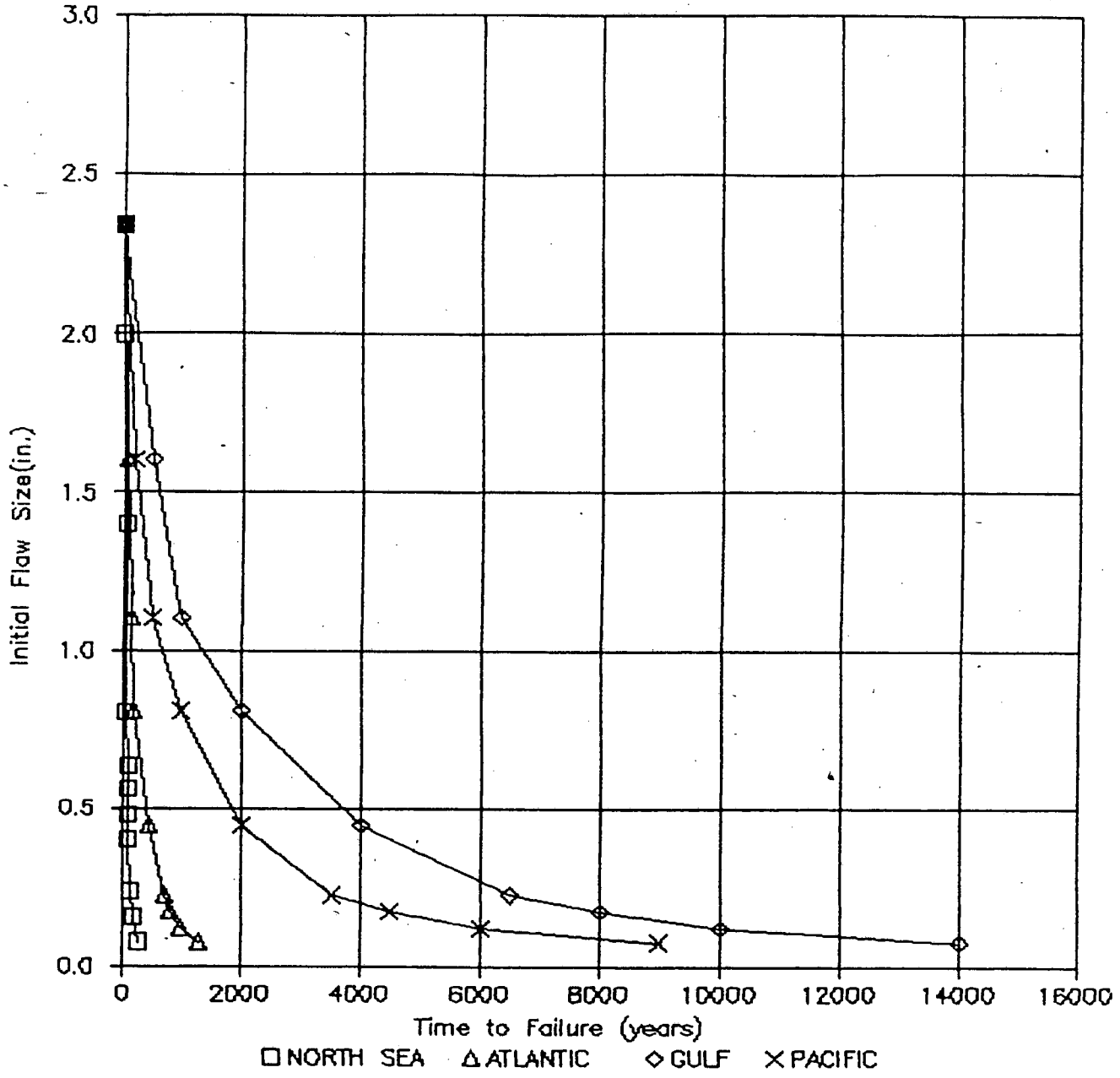


Figure 7.6b - Initial Flaw Size versus Time to Failure. A Comparison of Platform Environments (Thin Walled).
Material Environment: Free Corrosion
Platform Environment: Dillingham
Tendon Cross Section: Last Box Thread
Stress Intensity Model: Semi-Elliptical Crack

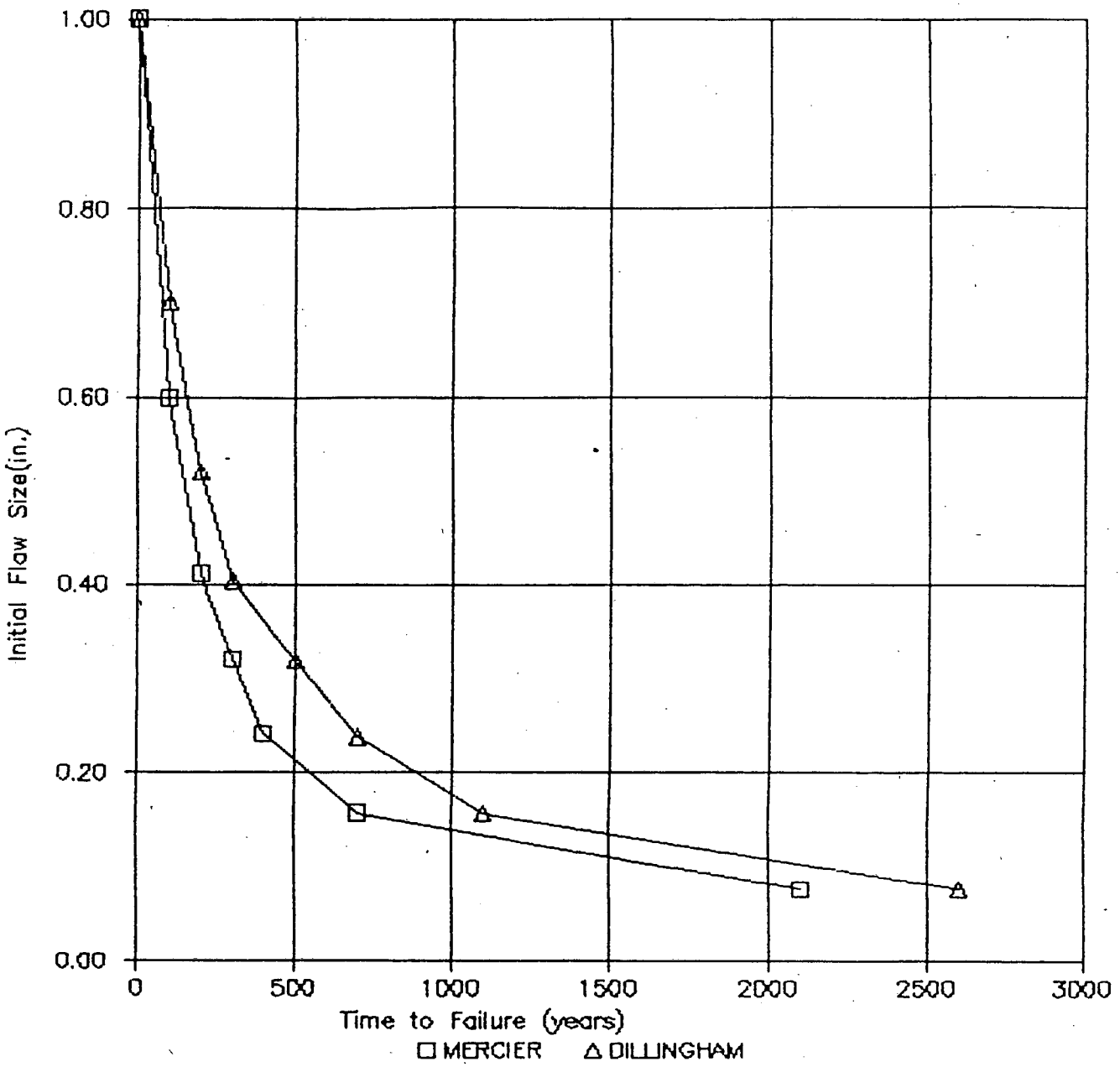


Figure 7.7 - Initial Flaw Size versus Time to Failure. A Comparison of Tendon Tension RAO (Thin Walled).
Material Environment: Free Corrosion
Platform Environment: Gulf of Mexico
Tendon Cross Section: Pipe
Stress Intensity Model: Semi-Elliptical Crack

Figure 7.8 - Probabilistic flow chart.

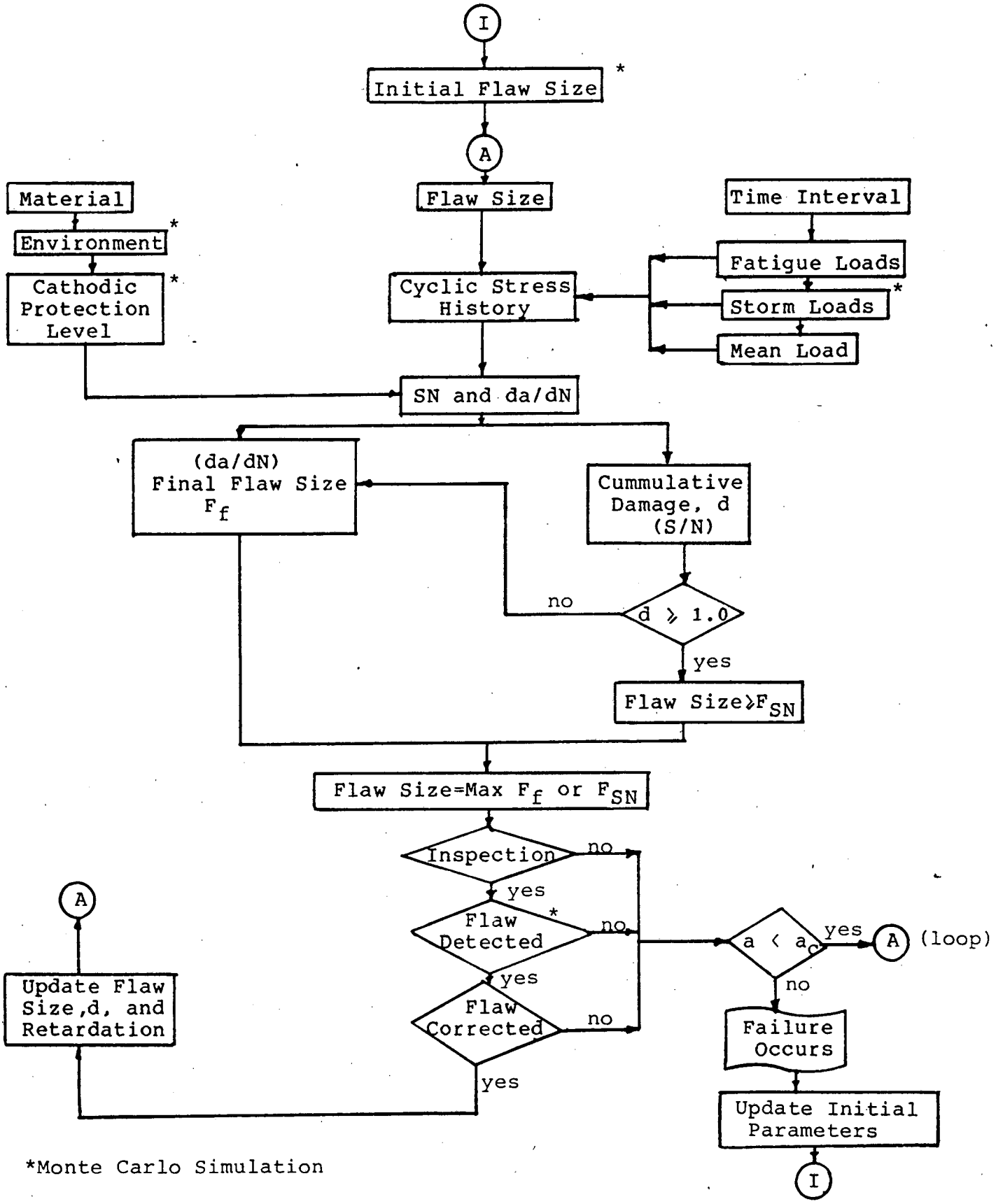


*Monte Carlo Simulation

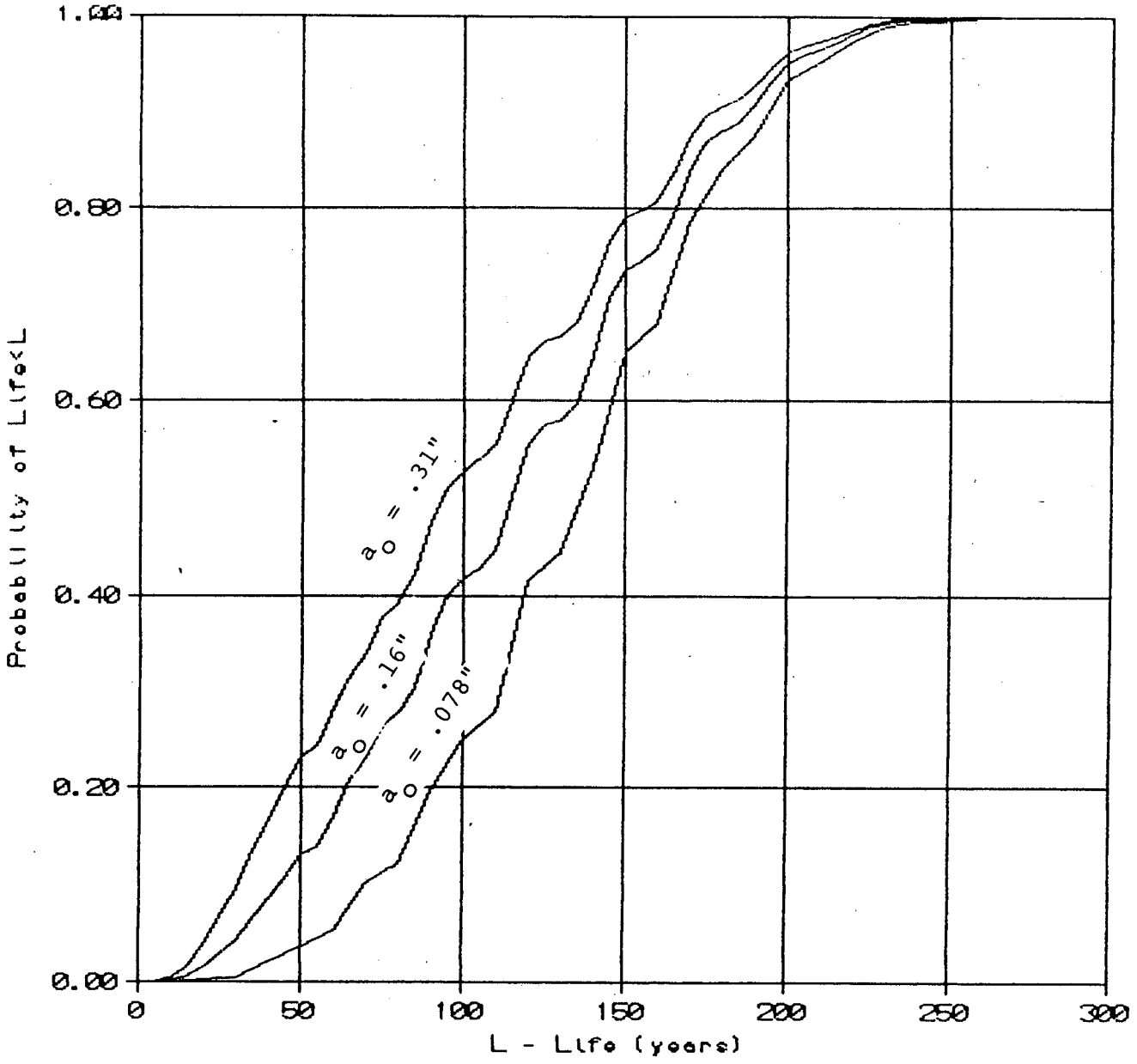


Figure 7.9a - Probability of Life < L.
Material Environment: Free Corrosion
Platform Environment: North Sea
Platform RAO: Dillingham
Tendon Cross Section: Pipe (thin walled)
Stress Intensity Model: Semi-Elliptical Crack

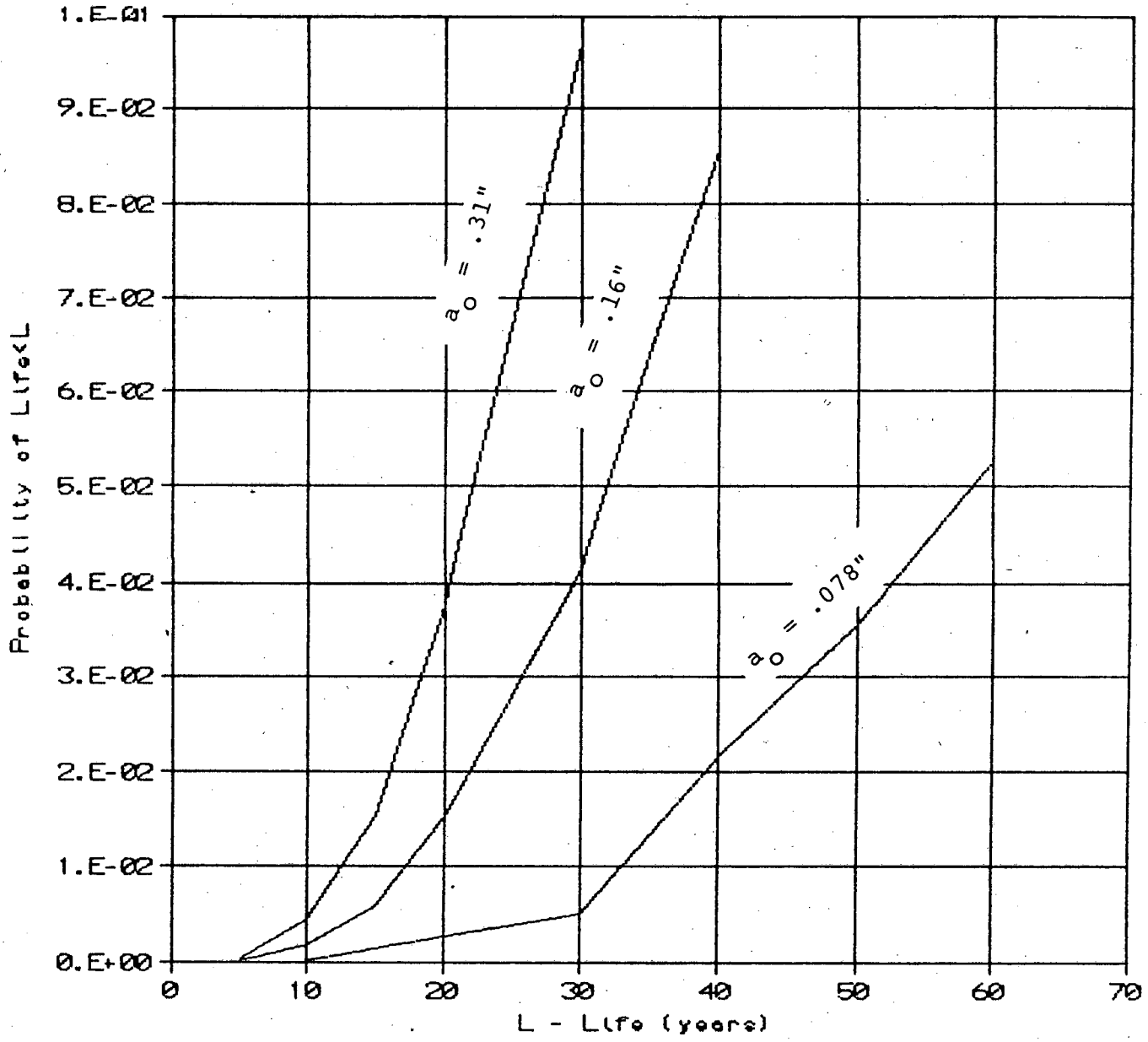


Figure 7.9b - Probability of Life < L. (exploded view)
Material Environment: Free Corrosion
Platform Environment: North Sea
Platform RAO: Dillingham
Tendon Cross Section: Pipe (thin walled)
Stress Intensity Model: Semi-Elliptical Crack

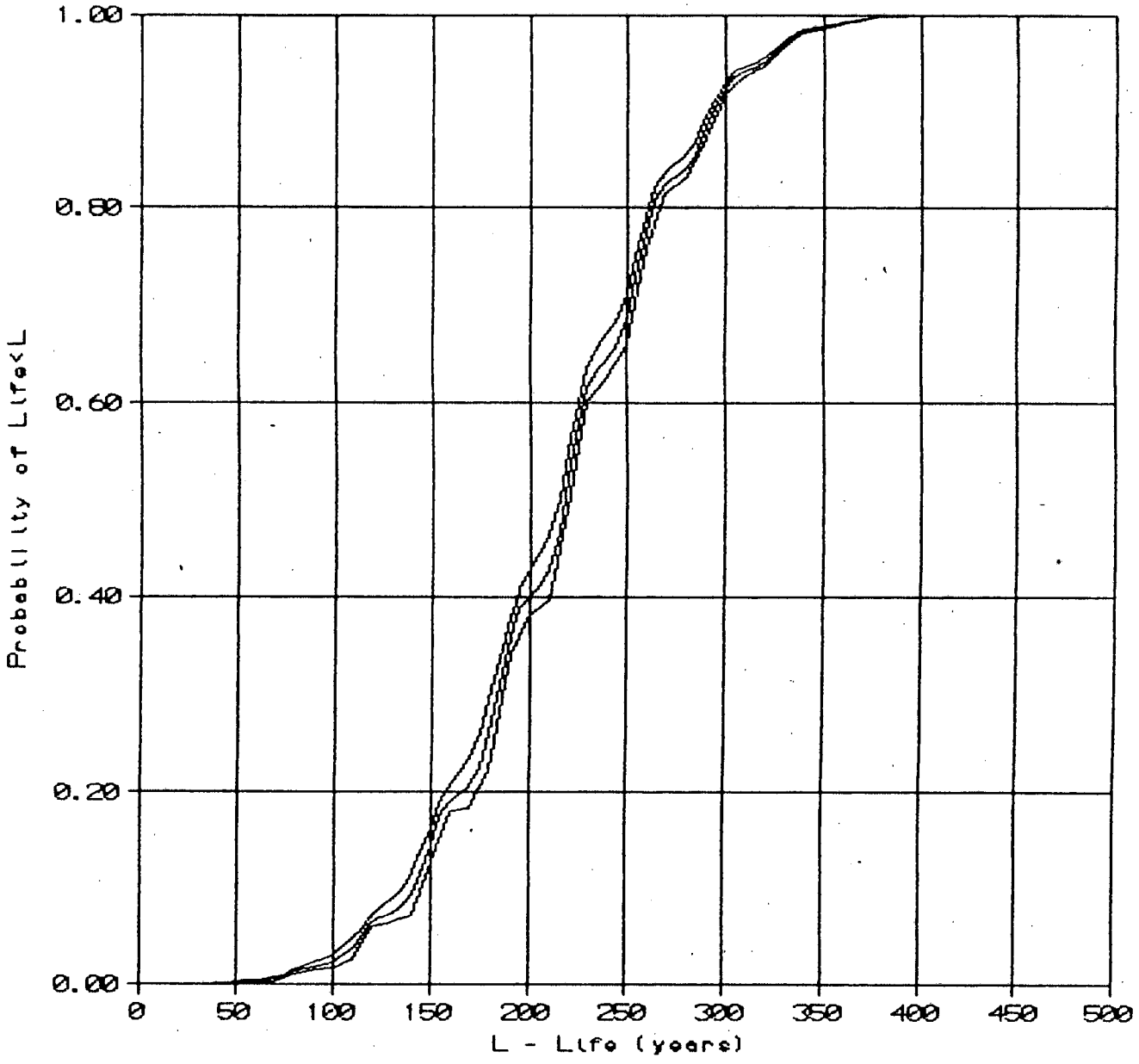


Figure 7.10a - Probability of Life < L.
Material Environment: Free Corrosion
Platform Environment: North Sea
Platform RAO: Dillingham
Tendon Cross Section: Last Pin Thread (thin walled)
Stress Intensity Model: Semi-Elliptical Crack

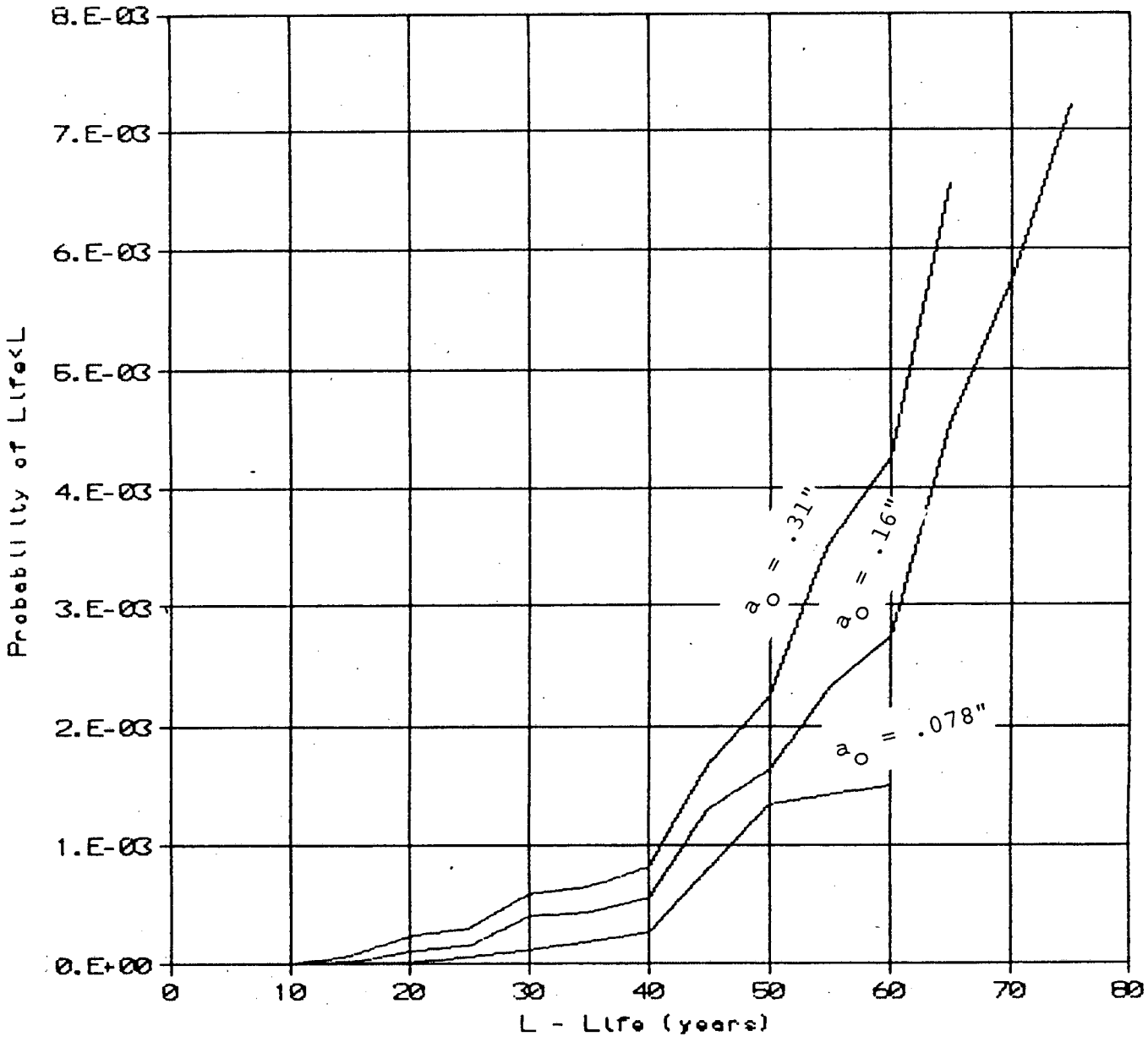


Figure 7.10b - Probability of Life < L. (exploded view)
Material Environment: Free Corrosion
Platform Environment: North Sea
Platform RAO: Dillingham
Tendon Cross Section: Last Pin Thread (thin walled)
Stress Intensity Model: Semi-Elliptical Crack

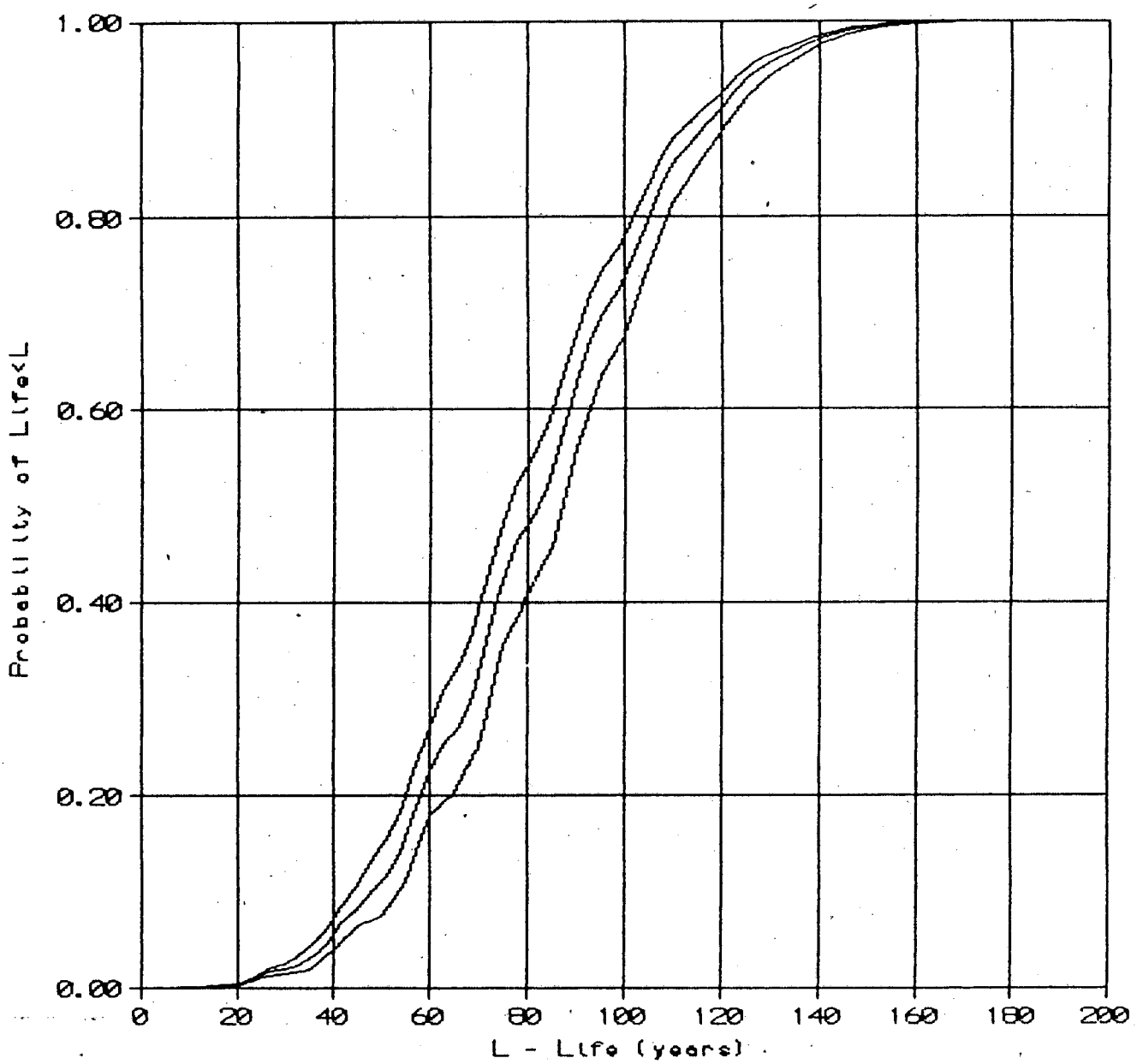


Figure 7.11a - Probability of Life < L.
Material Environment: Free Corrosion
Platform Environment: North Sea
Platform RAO: Dillingham
Tendon Cross Section: Last Pin Thread (thin walled)
Stress Intensity Model: Circumferential Crack

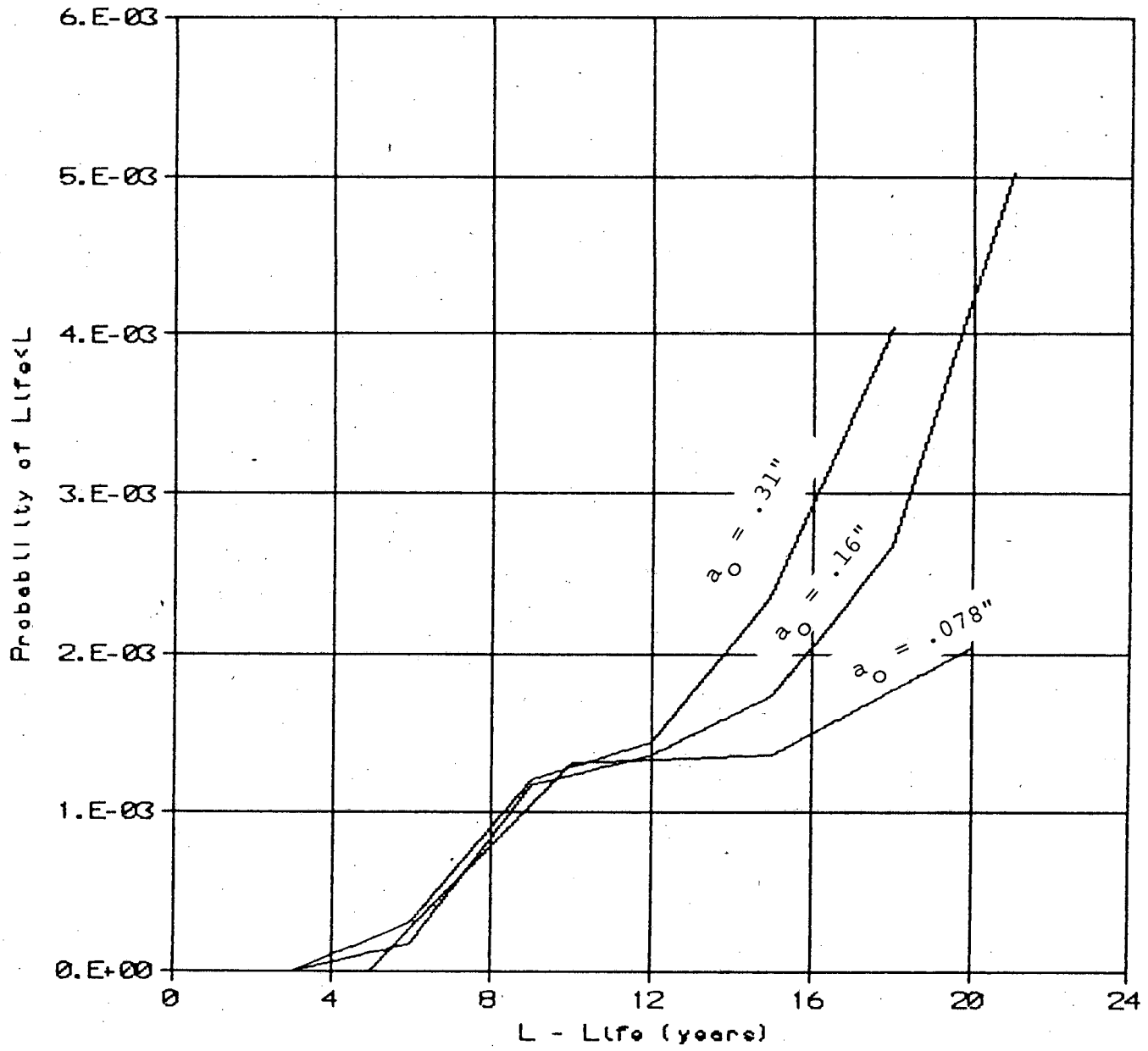


Figure 7.11b - Probability of Life < L. (exploded view)
Material Environment: Free Corrosion
Platform Environment: North Sea
Platform RAO: Dillingham
Tendon Cross Section: Last Pin Thread (thin walled)
Stress Intensity Model: Circumferential Crack

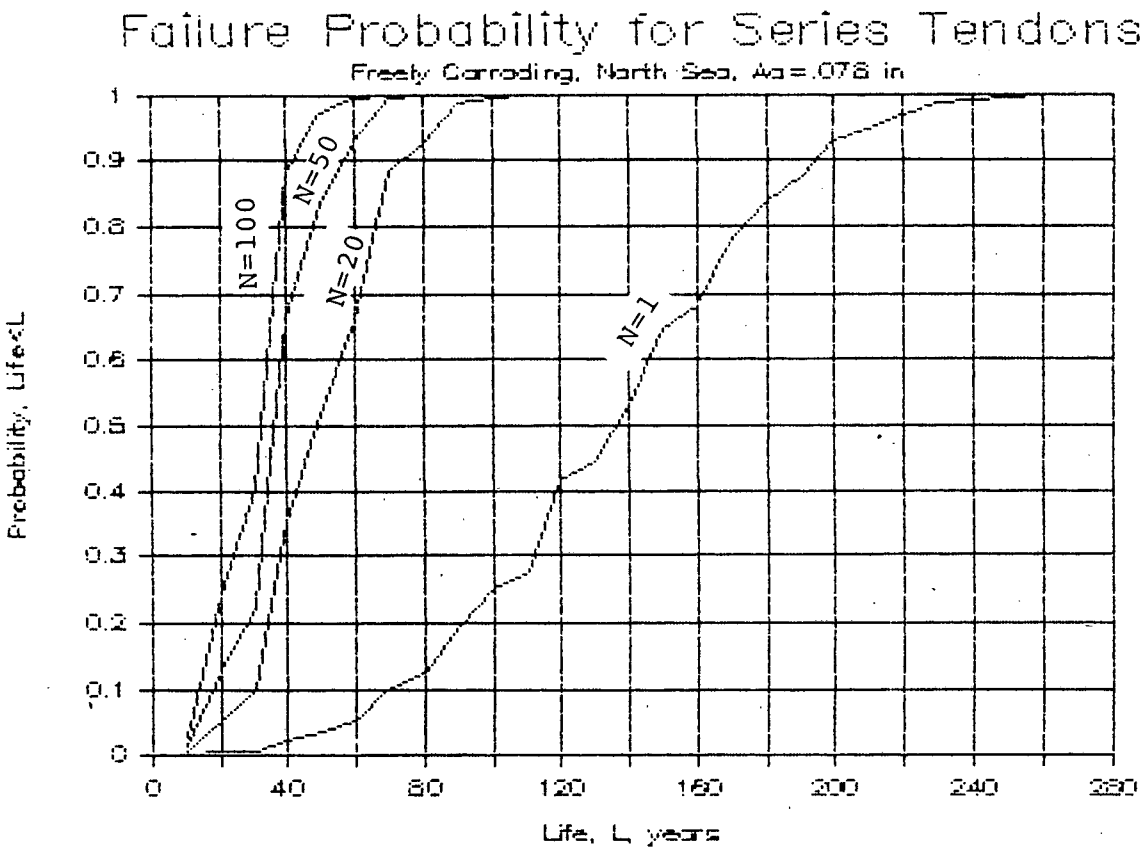


Figure 7.12a
(thin walled pipe section)

Figure 7.12b
(thin walled pipe section)

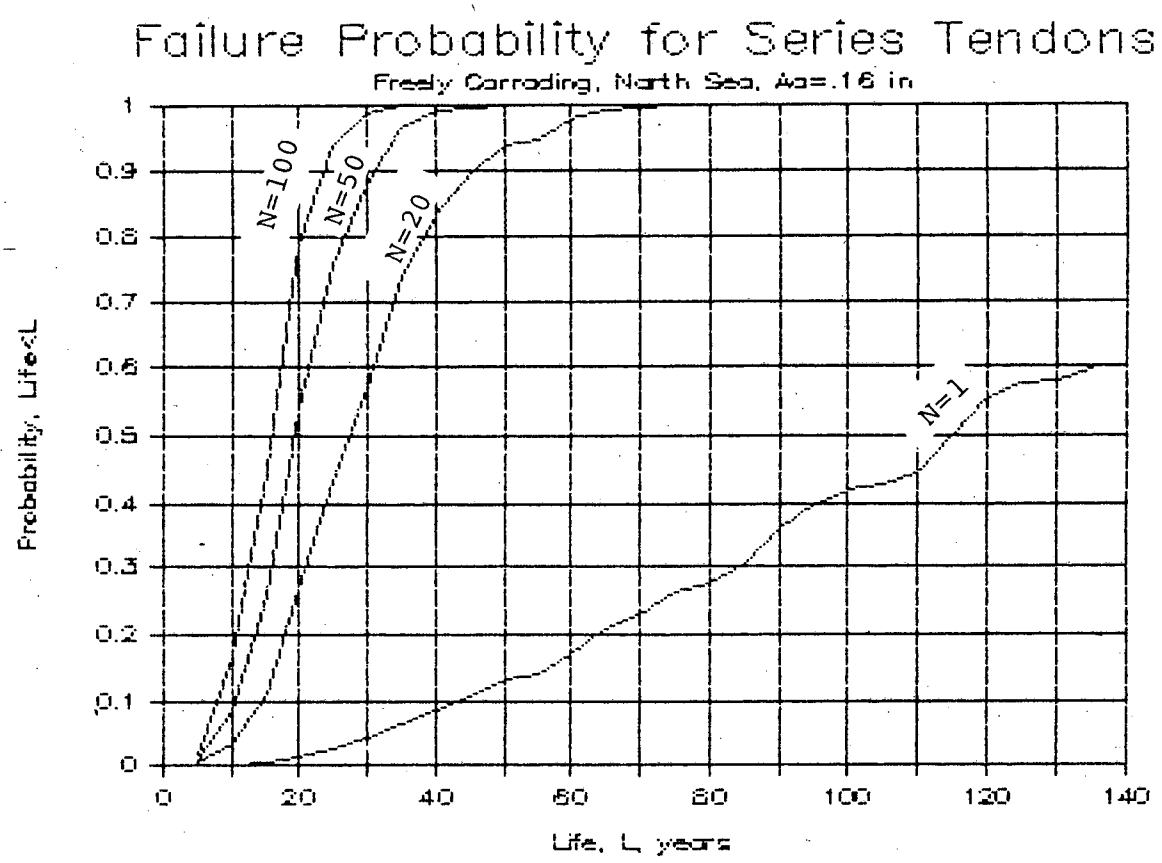


Figure 7.12c
(thin walled pipe section)

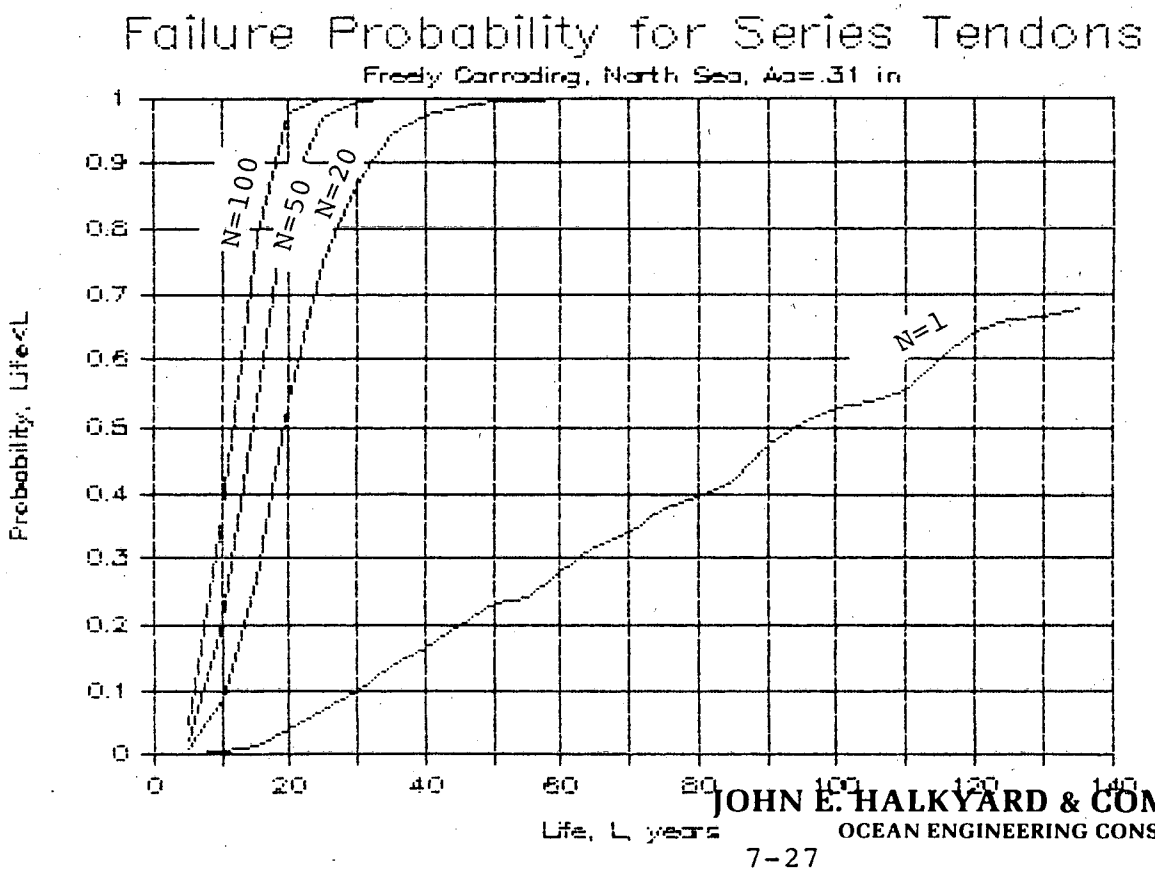

Figure 7.13
(Last Pin Thread, Circumferential Crack)

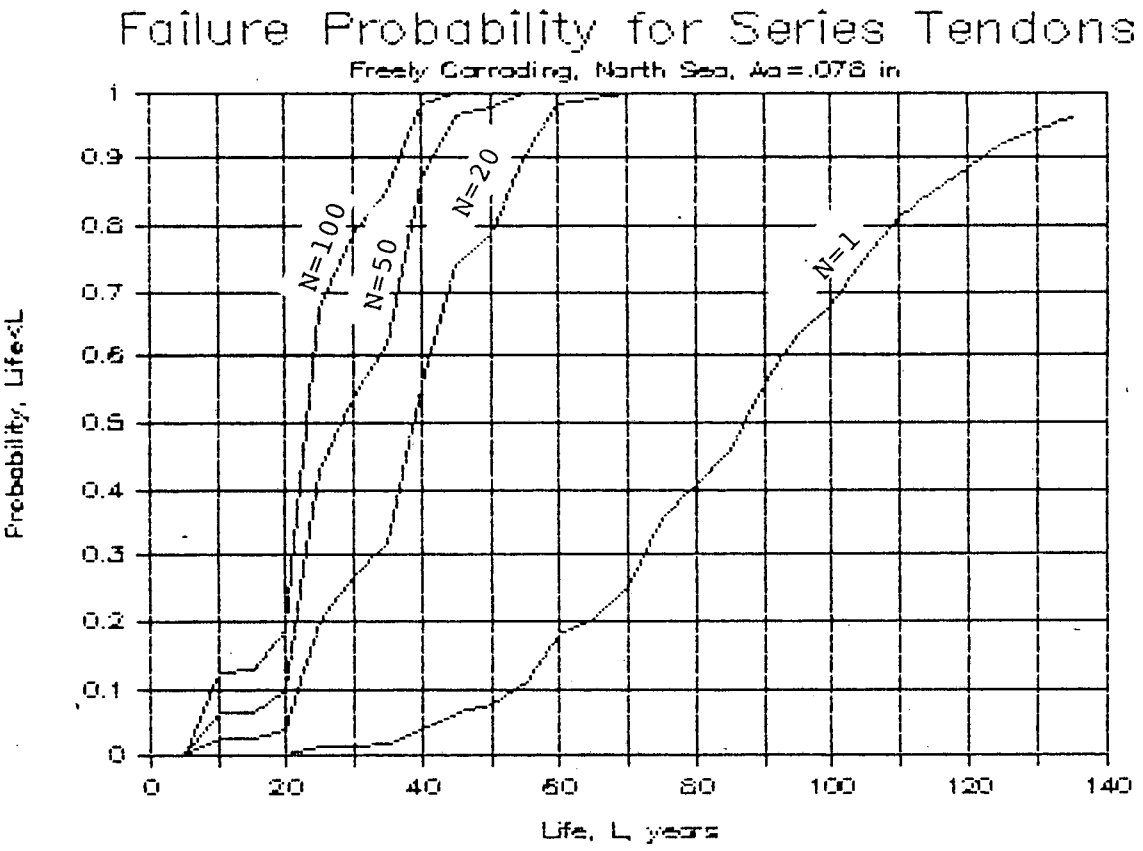


Figure 7.14
(Last Pin Thread, Semi-elliptical Crack)

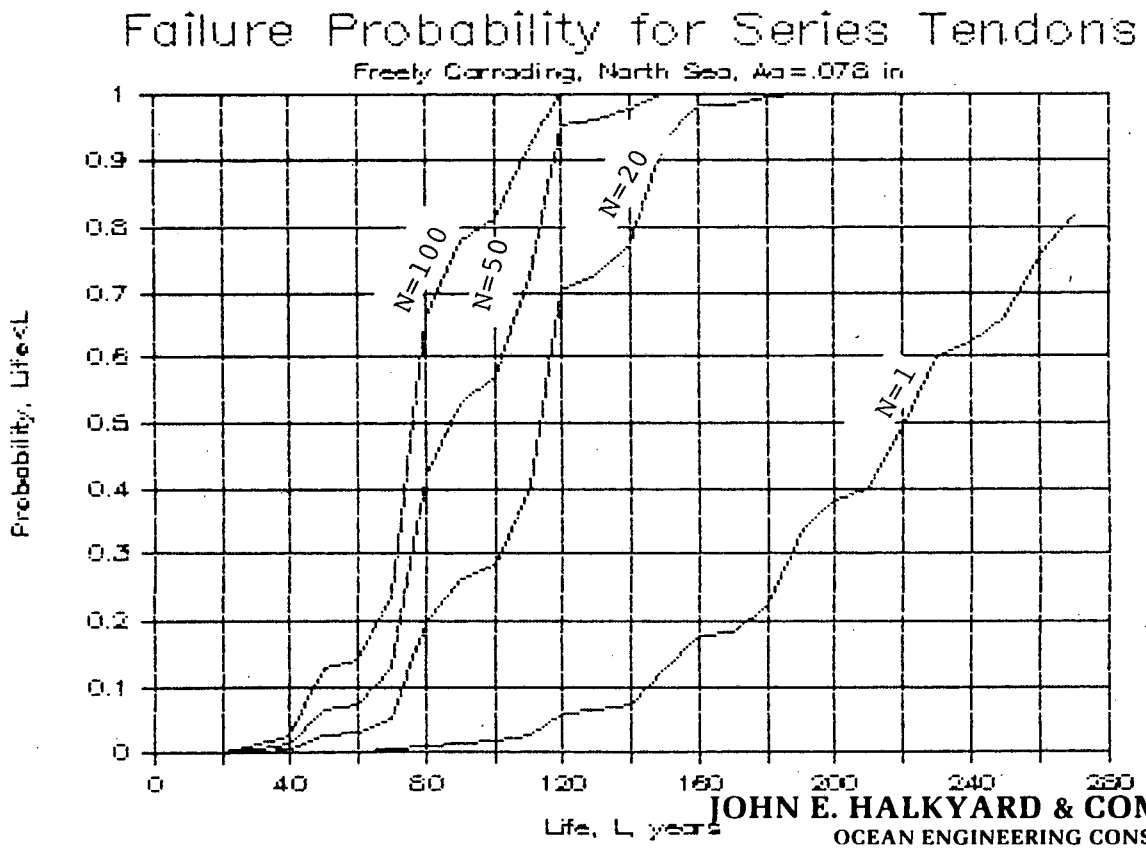

# 8.0 Future Research Recommendations

## 8.1 Objectives

The primary objective of this work is to determine the effectiveness of tendon system inspection as a means for insuring the structural reliability of TLP tendons, and to specify methods for evaluating inspection criteria. During Phase I, theoretical models for ultrasonic inspection and tendon fatigue failure under realistic conditions were developed. This work showed that in place inspection could provide an effective means of early crack detection provided assumptions of our model are correct. The objective of future research is, therefore, to verify our assumptions and theoretical models.

## 8.2 Approach

Our assessment indicates the following are key factors relating to the effectiveness of an inspection program and predicted life of a TLP system:

I. Inspection Device Performance
   a) Location and shape of critical cracks
   b) Reflection or 'shadowing' characteristics of actual cracks in tendon material.
   c) Material acoustic attenuation.
   d) Effect of surface treatments (e.g. flame spraying) on acoustic responses.

II. Failure Model
   a) Actual load/stress histories.
   b) Environment at critical locations.
   c) Form of fatigue cracks, i.e. number of nucleation sites.
   d) Crack growth for high R, low $\Delta K$, short cracks under actual environments.

The failure model is used to evaluate the effectiveness of different inspection schemes under different loading/environmental scenarios.

In order to verify both the inspection device performance and the failure model, five separate but related activities are suggested:

1. Ultrasonic Model Developemnt
2. Tubular Joint Fatigue Testing

3. Materials Testing
4. TLP Tendon Analysis
5. Full Scale Tendon Component Testing

The first three activities are 'generic' and not directed at a specific tendon design or location. The latter two activities deal with specific locations, loads and/or tendon designs.

The purpose of activities 1-3 is to develop a data base and level of confidence in our approach which can be utilized to evaluate actual tendon designs. At this time, tendon designs are proprietary and may not be available for testing.

The following section discusses the specific activities in more detail. Appendix B provides an outline of these tasks. Note that our proposed Phase II program does not include the entire scope of the suggested activities.

## 8.3 Ultrasonic Model Development and Verification

The ultrasonic model includes assumptions about acoustic attenuation, transmissivity, reflectivity and the reflection and scattering properties of cracks and threads. The assumed conditions are a function of material (i.e. grain size) and surface properties, flaw location and geometry, thread geometry, ultrasonic frequency and beam angles.

To develop this model, basic tests should be conducted on plates with machined taper, notches and threads. The plates should have representative metallurgy and should be sized to correspond to the thickness of the 'thick walled' connector (6.8 inch w.t.), the 'thin walled' (2.5 inch w.t.), and a connector corresponding to the connector to be tested in the fatigue test program. This 'generic' connector could, for example, be a rotary shouldered tool joint or an integral casing joint with buttress threads.

These tests would result in detection levels as a function of flaw size and shape, location (i.e. distance from source and detection, and beam angle), and thread form.

Following these tests, the model would be refined and an inspection system designed for the joints to be fatigue tested.

An optional experiment could be run on actual tendon elements if

they would be available. In this case, an additional inspection system would be designed and built.

Static tests could then be conducted on the tool joint and/or the tendon joint. These tests would be designed to establish inspection limits for different sized machined cracks at different locations. Two experiments could be run:

a) Calibration experiments on known cracks.

b) 'Blind' inspection to determine the probability of detecting unknown cracks of various sizes at different locations.

## 8.4 Fatigue Testing on 'Generic' Connector

The effectiveness of an inspection program depends on the ability to detect actual fatigue cracks early enough to allow repair or replacement of the defective component. The above experiments are based on 'ideal' machined cracks of circular or elliptical form. If a crack tends to form as a long shallow crack (i.e. from several nucleation sites) before it grows into the wall appreciably then the length of time required for growth to critical flaw size is reduced significantly (at least one order of magnitude) over that of an elliptical crack growing through the wall. Only fatigue tests under realistic geometrical or stress conditions can address this issue.

An important consideration in the testing is the environment, loading and frequency. Tendons will probably (but not necessarily always) be cathodically protected on the outside and have a benign fluid or air on the inside. The Hutton tendons have a flame sprayed aluminum coating, which acts as a sacrificial anode.

The connector threads are nominally sealed from the external fluid by a metalic and/or elastomeric seal. However, from a reliability standpoint, the possibility of sea water leakage needs to be considered.

Table 8.1 indicates the possible environments for a tendon connector and pipe.

In order to satisfy all of our objectives, the following tentative test plan is proposed:

A. Test connectors with machined crack to monitor crack growth.

1) Fresh water on I.D., air outside
2) Sea water on I.D. and in threads, freely corroding
3) Sea water on I.D. and in threads, cathodically protected

B. Test connector to determine location and form of fatigue crack nucleation sites.

1) Fresh water on I.D., sea water on O.D., freely corroding.
2) Fresh water on I.D., sea water on O.D., cathodically protected.
3) Fresh water on I.D., sea water on O.D., flame sprayed.
4) Seawater on O.D., I.D. and in threads, freely corroding.

These tests would be conducted with redundant means of detecting crack initiation and growth. Acoustic emission monitoring could be used to detect crack initiation. External ultrasonic inspection would identify and size cracks and would establish a comparison for the internal probe.

Test series A. should consist of relatively short duration tests. Crack growth near threshold stress intensities should be monitored to confirm the Region I da/dN curve. Resolution will be limited to that attainable by ultrasonic or other means of NDT inspection.

Series B tests could be several months duration to adequately account for environmental effects and high cycle fatigue life.

## 8.5 TLP Tendon Analysis

### 8.5.1 Tendon Loads

Our conclusions regarding tendon reliability depend to a large degree on confidence in the wave/environmental data, and the loads and computed stress and stress intensities in our failure model. In Phase I we utilized hindcast SOWM environmental data, which should be as accurate as any method available. The tendon tension responses derived from published data show a large scatter, however, and the reasons for the scatter can't be pinpointed because of the lack of specific data or analytical procedures and program verification in the published sources.

While the exact loads can not be determined without an actual

platform preliminary design, a self consistent set of calculations considering parametric changes in platform and tendon parameters would be useful in assessing the sensitivity of tendon fatigue life to changes in platform parameters (e.g. displacement, column/pontoon volume ratios, number and spacing of columns).

Also, linear RAO's do not account for wave springing forces and diffraction effects for waves less than 8-10 second periods. Since these waves account for a significant percentage of fatigue damage, these effects should be evaluated.

### 8.5.2 Stress Analysis

During Phase I, connector stresses and stress intensities were estimated using hand calculation methods and stress intensity results from simple geometries. The crack growth predictions are highly sensitive to stress intensities, hence any inaccuracies in these would be amplified in our life estimates.

To eleviate this, 3-dimensional finite element analysis of the threaded joints with cracks could be conducted to determine stress intensities. The FEA results would then be utilzied to develop algorythms for stress intensity in the threads for various crack depths and widths. These algorythms could be generalized to handle various connector shapes and thread forms by examining parametric relationships between the through thickness stress profile of an uncracked connector and the stress intensities for various crack geometries.

Finally, utilizing revised load and stress data, reliability calculations for the TLP could be updated.

## 8.6 Material Tests

This work has revealed a need for additional fatigue data. While several investigators are currently working on material data for TLP tendons, much of the data is proprietary or not published yet. In particular, the following data is needed:

A. da/dN data for high R ratio, low stress intensities (Region I), short crack, cathodically protected and flame sprayed low alloy high strength steels.

B. S-N data under similar conditions, especially data on the transition from crack initiation to crack growth.

A plan for these tests needs to be developed. Standard da/dN tests using compact tension test specimens could be used with fatigue cracks initiated by high cyclic loadings. The transition from crack initiation could be investigated using microscopic examination, magnetic flux techniques, radiography or other methods to detect small cracks.

Another alternative might be to simulate the thread stress profile with notches machined into pipe or rods. The process of crack nucleation and growth could then be examined on a smaller scale than the tool joint fatigue tests.

## 8.7 Full Scale Tendon Fatigue Tests

The above research should lead to rational criteria for TLP tendon design (and platform preliminary design). Once an actual tendon has been built, full scale fatigue tests should be conducted to confirm failure analysis.

This work is beyond the scope of the current project, but should be considered as a logical extension.

**APPENDIX A**

Environmental Data

DATA FOR GRID POINT 212(GULF OF MEXICO). BASED ON 26540 RECORDS-20 YEARS.
DIRECTIONS MEASURED CLOCKWISE FROM NORTH. LATITUDE=25.6 DEGREES.
LONGITUDE=92.4 DEGREES.

PEAK FREQUENCY VERSUS H-SIGNIFICANT - FREQUENCY OF OCCURANCE

| FREQ | PERIOD | H-SIGNIFICANT [FEET] | | | | | | | | | | | |
|---|---|---|---|---|---|---|---|---|---|---|---|---|---|
| | | 0-1 | 1-3 | 3-5 | 5-7 | 7-9 | 9-11 | 11-13 | 13-18 | 18-25 | 25-35 | 35-45 | 45-60 |
| .308 | 3.25 | .644 | 2.961 | .000 | .000 | .000 | .000 | .000 | .000 | .000 | .000 | .000 | .000 |
| .208 | 4.81 | .000 | .844 | 1.876 | .000 | .000 | .000 | .000 | .000 | .000 | .000 | .000 | .000 |
| .158 | 6.33 | 3.591 | 17.128 | 12.746 | 4.404 | .053 | .000 | .000 | .000 | .000 | .000 | .000 | .000 |
| .133 | 7.52 | .904 | 5.150 | 5.147 | 6.446 | 2.490 | .053 | .000 | .000 | .000 | .000 | .000 | .000 |
| .117 | 8.55 | 1.533 | 7.328 | 4.740 | 3.278 | 3.086 | 1.413 | .173 | .004 | .000 | .000 | .000 | .000 |
| .103 | 9.71 | .452 | 2.400 | 1.567 | 1.074 | 1.006 | 1.243 | 1.100 | .373 | .000 | .000 | .000 | .000 |
| .092 | 10.87 | .147 | .550 | .426 | .294 | .117 | .124 | .173 | .588 | .026 | .000 | .000 | .000 |
| .081 | 12.35 | .038 | .241 | .147 | .064 | .109 | .034 | .030 | .154 | .166 | .004 | .000 | .000 |
| .072 | 13.89 | .113 | .203 | .064 | .030 | .004 | .019 | .008 | .000 | .026 | .000 | .000 | .000 |
| .067 | 14.93 | .015 | .185 | .068 | .011 | .000 | .000 | .004 | .004 | .004 | .008 | .000 | .000 |
| .061 | 16.39 | .132 | .347 | .075 | .011 | .008 | .015 | .004 | .000 | .000 | .000 | .000 | .000 |
| .056 | 17.86 | .000 | .000 | .000 | .000 | .000 | .000 | .000 | .000 | .000 | .000 | .000 | .000 |
| .050 | 20.00 | .000 | .000 | .000 | .000 | .000 | .000 | .000 | .000 | .000 | .000 | .000 | .000 |
| .044 | 22.73 | .000 | .000 | .000 | .000 | .000 | .000 | .000 | .000 | .000 | .000 | .000 | .000 |
| .039 | 25.64 | .000 | .000 | .000 | .000 | .000 | .000 | .000 | .000 | .000 | .000 | .000 | .000 |

DIRECTION OF MAXIMUM S(THETA) VERSUS H-SIGNIFICANT - FREQUENCY OF OCCURANCE

| DIRECTION | H-SIGNIFICANT [FEET] | | | | | | | | | | | |
|---|---|---|---|---|---|---|---|---|---|---|---|---|
| | 0-1 | 1-3 | 3-5 | 5-7 | 7-9 | 9-11 | 11-13 | 13-18 | 18-25 | 25-35 | 35-45 | 45-60 |
| 53.8 | .46 | 2.31 | 2.40 | 2.30 | 1.24 | .90 | .50 | .42 | .07 | .01 | .00 | .00 |
| 23.8 | .26 | 2.08 | 1.88 | 1.82 | 1.36 | .72 | .49 | .46 | .10 | .00 | .00 | .00 |
| 353.8 | .08 | .64 | .77 | .67 | .44 | .28 | .15 | .09 | .04 | .00 | .00 | .00 |
| 323.8 | .22 | .90 | .48 | .24 | .09 | .03 | .00 | .00 | .00 | .00 | .00 | .00 |
| 293.8 | .02 | .11 | .04 | .03 | .01 | .00 | .00 | .00 | .00 | .00 | .00 | .00 |
| 263.8 | .03 | .04 | .02 | .02 | .00 | .00 | .00 | .00 | .00 | .00 | .00 | .00 |
| 233.8 | .02 | .07 | .05 | .03 | .00 | .00 | .00 | .00 | .00 | .00 | .00 | .00 |
| 203.8 | .03 | .17 | .13 | .07 | .02 | .00 | .02 | .00 | .00 | .00 | .00 | .00 |
| 173.8 | .17 | .71 | .53 | .33 | .11 | .05 | .04 | .02 | .01 | .00 | .00 | .00 |
| 143.8 | 2.60 | 9.21 | 3.79 | 1.71 | .66 | .20 | .04 | .02 | .00 | .00 | .00 | .00 |
| 113.8 | 2.88 | 15.97 | 11.80 | 5.34 | 1.80 | .45 | .08 | .01 | .00 | .00 | .00 | .00 |
| 83.8 | .79 | 5.12 | 4.97 | 3.06 | 1.13 | .27 | .18 | .11 | .00 | .00 | .00 | .00 |

WIND SPEED[KNOTS] VERSUS H-SIGNIFICANT - FREQUENCY OF OCCURANCE

| WIND SPEED | H-SIGNIFICANT [FEET] | | | | | | | | | | | |
|---|---|---|---|---|---|---|---|---|---|---|---|---|
| | 0-1 | 1-3 | 3-5 | 5-7 | 7-9 | 9-11 | 11-13 | 13-18 | 18-25 | 25-35 | 35-45 | 45-60 |
| 0-- 5 | 3.30 | 6.16 | 1.28 | .23 | .06 | .01 | .00 | .00 | .00 | .00 | .00 | .00 |
| 5--10 | 4.27 | 22.16 | 7.18 | 1.41 | .39 | .07 | .01 | .00 | .00 | .00 | .00 | .00 |
| 10--15 | .00 | 8.84 | 15.86 | 6.31 | 1.31 | .31 | .04 | .02 | .00 | .00 | .00 | .00 |
| 15--20 | .00 | .17 | 2.49 | 7.34 | 3.04 | .73 | .23 | .05 | .00 | .00 | .00 | .00 |
| 20--25 | .00 | .02 | .05 | .28 | 1.97 | 1.47 | .50 | .16 | .00 | .00 | .00 | .00 |
| 25--30 | .00 | .00 | .01 | .04 | .07 | .28 | .60 | .44 | .02 | .00 | .00 | .00 |
| 30--35 | .00 | .00 | .00 | .01 | .03 | .04 | .08 | .34 | .05 | .00 | .00 | .00 |
| 35--40 | .00 | .00 | .00 | .00 | .00 | .00 | .02 | .08 | .09 | .00 | .00 | .00 |
| 40--45 | .00 | .00 | .00 | .00 | .00 | .00 | .00 | .02 | .04 | .01 | .00 | .00 |
| 45--50 | .00 | .00 | .00 | .00 | .00 | .00 | .00 | .01 | .02 | .00 | .00 | .00 |
| 50--55 | .00 | .00 | .00 | .00 | .00 | .00 | .00 | .00 | .01 | .00 | .00 | .00 |
| 55--60 | .00 | .00 | .00 | .00 | .00 | .00 | .00 | .00 | .00 | .00 | .00 | .00 |

MEAN SPECTRA [FT**2] VERSUS H-SIGNIFICANT

| FREQ | PERIOD | H-SIGNIFICANT [FEET] | | | | | | | | | | | |
|---|---|---|---|---|---|---|---|---|---|---|---|---|---|
| | | 0-1 | 1-3 | 3-5 | 5-7 | 7-9 | 9-11 | 11-13 | 13-18 | 18-25 | 25-35 | 35-45 | 45-60 |
| .308 | 3.25 | .006 | .068 | .146 | .193 | .210 | .223 | .237 | .274 | .349 | .410 | .000 | .000 |
| .208 | 4.81 | .000 | .010 | .193 | .432 | .587 | .685 | .772 | .822 | .917 | 1.013 | .000 | .000 |
| .158 | 6.33 | .018 | .100 | .336 | .677 | .984 | 1.198 | 1.363 | 1.475 | 1.615 | 1.653 | .000 | .000 |
| .133 | 7.52 | .004 | .033 | .139 | .377 | .730 | 1.050 | 1.319 | 1.532 | 1.750 | 1.900 | .000 | .000 |
| .117 | 8.55 | .007 | .038 | .118 | .321 | .765 | 1.352 | 1.923 | 2.467 | 3.124 | 3.563 | .000 | .000 |
| .103 | 9.71 | .001 | .010 | .040 | .120 | .375 | .886 | 1.553 | 2.463 | 3.614 | 4.283 | .000 | .000 |
| .092 | 10.87 | .001 | .004 | .016 | .049 | .160 | .478 | 1.075 | 2.592 | 4.964 | 6.917 | .000 | .000 |
| .081 | 12.35 | .000 | .001 | .006 | .017 | .065 | .180 | .468 | 1.741 | 6.146 | 10.893 | .000 | .000 |
| .072 | 13.89 | .000 | .001 | .001 | .003 | .008 | .027 | .061 | .329 | 2.004 | 5.460 | .000 | .000 |
| .067 | 14.93 | .000 | .000 | .001 | .001 | .004 | .014 | .024 | .142 | 1.001 | 5.910 | .000 | .000 |
| .061 | 16.39 | .000 | .001 | .001 | .002 | .004 | .013 | .009 | .045 | .406 | 1.200 | .000 | .000 |
| .056 | 17.86 | .000 | .000 | .000 | .000 | .000 | .000 | .001 | .002 | .046 | .167 | .000 | .000 |
| .050 | 20.00 | .000 | .000 | .000 | .000 | .000 | .000 | .000 | .000 | .011 | .080 | .000 | .000 |
| .044 | 22.73 | .000 | .000 | .000 | .000 | .000 | .000 | .000 | .000 | .001 | .010 | .000 | .000 |
| .039 | 25.64 | .000 | .000 | .000 | .000 | .000 | .000 | .000 | .000 | .000 | .000 | .000 | .000 |

WIND DIRECTION VERSUS WIND SPEED(KNOTS) -FREQUENCY OF OCCURANCE

| DIRECTION | WIND SPEED (KNOTS) | | | | | | | | | | | |
|---|---|---|---|---|---|---|---|---|---|---|---|---|
| | 0-5 | 5-10 | 10-15 | 15-20 | 20-25 | 25-30 | 30-35 | 35-40 | 40-45 | 45-50 | 50-55 | 55-60 |
| 53.8 | 1.60 | 6.07 | 6.62 | 2.89 | .72 | .18 | .05 | .00 | .00 | .00 | .00 | .00 |
| 23.8 | 1.53 | 3.24 | 3.82 | 2.78 | 1.59 | .67 | .27 | .09 | .02 | .01 | .00 | .00 |
| 353.8 | .70 | 1.56 | 1.65 | 1.37 | .83 | .44 | .21 | .10 | .05 | .02 | .01 | .00 |
| 323.8 | .40 | .92 | .78 | .39 | .14 | .05 | .00 | .00 | .00 | .00 | .00 | .00 |
| 293.8 | .31 | .41 | .29 | .07 | .01 | .00 | .00 | .00 | .00 | .00 | .00 | .00 |
| 263.8 | .26 | .19 | .08 | .03 | .00 | .00 | .00 | .00 | .00 | .00 | .00 | .00 |
| 233.8 | .24 | .17 | .08 | .03 | .00 | .00 | .00 | .00 | .00 | .00 | .00 | .00 |
| 203.8 | .34 | .27 | .14 | .04 | .00 | .00 | .00 | .00 | .00 | .00 | .00 | .00 |
| 173.8 | .54 | .92 | .55 | .21 | .05 | .01 | .01 | .00 | .00 | .00 | .00 | .00 |
| 143.8 | 1.21 | 3.35 | 2.79 | 1.12 | .26 | .03 | .01 | .00 | .00 | .00 | .00 | .00 |
| 113.8 | 1.79 | 8.97 | 7.41 | 2.57 | .49 | .06 | .00 | .00 | .00 | .00 | .00 | .00 |
| 83.8 | 2.11 | 9.43 | 8.49 | 2.54 | .35 | .03 | .00 | .00 | .00 | .00 | .00 | .00 |

TABLE 1B

DATA FOR GRID POINT 260(ATLANTIC-EAST COAST). BASED ON 27000 RECORDS-20 YEARS.
DIRECTIONS MEASURED CLOCKWISE FROM NORTH. LATITUDE=34.5 DEGREES.
LONGITUDE=74.9 DEGREES.

PEAK FREQUENCY VERSUS H-SIGNIFICANT - FREQUENCY OF OCCURANCE

| FREQ | PERIOD | H-SIGNIFICANT [FEET] | | | | | | | | | | | |
|---|---|---|---|---|---|---|---|---|---|---|---|---|---|
| | | 0-1 | 1-3 | 3-5 | 5-7 | 7-9 | 9-11 | 11-13 | 13-18 | 18-25 | 25-35 | 35-45 | 45-60 |
| .308 | 3.25 | .54 | 3.51 | .00 | .00 | .00 | .00 | .00 | .00 | .00 | .00 | .00 | .00 |
| .208 | 4.81 | .00 | 1.54 | 3.80 | .00 | .00 | .00 | .00 | .00 | .00 | .00 | .00 | .00 |
| .158 | 6.33 | 1.88 | 8.02 | 6.96 | 3.93 | .11 | .00 | .00 | .00 | .00 | .00 | .00 | .00 |
| .133 | 7.52 | 1.21 | 4.82 | 2.56 | 3.72 | 2.02 | .10 | .00 | .00 | .00 | .00 | .00 | .00 |
| .117 | 8.55 | 1.14 | 4.80 | 2.56 | 2.26 | 2.94 | 2.12 | .50 | .03 | .00 | .00 | .00 | .00 |
| .103 | 9.71 | 1.14 | 4.85 | 1.97 | 1.13 | .93 | 1.25 | .98 | .50 | .00 | .00 | .00 | .00 |
| .092 | 10.87 | .62 | 3.61 | 1.76 | .87 | .56 | .37 | .42 | .97 | .04 | .00 | .00 | .00 |
| .081 | 12.35 | .46 | 2.77 | 1.80 | .87 | .56 | .37 | .27 | .40 | .30 | .00 | .00 | .00 |
| .072 | 13.89 | .24 | 1.44 | .88 | .65 | .28 | .15 | .09 | .08 | .10 | .03 | .00 | .00 |
| .067 | 14.93 | .20 | 1.23 | .67 | .42 | .29 | .14 | .09 | .14 | .11 | .04 | .00 | .00 |
| .061 | 16.39 | .12 | .39 | .37 | .23 | .16 | .09 | .04 | .06 | .07 | .09 | .01 | .00 |
| .056 | 17.86 | .00 | .03 | .05 | .01 | .01 | .02 | .01 | .00 | .02 | .03 | .00 | .00 |
| .050 | 20.00 | .00 | .01 | .01 | .00 | .00 | .00 | .00 | .00 | .01 | .01 | .00 | .00 |
| .044 | 22.73 | .00 | .01 | .00 | .00 | .00 | .00 | .00 | .00 | .00 | .00 | .00 | .00 |
| .039 | 25.64 | .00 | .00 | .00 | .00 | .00 | .00 | .00 | .00 | .00 | .00 | .00 | .00 |

DIRECTION OF MAXIMUM S(THETA) VERSUS H-SIGNIFICANT - FREQUENCY OF OCCURANCE

| DIRECTION | H-SIGNIFICANT [FEET] | | | | | | | | | | | |
|---|---|---|---|---|---|---|---|---|---|---|---|---|
| | 0-1 | 1-3 | 3-5 | 5-7 | 7-9 | 9-11 | 11-13 | 13-18 | 18-25 | 25-35 | 35-45 | 45-60 |
| 240.2 | .49 | 3.28 | 3.15 | 1.83 | .99 | .50 | .24 | .13 | .01 | .00 | .00 | .00 |
| 210.2 | 1.15 | 5.71 | 3.81 | 2.14 | 1.04 | .67 | .42 | .37 | .08 | .00 | .00 | .00 |
| 180.2 | .17 | 1.07 | .69 | .45 | .27 | .12 | .09 | .04 | .00 | .00 | .00 | .00 |
| 150.2 | .99 | 2.12 | .54 | .20 | .10 | .05 | .03 | .00 | .00 | .00 | .00 | .00 |
| 120.2 | 2.64 | 11.38 | 4.51 | 1.48 | .61 | .22 | .07 | .08 | .00 | .00 | .00 | .00 |
| 90.2 | .64 | 1.56 | .67 | .38 | .19 | .13 | .07 | .13 | .00 | .00 | .00 | .00 |
| 60.2 | .41 | 3.20 | 2.81 | 2.30 | 1.48 | 1.05 | .64 | .80 | .37 | .15 | .00 | .00 |
| 30.2 | .79 | 5.45 | 3.92 | 2.58 | 1.60 | .87 | .45 | .39 | .12 | .04 | .01 | .00 |
| 0.2 | .20 | 2.43 | 2.34 | 2.00 | 1.17 | .64 | .27 | .19 | .05 | .00 | .00 | .00 |
| 330.2 | .02 | .28 | .29 | .25 | .14 | .06 | .01 | .00 | .00 | .00 | .00 | .00 |
| 300.2 | .03 | .23 | .33 | .26 | .19 | .21 | .11 | .04 | .00 | .00 | .00 | .00 |
| 270.2 | .01 | .31 | .33 | .22 | .09 | .10 | .02 | .03 | .00 | .00 | .00 | .00 |

WIND SPEED[KNOTS] VERSUS H-SIGNIFICANT - FREQUENCY OF OCCURANCE

| WIND SPEED | H-SIGNIFICANT [FEET] | | | | | | | | | | | |
|---|---|---|---|---|---|---|---|---|---|---|---|---|
| | 0-1 | 1-3 | 3-5 | 5-7 | 7-9 | 9-11 | 11-13 | 13-18 | 18-25 | 25-35 | 35-45 | 45-60 |
| 0— 5 | 3.58 | 8.77 | 2.49 | .74 | .27 | .09 | .06 | .04 | .03 | .01 | .00 | .00 |
| 5—10 | 3.97 | 18.59 | 5.48 | 1.78 | .72 | .24 | .09 | .13 | .03 | .01 | .00 | .00 |
| 10—15 | .00 | 9.10 | 11.27 | 3.42 | 1.22 | .47 | .24 | .12 | .04 | .01 | .00 | .00 |
| 15—20 | .00 | .54 | 3.81 | 6.85 | 2.55 | .75 | .31 | .21 | .07 | .02 | .00 | .00 |
| 20—25 | .00 | .02 | .30 | 1.08 | 2.69 | 2.05 | .53 | .34 | .05 | .01 | .00 | .00 |
| 25—30 | .00 | .00 | .03 | .19 | .33 | .82 | .92 | .66 | .09 | .03 | .00 | .00 |
| 30—35 | .00 | .00 | .00 | .02 | .07 | .16 | .21 | .52 | .16 | .01 | .00 | .00 |
| 35—40 | .00 | .00 | .00 | .00 | .01 | .02 | .05 | .15 | .12 | .03 | .00 | .00 |
| 40—45 | .00 | .00 | .00 | .00 | .00 | .00 | .00 | .03 | .04 | .05 | .00 | .00 |
| 45—50 | .00 | .00 | .00 | .00 | .00 | .00 | .00 | .00 | .01 | .01 | .00 | .00 |
| 50—55 | .00 | .00 | .00 | .00 | .00 | .00 | .00 | .00 | .00 | .00 | .00 | .00 |
| 55—60 | .00 | .00 | .00 | .00 | .00 | .00 | .00 | .00 | .00 | .00 | .00 | .00 |

MEAN SPECTRA [FT**2] VERSUS H-SIGNIFICANT

| FREQ | PERIOD | H-SIGNIFICANT [FEET] | | | | | | | | | | |
|---|---|---|---|---|---|---|---|---|---|---|---|---|
| | | 0-1 | 1-3 | 3-5 | 5-7 | 7-9 | 9-11 | 11-13 | 13-18 | 18-25 | 25-35 | 35-45 | 45-60 |
| .308 | 3.25 | .006 | .068 | .141 | .182 | .200 | .217 | .229 | .250 | .262 | .290 | .407 | .000 |
| .208 | 4.81 | .000 | .015 | .232 | .455 | .570 | .666 | .696 | .733 | .731 | .766 | .970 | .000 |
| .158 | 6.33 | .011 | .058 | .230 | .574 | .858 | 1.069 | 1.198 | 1.331 | 1.387 | 1.502 | 1.573 | .000 |
| .133 | 7.52 | .006 | .028 | .094 | .293 | .619 | .910 | 1.139 | 1.342 | 1.447 | 1.635 | 1.650 | .000 |
| .117 | 8.55 | .006 | .028 | .089 | .259 | .688 | 1.280 | 1.816 | 2.278 | 2.680 | 3.005 | 3.487 | .000 |
| .103 | 9.71 | .004 | .020 | .054 | .125 | .344 | .757 | 1.345 | 2.124 | 2.931 | 3.366 | 4.120 | .000 |
| .092 | 10.87 | .003 | .018 | .053 | .110 | .244 | .525 | 1.114 | 2.434 | 4.260 | 5.224 | 6.560 | .000 |
| .081 | 12.35 | .002 | .014 | .049 | .102 | .215 | .388 | .801 | 1.927 | 5.712 | 8.640 | 11.637 | .000 |
| .072 | 13.89 | .001 | .005 | .018 | .042 | .073 | .119 | .226 | .557 | 2.666 | 5.813 | 8.083 | .000 |
| .067 | 14.93 | .001 | .004 | .014 | .033 | .069 | .108 | .182 | .399 | 2.307 | 6.693 | 9.640 | .000 |
| .061 | 16.39 | .000 | .002 | .008 | .018 | .039 | .063 | .111 | .242 | 1.746 | 7.586 | 13.167 | .000 |
| .056 | 17.86 | .000 | .000 | .002 | .003 | .012 | .023 | .036 | .076 | .742 | 5.033 | 11.700 | .000 |
| .050 | 20.00 | .000 | .000 | .000 | .000 | .002 | .004 | .007 | .022 | .211 | 1.655 | 8.293 | .000 |
| .044 | 22.73 | .000 | .000 | .000 | .000 | .000 | .000 | .001 | .003 | .064 | .218 | .540 | .000 |
| .039 | 25.64 | .000 | .000 | .000 | .000 | .000 | .000 | .000 | .000 | .002 | .037 | .093 | .000 |

WIND DIRECTION VERSUS WIND SPEED(KNOTS) -FREQUENCY OF OCCURANCE

| DIRECTION | WIND SPEED [KNOTS] | | | | | | | | | | | |
|---|---|---|---|---|---|---|---|---|---|---|---|---|
| | 0-5 | 5-10 | 10-15 | 15-20 | 20-25 | 25-30 | 30-35 | 35-40 | 40-45 | 45-50 | 50-55 | 55-60 |
| 240.2 | 1.19 | 2.71 | 2.60 | 1.58 | .87 | .45 | .15 | .07 | .01 | .00 | .00 | .00 |
| 210.2 | 2.39 | 4.50 | 4.67 | 2.92 | 1.16 | .58 | .20 | .05 | .02 | .00 | .00 | .00 |
| 180.2 | 1.65 | 3.67 | 2.45 | 1.06 | .47 | .18 | .10 | .04 | .01 | .01 | .00 | .00 |
| 150.2 | 1.44 | 2.38 | 1.08 | .42 | .16 | .04 | .01 | .00 | .00 | .00 | .00 | .00 |
| 120.2 | 1.18 | 1.61 | .91 | .37 | .13 | .03 | .00 | .00 | .00 | .00 | .00 | .00 |
| 90.2 | 1.16 | 1.94 | 1.03 | .50 | .22 | .10 | .03 | .01 | .00 | .00 | .00 | .00 |
| 60.2 | 1.23 | 2.63 | 2.28 | 1.22 | .53 | .22 | .09 | .05 | .01 | .00 | .00 | .00 |
| 30.2 | 1.50 | 3.16 | 3.09 | 1.89 | .93 | .37 | .13 | .06 | .03 | .01 | .00 | .00 |
| 0.2 | 1.14 | 2.65 | 2.48 | 1.56 | .73 | .32 | .10 | .03 | .03 | .01 | .00 | .00 |
| 330.2 | 1.11 | 2.17 | 2.29 | 1.59 | .74 | .28 | .12 | .02 | .00 | .00 | .00 | .00 |
| 300.2 | 1.04 | 1.88 | 1.72 | 1.20 | .68 | .31 | .11 | .03 | .01 | .00 | .00 | .00 |
| 270.2 | 1.05 | 1.74 | 1.32 | .83 | .45 | .20 | .10 | .03 | .01 | .00 | .00 | .00 |

## TABLE 1C

DATA FOR GRID POINT 175(PACIFIC-WEST COAST). BASED ON 16070 RECORDS-11 YEARS.
DIRECTIONS MEASURED CLOCKWISE FROM NORTH. LATITUDE=32.8 DEGREES.
LONGITUDE=119.5 DEGREES.

PEAK FREQUENCY VERSUS H-SIGNIFICANT - FREQUENCY OF OCCURANCE

| FREQ | PERIOD | H-SIGNIFICANT [FEET] | | | | | | | | | | |
|---|---|---|---|---|---|---|---|---|---|---|---|---|
| | | 0-1 | 1-3 | 3-5 | 5-7 | 7-9 | 9-11 | 11-13 | 13-18 | 18-25 | 25-35 | 35-45 | 45-60 |
| .308 | 3.25 | .959 | 3.953 | .000 | .000 | .000 | .000 | .000 | .000 | .000 | .000 | .000 | .000 |
| .208 | 4.81 | .000 | 3.000 | 5.845 | .000 | .000 | .000 | .000 | .000 | .000 | .000 | .000 | .000 |
| .158 | 6.33 | .622 | 4.177 | 8.273 | 4.893 | .081 | .000 | .000 | .000 | .000 | .000 | .000 | .000 |
| .133 | 7.52 | .430 | 2.714 | 3.019 | 4.413 | 2.359 | .044 | .000 | .000 | .000 | .000 | .000 | .000 |
| .117 | 8.55 | .342 | 2.235 | 1.849 | 1.500 | 2.608 | 1.401 | .162 | .000 | .000 | .000 | .000 | .000 |
| .103 | 9.71 | .510 | 2.944 | 2.017 | 1.338 | 1.120 | 1.127 | .822 | .162 | .000 | .000 | .000 | .000 |
| .092 | 10.87 | .293 | 2.011 | 1.226 | .859 | .548 | .311 | .149 | .243 | .000 | .000 | .000 | .000 |
| .081 | 12.35 | .454 | 2.135 | 1.345 | .691 | .479 | .249 | .106 | .143 | .006 | .000 | .000 | .000 |
| .072 | 13.89 | .380 | 2.179 | 1.357 | .909 | .305 | .143 | .056 | .068 | .000 | .000 | .000 | .000 |
| .067 | 14.93 | .560 | 2.378 | 1.550 | .784 | .342 | .137 | .081 | .062 | .000 | .000 | .000 | .000 |
| .061 | 16.39 | 1.226 | 5.235 | 2.340 | 1.208 | .367 | .230 | .100 | .056 | .000 | .000 | .000 | .000 |
| .056 | 17.86 | .012 | .243 | .174 | .093 | .075 | .056 | .025 | .019 | .006 | .000 | .000 | .000 |
| .050 | 20.00 | .012 | .075 | .112 | .068 | .025 | .044 | .019 | .031 | .006 | .000 | .000 | .000 |
| .044 | 22.73 | .000 | .019 | .025 | .006 | .019 | .019 | .006 | .000 | .006 | .000 | .000 | .000 |
| .039 | 25.64 | .006 | .037 | .006 | .006 | .012 | .000 | .000 | .000 | .000 | .000 | .000 | .000 |

DIRECTION OF MAXIMUM S(THETA) VERSUS H-SIGNIFICANT - FREQUENCY OF OCCURANCE

| DIRECTION | H-SIGNIFICANT [FEET] | | | | | | | | | | | |
|---|---|---|---|---|---|---|---|---|---|---|---|---|
| | 0-1 | 1-3 | 3-5 | 5-7 | 7-9 | 9-11 | 11-13 | 13-18 | 18-25 | 25-35 | 35-45 | 45-60 |
| 281.4 | 1.438 | 9.430 | 6.829 | 3.978 | 1.861 | .772 | .367 | .237 | .012 | .000 | .000 | .000 |
| 251.4 | .716 | 2.876 | 1.886 | .741 | .349 | .193 | .050 | .050 | .000 | .000 | .000 | .000 |
| 221.4 | .019 | .187 | .205 | .212 | .156 | .131 | .050 | .093 | .000 | .000 | .000 | .000 |
| 191.4 | .019 | .037 | .044 | .044 | .106 | .068 | .050 | .062 | .000 | .000 | .000 | .000 |
| 161.4 | .075 | .218 | .162 | .118 | .031 | .025 | .037 | .000 | .006 | .000 | .000 | .000 |
| 131.4 | .037 | .118 | .025 | .006 | .006 | .000 | .000 | .000 | .000 | .000 | .000 | .000 |
| 101.4 | .068 | .324 | .342 | .075 | .025 | .000 | .000 | .000 | .000 | .000 | .000 | .000 |
| 71.4 | .168 | 1.064 | .566 | .100 | .025 | .000 | .000 | .000 | .000 | .000 | .000 | .000 |
| 41.4 | .149 | 1.108 | .641 | .131 | .000 | .006 | .000 | .000 | .000 | .000 | .000 | .000 |
| 11.4 | .137 | 1.058 | .753 | .255 | .075 | .006 | .000 | .000 | .000 | .000 | .000 | .000 |
| 341.4 | .255 | 2.004 | 1.656 | .797 | .535 | .224 | .037 | .019 | .000 | .000 | .000 | .000 |
| 311.4 | 2.726 | 14.908 | 16.029 | 10.314 | 5.173 | 2.334 | .934 | .324 | .006 | .000 | .000 | .000 |

WIND SPEED[KNOTS] VERSUS H-SIGNIFICANT - FREQUENCY OF OCCURANCE

| WIND SPEED | H-SIGNIFICANT [FEET] | | | | | | | | | | | |
|---|---|---|---|---|---|---|---|---|---|---|---|---|
| | 0-1 | 1-3 | 3-5 | 5-7 | 7-9 | 9-11 | 11-13 | 13-18 | 18-25 | 25-35 | 35-45 | 45-60 |
| 0— 5 | 1.706 | 3.150 | 1.201 | .367 | .112 | .118 | .012 | .000 | .000 | .000 | .000 | .000 |
| 5—10 | 4.102 | 16.857 | 4.034 | 1.133 | .517 | .156 | .062 | .031 | .000 | .000 | .000 | .000 |
| 10—15 | .000 | 12.979 | 17.448 | 3.063 | .672 | .212 | .149 | .087 | .000 | .000 | .000 | .000 |
| 15—20 | .000 | .342 | 6.331 | 10.688 | 2.278 | .398 | .118 | .062 | .006 | .000 | .000 | .000 |
| 20—25 | .000 | .006 | .118 | 1.438 | 4.556 | 1.942 | .187 | .075 | .006 | .000 | .000 | .000 |
| 25—30 | .000 | .000 | .006 | .075 | .199 | .921 | .859 | .330 | .006 | .000 | .000 | .000 |
| 30—35 | .000 | .000 | .000 | .006 | .006 | .012 | .137 | .187 | .000 | .000 | .000 | .000 |
| 35—40 | .000 | .000 | .000 | .000 | .000 | .000 | .000 | .012 | .006 | .000 | .000 | .000 |
| 40—45 | .000 | .000 | .000 | .000 | .000 | .000 | .000 | .000 | .000 | .000 | .000 | .000 |
| 45—50 | .000 | .000 | .000 | .000 | .000 | .000 | .000 | .000 | .000 | .000 | .000 | .000 |
| 50—55 | .000 | .000 | .000 | .000 | .000 | .000 | .000 | .000 | .000 | .000 | .000 | .000 |
| 55—60 | .000 | .000 | .000 | .000 | .000 | .000 | .000 | .000 | .000 | .000 | .000 | .000 |

MEAN SPECTRA [FT**2] VERSUS H-SIGNIFICANT

| FREQ | PERIOD | H-SIGNIFICANT [FEET] | | | | | | | | | | |
|---|---|---|---|---|---|---|---|---|---|---|---|---|
| | | 0-1 | 1-3 | 3-5 | 5-7 | 7-9 | 9-11 | 11-13 | 13-18 | 18-25 | 25-35 | 35-45 | 45-60 |
| .308 | 3.25 | .012 | .096 | .172 | .202 | .212 | .216 | .234 | .255 | .250 | .000 | .000 | .000 |
| .208 | 4.81 | .000 | .035 | .313 | .534 | .638 | .691 | .718 | .720 | .780 | .000 | .000 | .000 |
| .158 | 6.33 | .005 | .034 | .202 | .554 | .857 | 1.017 | 1.124 | 1.167 | 1.090 | .000 | .000 | .000 |
| .133 | 7.52 | .003 | .018 | .075 | .283 | .627 | .882 | 1.075 | 1.173 | 1.125 | .000 | .000 | .000 |
| .117 | 8.55 | .003 | .017 | .056 | .197 | .651 | 1.175 | 1.666 | 1.957 | 1.655 | .000 | .000 | .000 |
| .103 | 9.71 | .003 | .014 | .040 | .109 | .335 | .772 | 1.369 | 1.802 | 1.538 | .000 | .000 | .000 |
| .092 | 10.87 | .002 | .010 | .030 | .075 | .188 | .482 | 1.042 | 1.969 | 1.560 | .000 | .000 | .000 |
| .081 | 12.35 | .003 | .013 | .035 | .073 | .150 | .306 | .713 | 1.958 | 2.345 | .000 | .000 | .000 |
| .072 | 13.89 | .002 | .008 | .019 | .046 | .072 | .112 | .244 | .667 | 1.480 | .000 | .000 | .000 |
| .067 | 14.93 | .002 | .009 | .021 | .040 | .065 | .096 | .213 | .476 | 1.495 | .000 | .000 | .000 |
| .061 | 16.39 | .005 | .016 | .028 | .061 | .082 | .215 | .230 | .422 | 1.593 | .000 | .000 | .000 |
| .056 | 17.86 | .000 | .001 | .003 | .007 | .017 | .062 | .090 | .205 | 2.638 | .000 | .000 | .000 |
| .050 | 20.00 | .000 | .000 | .002 | .004 | .008 | .035 | .065 | .362 | 2.168 | .000 | .000 | .000 |
| .044 | 22.73 | .000 | .000 | .000 | .001 | .004 | .014 | .020 | .086 | 5.968 | .000 | .000 | .000 |
| .039 | 25.64 | .000 | .000 | .000 | .001 | .001 | .003 | .001 | .010 | .035 | .000 | .000 | .000 |

WIND DIRECTION VERSUS WIND SPEED(KNOTS) -FREQUENCY OF OCCURANCE

| DIRECTION | WIND SPEED (KNOTS) | | | | | | | | | | | |
|---|---|---|---|---|---|---|---|---|---|---|---|---|
| | 0-5 | 5-10 | 10-15 | 15-20 | 20-25 | 25-30 | 30-35 | 35-40 | 40-45 | 45-50 | 50-55 | 55-60 |
| 281.4 | .815 | 4.712 | 6.909 | 3.648 | 1.376 | .423 | .062 | .006 | .000 | .000 | .000 | .000 |
| 251.4 | .473 | .971 | .716 | .398 | .156 | .012 | .000 | .000 | .000 | .000 | .000 | .000 |
| 221.4 | .342 | .311 | .355 | .299 | .168 | .056 | .012 | .000 | .000 | .000 | .000 | .000 |
| 191.4 | .199 | .411 | .305 | .274 | .168 | .100 | .044 | .000 | .000 | .000 | .000 | .000 |
| 161.4 | .212 | .237 | .174 | .149 | .118 | .037 | .012 | .000 | .000 | .000 | .000 | .000 |
| 131.4 | .218 | .261 | .193 | .075 | .012 | .006 | .000 | .000 | .000 | .000 | .000 | .000 |
| 101.4 | .330 | .405 | .268 | .100 | .025 | .019 | .000 | .000 | .000 | .000 | .000 | .000 |
| 71.4 | .448 | 1.077 | .946 | .286 | .093 | .025 | .000 | .000 | .000 | .000 | .000 | .000 |
| 41.4 | .604 | 1.973 | 1.301 | .373 | .075 | .025 | .000 | .000 | .000 | .000 | .000 | .000 |
| 11.4 | .815 | 3.056 | 1.892 | .579 | .106 | .012 | .006 | .000 | .000 | .000 | .000 | .000 |
| 341.4 | 1.282 | 4.743 | 4.457 | 2.004 | .685 | .212 | .019 | .000 | .000 | .000 | .000 | .000 |
| 311.4 | .927 | 8.733 | 17.093 | 12.039 | 5.347 | 1.469 | .193 | .012 | .000 | .000 | .000 | .000 |

**APPENDIX B**

Outline of Future Tasks

Appendix B
Outline of Future Tasks

Phase II Work

1.0 Ultrasonic Model Validation

- 1.1 Define Flaw Types
- 1.2 Fabricate Test Samples
  - 1.2.1 Attenuation Samples (4x4x4, 4x4x8)
  - 1.2.2 Thick Walled (8x36x6.8) (2)
  - 1.2.3 Thin Walled (8x16x2.5) (2)
  - 1.2.4 Tool Joint (8x10x1.5) (2)
- 1.3 Detection as Function of Flaw Size and Location (no threads)
- 1.4 Effect of Thread Form
- 1.5 Refine Model
- 1.6 Design Inspection System for Tool Joints
- 1.7 Fabricate Tool Joints (5)
- 1.8 Calibration Experiment
- 1.9 'Blind' Test
- 1.10 Flame Spray Experiment

2.0 Fatigue Testing (Tool Joints)

- 2.1 Tool Joint Analysis (FEA, S-N, da-dN)
- 2.2 Test Planning
- 2.3 Test Facility Design and Construction (optional)
- 2.4 Test Specimen Procurement (20)
- 2.5 Instrumentation (AE, Radiography, Ultrasonic)
- 2.6 Short Term Testing
- 2.7 Long Term Testing (check effects of CiPo, sea water leakage, flame spraying, etc.)

3.0 TLP Tendon Analysis

- 3.1 Loads Characterization
  - 3.1.1 Non-linear wave responses
  - 3.1.2 Platform Criteria and Optimization
  - 3.1.3 Other Loads
- 3.2 Connector Analysis
  - 3.2.1 FEA Stress Analysis (Axisyummetric)
  - 3.2.2 Crack Propagation Modeling (FEA)
- 3.3 Failure Analysis

4.0 Material Tests

- 4.1 High R, Low $\Delta K$, CP da/dN tests
- 4.2 High R, Low $\Delta S$, CP S-N tests
- 4.3 High R, Low $\Delta S$, Flame Spray, S-N tests
- 4.4 High R, Low $\Delta K$, Flame Spray, da/dN tests

5.0 Full Scale Component Testing